Annual Reports on
NMR SPECTROSCOPY

VOLUME **68**

Edited by

GRAHAM A. WEBB
Royal Society of Chemistry
Burlington House
Piccadilly, London, UK

Notice
No responsibility is assumed by the publisher for any injury and/or damage to persons
or property as a matter of products liability, negligence or otherwise, or from any use
or operation of any methods, products, instructions or ideas contained in the material
herein. Because of rapid advances in the medical sciences, in particular, independent
verification of diagnoses and drug dosages should be made

For information on all Academic Press publications
visit our web site at elsevierdirect.com

Printed and bound in Great Britain

09 10 11 12 10 9 8 7 6 5 4 3 2 1

CONTRIBUTORS

David J. Craik
Division of Chemistry and Structural Biology, Institute for Molecular Bioscience, The University of Queensland, Brisbane, Qld 4072, Australia

Norelle L. Daly
Division of Chemistry and Structural Biology, Institute for Molecular Bioscience, The University of Queensland, Brisbane, Qld 4072, Australia

Stefan Jankowski
Institute of Organic Chemistry, Faculty of Chemistry, Technical University of Lodz, Zeromskiego 116, 90-924 Lodz, Poland

G. Kummerlöwe
Department Chemie, Technische Universität München, LS OC II, Lichtenberg-strasse 4, D-85747 Garching, Germany

B. Luy
Department Chemie, Technische Universität München, LS OC II, Lichtenberg-strasse 4, D-85747 Garching, Germany

Roberta Musio
Dipartimento di Chimica, Università degli Studi di Bari, Via E. Orabona 4, I-70126 Bari, Italy

K. Johan Rosengren
Division of Chemistry and Structural Biology, Institute for Molecular Bioscience, The University of Queensland, Brisbane, Qld 4072, Australia

PREFACE

Volume 68 of *Annual Reports of NMR* contains accounts of developments and progress in many areas of NMR studies. The volume opens with an account by R. Musio on 'Applications of ^{33}S NMR Spectroscopy'; 'NMR of Peptide Toxins' is reported on by K.J. Rosengren, N.L. Daly and D.J. Craik; S. Jankowski reports on 'Application of NMR Spectroscopy in Isotope Effects Studies', finally G. Kummerlöwe and B. Luy cover 'Residual Dipolar Couplings for the Configurational and Conformational Analysis of Organic Molecules'. It is my pleasure to thank all of these authors for their timely and interesting contributions.

G.A. Webb
Royal Society of Chemistry
Burlington House
Piccadilly
London, UK

CHAPTER 1

Applications of ^{33}S NMR Spectroscopy

Roberta Musio

Dipartimento di Chimica, Università degli Studi di Bari, Via E. Orabona 4, I-70126 Bari, Italy

Abstract   Results so far reported in the literature have demonstrated that [33]S NMR spectroscopy is a valuable tool, not only in the determination of molecular structure, but also in the study of the electronic distribution in organic and inorganic molecules, association and exchange phenomena in solution, effects of intermolecular interactions in different aggregation states and qualitative and quantitative analyses of mixtures of sulphur compounds. Notwithstanding this importance, [33]S NMR spectroscopy has so far been under-utilized because [33]S is a difficult nucleus to detect. However, the availability of a new generation of high-field spectrometers gives hope for further developing this technique. Preliminary results obtained in the field of solid-state NMR spectroscopy demonstrate its potential. This review discusses the most important applications of [33]S NMR spectroscopy. Moreover, since knowledge of the correlation between NMR parameters and structure is a prerequisite for any application, it also addresses the way in which [33]S NMR parameters change due to structural modifications in different functional groups. A compilation of [33]S parameters in different organic and inorganic functional groups has been provided.

Keywords: [33]S NMR spectroscopy; [33]S chemical shift; [33]S nuclear relaxation; [33]S solid state NMR spectroscopy

1. INTRODUCTION

[33]S was one of the first nuclei to be detected by nuclear magnetic resonance (NMR).[1] After the first papers by Retcofsky and Friedel[2,3] and Lutz et al.,[4,5] [33]S NMR spectroscopy received a certain amount of attention in the 1980s, with the availability of FT spectrometers at high magnetic field. In 1981, Faure et al.[6] presented the first application of FT [33]S NMR spectroscopy to characterize organic and biological compounds. During the successive decade, some important functional groups containing sulphur were extensively characterized, and numerous chemical applications were presented. Up to 1992, four reviews[7–10] and dedicated chapters in some important NMR books[11] were published.

Notwithstanding the first encouraging results, [33]S NMR spectroscopy has been largely under-utilized, partly because it is considered a difficult experimental technique. However, the relative paucity of [33]S NMR studies in the literature is largely compensated for by the relevant significance of most of them. Indeed, many of the published works clearly demonstrate the important and, in certain cases, unique role that [33]S NMR can play in understanding structure and electronic distribution in organic and inorganic molecules, as well as in the study of many chemical problems, including association and exchange phenomena in solution, effects of intermolecular interaction in different aggregation states and qualitative and quantitative analysis of mixtures of sulphur compounds.

Many of the difficulties encountered in the acquisition of [33]S NMR spectra can now be circumvented by the use of modern spectrometers operating at very high magnetic fields, as the early successes of solid-state [33]S NMR spectroscopy have demonstrated.

There is hope for future growth and development of ^{33}S NMR spectroscopy, and the aim of this work is to draw attention also to the potential of this technique. In Chapter 2, a brief outline of the most relevant problems associated with the acquisition of ^{33}S NMR spectra is reported. Chapter 3 gives a general survey of the ^{33}S NMR parameters and of their correlations with molecular structure. Chapter 4 is dedicated to an analysis of the most relevant applications of ^{33}S NMR spectroscopy in different fields, with particular attention to the use of ^{33}S NMR parameters in the study of structural problems. In Chapter 5, the utility of theoretical calculations of ^{33}S NMR parameters as a tool in interpreting experimental data has been examined.

2. NMR SPECTROSCOPIC PROPERTIES OF SULPHUR-33

2.1 ^{33}S nuclear properties

The most important NMR properties[12] of ^{33}S, which is the only isotope of sulphur with a non-zero spin, are shown in Table 1.

   ^{33}S is a quadrupolar nucleus characterized by a low magnetogyric ratio and scarce natural abundance, resulting in a very low receptivity. The moderate quadrupole moment results in efficient quadrupolar relaxation and broad NMR signals (from few to thousands of Hz). Reasonably narrow signals can be obtained only for small molecules in which the sulphur atom is located at sites of high electronic symmetry, such as the tetrahedral SO_4^{2-} anion and low molecular weight sulphones and sulphonates. In thiols, sulphides, sulphoxides and other organic and inorganic functional groups with a low electronic symmetry, ^{33}S line widths are often larger than 10,000 Hz, and the signals are observable only in a limited number of cases.

   Besides electronic symmetry, other factors that can affect NMR line widths, such as chemical exchange, viscosity and temperature, can often preclude the detection of ^{33}S NMR signals.

   Large line widths (i) prevent the accurate measurement of chemical shifts, (ii) may cause the overlap of resonances when more than one type of sulphur atom is present in a molecule or sample and (iii) have a significant influence on the achievable signal-to-noise ratio (S/N) and, consequently, on the experimental times needed to obtain readable spectra.

Table 1 Basic spin properties of ^{33}S nucleus

I	Natural abundance	Magnetogyric ratio $\gamma/10^7\,\mathrm{rad\,s^{-1}\,T^{-1}}$	Magnetic moment μ/μ_N	Quadrupole moment Q/barn	Receptivity[a]	
					D^p	D^C
3/2	0.76%	2.055685	0.8311696	−6.78	1.72×10^{-5}	0.101

[a]D^p is the receptivity relative to that of ^{1}H and D^C is relative to ^{13}C.

Moreover, the low magnetogyric ratio results in very low resonance frequencies and accentuates the effects of spurious signals in the first part of the FID. These signals cause severe baseline distortions in the FT spectrum, thus preventing a precise measurement of spectral parameters (chemical shift, line width and signal amplitude), especially in the case of broad resonances.

With these features, ^{33}S is one of the most difficult nuclei to detect by NMR. However, the increasing availability of high-field NMR spectrometers and the development of hardware and probe technology can partly facilitate its detection.

2.2 Experimental details

As previously pointed out, the ^{33}S NMR signal is often difficult to detect. Acquiring ^{33}S spectra with an acceptable S/N may require from a few minutes to several days, depending on the symmetry of the sulphur electronic environment and molecular size. Therefore, a suitable choice of acquisition parameters and other experimental conditions (e.g. solvent and concentration in liquid phase, density in gas phase, temperature and so on) is particularly important. In addition, signal-processing methodologies can be critical for extracting all the information contained in a FID, especially when the S/N is not satisfactory.

Some practical aspects of ^{33}S NMR spectroscopy are outlined in the following section. For a deeper discussion, the reader can refer to the literature.[13]

2.2.1 Acquisition

In the case of signals with large line widths, some aspects that can be ignored in routine FT NMR become significant. First, fast nuclear relaxation rate is usually considered a limiting factor in the achievement of a good S/N, but it can become an advantage under suitable conditions. For a signal with a line width of 100 Hz (very common for ^{33}S), the longitudinal relaxation time T_1 is 3 ms, meaning that a delay time of 0.015 s between two pulses is sufficient to avoid signal saturation. If the line width is 4 Hz and T_1 is 80 ms, the delay between two pulses has to be 0.4 s. It is evident that a large number of scans can be acquired in a reasonable time (in ^{33}S spectra, a number of transients on the order of 10^6 is quite common to reach a suitable S/N), and the fast repetition rate can at least partly compensate for the loss in S/N due to large line widths.

Other experimental factors that must be considered attentively are temperature, nature of the solvent and solution concentration. A substantial improvement in S/N and sensitivity can be achieved by increasing the temperature of acquisition. Indeed, raising the temperature can lead to a decrease in the line width, due to faster molecular tumbling, and to an increase in the solubility or miscibility of the solute, if necessary. Low-viscosity solvents should be preferred, since molecular tumbling depends on the medium viscosity.

In acquiring ^{33}S FT NMR spectra, further problems arise from the presence of spurious transitory signals at the beginning of the FID that cause baseline rolling in the FT spectrum. These baseline distortions prevent the sufficiently precise measurement of NMR parameters and sometimes the unambiguous identification of resonances. This problem is common to all fast-relaxing nuclei with low

resonance frequency, but it often becomes dramatic in ^{33}S NMR spectra, especially in the case of dilute samples and very broad resonances. It has been extensively discussed and reviewed in the literature.[14] Here, only some general indications are given.

Transitory signals are detected together with the magnetization, and their amplitude decays exponentially with a constant time that can be comparable to the relaxation time of the nucleus observed. They can obscure the signal if it is weak and of short duration. These transitory signals have been attributed to a variety of factors such as (i) leakage from pulse breakthrough; (ii) acoustic waves generated from the metallic probe parts; (iii) ringing originated in different parts of the spectrometer, particularly in the receiver coil, filters and cable; and (iv) piezoelectric resonances in solid samples. Among these, pulse breakthrough and probe acoustic waves are considered the most relevant problems.

The effects of ring-down due to any of the previously reported causes can be reduced in three different ways: (i) by acquiring spectra at high magnetic fields; (ii) by using suitable pulse sequences; and (iii) by introducing a delay time between the end of the pulse and the beginning of the acquisition.

With more recent spectrometers working at very high magnetic fields, the quality of the baseline of ^{33}S FT spectra have partially improved for two main reasons. First, the nuclear resonance frequency increases with magnetic field strength (see ^{33}S resonance frequencies in Table A.1), and second, recent probes give better results because particular attention is paid to the choice of materials and to the optimization of circuit design.

During the acquisition, it is possible to reduce the baseline rolling by using suitable pulse sequences. The most commonly used are the RIDE (ring-down elimination) sequence, first proposed by Ellis[7,14] (slightly different from a sequence introduced by Canet et al.[15]), the ACOUSTIC sequence, proposed by Patt,[16] and a series of extended spin-echo sequences.[14] However, all these sequences result in inefficient excitation over a wide range of frequencies, and therefore they can be applied only to restricted spectral widths.

A very easy way to reduce the strong baseline distortions in the FT spectrum is to introduce a delay time between the switch-off of the transmitter and the beginning of the acquisition. This pre-acquisition delay can also be useful to avoid saturating the memory with transitory signals. However, the use of a pre-acquisition delay in a one-pulse experiment is very critical, and care must be taken in correctly setting its duration. If the pre-acquisition delay is too short, no significant improvement is achieved. If it is too long, the first part of the FID is not sampled, and as a consequence there is a significant loss of the signal intensity, as well as phase coherence if two or more resonances are present.

When acquiring gas phase ^{33}S spectra, other problems must be considered. Spectrometers used for liquid phase studies can be employed for gas phase studies without any modification, but signals are generally much broader than in the liquid phase. Care must be taken in preparing samples. These should be no longer than 3–4 cm, in order to minimize the diffusion of molecules and temperature gradients,[17] and should match exactly the active region of the probe.

In their works on [33]S NMR spectroscopy in the gas phase, Jackowski et al.[18,19] have used 4–8 mm o.d. glass tubes filled with gaseous mixtures and sealed. These tubes were fitted into a standard 5–10 mm o.d. tube filled with a deuterated solvent (toluene-d_8, benzene-d_6, acetone-d_6) in the annular space to generate the lock signal.

2.2.2 Signal processing

Signal processing is a critical point in the accurate determination of NMR parameters.[20]

As previously outlined, in most cases, [33]S NMR spectra are characterized by low S/N, and the first points of the FID are corrupted by acoustic ringing and pulse breakthrough.

The effects of acoustic ringing and pulse breakthrough can be significantly reduced but not completely eliminated during the acquisition of the spectra, and sometimes polynomial correction of the spectrum baseline is not an advisable way to eliminate the problem, especially if resonances are broad. It can be very helpful to delete the first corrupted points of the FID before FT (left-shift procedure). However, eliminating a large number of data points at the beginning of the FID produces a loss of signal intensity and phase coherence between different signals in the spectrum.

To further improve the quality of the FT spectrum, linear prediction[21] can be applied to reconstruct the first FID data points.[22,23]

A remarkable improvement in the visualization of the signal can be obtained by displaying the [33]S power spectrum,[22] although this is feasible only when a single signal is present (information about the phases and intensities of peaks are lost in the power spectrum representation).

2.2.3 2D [33]S NMR

2D HMQC [33]S/^{19}F correlation spectra of SF_6 have been reported. The spectra were acquired at 11.7 T, on a gas sample at high pressure[24] (approximately 20 atm, $T = 298$ K) and on SF_6 dissolved in thermotropic liquid crystals.[25] At present, [33]S 2D NMR does not seem to have great prospects for future development. SF_6 is the only molecule in which [33]S is strongly coupled to another nucleus ($^1J_{S-F} = 250$ Hz ca.) and shows a multiplet with very narrow line widths (1 Hz ca. in pure liquid).

2.3 Reference standard for chemical shift

The individuation of a suitable reference standard to determine chemical shift is an inconvenience for many nuclei, but in the case of [33]S it is a serious difficulty. Indeed, there is an unfortunate lack of standardization in the choice of reference compounds, which often makes it difficult to compare different data in the literature.

Many compounds have been used as reference standards, including CS_2, some inorganic sulphates in aqueous solutions at different concentrations and

sulpholane, but none of them satisfies the specific requirements for a good NMR reference completely. A good NMR reference compound should have one sharp signal with a high intensity, a shielding constant independent of concentration, pH, and temperature, absence of nuclear spin coupling with other nuclei and a very high shielding constant so that all signals are at positive chemical shifts.

The use of CS_2 was proposed for the first time by Retcofsky and Friedel.[3] CS_2 has two chemically equivalent ^{33}S nuclei, so it gives quite an intense signal when used as neat liquid. Its shielding constant does not depend on the experimental conditions, it is chemically inert and the sulphur is not spin coupled. In addition, ^{33}S is highly shielded, and its NMR signal lies towards the right end of the resonance frequency range, so that the chemical shifts are generally positive. However, the electronic environment of sulphur is characterized by a low symmetry, and the NMR signal is quite broad (LW = 160–360 Hz), preventing accurate measurements of chemical shifts.

Lutz et al.[4] proposed the use of the ^{33}S resonance of Cs_2SO_4 4M in D_2O, since they found that the line width of SO_4^{2-} anion is small compared to that of CS_2 and that the solubility of Cs_2SO_4 is high enough to obtain spectra with good S/N in a reasonable time. Successively, Cs_2SO_4, Na_2SO_4 and $(NH_4)_2SO_4$ in different concentrations have been often used as references. Belton et al.[7,26] showed for the first time that ^{33}S resonance frequency in SO_4^{2-} is affected by the nature of the counterion, temperature, concentration and pH, and they suggested the use of a solution of Cs_2SO_4 2M in D_2O at pH 7.5, because in these conditions ^{33}S gives rise to a very sharp signal (6.5 Hz). However, the variations in chemical shift among Cs_2SO_4, Na_2SO_4 and $(NH_4)_2SO_4$ (Table 2) are not very significant if compared to the error normally introduced in the determination of chemical shift. The only inconvenience of SO_4^{2-} is that the ^{33}S nucleus is quite deshielded, and chemical shifts are often negative in its scale.

In 2001, IUPAC[12] has recommended the use of a saturated solution of $(NH_4)_2SO_4$ in D_2O as a standard for ^{33}S.

In this work, all chemical shifts have been referred to SO_4^{2-}, if not otherwise specified. Chemical shifts reported in the literature and referred to CS_2 or

Table 2 ^{33}S NMR chemical shift, δ, and line widths, LW (in Hz), of the SO_4^{2-} anion in water as a function of counterion, concentration and pH

Counterion	Concentration, pH	δ	LW (Hz)
$Cs^{+7,26}$	2 M, pH = 7.5	0.0	6.5
NH_4^{+7}	2.0 M	−0.8	3.5
NH_4^{+26}	2.0 M, pH = 5.7	−1.0	3.3
Na^{+26}	1.0 M, pH = 6.4	−0.55	9.5
Mg^{2+26}	2.0 M, pH = 7.8	−1.45	18.0
Mg^{2+26}	0.1 M, pH = 6.8	−1.2	7.0
Al^{3+26}	0.4 M, pH = 2.9	−1.6	46.0

sulpholane have been converted using the following relationships,[10] obtained from the chemical shift values reported by Belton et al.[7] (referred to Cs_2SO_4 2M in water):

$$\delta(SO_4^{2-}) = \delta(CS_2) - 333$$

$$\delta(SO_4^{2-}) = \delta(\text{sulpholane}) + 36.7$$

Of course, these relationships do not take into account the variations in SO_4^{2-} chemical shift due to the effects of counterions, pH, concentration and temperature. It has not been possible to adopt the IUPAC chemical shift scale exactly, because that would require measuring the chemical shifts of all secondary references reported in the literature with respect to the standard suggested by IUPAC.

Another important problem to examine is the method used for referencing procedures. ^{33}S NMR chemical shifts are generally measured with respect to an external standard. In liquid phase spectroscopy, the standard is placed in a capillary tube concentric with the sample, and a single spectrum is recorded that includes signals from both the sample and the reference substance. This method is largely followed when high diameter sample tubes are employed (10 mm or higher). At present, the so-called replacement technique is preferred, since with the advent of high-field spectrometers, multinuclear 5 mm probes can have sufficient sensitivity and are more frequently used. Both methods are accepted by IUPAC,[12] but it must be considered that they are not always expected to give identical results. Some problems can arise with the substitution method, especially when locking is not used. In this case the magnet has to be shimmed separately when the spectrum of the sample and that of the reference are acquired, and this can change the applied magnetic field. Usually no bulk susceptibility corrections are applied, since they are smaller than other errors in measuring chemical shift. In ^{33}S solid-state NMR spectroscopy, the replacement technique is used.

## 3. ^{33}S NMR PARAMETERS

3.1 Chemical shift

3.1.1 Overview

The ^{33}S chemical shift range is on the order of 1,000 ppm, including organic and inorganic sulphur compounds. This large range implies that the ^{33}S screening constant is very sensitive to small variations in sulphur electronic environment, and hence it can be a valuable tool for determining molecular structure and studying the electronic properties of sulphur-containing molecules.

Sulphur can assume three formal oxidation states and forms as many as six bonds: S(II), in which it forms two covalent bonds and has two lone pairs (i.e. H_2S and $(CH_3)_2S$) or forms three covalent bonds and has one electron lone pair $((CH_3)_3S^+)$, and S(IV) and S(VI), in which it is hypervalent and can use its lone

pairs and empty d orbitals to form four- and six-coordinated structures, respectively.

The ^{33}S chemical shift is only partly related to the oxidation state. S(II) spans approximately over the entire chemical shift range. Inorganic sulphides are the most shielded species and lie at the upfield extreme of the chemical shift range (ammonium polysulphide at -584 ppm,[7] Li$_2$S at -680 ppm[27]). Proceeding towards downfield shifts, aliphatic sulphides and thiols, thiophene and its substituted derivatives, other organic compounds and thiometallate anions are found. The most deshielded compound is SO$_2$ (375 ppm[28]). It had previously been found that at the downfield extreme there was the cation **1**, whose chemical shift was reported at 417 ppm,[29] but this value has been recently revised.[30,31] Sulphoxides, sulphones, sulphonates, sulphimides, sulphoximides and, more generally, compounds containing S(IV) or S(VI) atoms lie in the central region of the spectral range, but a net separation of chemical shifts on the basis of sulphur functional group is not possible.

1
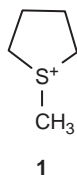
As for all nuclei, the ^{33}S nuclear screening constant σ can be approximated as the sum of two independent terms of opposite sign, the diamagnetic and the paramagnetic contribution:[32]

$$\sigma = \sigma_\mathrm{d} + \sigma_\mathrm{p} \tag{1}$$

The most significant contribution to the overall screening constant is due to the diamagnetic term, which arises from the electrons in the filled shells surrounding the nucleus. It depends on the electronic ground state of the molecule and has a shielding effect. The variations in chemical shift can be ascribed mainly to variations in the paramagnetic term. This has been demonstrated experimentally for ^{33}S in 3- and 4-substituted benzenesulpho-nates.[33]

The paramagnetic term, which generally has a deshielding effect, is associated with the orbital angular momentum of electrons and hence arises from non-spherical valence orbitals. It involves the mixing of the electronic ground and excited states of the molecule. According to the formalism of Jameson and Gutowsky,[34] the paramagnetic term for ^{33}S is:

$$\sigma_\mathrm{p} = -\frac{2e^2\hbar^2}{3m^2c^2}\frac{1}{\Delta E}\left[\frac{P_u}{\langle r^3\rangle_{3\mathrm{p}}} + \frac{D_u}{\langle r^3\rangle_{3\mathrm{d}}}\right] \tag{2}$$

where m and e denote the electron mass and charge, respectively; ΔE is an average excitation energy generally approximated as the energy of the HOMO–LUMO

transition; $\langle r^3 \rangle$ is the expected value of the cube of the mean radius of 3p and 3d orbitals; and P_u and D_u are the so-called unbalance of the 3p and 3d orbitals and are functions of the p and d orbital populations, respectively. In principle, for hypervalent sulphur, the contribution of sulphur d orbitals should be considered, although it is expected to be negligible because of the significantly lower density of d orbitals in the region close to the nucleus. In the case of 3- and 4-substituted benzenesulphonates[33] and 2-substituted ethanesulphonates,[35] it has been demonstrated that the contribution of sulphur d orbitals is minimally effective in determining the variations of σ_p. According to Equation (2), all structural factors that induce variations in the electron distribution around the nucleus and in the energies of molecular levels can determine variations of the ^{33}S paramagnetic shielding term. In many cases, the analysis of the paramagnetic term has provided interesting information about the electronic distribution around the sulphur nucleus and the formation of chemical bonds.

It can be helpful to compare the behaviour of ^{33}S chemical shifts with those of other nuclei whose properties have been fully investigated. Considering ^{29}Si and ^{31}P, also belonging to the third row of the periodic table, and ^{77}Se, their chemical shifts cover ranges of about 400, 700 and 3,000 ppm, respectively. An increase in the whole chemical shift range is evident moving along the third row and the group VI. This can be directly correlated to the relative sizes of $\langle r^{-3} \rangle_{np}$ for the different atoms.

There are many analogies in the structural influences on ^{33}S, ^{31}P and ^{77}Se NMR chemical shifts. Wasylishen et al.[36] have compared the relative ^{33}S and ^{77}Se chemical shift scales and found that the correspondence is noticeable. For example, the resonances of the hydrides H_2S and PH_3 lie at the extreme upfield end of the total spectral range. Substitution of a hydrogen atom with a methyl group provokes downfield shifts of 44.7 and 64.5 ppm, respectively. Further substitution of a second hydrogen atom with a methyl causes downfield shifts by 31 and 64.9 ppm, respectively.

It is also interesting that a parallel trend is observed for ^{33}S, ^{31}P and ^{77}Se chemical shifts when lone pairs are used to form hypervalent species. When one lone pair is used to coordinate one oxygen atom, ^{33}S, ^{31}P and ^{77}Se chemical shifts increase significantly, which means that the nuclei are more deshielded (as expected, since the electron density around the nucleus decreases). However, in coordinating another oxygen atom, the loss of the second lone pair produces a shielding effect.

	$(CH_3)_2Se$	$(CH_3)_2SeO$	$(CH_3O)_2SeO$	$(CH_3)_2SeO_2$
δ(ref. Me$_2$Se)[37a]	0	+812	+1,339	+1,076
	$(CH_3)_2S$	$(CH_3)_2SO$		$(CH_3)_2SO_2$
δ(ref. SO$_4^{2-}$)	−459	−20		−13
	$P(CH_3)_3$	$(CH_3)_3PO$	$P(OCH_3)_3$	$PO(OCH_3)_3$
δ(ref. H$_3$PO$_4$ 80%)[37b]	−61	36.2	140	−2.4

The ^{33}S chemical shift trend has been compared to the behaviour of more common nuclei, such as ^{13}C, ^{17}O and ^{15}N, and in many cases it has been demonstrated that the ^{33}S chemical shift is a better probe of structural properties. Many correlations among the chemical shifts of these nuclei in similar electronic environments have been found (e.g. between the ^{33}S chemical shifts in sulphonates and the ^{13}C chemical shift carboxylic acids[38] or between the ^{33}S chemical shift in sulphones and ^{17}O in ethers or ^{13}C in alkanes[39]). This suggests that ^{33}S is affected by the same kind of electronic and steric influences as ^{13}C, ^{15}N and ^{17}O.

A list of ^{33}S chemical shifts and line width values reported in the literature for relevant organic and inorganic compounds can be found in Tables A.2–A.10 in the appendix. With respect to the reviews previously published[8–11], here the tables have been reformulated to refer all chemical shifts to SO_4^{2-} ion in aqueous solution, even when the literature data were referred to different standards. The original standards indicated in the literature have been reported. In many cases, data in the literature show sizeable differences, often due to the different experimental conditions used in the acquisition of the spectra and also to large errors in the case of broad signals, especially at low magnetic fields. This is the reason why the most relevant experimental conditions (solvent, temperature, pH, ^{33}S resonance frequency) have also been reported in Tables A.2–A.10. It is evident that some standardization of recording techniques is desirable.

^{33}S chemical shift is particularly sensitive to small variations in the electronic distribution in the nuclear environment induced by:

- effect of substituents on the molecules,
- variation in molecular conformation,
- ring strain,
- solvent,
- temperature
- and sometimes also concentration effects, especially when dealing with ionic species.

In the following section, a brief summary of the most relevant properties of the ^{33}S chemical shift (and in some cases line widths) in organic and inorganic compounds is given.

3.1.2 Organic compounds

As previously pointed out, only sulphur functional groups with a highly symmetric electronic environment have been extensively characterized: sulphones, sulphonates and to a lesser extent thiols, sulphides, sulphoxides and sulphur–nitrogen compounds such as sulphimides, sulphoximides and sulphonamides.

3.1.2.1 Recent results. Riddel et al.[40] have reported the spectral parameters of some significant sulphur compounds, including some previously unobserved functional groups: phenyl isothiocyanate (PhNCS), methyl thiocyanate (MeSCN), thiophenol (PhSH), methyl phenyl sulphide (PhSMe), 2-methylthiazole,

3-methylisothiazole, potassium persulphate ($K_2S_2O_8$), phenylsulphinic acid ($PhSO_2H$) and its sodium salt, a sulphonyl hydrazide, and some sulphonyl fluorides and chlorides. The spectra have been acquired at 11.7 T, thus demonstrating that at high magnetic field strength, it is possible to obtain ^{33}S NMR signal from species previously considered not detectable. As pointed out by the authors, in many cases the errors in reported ^{33}S chemical shifts are significant because the detected signals are very broad (23,000 Hz for PhNCS, 19,800 Hz for PhSMe, 500 Hz for $HOCH_2SO_2Na$).

^{33}S NMR spectra of thiocarbonyl, thiophosphoryl compounds, and of some sulphonium salts have also been published. Machiguchi et al. have reported the ^{33}S NMR spectrum of tropothione[41] **2**, a thiocarbonyl compound, and of its corresponding S-oxide, **3** and sulphenic acid, **4**.[42]


2   **3**   **4**
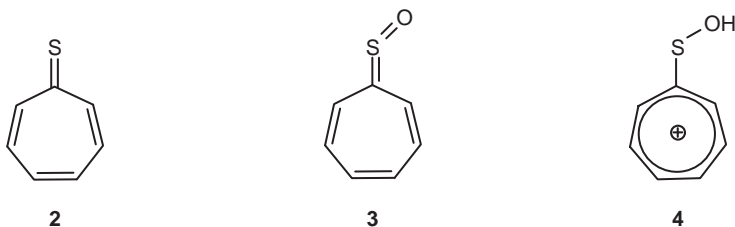
The resonance signal of **2** is at -287 ppm (in $CDCl_3$ at 233 K), downfield relative to sulphides. The same behaviour has been observed for ^{17}O in ketones[43] and ethers.[44] For **3** and **4**, the ^{33}S chemical shifts are -6 and -85 ppm, respectively.

The ^{33}S chemical shifts of the following thiophosphoryl compounds have been determined:[45] $(CH_3)_3PS$ (-536 ppm in $CDCl_3$ at 295 K), Cl_3PS (-105 ppm, 90% solution containing 10% of deuterobenzene) and $(C_6H_5)_3PS$ (-408 ppm in $CDCl_3$ at 293 K). As outlined by the authors of the paper, these chemical shifts are to be considered highly tentative, because the signals are very broad (line widths are larger than 3,000 Hz), and the spectra are affected by severe rolling baselines.

Quin et al.[30,31] have determined the ^{33}S chemical shifts and line widths of trimethylsulphonium iodide **5** (-285 ppm, 5,400 Hz, in D_2O at 318 K) and S-methyltetrahydrothiophenium iodide **1** (-238 ppm, 5,600 Hz, in D_2O at 318 K). The chemical shift previously reported for **1** was 417 ppm.[29]

5
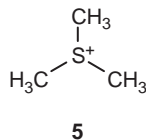
Moreover, a series of Cl and Br derivatives of sulpholane **6** have been characterized.[46]

$$X, X', Y, Y' = H, Cl, Br$$

6
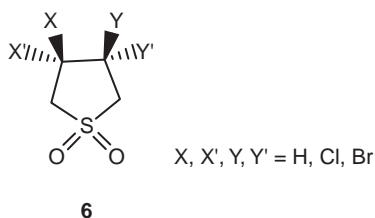
Their chemical shifts and line widths are in the ranges −1.2 to 38.4 ppm and 3.5 to 210 Hz, respectively, in agreement with the data already reported for other substituted sulpholanes.[29]

3.1.2.2 Organic thiols and sulphides (−SH, −S−). Spectral parameters of few thiols and sulphides have been reported in the literature (Table A.2).[3,7,29,36,40,47] Dicoordinated sulphur has a low electronic symmetry. The observed line widths vary from 2,000 to 20,000 Hz, and the signals become undetectable as the molecular size increases. [33]S resonance lies upfield with respect to the SO_4^{2-} signal, and chemical shifts are in the range −460 to −300 ppm, with the exception of thiirane $(CH_2)_2S$ (−573 ppm). More upfield, only inorganic sulphides can be found. This strong shielding effect can be attributed to the sulphur lone pairs. In thiophene and its derivatives,[3] [33]S is much more deshielded than in tetramethylenesulphide and shows narrower line widths.

3.1.2.3 Sulphoxides (−SO₂−). Also in this case the [33]S spectra of a very limited number of compounds have been reported (Table A.3).[3,7,29,36,40,47] The [33]S nucleus is significantly deshielded with respect to sulphides, with its chemical shift ranging from 32 to −213 ppm, and signals are significantly broader than in the corresponding sulphides. Evidently, when one sulphur lone pair is used to bond an oxygen atom, there is a decrease in the electron density around the sulphur nucleus, due also to the electronegativity of the oxygen atom, and a loss in symmetry of the electron distribution.

3.1.2.4 Sulphones (−SO₃⁻). Aliphatic, vinyl and aryl sulphones have been extensively characterized (Tables A.4.1–A.4.3).[6,9,29,40,46–54] Reported chemical shifts cover a range of about 80 ppm (−40 to +40 ppm, with the only known exception of thiirane 1,1-dioxide, $(CH_2)_2SO_2$, whose chemical shift is −88 ppm[47]). Signals are relatively sharp, with line widths varying from a few hertz to about 1,500 Hz.

Many attempts to correlate chemical shift and molecular structure have been made, and various empirical correlations have been found. Three important effects are evident:

(1)   branching of the attached hydrocarbons leads to a deshielding of the sulphur atom;

(2)   unsaturated substituents bonded to the sulphur atom have a shielding effect on the ^{33}S nucleus;

(3) ^{33}S chemical shift is sensitive to the electronic effect of substituents at different sites of the molecule.

Taking dimethyl sulphone as reference compound, symmetric replacement of a hydrogen of the C_α atom (β-hydrogen) with a methyl group[48] (–S–C–**H**→S–C–**CH₃**) leads to a deshielding of approximately 15 ppm ('β-methyl effect,' 7–8 ppm/CH₃). The β-methyl effect is nearly additive in the range of the experimental error. Methyl substitution of a hydrogen atom in the γ position to sulphur (S–C–C–**H**→S–C–C–**CH₃**) produces a shielding effect (γ effect) of approximately –3 ppm. Replacement of a hydrogen atom with a methyl group beyond the C_γ carbon exerts a minimal influence on the ^{33}S chemical shift. The trend of β, γ and δ effects parallels those observed for ^{13}C in alkanes,[55] for the carbonyl carbon in dialkyl ketones,[55] for ^{17}O in ethers and alcohols[44] and for ^{15}N in amines.[56]

Aryl and vinyl groups exert a shielding effect on the ^{33}S nucleus (about –5 ppm/Ph and –7.5 ppm/CH₂=CH).[50] It is important to observe that, as found for most nuclei, substituent effects on ^{33}S are additive, within the limits of experimental error. If the shielding effect of a phenyl group is about –5 ppm and the shielding effect of a vinyl group is –7 to –8.5 ppm, it is significant that the ^{33}S chemical shift of vinyl phenyl sulphone is –25 ppm. A resulting shielding effect of –12 ppm is observed with respect to dimethyl sulphone.

Moreover, the substituent effect exerted by polar groups at the α, β and γ positions to sulphur must be considered. Substituents can have a shielding or deshielding effect, depending on their electronic properties. For example, in dimethyl sulphone, when a methyl group is substituted by a fluorine or chlorine atom, a downfield shift of about 15–16 ppm is observed.[52,53] The effect of a bromine atom is smaller whilst iodide induces an upfield shift. A methoxy group also induces a downfield shift of about 16 ppm. At a first approximation, the ^{33}S chemical shift in substituted sulphones can be related to the electronegativity of the substituent: atoms or groups more electronegative than sulphur exert a deshielding effect, and a downfield shift of the ^{33}S resonance is then observed.

Also the replacement of a hydrogen atom of the C_a with an X substituent (–S–C–**H**→S–C–**X**) can have a shielding or deshielding effect.

Hoyle et al.[39] have found good linear correlations between $\delta(^{33}\mathrm{S})$ in substituted alkyl sulphones and the Taft polar substituent constant, σ^*:

$$\delta(^{33}\mathrm{S}) = -155\sigma^* - 133 \quad \text{corr. coeff.} = 0.967 \quad \text{symmetric dialkyl sulphones}$$

$$\delta(^{33}\mathrm{S}) = 8.78\sigma^* - 18.0 \quad \text{corr. coeff.} = 0.991 \quad \text{monosubstituted dimethyl sulphones}$$

These correlations, which are only indicative because they were obtained for a limited number of compounds, seem to suggest that the origin of the substituent effect on C_α can be of inductive origin, but no interpretation of these data has been reported.

The γ effect (S–C–C–**H**→S–C–C–**X**) can be significant. Rozhenko et al.[46] have found that in sulpholane derivatives, **6,** the successive substitution of hydrogen

atoms in 3- and 4-positions with chlorine and bromine atoms has a shielding effect. The substituent effect is additive, and the variation of ^{33}S nuclear shielding with increasing numbers of Cl and Br atoms ($\Delta\delta = 39.6$) is determined by through-space electrostatic influence of halogen atoms.

Also in vinyl sulphones, the substitution of a β-hydrogen of the vinyl group causes some variations in the ^{33}S chemical shift.[50] A fluorine atom causes an upfield shift of about -4 ppm, while chlorine and bromine atoms induce a decrease in chemical shift of 1–2 ppm.

The effect of the substituents on the aromatic ring in aryl sulphones is also significant. For 4-substituted methyl phenyl sulphones, the variations of chemical shift induced by substituents range from -12 ppm (–OCH$_3$) to $+4$ ppm (p-NO$_2$-), with a total variation of 16 ppm.[9] Clearly, chemical shift depends on the electronic properties of substituents: electron-withdrawing groups such as –NO$_2$ induce a downfield shift, whilst electron-releasing groups induce an upfield shift. This is a so-called normal effect, opposite to the one found for benzenesulphonates. The origin of this effect in sulphones has not been studied.

3.1.2.5   Sulphonic acids (–SO$_3$H) and sulphonates (–SO$_3^-$).   Sulphonic acids and sulphonates are the most studied organosulphur compounds, due to the quite narrow line widths of their ^{33}S resonances (Table A.5).[22,33,35,38,57–63]

They are very strong acids, completely ionized at 1–3 M concentrations in water; therefore, in this range of concentrations and at pH values from 1 to 14, they exist as sulphonates, and no significant variations of chemical shift are observed. At higher concentrations and/or in different solvents, the spectral parameters can change significantly due to differences in degrees of ionization, ion pairing and proton transfer rates. Most of the data reported in the literature refer to sulphonates in aqueous solution. Signals are quite narrow (less than 100 Hz). Chemical shifts lie in the same spectral region of sulphones but cover a more limited range ($+5$ to -20 ppm).

There exists a linear correlation between the ^{33}S chemical shifts in sodium sulphonates, RSO$_3$Na, and ^{13}C chemical shifts of the carboxylic carbon in the corresponding sodium carboxylates, RCOONa:[38]

$$\delta(^{33}\text{S}) = -390.37 + 2.1296\,\delta(^{13}\text{C}) \qquad \text{corr. coeff.} = 0.990$$

This implies that substituent effects on ^{13}C shielding in carboxylic acids and ^{33}S shielding in sulphonates are closely related, but –SO$_3^-$ resonances appear to be almost twice as sensitive to substituent effects as –COO$^-$.

Some general trends have been observed:[38] (i) as for sulphones, resonances of aryl and vinyl sulphonates occur at appreciably higher fields than those of alkyl sulphonates; (ii) in alkyl, aryl and vinyl sulphonates, the ^{33}S chemical shift strongly depends on the electronic properties of substituents on the molecule. In the case of 2-substituted ethanesulphonates[22] and 3- and 4-substituted benzenesulphonates,[33,57,59,61,63] the occurrence of a 'reverse' substituent effect has been observed: electron-withdrawing substituents cause un upfield shift of the ^{33}S resonance, whereas electron-releasing groups produce a downfield shift.

3.1.2.6   Sulphur–nitrogen compounds.   [33]S spectra of some sulphimides, sulphox-imides and sulphonamides[29,64,65] have been reported, but the available data are not sufficient for a detailed discussion of the correlation between chemical shifts and molecular structure (Table A.6).

Sulphimides **7** can be considered to be derived from sulphoxides by substitution of the oxygen atom with an $=NR$ group. Sulphoximides **8** and sulphonamides **9** can be considered to be derived from sulphones by substitution of an oxygen atom and an R group, respectively, with an NR'(R'') group.
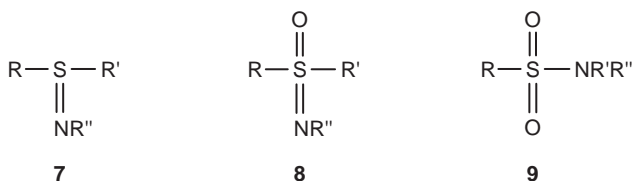
[33]S in sulphimides resonates approximately 20 ppm downfield with respect to the corresponding sulphoximides ([33]S nucleus is less shielded).[29] On going from $-S(=NR)-$ to $-S(=NR)O-$, the chemical shift trend is similar to that observed for $CH_3S(O)CH_3$ and $CH_3SO_2CH_3$ (and more generally for analogous phosphorous and selenium compounds). In other words, the shielding of the central atom increases when it loses one lone pair.

Sulphoximides resonate at higher field than sulphones. This shielding effect can be partly ascribed to the lower polarity of the S–N bond with respect to the S–O bond, but much evidence also suggests a significant role for the nitrogen lone pair.
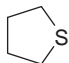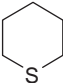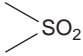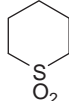
This is more evident if the chemical shift in sulphonamides is considered. Replacing the methyl group of phenyl methyl sulphone (-17 ppm) with $-NH_2$ to obtain phenyl sulphonamide (-25 ppm) leads to the shielding of the [33]S nucleus. Evidently, the deshielding effect of the nitrogen atom due to its greater electronegativity is compensated for and overwhelmed by the presence of the nitrogen lone pair, which can contribute to the double bond character of the S–N bond.[64]
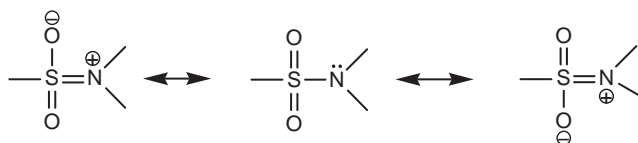
In sulphonamides, the [33]S chemical shift is sensitive to the electronic properties of both the α-group and of the substituent on the nitrogen atom.[64] The replacement of both hydrogen atoms of the $-NH_2$ moiety with methyl groups induces a downfield shift of 23 ppm, and the substitution of one hydrogen bond with another NH_2 group causes a downfield shift of 18 ppm.

Line widths of sulphoximides are 10–20 times greater than those of the corresponding sulphones. Sulphimides show line widths that are twice those of sulphoximides.

3.1.2.7 Cyclic sulphides, sulphoxides and sulphones. In the following scheme, the [33]S chemical shifts of simple cyclic sulphides, sulphoxides and sulphones are reported.[47]

>S	▷S	☐S	⬠S	⬡S
−428	−573	−302	−336	−363

>SO	▷SO	☐SO	⬠SO
−8	−213	32	27

>SO₂	▷SO₂	☐SO₂	⬠SO₂	⬡S O₂
−13	−88	−2	35	−12

The influence of ring strain tension is evident. By comparing dimethyl derivatives and the corresponding thiiranes, in all cases a marked upfield shift is observed upon cyclization (−145 ppm for thiirane, −205 ppm for thiirane 1-oxide and −75 ppm for thiirane 1,1-dioxide). Three-membered ring compounds are markedly more shielded than larger rings. On going from three- to four-membered rings, a significant downfield shift is observed, but from four- to five-membered rings, a further downfield shift is found only in the case of sulphonyl compounds. In six-membered rings, [33]S is more shielded than in five-membered rings by approximately 40–50 ppm, and it resonates in the same range as open-chain compounds. This is probably due to the absence of ring–strain interactions and to the well-known geometric stability of six-membered rings. Similar behaviours have been observed for the [17]O chemical shift in cyclic ethers.[44,66]

For three-membered ring compounds, Barbarella et al.[47] found that there is proportionality between the [33]S chemical shift and the atomic charge of the sulphur atom.

3.1.3 Inorganic compounds

The study of inorganic sulphur compounds, particularly sulphides and sulphates, has received a substantial boost during the last decade with the development of very high-field spectrometers and solid-state NMR methodologies (Tables A.8–A.10).

The ^{33}S chemical shift of Na_2S has been determined by Retcofsky and Friedel[3] and by Belton et al.,[67] but very large line widths have not encouraged further investigations on sulphides in solution. In contrast, inorganic sulphates in water solution have received much more attention, since they give rise to very narrow ^{33}S signals and are used as standard references for chemical shift. In 1986, Eckert and Yesinowsky[27] published the first comprehensive study on metal sulphides and sulphates in the solid state, using a spectrometer at 11.7 T working in static conditions. All the compounds examined are characterized by very broad ^{33}S resonances. More recently, with the development of high-field spectrometers dedicated to solid-state analysis, spectra of inorganic sulphides and sulphates have become more accessible.[23,68,69]

^{33}S in sulphides is expected to be highly shielded, but resonances are spread over a wide range: from -680 ppm (Li_2S, the upfield limit of the total ^{33}S chemical shift range) to -42 ppm (BaS). Line widths in static samples are between 1,380 Hz (Li_2S) and 100 Hz (CaS and SrS). ^{33}S MAS spectra are characterized by much narrower resonances.[23,68]

Both in solution[26] and solid state,[68,69] ^{33}S chemical shifts in simple sulphates do not show very large variations with the counterion (-7 to $+4$ ppm), with the sole exception of $TlSO_4$ (-13 ppm). Much more significant are the variations of line widths, which are evidently produced by variations of the electric field gradient at the ^{33}S nucleus.

Besides metal sulphates and sulphides, thiomolybdates and thiotungstates have also been investigated by ^{33}S NMR spectroscopy. Kroneck et al.[70] have reported the first ^{33}S NMR spectrum of diammonium tetrathiomolybdate $(NH_4)_2MoS_4$, in aqueous solution. The chemical shift is 343 ppm, and the line width is 40 Hz. A larger series of thiomolibdates and thiotungstates, $[MS_nO_{4-n}]^{2-}$ (with M = Mo, W, n = 1–4), have been characterized in aqueous solution,[71] in CH_3CN[72], and in the solid state.[73] In solution, ^{33}S chemical shifts of the Mo complexes are in the range -25 to 345 ppm, about 180 ppm downfield from the analogous tungsten complexes. The ^{33}S MAS spectrum of $(NH_4)_2MoS_4$ shows three different resonances (209.3, 187.5 and 162.9 ppm) corresponding to three crystallographically independent S sites. The chemical shift varies with the number of sulphur atoms in the complex; namely, the larger the sulphur complex, the more positive the chemical shift.

Other sparse inorganic compounds have also been characterized: CS_2,[3,7,36] SO_2,[19,28,36] OCS[18,36] and SF_6, both in liquid and in gas phase,[24,25,36] H_2SO_4,[3,74] H_2S,[36] $S_2O_3^{2-}$ (only one signal has been observed, which has been assigned to the internal sulphur atom)[5,36,74,80] and some bi- and trinuclear complexes,[72] [(CN)M'S$_2$MS$_2$]$^{2-}$ (M' = Cu and Ag, M = Mo and W) and [(CN)CuS$_2$MS$_2$Cu(CN)]$^{2-}$ (M = Mo and W).

3.2 Spin–spin coupling constants

As for most of the quadrupolar nuclei, ^{33}S nuclear spin–spin coupling constants have seldom been observed because the signals are very broad and the fine structure of the spectrum is not observed. The evidence of the existence of a ^2J

(^{33}S,^{1}H) spin–spin coupling in the ^{33}S spectra of dimethyl sulphone, sulpholane **10**, and butadiene sulphone **11** was reported for the first time by Hinton.[75] Afterward, the values of $^2J(^{33}$S,^{1}H) in dimethyl sulphone[49] and sulpholane[76] **10** have been estimated by comparing the line width value of the ^{33}S resonance lines in ^{1}H-coupled spectra and in spectra obtained under broadband proton decoupling.

Table 3 collects the values of the experimental coupling constants involving the ^{33}S nucleus so far reported in the literature.

Table 3 Values of experimental spin–spin coupling constants involving ^{33}S, reported in the literature

Coupling	Compound	Experimental conditions	J (Hz)	Refs.
$^2J(^{33}$S,^{1}H)	(CH$_3$)$_2$SO$_2$	CDCl$_3$	3	49
$^2J(^{33}$S,^{1}H)	Sulpholane **10**	80% in benzene	4.5	76
$^2J(^{33}$S,^{1}H)	Butadiene sulphone **11**	2 M in (CH$_3$)$_2$CO	6	7
$^1J(^{33}$S,^{19}F)	SF$_6$	Gas, 3 atm, 223 K	245	25
		Gas, 3 atm 297 K	242	25
		Gas, 20 atm	250.1(4)	24
		Supercritical fluid	251.4(2)	24
		Neat liquid	251.8, 251.6	24,36
		In CS$_2$	253.1(2)	24
		In n-C$_5$H$_{12}$, n-C$_6$H$_{14}$, C$_6$F$_6$, [(CH$_3$)$_2$Si]$_2$O, CH$_3$CN	253.4(2)	24
		In (CH$_3$)$_2$CO	253.8(2)	24
		In CCl$_4$ and c-C$_6$H$_{12}$	254.0(2)	24
		(CH$_3$)$_2$SO and C$_6$H$_6$	255.2(2)	24
		CH$_3$I	255.7(2)	25
		Liquid crystal, ZLI 2806	253.3	25
		HAB	253.9	25
		Liquid crystal, ZLI 3125	255.5	25
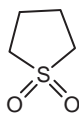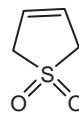
10   **11**

Coupling constants have been measured with good precision in only two cases: $^2J(^{33}$S,^{1}H) in butadiene sulphone[7] and $^1J(^{33}$S,^{19}F) in SF$_6$.[24,25,36]

In butadiene sulphone **11**, the ^{33}S spectrum shows a partially resolved triplet that collapses to a singlet under proton decoupling.

For SF$_6$, the ^{33}S signal has the symmetric pattern typical of an AX$_6$ spin system, due to the coupling of the ^{33}S nucleus with six equivalent fluorine atoms.[36] In the liquid, each component has a line width of 1 Hz ca., so the seven components are very well resolved, and $^1J(^{33}S,^{19}F)$ has been measured with an elevated precision. This peculiarity makes SF$_6$ an ideal molecule for studies in the gas phase and in high viscosity media because the broadening of the signals does not produce any loss of the fine structure. $^1J(^{33}S,^{19}F)$ has been determined in pure liquid, different solvents, gas phase, liquid crystals and supercritical fluids (Table 3), and its dependence on intermolecular interactions has been examined. According to Jackowski et al.,[24] $^1J(^{33}S,^{19}F)$ seems to increase slightly upon going from the gas phase at 20 atm to supercritical fluid and pure liquid, as well as with the density of the gas sample (only high-density samples have been examined, but the precision of the ^{33}S NMR measurements for the sample was not satisfactory enough to extrapolate values at infinite dilution). As evident from Table 3, variations are very small (less than 1 Hz), and it is difficult to assess whether they are within the limits of experimental error. More significant variations ($\Delta J = 4.9$ Hz) are observed in different solvents. According to Jackowski et al., this is proof of the dependence of $^1J(^{33}S,^{19}F)$ on intermolecular interactions, considering that experimental data would suggest that different media permittivities have no influence.

Different conclusions have been reached by Tervonen et al.,[25] who have measured $^1J(^{33}S,^{19}F)$ in liquid crystal solutions at variable temperatures, from the ^{33}S satellites of 1D ^{19}F spectra, and in gaseous samples at 3 atm, by 2D HMQC experiments at two different temperatures (in the ^{19}F spectrum, the dominant peak of the most abundant ^{32}SF$_6$ is quite broad and completely masks the quartet structure of ^{33}S satellite of the ^{33}SF$_6$ isotopomer). Significantly, $^1J(^{33}S,^{19}F)$ increases by ca. 10 Hz on going from the gas phase to termotropic liquid crystal solutions, but the values measured in the gas phase at different temperatures can be considered equal within the limits of experimental error. Analogously, because of the broad lines in the spectra, no significant changes can be detected in different liquid crystals and isotropic liquids, thus suggesting, according to the authors, that $^1J(^{33}S,^{19}F)$ seems to be fairly insensitive to solvent properties.

3.3 Line widths and relaxation times

^{33}S has a moderate quadrupolar moment, eQ, arising from its non-spherical charge distribution. The interaction between the nuclear quadrupole moment and the electric field gradient, which is generated at the nucleus itself by the surrounding electronic distribution, is modulated by molecular reorientational motion and provides the only effective relaxation mechanism in liquid. The resulting relaxation times are on the order of milliseconds.

In the motional narrowing limit ($\omega_0 \tau_c \ll 1$, where ω_0 is the Larmor angular precession rate), the longitudinal and transverse relaxation times, T_1 and T_2, in

solution can be considered numerically equal, and the following equations hold.[77]

$$LW = \frac{1}{\pi T_1} = \frac{1}{\pi T_2} = 1.257\chi^2\left(1 + \frac{\eta^2}{3}\right)\tau_q \tag{3}$$

where LW is the half height signal line width,

$$\chi = \frac{e^2 Q q_{zz}}{h} \tag{4}$$

χ the [33]S nuclear quadrupole coupling constant (expressed in frequency units), and η the asymmetry parameter of the electric field gradient tensor ($0 \leq \eta \leq 1$):

$$\eta = \frac{q_{xx} - q_{yy}}{q_{zz}} \qquad |q_{zz}| \geq |q_{yy}| \geq |q_{xx}| \tag{5}$$

q_{xx}, q_{yy} and q_{zz} are the components of the electric field gradient tensor at the sulphur nucleus. τ_q is the effective quadrupolar correlation time characterizing the motional modulation of the interaction between the [33]S quadrupole moment and the electric field gradient. For rigid molecules with isotropic reorientational motion, τ_q is often approximated as τ_c, the rotational correlation time of the molecule (i.e. the average time for a molecular axis to change its direction by one radian).

As a consequence of the fast quadrupolar relaxation, [33]S NMR signals are quite narrow only when the sulphur nucleus is in small molecules and is characterized by a highly symmetric electronic environment, that is to say, when χ is quite small and η is near to zero. This is the case for inorganic sulphates, sulphonates and sulphones. When these features are not verified, signals are broad and often undetectable, but in some cases it is possible to modify the experimental conditions (temperature, solvent viscosity, concentration) in order to obtain a narrowing of the signals.

In principle, T_1 and T_2 can be measured experimentally by the inversion recovery sequence ($180° - \tau - 90°$) and the Hahn spin-echo sequence, respectively. In practice, these experiments can be easily performed only when the [33]S signal is very narrow. If the signal is broad, the difficulties in obtaining [33]S spectra with a good S/N make the direct measurements very time-consuming and less precise. The problem can be easily circumvented because T_2 (and T_1) can be obtained with good precision directly from line width.

As a consequence, only in a few cases the T_1 values reported in the literature have been measured directly (Table 4). In most cases, they have been obtained from line width values.

The dependence of T_1 on temperature, concentration and viscosity has been studied in the pioneering works by Haid et al.[79] and Hinton et al.[75,78,80]

Haint et al.[79] have measured [33]S T_1 of Cs_2SO_4 in H_2O as a function of concentration. Hinton and Shungu[78] have also considered the dependence on temperature for $(NH_4)_2SO_4$ (Table 4). Independently of the counterion

Table 4   [33]S T_1 relaxation times in some compounds, measured by inversion-recovery sequence (180°−τ−90°)

	Experimental conditions	T_1 (ms)	Refs.
$(NH_4)_2SO_4$	0.9 M in D_2O, 297 K	138.5	78
	0.9 M in D_2O, 311 K	161.8	78
	0.9 M in D_2O, 327 K	204.4	78
	0.9 M in D_2O, 339.5 K	239.3	78
	1 M in D_2O, 311 K	157.7	78
	4 M in D_2O, 297 K	98.9	78
	4 M in D_2O, 311 K	125.2	78
	4 M in D_2O, 327 K	149.5	78
	4 M in D_2O, 339.5 K	165.2	78
	2 M in H_2O, pH = 5.7	95[a]	7
Cs_2SO_4	1.0 M in H_2O	91	79
	2.0 M in H_2O	76	79
	3.0 M in H_2O	65	79
	4.0 M in H_2O	36	79
	2 M in H_2O, pH = 7.5	78[b]	7
CS_2	Neat liquid	1.0	7
$CH_3C_6H_4SO_3^-$	2 M in H_2O	5.0	7
Sulpholane **10**	In DMSO, 307 K	28.5	75
	In DMSO, 321 K	32.9	75
	In DMSO, 349 K	64.4	75
	In $CDCl_3$, 303 K	40.4	75
	In $CDCl_3$, 323 K	66.9	75
Butadiene sulphone **11**	In DMSO, 307 K	40.3	75
	In DMSO, 321 K	44.5	75
	In DMSO, 349 K	71.2	75
	In $CDCl_3$, 303 K	39.4	75
	In $CDCl_3$, 323 K	52.7	75
Dimethyl sulphone	In DMSO, 307 K	16.2	75
	In DMSO, 321 K	24.4	75
	In DMSO, 349 K	45.1	75
	In $CDCl_3$, 303 K	25.9	75
	In $CDCl_3$, 323 K	33.5	75
$S_2O_3^{2-}$	1.0 M in D_2O, 298 K	10.4	80
	2.0 M in D_2O, 298 K	8.4	80
	3.0 M in D_2O, 298 K	7.2	80
	3.0 M in D_2O, 316 K	11.2	80
	3.0 M in D_2O, 332 K	17.5	80

[a]T_2 = 90 ms.
[b]T_2 = 65 ms.

considered, a strong increase in T_1 is observed with decreasing concentration and increasing temperature, as expected. T_1 for ^{33}S in Cs_2SO_4 extrapolated to infinite dilution is 111 ± 20 ms.

Temperature-dependent measurements of T_1 have also been performed for the ^{33}S in the thiosulphur position of the $S_2O_3^{2-}$ anion (as a function of concentration and temperature),[80] as well as for sulpholane **10**, butadiene sulphone **11** and dimethyl sulphone (in DMSO-d$_6$ and CDCl$_3$).[75]

For the $S_2O_3^{2-}$ dianion, T_1 is significantly shorter than for SO_4^{2-} because of the lower electron symmetry around the sulphur nucleus.

For sulpholane, butadiene sulphone and dimethyl sulphone,[75] the linear dependence of $1/T_1$ on the factor η/T has been verified in both solvents. However, the correlation is different for the three compounds, suggesting that different molecular association processes take place for the three compounds in different solvents.

3.4 ^{33}S nuclear quadrupole coupling constants

While ^{33}S relaxation behaviour can provide interesting information about interactions in solution, nuclear quadrupole coupling constants are a very sensitive probe in the study of the electronic distribution around the sulphur nucleus.

Expressing q_{zz} in Equation (4) as a function of valence orbital populations, the dependence of ^{33}S χ on the electronic distribution around the nucleus is given by the following relationship:[81]

$$\chi = (1 - \gamma_\infty) \frac{e^2 Q}{h} \left[\frac{4}{5} \langle r^{-3} \rangle_{3p} \, P'_u + \frac{4}{7} \langle r^{-3} \rangle_{3d} \, D'_u \right] \qquad (6)$$

where e is the electron charge, eQ the ^{33}S quadrupole moment, $\langle r^{-3} \rangle$ the expected values of the inverse cube of the mean radius of the 3p and 3d orbitals, P'_u and D'_u are functions of the p and d orbital populations, respectively and γ_∞ the Sternheimer antishielding factor.[82] Generally, it is assumed that closed shell electrons, having a spherical symmetry, do not contribute to the electric field gradient, which should arise predominantly from valence electrons. However, since inner shell electrons are very close to the nucleus, small distortions from spherical symmetry induced by changes in the electron distribution of valence electrons can modify the resultant electric field gradient acting on the nucleus. The electric field gradient must be corrected with the introduction of γ_∞:

$$q_{zz} = q_{zz}^0 [1 - \gamma_\infty(r)] \qquad (7)$$

The distortion of closed shell electrons can be very significant in the case of charged species. The Sternheimer antishielding factor has been determined for sp^{3}d^2 hybridized sulphur by evaluation of the ion–water contribution to the ^{33}S relaxation rate in aqueous SO_4^{2-}.[83] The value found ($\gamma_\infty = -43.9$) is in good agreement with the value reported for S^{2-} ($\gamma_\infty = -52.2$) in the crystalline state.[84]

From relaxation times or line widths in liquids (Equation (3)), it is possible to determine the term $\chi^2(1+\eta^2/3)$ provided that correlation time values are known. The absolute values of χ can be obtained if the asymmetry parameter η is known, or they can be deduced using symmetry considerations regarding the electronic distribution around the nucleus.

The determination of correlation times requires particular attention and is not a problem that can be easily resolved. It is necessary to consider not only the overall molecular tumbling, but also internal rotation motions, which can modulate the interaction between the nuclear quadrupole moment and the electric field gradient. In any case, it must be considered that χ depends on the square root of τ_q and, even if in most cases it is not possible to measure or calculate precise values of τ_q, the uncertainties introduced in the values of χ may often be accepted.

^{33}S nuclear quadrupole coupling constants have been determined from line width values in some 3- and 4-substituted sodium benzenesulphonates[33,63] and in 2-substituted sodium ethanesulphonates.[35] Reasonably, in sulphonates $R-SO_3^-$, (i) η is near zero due to the tetrahedral symmetry of the electronic distribution at the ^{33}S nucleus, and (ii) q_{zz} is the component of the electric field gradient along the C–S axis. In the benzenesulphonate anion, the correlation time has been obtained from ^{13}C spin–lattice relaxation time and NOE measurements. In substituted benzenesulphonates, it has been obtained by the Debye–Stokes–Einstein relationship, corrected by an empirically determined microviscosity factor. In 2-substituted ethanesulphonates, the molecular correlation time of the sphere having a volume equal to the molecular volume has been considered.

The χ values of ^{33}S in liquid H_2S[85] (45.5 and 52.5 MHz for $\eta = 0$ and 1, respectively) have been measured from ^{33}S and deuterium T_1 together with χ values for deuterium.

More precise values of χ (and in principle η) can be obtained from solid-state spectra or spectra of oriented systems. In ordered media, NMR spectra of quadrupolar nuclei exhibit quadrupolar splittings that are not observed in isotropic media because of complete motional averaging.

Ruessink et al.[76] have measured the quadrupolar coupling tensor of ^{33}S in sulpholane from the analysis of ^{33}S and ^{2}H spectra of the liquid aligned by a strong electric field, in combination with T_1 measurements in non-aligned liquid and *ab initio* calculations. The dependence of ^{33}S and ^{2}H T_1 values on temperature suggests that the molecular reorientational motion of liquid sulpholane is essentially isotropic. Spectra of the oriented systems have allowed the determination of χ for the ^{33}S nucleus. It has been found that the major principal component of the ^{33}S quadrupole coupling tensor is +1.34 MHz, perpendicular to the five-membered molecule ring. The intermediate component is along the C_2 molecular axis of symmetry and is −1.05 MHz.

Lowenstein and Igner[86] have determined the quadrupole coupling tensor of ^{33}S in dimethyl sulphone, both in liquid crystalline solvents and in $CHCl_3$ solutions. In solution, an approximate value of τ_c has been measured from ^{2}H χ and T_1. ^{33}S χ values are as follows: 1.63 MHz for $\eta = 0$ and 1.41 MHz for $\eta = 1$. In liquid crystals, χ is about 1.8 MHz. These values seem to be in agreement within

the limits of experimental error. However, according to the authors, the possibility cannot be excluded that the difference could also be partly ascribed to solvent effects. For CS$_2$ in liquid crystals, ^{33}S χ is about 13.2 MHz.

^{33}S χ values in many sulphides and sulphates have been determined from solid-state spectra (see Chapter 4).

4. ^{33}S NMR PARAMETERS AND MOLECULAR STRUCTURE

4.1 Investigation of the electronic properties of sulphur-containing molecules

As already outlined in Chapter 3, the variation in ^{33}S chemical shift with molecular structure has been quite extensively studied in sulphinyl, –SO–, sulphonyl, –SO$_2$–, and sulphonic, $-SO_3^-$, moieties. It has been found that the ^{33}S chemical shift is much more sensitive to structural variation than the chemical shift of other nuclei, such as ^{13}C, ^{15}N or ^{17}O. For this reason, ^{33}S NMR is a powerful method for structural elucidation and in many cases a unique probe for assessing the properties of the electronic distribution around the sulphur atom.

In many cases, experimental data have been discussed in terms of variations of the paramagnetic contribution, σ_P, to the nuclear shielding constant (Equation (2)). Empirical correlations with parameters related to the electronic properties of other substituents in the molecule (electronegativities, Hammett substituent constants etc.) have been found. This kind of investigation has provided useful information about the electronic structure of the sulphur atom in different bonding situations and most of all about the electronic properties of the S–O bond, which is still a rather controversial matter.

One of the most significant problems to have been analysed is the apparently anomalous variation in the ^{33}S chemical shift on going from –S– to –SO– to –SO$_2$– functional groups. As the sulphur oxidation number and the oxygen number increase, a downfield shift of the ^{33}S resonance should be expected, due to the decrease in the electron density at the sulphur nucleus. This is verified when passing from –S– to –SO– functionalities, but on going from –SO– to –SO$_2$–, an upfield shift is observed, which suggests that the bonding of a second oxygen atom exerts a shielding effect.

	CH$_3$–S–CH$_3$	CH$_3$–SO–CH$_3$	CH$_3$–SO$_2$–CH$_3$
$\delta(^{33}$S)	−428	−8	−13

This behaviour has been studied by Barbarella et al.,[47,87] who have reported the chemical shifts for a series of cyclic and acyclic sulphides, sulphoxides and sulphones. They have found that there is a proportionality between the ^{33}S chemical shift and the sulphur atomic charge only for thiirane derivatives. According to the authors, this behaviour can be explained if one considers the complex dependence of the paramagnetic contribution to the shielding constant, σ_P, on the three terms ΔE, $\langle r^{-3} \rangle$ and bond order character (Equation (2),

according to the Karplus and Pople notation[88]). As the nuclear positive charge increases, the electron density around the sulphur atom decreases, leading to a contraction of the 3p orbitals and a consequent decrease in the nuclear shielding constant. A downfield shift of the ^{33}S resonance is observed. The effect of nuclear charge and electron density seems to be predominant when going from sulphides to sulphoxides, since ΔE has similar values in the two classes of compounds. From sulphoxides to sulphones, the increase in the S–O π-bond character also leads to an increase in the bond order term. However, the ΔE term is also expected to increase since the HOMO–LUMO transition does not involve sulphur lone pairs; evidently, the ΔE contribution counterbalances or overwhelms the effects of the other two terms. The shielding of the ^{33}S nucleus increases, and an upfield shift is observed.

It has been found that ^{33}S NMR parameters can depend strongly on the electronic properties of substituents on the molecule.

For example, for the sulphonyl group, the substituent effects on the ^{33}S and ^{17}O chemical shifts in the series CH_3SO_2Y (Y = I, Br, Cl, F, SeC_6H_4, SCH_3, OCH_3, $N(CH_3)_2$ and CH_3) and p-$CH_3C_6H_4SO_2Y$ (Y = Cl, Br, I, OH and CH_3) have been examined.[52,53] In both series, it has been found that the ^{33}S chemical shift decreases with decreasing Y electronegativity. An opposite trend has been observed for the ^{17}O nucleus. The behaviour of both the ^{33}S and ^{17}O chemical shifts can be rationalized in terms of a balance between the effect of substituent electronegativity and $n_O \rightarrow \sigma^*(S–Y)$ hyperconjugative interactions between an occupied molecular orbital containing an oxygen lone pair and the empty $\sigma^*(S–Y)$ antibonding orbital. Conjugative interactions and electronegativity effects may operate in the same or in opposite directions. As the electronegativity of Y decreases down a column of the periodic table, the energy of the $\sigma^*(S–Y)$ antibonding orbital decreases. Consequently, the $n_O \rightarrow \sigma^*(S–Y)$ interaction becomes stronger, with an increase of the electron transfer from oxygen to sulphur and a shielding of the ^{33}S nucleus. This means that moving down the same column of the periodic table, hyperconjugative interactions and electronegativity act on the ^{33}S chemical shift in the same way, causing an increase in the electron density around the sulphur atom. Moving along a row, conjugative interactions should be very small, due to the large energy difference between lone pair and $\sigma^*(S–Y)$ orbitals; hence the electronegativity effects prevail. This model also accounts for the opposite substituent effect on the ^{17}O chemical shift. Other series X-SO-Y and X-SO_2-Y have been studied.[52,53,87]

Replacing a methyl group in dimethyl sulphone, $CH_3SO_2CH_3$, with a phenyl and/or vinyl group causes an upfield shift of the ^{33}S resonance.[50] The effect is larger for the vinyl (−7 to −8.5 ppm) than for the phenyl group (−4 to −5 ppm), and it is additive within the limits of experimental error. A much more remarkable downfield effect is observed for ^{17}O in the corresponding ethers and for ^{77}Se in selenides (CH_3OCH_3, CH_3SeCH_3 and substituted compounds). Since this deshielding effect for ^{17}O and ^{77}Se has been attributed to the delocalization of lone pairs caused by conjugation with the π-electron system of the substituent, the shielding effect on ^{33}S could be due to a weak

(3p–2p)π or (3d–2p)π interaction between the sulphur atom and the π system of the substituent.

A deeper insight into the electronic properties of S–O and S–C bonds in sulphonates has been obtained by studying the substituent effect on [33]S NMR parameters in some 3- and 4-substituted benzenesulphonates[33,63] and 2-substituted ethanesulphonates.[35]

In a series of 3- and 4-substituted benzenesulphonates[33,63] (with substituents X = 3-NO$_2$, 4-NO$_2$, 4-COCH$_3$, 4-Cl, 4-F, H, 3-CH$_3$, 4-CH$_3$, 3-OH, 4-OH, 3-O$^-$, 4-O$^-$, 3-NH$_2$, 4-NH$_2$, 3-NH$_3^+$, 4-NH$_3^+$, 4-N(CH$_3$)$_2$, 4-NH(CH$_3$)$_2^+$, 3-CF$_3$, 3-SO$_3^-$ and 4-SO$_3^-$), the overall variation in chemical shift is not large ($\Delta\delta = 7.8$), but it is still significant. [33]S chemical shift shows the occurrence of a so-called reverse substituent effect: electron-withdrawing substituents cause an upfield shift of the [33]S resonance, whereas electron-releasing groups produce a downfield shift. Dual substituent parameter (DSP) analysis of $\Delta\delta$ for 3- and 4-substituted benzenesulphonates suggests that in both series of compounds, the inductive contribution predominates over the resonance one, and the resonance effect operates without direct conjugation between the sulphonate group and the aromatic ring. Through–space interaction of the C–X dipole with the π-system of the sulphonate group induces a change in the electron density at the [33]S nucleus (localized polarization). The conjugative effect of the substituent with the ring electrons should cause changes in the electron density at the carbon atom bonded to sulphur, thus affecting the $-$SO$_3^-$ d–p π-polarization and producing a shift of π-electrons between the oxygen and sulphur atoms.

Also line widths depend on the electronic properties of the substituents. Both electron-withdrawing and electron-releasing substituents provoke a broadening of the signal with respect to unsubstituted benzenesulphonate. This could be evidence for an inversion of the electric field gradient at the sulphur nucleus on going from electron-releasing to electron-withdrawing substituents.

The existence of a linear correlation between the [33]S chemical shift and nuclear quadrupole coupling constant

$$\delta(^{33}\text{S}) = 2.01\chi - 12.66 \qquad \text{corr. coeff.} = 0.993$$

suggests that substituent effects on both parameters have a common origin and seem to be mainly controlled by the term $\langle r^{-3} \rangle_{3p}$.

Also in 2-substituted ethanesulphonates,[35] the [33]S chemical shift has a reverse substituent effect and correlates with both Taft substituent constants and the chemical shift of the carboxylic carbon in related carboxylic acids. It seems that the substituent effect does not depend on conformation, but prevailingly on intramolecular electronic effects. Density functional theory (DFT) calculations of [33]S nuclear shielding constants and natural bond orbital (NBO) analysis made it possible to conclude that substituents cause a variation in the polarization of the S–C and S–O bonds and of the oxygen lone pairs of the C $-$ SO$_3^-$ moiety. This affects the electron density in the surroundings of the sulphur nucleus and consequently the expansion or contraction of 3p sulphur orbitals.

Interesting information has been obtained about the equilibria in aqueous solutions and the bond properties of thiomolybdate and thiotungstate anions, $[MS_nO_{4-n}]^{2-}$ with M = Mo, W.[71] An aqueous solution of $(NH_4)_2[MoS_2O_2]$ shows four ^{33}S sharp resonances, whose intensities vary with time. The kinetics of this equilibrium have been monitored by ^{33}S NMR. The four peaks have been assigned to the species $[MoS_4]^{2-}$ (345 ppm, 38 Hz), $[MoS_3O]^{2-}$ (240 ppm, 170 Hz), $[MoS_2O_2]^{2-}$ (123 ppm, 250 Hz) and $[MoSO_3]^{2-}$ (−25 ppm, 200 Hz). A similar trend has been observed for thiotungstate anions, which have narrower resonances than molybdenum complexes. The bonding properties of these complexes have also been analysed with the aid of ^{17}O NMR. Linear correlations exist between (i) ^{33}S chemical shifts in Mo and W complexes; (ii) ^{17}O chemical shifts in Mo and W complexes; and (iii) ^{33}S and ^{17}O chemical shifts in Mo and W complexes. Moreover, the variations in ^{33}S and ^{17}O chemical shifts, which can be ascribed to the paramagnetic term σ_p, linearly correlate to $1/\Delta E$, the reciprocal of the lowest energy electronic transitions of the complexes. This means that the electronic structure of thiomolybdate and thiotungstate anions must be similar. ^{33}S line widths decrease with the increase in the sulphur atom number, due to both molecular dimensions and the electric field gradient at the sulphur nucleus. According to the Townes and Dailey model,[89] the electric field gradient can be related to the population of the sulphur p orbitals. The narrower resonances in W complexes, compared to Mo complexes, could confirm that W complexes possess a stronger interaction between sulphur lone pairs and metal orbitals, which leads to higher π-bond order.

4.2 Determination of the molecular structure of sulphur-containing compounds; identification of sulphur functional groups

For more diffuse nuclei such as ^{13}C and ^1H, the analysis of chemical shift values is often sufficient to individuate the functional groups that constitute a molecule. For ^{33}S, it is often not possible to determine the nature of sulphur functional groups solely by examining their chemical shifts. For some functionalities, there is no net separation of chemical shift ranges. In such cases, parallel analysis of both ^{33}S NMR chemical shift and line width can sometimes provide the desired information.

A typical case is the structural assignment of the product obtained by addition of sodium bisulphite to anthocyanins.[90]

Anthocyanins are naturally occurring compounds. Among numerous other applications, they show a potential use as colouring agents for beverages and foods (E163). Their use is seriously limited, however, because in the presence of sulphur dioxide, widely used in the food industry as a preservative, they undergo a decolourization process. It was already known that this phenomenon is due to the nucleophilic addition of sodium bisulphite to anthocyanins, but many hypotheses had been made about the structure of the adduct obtained. The reaction between sodium bisulphite and a particular anthocyanin, malvidin 3-O-glucoside **12**, has recently been investigated.

By ^{1}H and ^{13}C 2D NMR, it has been demonstrated that the addition of bisulphite takes place on the C-4, but it has not been possible to assess whether the adduct is a sulphinate or a sulphonate. Only ^{33}S NMR spectroscopy has allowed the unambiguous determination of the structure of the product. Indeed, the ^{33}S spectrum of the adduct shows a single signal that can be attributed only to sulphonate **13** on the basis of chemical shift (-3.3 ppm) and line width (40 Hz). The line width value is particularly indicative of the formation of an $-SO_3^-$ moiety because it suggests that the sulphur electronic environment should be highly symmetric. In the case of a sulphur atom with an unsymmetrical electronic environment, such as in sulphinates, a broader signal should be expected.

12

13
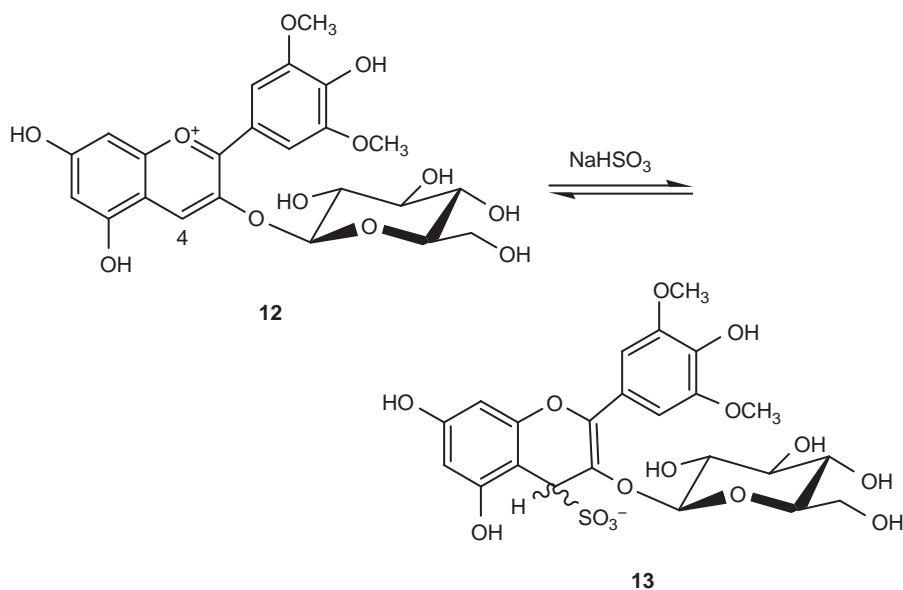
As already reported, ^{33}S NMR spectroscopy has also been useful in characterizing tropothione **2** and its derivatives. It has been found that tropone can be directly sulphurized at the exocyclic position, giving tropothione **2**. The reaction can be accomplished under mild conditions using tetraphosphorous decasulphide and triethylamine as catalysts in anhydrous organic solvents. ^{33}S NMR spectrum,[41] acquired at 9.4 T on a 0.4 M CDCl$_3$ solution at a temperature of 233 K, exhibits a signal at -287 ppm with a line width of 11,500 Hz. This signal is downfield with respect to sulphides, thus showing the same trend found for ^{17}O in ethers and ketones.[43,44] This is the only spectrum of a thioketone reported in the literature.

Tropothione **2** can be oxidized with an equimolar amount of *m*-chloroperbenzoic acid. Below 213 K, a sulphinic species, tropothione-*S*-oxide **3**, has been isolated.[42] In turn, S-oxide **3** with CF$_3$COOH forms a sulphenic acid **4**, which is quite stable at room temperature. Compounds **3** and **4** have been characterized with the aid of ^{33}S NMR spectroscopy. The ^{33}S chemical shift is -6 ppm for **3** and -85 ppm for **4**. In agreement with findings for sulphides and sulphoxides, the bonding of an oxygen atom to sulphur in tropothione induces a downfield shift of the ^{33}S resonance.

4.3 Studies of intermolecular interactions by relaxation times in solution

T_1 and T_2 are strongly dependent on the electron distribution around the nucleus and on the intra- and intermolecular interactions that can modify the electron distribution, such as:

(i)   solute–solvent interactions,
(ii)   formation of aggregates,
(iii)   hydrogen bonding,
(iv)   protonation, and, more generally, equilibria effects.

The study of ^{33}S relaxation times and line widths has provided much information about dynamic behaviour and molecular association for sulpholane, sulphonic acids and sulphonate anions. It is interesting to observe that in all cases, ^{33}S is an internal nucleus and is particularly sensitive to solvent and association effects, even though it is not directly exposed to these interactions.

The effect of counterion on the ^{33}S NMR spectrum of SO_4^{2-} anion has been studied by Belton et al.[26] The nature of counterion has a marked effect on signal line width (Table 2). One to two molar solutions of $CsSO_4$, $(NH_4)_2SO_4$ and Na_2SO_4 show variable but always narrow line widths (3.3–9.5 Hz); $MgSO_4$ and $Al_2(SO_4)_3$ give rise to particularly broad signals (46 Hz for Al^{+3}, from 7 to 37 Hz for Mg^{+2} in the concentration range 0.1–4 M). This line broadening effect indicates the existence in solution of ion binding interactions, as confirmed by the dramatic broadening of the ^{33}S signal after the addition of low concentration Ce(IV) to a solution of $(NH_4)_2SO_4$.

The same authors[26] have also studied the effect of pH on the ^{33}S line width of a solution of Na_2SO_4. In the pH range 0.9–6.4, the overall line width change is 190 Hz, and the chemical shift variation is 3 ppm. The origin of these variations is not due to exchange phenomena but probably to the interaction of the unprotonated species with sodium ions. Ion pairs should relax faster than not complexed species.

The behaviour of the ^{33}S line width and relaxation time in sulpholane **10** has been analysed as a function of concentration and temperature in acetic acid, trifluoroacetic acid, methyl acetate and methyl trifluoroacetate.[91] In the two esters, a normal trend for ^{33}S line width is observed. That is, at 313 K line width increases with sulpholane concentrations (from 4.6 to 18 Hz in CF_3COOCH_3 and from 4.9 to 18 Hz in CH_3COOCH_3). In contrast, line width decreases significantly in CH_3COOH (from 40 to 17 Hz) and dramatically in CF_3COOH (from 190 to 21 Hz) as the concentration increases. The data for ester solutions indicate that no significant solute–solvent interactions operate, as expected. Acetic acid should weakly interact with sulpholane molecules, causing minor perturbations of the electric field gradient at both ^{17}O and ^{33}S. Moreover, solute–solvent interactions, probably hydrogen bonds, should not have any influence on the macroscopic viscosity, but they could alter the microscopic viscosity, causing the slowing of the molecular reorientational motion. In contrast, trifluoroacetic acid should interact with sulpholane molecules, probably inducing weak protonation. A rapid exchange between protonated and non-protonated sulpholane should make it possible to observe only one signal. The line width of protonated species

should be several kilohertz, which is consistent with the findings that, by addition of a small amount of sulphuric acid, the ^{33}S signal becomes undetectable. The ^{17}O line width of CF$_3$COOH shows a typical dependence on the solution viscosity, thus confirming that the degree of protonation of sulpholane should be quite low.

Crumrine et al.[92,93] have found that when dealing with strong electrolytes, such as sulphonates and sulphonic acids, the classical Debye–Stokes–Einstein model does not hold, and the experimental behaviour cannot be interpreted considering the solvent as a continuous medium whose viscosity has the sole effect of varying the rate of reorientational motion. The ^{33}S line widths and relaxation times of benzenesulphonic acid[92] have been measured in different solvents (water, formamide, N-methylformamide and a binary mixture of formamide plus 18 mol % water) at variable concentrations, whereas methanesulphonic and trifluoro-methanesulphonic acid have been studied at different concentrations in aqueous solutions.[93] In benzenesulphonic acid, the ^{33}S relaxation time decreases linearly with increasing concentration in all the solvents considered. The relaxation times at infinite dilution are as follows: 28.2 ms in water, 6.5 ms in formamide, 7.0 ms in formamide/water, and 3.0 ms in N-methylformamide. T_1 values in water, formamide and formamide/water do not satisfy the dependence on solution viscosity predicted by the Debye–Stokes–Einstein equation. Moreover, if the solution viscosity was the principal solvent property determining nuclear relaxation, the relaxation time at infinite dilution (but also over the whole concentration range) in formamide should be shorter than that in N-methylforma-mide (the viscosities of formamide and N-methylformamide at 298 K are 3.30 and 1.65 cP, respectively). Data have been interpreted on the basis of the electrostatic model proposed by Hertz. At finite concentration, the ^{33}S relaxation originates not only from the interaction of the nuclear quadrupole moment with the electric field gradient generated at the nucleus by its electronic distribution, but also from interactions with the counterions and solvent dipoles constituting the solvation sphere of the $-SO_3^-$ moiety. As the acid concentration decreases, the sulphonate anion tends to be surrounded only by solvent molecules. The contribution of ion–ion interactions tends to become negligible, and the ^{33}S relaxation time increases. T_1 at infinite dilution is a measure of the efficiency of solute–solvent interactions in determining relaxation. In N-methylformamide, the shorter relaxation time is due to a stronger solvation of the benzenesulphonate anion with respect to water and formamide. Solvent dipoles are strongly oriented and tightly bound to the $-SO_3^-$ moiety, thus forming a compact solvation sphere. In water and formamide, benzenesulphonate anion is weakly solvated, and solvent dipoles are randomly distributed so that a solvation sphere is absent.

The same model can be applied to methane- and trifluoromethanesulphonic acids.[93] Also in these two cases, there is a linear dependence of ^{33}S T_1 on concentration in very large ranges (approximately 0.1–8 M for methanesulphonic acid and 0.1–5 M for trifluoromethanesulphonic acid). Moreover, T_1 in methane-sulfonic acid increases linearly with the degree of ionization of the acid. In both cases, ^{17}O T_1 has a parallel behaviour. For methanesulphonic acid, T_1 at infinite dilution is 11.6 ms at 293 K and 13.5 ms at 313 K. For trifluoromethanesulphonic

acid, these values are significantly shorter (1.5 ms at 293 K and 1.9 ms at 323 K), reasonably because the inductive effect of the three fluorine atoms causes a larger electric field gradient at the sulphur, hence giving a more efficient intramolecular effect on relaxation. The dependence of T_1 on concentration and degree of ionization reflects the variations in intermolecular interactions. As for benzene-sulphonate, only solute–solvent interactions are active at infinite dilution. As the acid concentration increases, other effects must be considered: protonation, variations in the composition of the solvation sphere surrounding the $-SO_3^-$ moiety (the number of counterions increases) and formation of aggregates. These changes decrease the symmetry of the environment around sulphur, and this is reflected in larger line widths and shorter T_1 values.

For benzenesulphonate, the counterion (Li^+, Na^+, K^+, Mg^{+2}) dependence of the ^{33}S relaxation rate in aqueous solution has also been studied.[83] Counterions influence the ^{33}S relaxation in the order $Mg^{+2} > Li^+ > Na^+ > K^+$.

4.4 Studies of intermolecular interactions in the gas phase

After 2000, Jackowski et al.[18,19,94–96] have published the first papers concerning ^{33}S NMR spectroscopy in the gas phase. The reported results can be considered preliminary, but they do show evidence for the potential utility of this technique in the study of the effect of intermolecular interactions on ^{33}S NMR parameters.

It is difficult to predict whether gas phase NMR applied to the ^{33}S nucleus can have a future. It cannot be ignored that the two major inconveniences in the observation of the ^{33}S resonances are amplified in gas phase NMR. Indeed, signals are weaker than in the condensed phases, due to the lower density of the samples (even at high pressure), and they are also broader. At the moment, it seems that the use of this technique is restricted only to the study of small molecules.

In the case of gaseous samples with low density, the nuclear magnetic shielding of a nucleus X in a molecule A can be expressed by a virial expansion as a power series in ρ density:[17]

$$\sigma(T) = \sigma_0(T) + \sigma_1(T)\rho + \sigma_2(T)\rho^2 + \ldots \tag{8}$$

For low-density systems, higher order terms can be neglected, and Equation (8) reduces to

$$\sigma(T) = \sigma_0(T) + \sigma_1(T)\rho \tag{8'}$$

where $\sigma_0(T)$ is the nuclear shielding of the nucleus X in the isolated A molecule at the temperature T, and $\sigma_1(T)$ a measure of the effects on nuclear shielding arising from bimolecular collisions. In gaseous mixtures of A and B, $\sigma_1(T)$ is the sum of two contributions, which take into account the effects of both A–A and A–B collisions:

$$\sigma_1(T) = \sigma_{AA}(T) + \sigma_{AB}(T) \tag{9}$$

If the density of A is low, only A–B collisions are significant, and $\sigma_1(T) \approx \sigma_{AB}(T)$.

According to Equation (8'), for low-density samples, a linear dependence of the nuclear shielding constant on gas density is generally observed, and $\sigma_0(T)$ can be determined by extrapolation to infinite diluition.[94]

The correlation between [33]S chemical shifts and density has been studied for OCS,[18,95] SF$_6$[24,25] and SO$_2$.[19]

In the case of OCS, the precise estimation of the [33]S chemical shift is complicated by the large broadening of the resonances. [33]S line width is 442 Hz at 323 K in the pure liquid, while in gas phase it varies from 1,020 to 1,450 Hz as the density decreases. Chemical shift at infinite dilution is 613.0 ppm (referred to (NH$_4$)$_2$SO$_4$ sat. in D$_2$O). Starting from this value, Jackowsky et al.[95] have recalculated the [33]S absolute shielding constant in OCS ($\sigma_0 = 817$ ppm at 323 K, against a value of 843 ppm previously reported by Wasylishen[36]) and defined a new absolute chemical shielding scale for [33]S.

The dependence of [33]S shielding on density has been studied for SF$_6$, both pure and in binary mixtures with Xe, CO$_2$ and NH$_3$ at 298 K.[24,25] In binary mixtures, the pressure of SF$_6$ has been kept constant, whereas the pressures of the gaseous solvents have been changed between 1 and 15 atm. In all cases, the [33]S shielding constant slightly decreases with increasing density, and Equation (8′) has been verified. This is consistent with the more general finding that intermolecular interactions have a net deshielding effect on a nucleus. The variations observed are very small, which is indicated by the values calculated for σ_1, suggesting that [33]S chemical shielding in SF$_6$ is not affected by intermolecular interactions. This conclusion is further supported by comparing the values of [33]S chemical shift at infinite dilution (-175.90 ppm) and in pure liquid (-176.79 ppm).

Also for SO$_2$,[19] the [33]S shielding decreases with increasing density, but it is much more sensitive than SF$_6$ to the effects of intermolecular interactions, as indicated by the value of σ_1 (-11.650 ppm L mol^{-1} at 333 K). The chemical shift at infinite dilution is 356.5 ppm.

Analysing these data, the most interesting result is the possibility of obtaining experimental values of [33]S chemical shift at infinite dilution, i.e. a measure of nuclear shielding in the absence of intermolecular interactions. These values can be compared with the ones obtained in condensed phases, providing an estimate of the effect of intermolecular interactions on nuclear shielding.

NMR spectroscopy in the gas phase has also been applied to determine the value of the [33]S magnetic dipole moment.[96]

4.5 Studies on deprotonation equilibria of sulphonic acids; determination of pK_a values

An acid–base reaction can alter the electronic distribution around the atoms involved in proton transfer, thus producing significant variations in the values of NMR parameters. Indeed, excluding the effect of other solute–solvent interactions and ion pair formations, one of the major factors determining [33]S spectral parameters in sulphonic acids is the degree of ionization. As examples, this is found for methanesulphonic acid in water at different concentrations and benzenesulphonic acid at constant concentration in different solvents.[58] At moderate concentrations (1–3 M) and within the pH range 1–14, sulphonic acids are generally completely ionized. Narrow [33]S NMR signals can be obtained due to the tetrahedral symmetry of the electronic distribution in sulphonate anions.

Upon protonation, ^{33}S line width increases as a consequence of the decreased electronic distribution symmetry around the sulphur nucleus. Also chemical shifts can undergo significant variations related to the structure of the species formed, but the pattern of the changes is unpredictable.

Ali et al.[91] have found that the ^{33}S chemical shift of sulpholane **10** in CF$_3$COOH depends linearly on concentration. Dilution provokes a deshielding of the ^{33}S nucleus, but a shielding of ^{17}O ($\Delta\delta(^{33}S) = +8.5$, $\Delta\delta(^{17}O) = -10$). According to the authors, this could be an effect of the protonation of sulpholane in CF$_3$COOH (as also suggested by relaxation time data), though a similar but weaker effect on chemical shift is observed in CH$_3$COOH ($\Delta\delta(^{33}S) = +1.7$, $\Delta\delta(^{17}O) = -3$), where protonation should be negligible according to the results of relaxation behaviour.

When sulphonic acids are not completely dissociated, so that both protonated and dissociated forms exist in solution, ^{33}S parameters measured experimentally have intermediate values between those of the two forms:

$$\delta(^{33}S) = \delta(AH)X_{AH} + \delta(A^-)X_{A^-}$$

$$LW(^{33}S) = LW(AH)X_{AH} + LW(A^-)X_{A^-}$$

where AH and A$^-$ are the acid and its conjugate base, respectively, and X represents the molar fractions of the two species. For both chemical shifts and line widths, it is possible to obtain NMR titration curves by simply measuring and plotting the values of NMR spectral parameters as a function of pH. A sigmoid is obtained that can be used as a classical titration curve, and its interpolation makes it possible to deduce precise values of pK_a values and NMR parameters for the ionized and undissociated forms. The ^{33}S NMR titration curve has been reported for methanesulphonic acid[58]; titration curves have also been determined[97] for 2-, 3- and 4-aminobenzenesulphonic acid **14**, 2-, 3-, and 4-hydroxybenzenesulphonic acid, taurine (2-aminoethanesulphonic acid), sulphonacetic acid, and 7-amino-1,3-naphthalene disulphonic acid. Some examples are reported in Figures 1–4.

These cases are particularly interesting since sulphonic acids bear an ionizable substituent. In the pH range 1–12, the sulphonic group of each compound is completely deprotonated, but the substituent changes its degree of ionization. Using ^{33}S NMR titration curves, it is possible to determine the second ionization constant. For example, aminobenzenesulphonic acids **14** exist in aqueous solution in zwitterionic form. By adding NaOH, the $-NH_3^+$ group is deprotonated, and the dissociation equilibrium is shifted towards the anionic form.
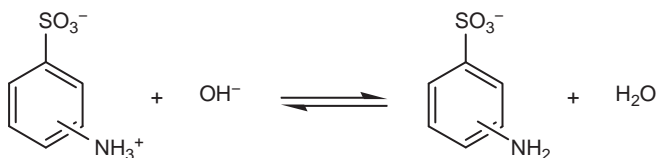
14

A significant variation of the ^{33}S NMR parameters is observed as a function of pH (Figures 1 and 2), even if deprotonation takes place at molecular sites distant
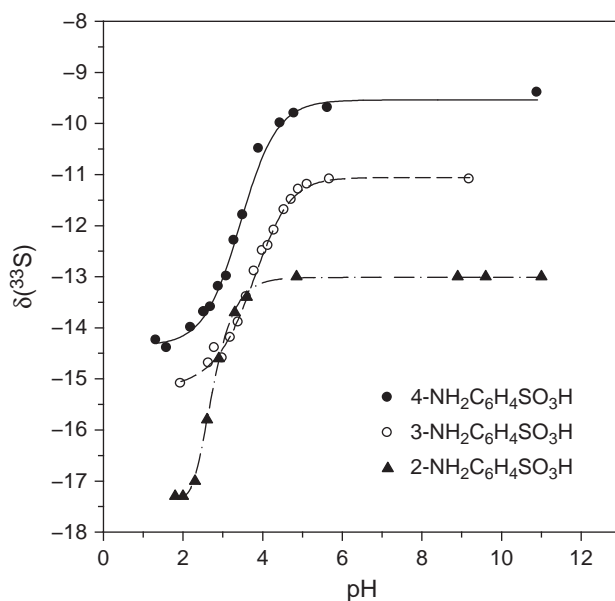
Figure 1 [33]S Chemical shift, δ([33]S), in 2-, 3- and 4-aminobenzensulphonic acids in water as a function of pH.
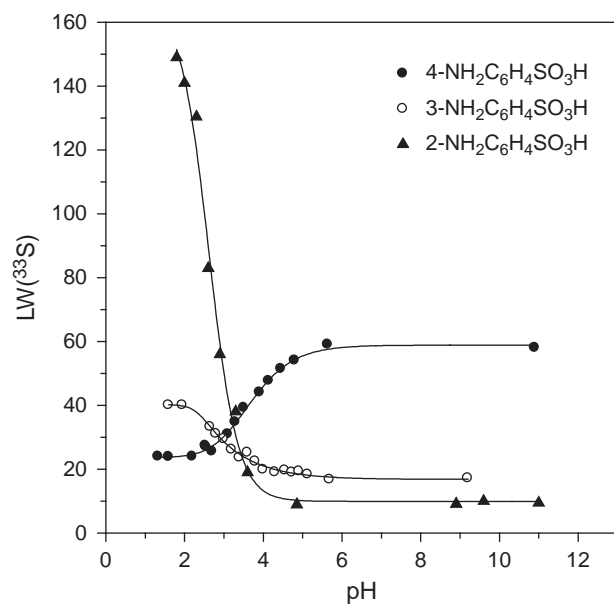

Figure 2 [33]S Line width, LW([33]S) in Hz, in 2-, 3- and 4-aminobenzensulphonic acids in water as a function of pH.
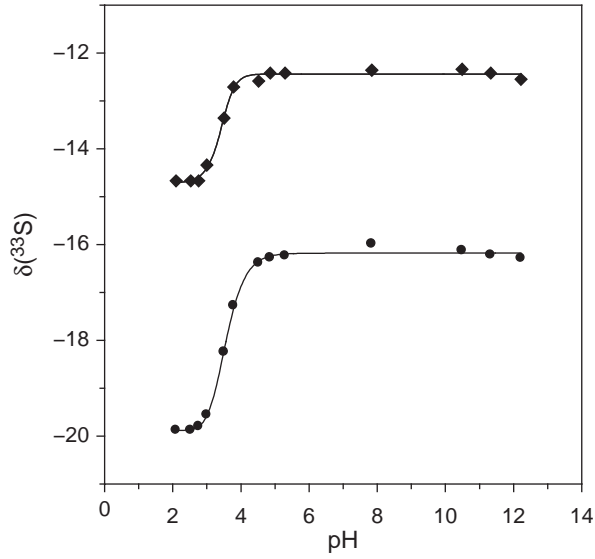
Figure 3 ^{33}S Chemical shift, $\delta(^{33}$S), of 7-amino-1,3-naphthalene disulphonic acid in water as a function of pH.
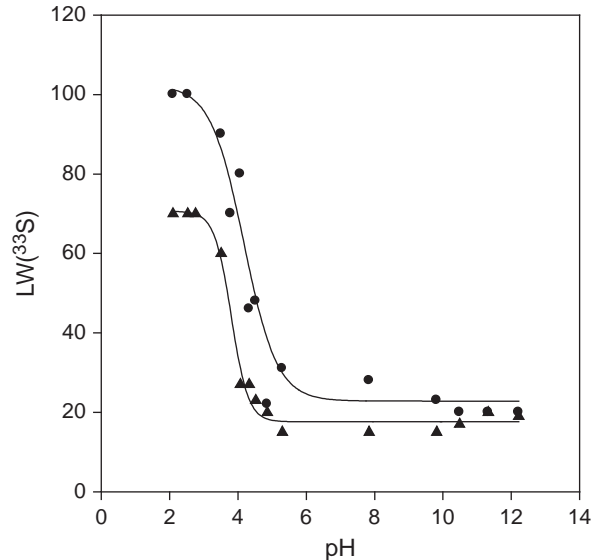

Figure 4 ^{33}S Line width, LW(^{33}S) in Hz, of 7-amino-1,3-naphthalene disulphonic acid in water as a function of pH.

from the sulphur atom. This behaviour is observed because [33]S NMR parameters are very sensitive to the electronic effect of the substituents, as previously discussed. The line width variations observed can be mainly ascribed to the variations of the electric field gradient at the sulphur nucleus induced by the different electronic properties of $-NH_3^+$ and $-NH_2$. Viscosity effects at high pH values seem to be negligible, as suggested by the decrease in line width values in 2- and 3-substituted compounds. The pK_a values determined by interpolating the experimental sigmoids (2.8 for 2-NH_2, 3.8 for 3-NH_2 and 3.4 for 4-NH_2) are in good agreement with the values reported in the literature (2.62 for 2-NH_2, 3.61 for 3-NH_2 and 3.14 for 4-NH_2).

Particularly interesting is the case of 7-amino-1,3-naphthalene disulphonic acid **15**:
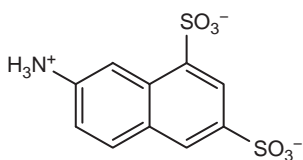
15

The two $-SO_3^-$ moieties are not equivalent, and two distinct signals with different line widths have been detected. The two $-SO_3^-$ groups are also differently influenced by the deprotonation of the $-NH_3^+$ group (Figures 3 and 4).

The effect of the deprotonation of the $-NH_2$ group on [33]S NMR parameters has also been studied for methanesulphonamide, $MeSO_2NH_2$.[98] Bagno and Comuzzi have found that in 0.1 M HCl, the [33]S resonance of $MeSO_2NH_2$ lies at -12 ppm and is deshielded by 13 ppm upon deprotonation in 1 M NaOH solution. This is in fair agreement with the variation of the nuclear isotropic shielding calculated at the HF/GIAO/6-311++G(2d,2p) level. It is interesting to point out that, as found in sulphonic acids, the [33]S chemical shift undergoes significant changes even though sulphur is not the deprotonation site. In contrast, ^{14}N, which is the deprotonation site, undergoes a smaller deshielding effect (only $+8$ ppm). Experimental longitudinal relaxation times do not show significant variations of the electric field gradient at the sulphur nucleus.

[33]S NMR spectroscopy could be a simple method to measure pK_a values of sulphonic acids in aqueous solutions. Indeed, it was shown that the [33]S chemical shifts of 3- and 4-substituted benzenesulphonates are linearly related to pK_a by the following equations,[59,61] derived respectively at 293 and 312 K:

$$pK_a = 0.130\delta(^{33}S) - 5.19 \quad \text{corr. coeff.} = 0.982 \quad T = 293 \text{ K}$$
$$pK_a = 0.139\delta(^{33}S) - 5.03 \quad \text{corr. coeff.} = 0.988 \quad T = 312 \text{ K}$$

The pK_a values determined by these relationships are comparable to the values obtained by UV spectroscopy, ^{1}H NMR spectroscopy and the Hammett plot. Analogous empirical relationships could be probably derived for different classes of sulphonic acids, e.g. alkyl and vinylsulphonic acids.

4.6 Detection of taurine in biological tissues

[33]S NMR spectroscopy was used for the first time to detect taurine in vivo.[22] Taurine, or 2-aminoethanesulphonic acid, is a naturally occurring β-amino acid that is widely distributed in the biosphere. Many of its biological functions are not completely understood due to the difficulty of detecting it in intact tissues. The great advantage in using [33]S NMR spectroscopy instead of ^{1}H and ^{13}C NMR is that sulphur functional groups normally occurring in biological samples, such as –S–, –SO_2–, SH, –SR and –S–S–, give rise to very broad signals not easily detectable at biological concentrations (and when they are detected, such signals lie in a different region of the spectral range and can be easily distinguished and assigned). On the contrary, the [33]S signal of taurine in tissues is quite narrow (40–80 Hz) and can be easily observed.

Lamb and calf heart, lamb brain and different molluscs have been examined, as intact tissues or as homogenates. A [33]S taurine spectrum in vivo has been obtained from *L. lithophaga*, due to its cylindrical shape, in about 8 min with a 10 mm probe (S/N = 3). Particularly important is the possibility of performing a quantitative determination of the taurine content. In this case, the major problem is to measure the intensity of the signals with good accuracy.

The results demonstrate that [33]S NMR spectroscopy can be a valuable and easy to use technique for observing sulphur metabolites in biological tissues and in living organisms. The method could be extended to the detection of other naturally occurring sulphonates, such as isethionate and coenzyme M.

4.7 Industrial applications of [33]S NMR spectroscopy

4.7.1 Analysis of mixtures and quantitative determinations

[33]S NMR spectroscopy is potentially an adequate method for both qualitative and quantitative analysis of mixtures of organosulphur compounds. Kosugi[62] has reported the [33]S spectra of mixtures of 1- and 2-naphthalenesulphonates and of 1,5- and 2,6-naphthalene disulphonates at concentrations of approximately 0.15 M in D_2O. In both cases, $(NH_4)_2SO_4$ was used as an internal standard to determine chemical shifts and for quantitative analysis. At a magnetic field of 5.9 T, the [33]S spectra of the two mixtures show two quite sharp and well-resolved resonances, and the results reported indicate that the quantitative analysis of these isomers is possible with a relative error of less than 10%.

Quantitative analysis can be performed by [33]S NMR using the classical methods, either (i) by adding a known amount of a standard to the sample and measuring the ratio of [33]S signal integrals, or (ii) by a calibration curve, obtained by measuring the integrals of the [33]S signals from samples of the examined compound at known concentrations.

Quantitative analysis is possible with good accuracy if the [33]S spectra are characterized by a good S/N and if the signals of the species to be determined are well resolved. It must be considered that in [33]S NMR spectra, baseline distortions can seriously endanger the final results.

## 4.7.2 ^{33}S NMR spectroscopy of fuel and coal

The application of ^{33}S NMR spectroscopy to the qualitative characterization of sulphur compounds in coals and petroleum has been another subject of a certain interest.[99–102] The presence of organic and inorganic sulphur derivatives in variable amounts in fuels has serious economic and environmental consequences. Coals and crude oils can be treated chemically to reduce sulphur content, and it is of fundamental importance to develop an analytical method to rapidly and accurately analyse sulphur before and after the desulphurization process.

^{33}S NMR could potentially be an adequate analytical technique, although the first attempts are not very encouraging. Sulphur occurs in different mineral forms in coals; in crude oils it is present as thiols, aromatic sulphides, aliphatic long chain sulphides and cycloalkyl sulphides. As already discussed, these compounds give rise to broad ^{33}S NMR signals and cannot be detected easily, especially considering the low concentrations and high viscosities of the samples. However, it is possible to selectively oxidize them to the corresponding sulphones. Ngassoum et al.[101] have characterized two low-boiling fractions of petroleum, previously oxidized, and assessed the absence of aryl, aliphatic or benzothiophene sulphones. The ^{33}S NMR spectrum of one fraction exhibited a sharp signal at 36 ppm and a broad one at 25 ppm, which could be attributed to non-aromatic five-membered cyclic sulphones and thiophene derivatives, respectively. The second fraction exhibited only one signal at about 28 ppm, due to thiophenic compounds.

Less encouraging are the results reported by McIntyre and Strauss,[102] who have tried to characterize a sample of asphaltene which, after oxidation, produced a signal in the spectral range of sulphones, but it was too broad to permit any assignment. Nevertheless, the results provide evidence of high molecular weight aliphatic sulphides. Although these results are not immediately encouraging, this field of application of ^{33}S NMR spectroscopy still deserves further investigation. The possibility cannot be excluded that the availability of high-field spectrometers with better standardization of experimental conditions and signal-processing methodologies could give better results.

4.7.3 Study of equilibria in molten binary system

The molten salt–gas system $K_2S_2O_7/KHSO_4/V_2O_5$–$SO_2/O_2/SO_3/CO_2/H_2O$ is a model of the industrial catalyst used for the oxidation of SO_2 to SO_3 by O_2. The molten $K_2S_2O_7/KHSO_4$ has been investigated by multinuclear NMR (^{39}K, ^{1}H, ^{17}O and ^{33}S).[103] ^{33}S NMR spectra, acquired at 9.4 T and at a temperature of 673 K for melts in the composition range X_{KHSO_4} 0.40–1, show a signal shifting downfield as the composition in $KHSO_4$ decreases. The presence of a single resonance line suggests that the anions $S_2O_7^{2-}$ and HSO_4^-, whose presence had been previously assessed by other spectroscopic techniques, are in fast exchange.

$$2HSO_4^- \rightleftharpoons S_2O_7^{2-} + H_2O$$
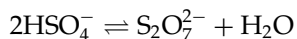
^{17}O NMR data confirms this conclusion. The ^{33}S chemical shifts reported vary from -6 to -3 ppm, but these values are not particularly indicative, since they

have been determined using 70% H_2SO_4 as a reference standard. Moreover, it must be pointed out that the ^{33}S chemical shift of pyrosulphate anion has not been previously reported in the literature.

4.8 Solid-state ^{33}S NMR spectroscopy

The majority of studies on ^{33}S NMR spectroscopy have been limited to liquid samples. ^{33}S solid-state NMR spectroscopy remained substantially unexplored until 2003, when the first systematic studies began to be published.

Previously, only three significant papers had been published. In 1986, an extensive study by Eckert and Yesinowsky[27] had evaluated the utility of solid-state ^{33}S NMR spectroscopy applied to metal sulphides and sulphates. The results were very interesting, but they were not particularly encouraging towards the pursuit of similar investigations, due to the large broadening of ^{33}S signals. Eckert and Yesinowsky used a spectrometer at a very high magnetic field (11.7 T, not common at that time), working in static conditions, and a modified RIDE sequence to reduce the problems arising from acoustic ringing. It was assessed that ^{33}S chemical shifts of sulphates in the solid state are in a narrow range and do not differ significantly from those determined in aqueous solutions, but the signals are very broad (950–18,000 Hz). Second-order quadrupolar broadening effects allowed to calculate ^{33}S nuclear quadrupole coupling constants (0.5–2.3 MHz), which show significant variations that could be related to differences in crystal lattice. In sulphides, ^{33}S chemical shifts (measured for the first time, since previously only the chemical shift of NaS in aqueous solution and ZnS in the solid state had been determined) are spread over a very large range (over 600 ppm) and are sensitive to small variations in crystal structure and composition. The variations in chemical shift can be explained by considering crystalline ionicities and bond polarities for ZnS, PbS and CdS, along with orbital overlap effects between ions for MgS, CaS, SrS and BaS. In 1988, Bastow and Stuart[104] characterized the cubic (sphalerite) and hexagonal (wurtzite) forms of ZnS.

In 1996, Daunch and Rinaldi[68] have demonstrated that a significant improvement in the sensitivity of solid-state ^{33}S spectra can be obtained by high-speed MAS. They have examined the ^{33}S spectra of some inorganic sulphides (PbS, ZnS (wurtzite), CaS) and sulphates (Cs_2SO_4, Li_2SO_4, Na_2SO_4, $BaSO_4$, $(NH_4)_2SO_4$, $NH_4Al(SO_4)_2 \cdot 12H_2O$ and $KAl(SO_4)_2 \cdot 12H_2O$) characterized by the different symmetries of their environments. The narrowing of the central transition under spinning rotation with respect to static lines is remarkable, more than an order of magnitude in some cases. In some cases, the typical second-order quadrupolar lineshape of the central transition has been observed.

Problems encountered in the acquisition of ^{33}S solid-state spectra are common to most of the quadrupolar nuclei, with the addition of the great inconvenience of the low sensitivity of ^{33}S.[105] In ^{33}S solid-state NMR,[69] the outer $(-3/2 \leftrightarrow -1/2)$ and $(1/2 \leftrightarrow 3/2)$ transitions are normally very broad as a consequence of

quadrupolar interactions.[69] In contrast, the central $(-1/2 \leftrightarrow 1/2)$ transition is not very broad, since it is not affected by quadrupolar interactions. Anyway, when the quadrupolar interactions are comparable to the nuclear resonance frequency, second-order quadrupolar effects can broaden the central transition. Second-order quadrupolar broadening (A) is inversely proportional to the strength of the static magnetic field, and [33]S line width can be reduced at higher magnetic field strength with a consequent sensitivity enhancement:[23]

$$A = \frac{3}{64} \frac{\chi^2}{\gamma}$$

Other factors that can influence spectral line widths in solid samples are dipolar coupling, chemical shift anisotropy (CSA), chemical shift dispersion (CSD) and spin–spin relaxation. Due to the low [33]S magnetogyric ratio, dipolar coupling is negligible or at least very small in most cases, but it can become important if nuclei with large magnetogyric ratios and high natural abundance are in close proximity to the [33]S nucleus. In any case, MAS technique can reduce the contributions from dipolar coupling, CSA and magnetic field inhomogeneity. CSD, however, cannot be reduced by MAS and increases proportionally to the magnetic field strength.

The effect of different contributions to the line width of the [33]S central transition has been extensively examined for sulphides[23,68] and sulphates.[68,69] In the case of sulphates,[69] it has been found that quadrupolar coupling is the most relevant contribution. In most of the sulphides examined,[23] the line widths broaden with increasing magnetic field strength. The measurement of the contributions due to different effects has confirmed the predominant role played by CSD, with the sole exception of ZnS, for which quadrupolar coupling is the dominant factor, and Li_2S, Na_2S and PbS, for which the quadrupolar contribution to the line width is very low. In these cases nuclear relaxation originates predominantly with dipole–dipole interactions between [33]S and [7]Li, [23]Na, and [207]Pb, all having high natural abundance and a high magnetogyric ratio.

A further improvement in the signal intensity of the central transition can be obtained using more sophisticated pulse sequences. Jakobsen et al.[107] have demonstrated that good sensitivity enhancement can be achieved by population transfer among the four energy levels of [33]S, by applying inversion pulses created by HS (hyperbolic secant) and WURST (wideband uniform rate smooth truncation) pulse shapes. The method has been tested on a series of inorganic sulphates, two cementitious materials, namely ettringite and thaumasite and two tetrathiometallates. The sensitivity enhancement factor measured is in the range 1.74–2.25. Very precise values of the nuclear quadrupole coupling constants and asymmetry parameters have been measured.

The first application of [33]S solid-state NMR spectroscopy is, of course, the determination of precise values of the [33]S nuclear quadrupole coupling constants that, as previously outlined, cannot be easily determined from liquid phase spectra. Jakobsen et al.[106] have demonstrated that it is possible to obtain very precise values of nuclear quadrupole coupling constants and asymmetry

parameters by analysing spinning sidebands (ssb) for the satellite transitions in natural abundance ^{33}S MAS spectra. The method has been applied to the ^{33}S spectra of $NH_4Al(SO_4)_2 \cdot 12H_2O$ and $KAl(SO_4)_2 \cdot 12H_2O$, which display a distinct first order ssb pattern. The iterative fitting of simulated to experimental intensities of ssb has not only given very accurate values of the nuclear quadrupole coupling constant and asymmetry parameter, but it has also made it possible to study the dependence of these two parameters on temperature. It has been found that in the range 238–343 K, the ^{33}S quadrupole coupling constant increases linearly with temperature with a gradient of 3.1 kHz/°C and 2.3 kHz/°C for NH_4^+ and K^+ salts, respectively. For $NH_4Al(SO_4)_2 \cdot 12H_2O$, the ^{33}S nuclear quadrupole coupling constant varies in the range 200.4 to -121.1 kHz, and for $KAl(SO_4)_2 \cdot 12H_2O$ it is in the range 680–452 kHz. For $NH_4Al(SO_4)_2 \cdot 12H_2O$, an inversion in the sign of the nuclear quadrupole coupling constant has been observed at 277 K.

Using the same technique, it has been possible to determine CSA data, the nuclear quadrupole coupling constants, and the asymmetry parameters for ^{33}S in $(NH_4)_2WS_4$ and $(NH_4)_2MoS_4$.[73] In these compounds, crystallographic analysis indicates that sulphur atoms can occupy three different sites. In the case of tetrathiotungstate anion, solid-state ^{33}S NMR spectra make it possible to distinguish these three non-equivalent sites. For tetrathiomolybdate, only one signal has been observed. This could be ascribed to the strongest and most organized N–H···S=M hydrogen bondings operating in $(NH_4)WS_4$, which determine a more ordered disposition of hydrogen atoms.

Very recent studies have examined the possibility of using ^{33}S MAS spectroscopy in the study of some structural problems in cementitious materials[107,108] and in sulphur speciation in silicate melts.[109] Several processes of the deterioration of cements and more generally lapideous materials can be correlated to the stability of sulphate, to changes in the sulphate phase and to the interaction of sulphate ions with water molecules and hydrates.[108] Since sulphate anion is one of the species that can be studied more easily by ^{33}S NMR solid-state spectroscopy, this technique can be a valuable tool in studying

(i)   the structure and local environment of sulphates in cement matrixes and
(i)   the modification of cementitious materials (sulphate) under the effect of temperature and different atmospheric agents, such as pollutants, acidic rain and so on.

In these studies, the parameters that could provide the most interesting information are likely to be the electric field gradient (nuclear quadrupole coupling constant) at the ^{33}S nucleus and its asymmetry parameter. Indeed, modifications of the lattice structure in different cement matrixes are expected to influence the symmetry of the electronic distribution around the sulphur nucleus more than the chemical environment of sulphur.

^{33}S solid-state MAS spectra at 19.6 T have been acquired for some bulk compounds representative of sulphate speciation in cement paste: ettringite, $[Ca_6Al_2(SO_4)_3(OH)_6 \cdot 26H_2O]$,[107,108] and three different samples of gypsum, $[CaSO_4 \cdot 2H_2O]$.[108] At ^{33}S natural abundance, the acquisition of spectra with a

reasonable S/N has required quite long experimental times, due to the low concentration of sulphate in different cements, but the problem can be avoided using [33]S enriched samples.[108] [33]S chemical shifts in different species vary in the small range of 2 ppm, but the variations of the lineshape and hence of the nuclear quadrupole coupling constant and asymmetry parameter are more significant. According to X-ray diffraction studies, ettringite has a hexagonal structure, and the sulphate anion occupies three different crystallographic sites. [33]S MAS spectra acquired with WURST PT inversion pulses[107] can be simulated by three distinct signals, in agreement with the X-ray structure, and the quadrupole coupling constants and the asymmetry parameters are as follows: 0.591 MHz $\eta_1 = 0.72$, 0.810 MHz $\eta_2 = 0.97$, 0.516 MHz $\eta_3 = 0.50$. In gypsum,[108] the nuclear quadrupole coupling constant and the symmetry parameter are 0.7 MHz and 1.0, respectively. Evidently, the sulphate anion in ettringite is much less distorted than in gypsum. Another sulphate-containing cementitious material, thaumasite $[Ca_3Si(OH)_6](SO_4)(CO_3) \cdot 12H_2O$, has also been characterized by [33]S MAS.[107]

[33]S MAS has been used to characterize a series of hydrous silicate glasses.[109] In this case also, [33]S isotopic enriched samples have been used. [33]S chemical shifts indicate that in the compounds examined, sulphur is present as sulphate. The line width is comparable to that observed in related crystalline sulphates, which means that the quadrupolar interactions are comparable in both phases, but a loss of the second-order lineshape is observed, which is typical for quadrupolar nuclei in glass systems. Chemical shift variations suggest that it could be possible to obtain information on the preferred association of sulphate with a specific cation. In a dry potassium silicate glass, two distinct [33]S signals have been observed. According to their chemical shift, the second signal can be assigned to nanocrystalline $K_2S_2O_3$.

5. THEORETICAL CALCULATIONS OF [33]S NMR PARAMETERS

Within the last two decades, significant progress has been achieved in the theoretical computation of NMR spectroscopic parameters,[110] particularly of nuclear screening constants. Theoretical calculations of [33]S NMR parameters have received a certain attention for two main reasons: (i) they can help in identifying and elucidating the structural properties of sulphur-containing molecules, and (ii) they can provide important information on the electron distribution and bonding situation around the sulphur atom.

5.1 Calculation of [33]S isotropic nuclear shielding

After some sparse papers published by different authors in the 1970s (see e.g. refs. 111–113), in 1987 Tossel et al.[114] performed *ab initio* CHFPT (coupled Hartree–Fock perturbation theory) calculations of σ_d and σ_p, the diamagnetic and

paramagnetic contributions to the screening constant σ, for a series of polysulphur anions (S_2^{2-}, S_4^{2+} and S_4^{2-}) and for S^{2-}, H_2S, HS^-, SO_2, and SO_4^{2-}. The calculated σ values satisfactorily reproduce the trend of the ^{33}S NMR chemical shift, but for those species whose chemical shifts have been determined experimentally (H_2S, HS^-, SO_2 and SO_4^{2-}), significant discrepancies have been found between calculated and experimental data. Free S^{2-} ion has the highest shielding among the species considered. Indeed, its σ_p is zero because calculations have been performed on the isolated molecule in the absence of any intermolecular and rovibrational contributions. In condensed phases, S^{2-} is expected to be less shielded because σ_p has a non-zero value, due to distortions of the electronic distribution caused by intermolecular interactions. The square planar S_4^{2+} ion ($\sigma = -564.9$ ppm) is predicted to be deshielded with respect to SO_2 ($\sigma = -154.1$ ppm), and in S_4^{2-} ion the terminal sulphur nucleus ($\sigma = 674.2$ ppm) is about 100 ppm more shielded than the internal one ($\sigma = 571.2$ ppm).

The ability of *ab initio* methods to reproduce ^{33}S chemical shifts with a sufficient accuracy has been extensively examined by Schindler[115] and Bagno.[116] Absolute shielding constants for a large series of sulphur compounds, covering approximately the whole chemical shift range, have been calculated at the MCSCF (multiconfiguration SCF) level by the IGLO (individual gauge for localized molecular orbitals) method[115] and at the HF/6-311++G(2d,2p) (Hartree–Fock) level[116] by the GIAO (gauge including atomic orbitals) method. With the exception of SO_2, the overall agreement between theoretical chemical shift values (referred to CS_2) and available experimental data in the liquid phase is satisfactory to good. At the HF level, theoretical values tend to overestimate the experimental ones by 12% (the correlation coefficient is 0.98); at the MCSCF level of theory, the mean absolute deviation is 25 ppm for an experimental chemical shift range of about 820 ppm.

As a general rule, *ab initio* methods reproduce the ^{33}S experimental chemical shift trend well, independently of the level of approximation used, provided that sufficiently expanded basis sets are used (according to Schindler, basis sets should include at least two sets of polarization functions for sulphur[115]). However, in many cases the introduction of electron correlation is mandatory. When this is the case, DFT methods[117] are usually preferred to Møeller–Plesset (MP) and coupled-cluster calculations because they are less time-consuming and can also be easily applied to complex molecular systems.

The most critical point is the calculation of σ_p. Indeed, ^{33}S σ_d values calculated for sulphur in various molecules at different levels of approximation do not deviate significantly from the value calculated for the free sulphur atom (1,050.5 ppm),[118] except for sulphurs directly bearing a positive or negative charge. For H_2S[112] and 2-substituted ethanesulphonates,[35] it has been demonstrated at different levels of theory that sulphur core electrons account for about 92–94% of σ_d, the remaining part being ascribed to valence bond electrons. σ_p depends on all the excited states of the molecule (the use of ΔE in Equation (2) is only an approximation). Since DFT methods tend to underestimate the energies

of the excited states, they overestimate the paramagnetic contribution, resulting in very low values of the total screening constant.

To avoid this problem, Chesnut[119] has proposed the use of a scaling factor derived by a least squares fit of DFT-calculated σ_p against the difference between the observed isotropic shielding and the calculated σ_d. The relationship derived for values calculated using the GIAO approach at B3LYP/6-311+G(2d,p) level is

$$\sigma = \sigma_d + 0.871(\pm 0.010)\sigma_p$$

with a root-mean-square error of 29.1 ppm. The method has been extended to the EMPI (estimated Møller–Plesset infinite-order) approximation[31] and has been tested on a large number of organic and inorganic sulphur compounds. Both the DFT and EMPI approaches are equivalent in reproducing experimental shielding values, and the error is about 3% of the experimental chemical shift range of about 1,000 ppm.

In any case, when dealing with theoretical calculations of NMR parameters, it must be considered that a quantitative agreement between theoretical and routine experimental data can hardly be expected. According to Chesnut and Quin,[31] differences of 30–50 ppm are not statistically significant. It must be considered that chemical shifts are almost exclusively calculated for idealized model systems, i.e. zero-temperature equilibrium geometries of free molecules, whereas NMR spectra are generally acquired on condensed-phase samples (liquid, solutions, solid or powders) at ambient temperatures. Consequently, experimental parameters are affected by intermolecular interactions and rotational and vibrational motions. Solvent effects on nuclear shielding can be significant, especially in the case of ionic compounds in protic solvents. An attempt to evaluate solvent effect on [33]S nuclear shielding has been reported for 2-substituted ethanesulphonates in water.[35] Applying the IEF–PCM method, it has been found that interactions with solvent molecules have a deshielding effect in the range 5.1–8.7 ppm, thus demonstrating that introducing a solvent effect can be a determinant, especially when small chemical shift differences must be reproduced.

Jackowski et al.[120] have examined the temperature dependence of the rovibrational corrections to the [33]S nuclear shielding constant in OCS by the GIAO method used at the MCSCF level with different basis sets. In the temperature range 170–420 K, the rovibrational correction has a deshielding effect that depends slightly on the basis set (−15 to −18.5 ppm ca. and −12.5 to −14.5 ppm ca. with two different basis sets).

Some interesting applications of theoretical calculations of [33]S shielding constants have been reported in the literature.

The conformational dependence of the [33]S isotropic σ in dimethyldisulphide, $(CH_3)_2S_2$, has been studied by HF calculations using the IGLO method.[121] $(CH_3)_2S_2$ is a good model for the disulphide linkage in polypeptides and proteins. [33]S σ has been calculated as a function of the dihedral angle C–S–S–C. Predicted chemical shifts vary between −84.4 ppm (<C–S–S–C = 0°) and −42.3 ppm (<C–S–S–C = 87.4°). Calculated values refer to CS_2 and cannot be converted to the SO_4^{2-} scale, since the absolute shielding of the SO_4^{2-} anion has not been reported

in the paper. In 1976, Retcofsky and Friedel[3] measured a chemical shift of -168 ± 88 ppm (referred to CS_2) for $(CH_3CH_2)_2S_2$. More recently, a value of 36 ppm (referred to CS_2, with a line width of 10,600 Hz) was reported.[40]

Combariza et al.[122] calculated the ^{33}S shielding tensor by the *ab initio* LORG (localized orbital local origin) method in the following oxothiomolybdates: $MoSO_3^{2-}$, $MoS_2O_2^{2-}$, MoS_3^{2-} and MoS_4^{2-}. An excellent correlation between calculated and experimental chemical shifts has been found with all the basis sets used:

$$\delta_{calc} = 1.447 \delta_{exp} + 156 \qquad corr.\ coeff. = 0.9995$$

The ^{33}S calculated and experimental chemical shifts correlate with the sulphur 3p and molybdenum 4d orbital populations.

Rasul et al.[123] have reported the ^{33}S NMR chemical shift values (referred to CS_2) of different forms of protonated and methylated dimethyl sulphoxide cations and dications at the GIAO-MP2 level. Unfortunately, the lack of experimental data does not allow any testing of the validity of theoretical values.

A typical demonstration of the utility of theoretical calculations in the assignment of uncertain signals is reported by Quin et al.[30,31] As already found by Bagno,[116] the experimental values reported in the literature for *S*-methyltetrahydrothiophenium salt **1**, 750 ppm (referred to CS_2), did not fit well with the scaled values, calculated by the B3LYP DFT approach and the EMPI method, which were 87.4 and 121 ppm respectively. With the aid of AIM calculations, it was verified that this discrepancy cannot be ascribed to intermolecular interactions in solution, neither salt formation nor interaction with counterions. The experimental redetermination of chemical shift values has given a value of 95 ppm (ext. ref. CS_2), in agreement with calculated values. For *S*-methylthianium ion **16**, a value of 68 ppm has been calculated, compared to an experimental value reported in the literature of 670 ppm.[29]
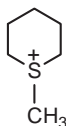
16

For a series of thiophosphoryl compounds R_3PS[31,45] with R = H, CH_3, OH, F, Cl, it has been found that σ values are in the range 692.9–890.6 ppm, with the exception of Cl_3PS. These values are close to the value calculated for sulphur in the reference species $HSPH_2$ ($\sigma = 741.5$ ppm) rather than in XP=S ($\sigma = -1,384.4$ ppm). This could suggest that, in R_3PS compounds, the P–S bond is not a conventional double bond. Cl_3PS is much more deshielded ($\sigma = 372.6$ ppm), but a satisfactory explanation of this behaviour has not been given.

The possibility of calculating ^{33}S NMR shielding constants has made it possible to obtain a better insight into the origin of substituent effects on ^{33}S NMR in 2-substituted ethanesulphonates.[35] Sulphur isotropic absolute shielding

constants have been calculated by the GIAO method at the B3LYP/6-311+G(2d,p) level and interpreted with the aid of the NBO method and NCS (nuclear chemical shielding) analysis. It has been found that the substituent effect is determined predominantly by the polarization of S–O and S–C σ-bonds that affect the electron density around the nucleus and the extension of the orbitals involved in the formation of the bonds.

5.1.1 Determination of an absolute shielding scale for ^{33}S

Calculated values of the isotropic nuclear shielding constants depend on the theoretical approximation and basis sets used. Hence, in order to evaluate the performance of a theoretical model, it is necessary to have reliable absolute shielding values. An absolute nuclear magnetic shielding scale for ^{33}S has been defined by Wasylishen et al.,[36] who have calculated the ^{33}S shielding constant in an isolated molecule of OCS in the ground vibrational state using Flygare's approximation for the estimation of σ_d and the molecular nuclear spin–rotation constant of OCS determined experimentally by molecular-beam electric resonance. With this semi-empirical procedure, the absolute ^{33}S nuclear shielding constant of OCS is 843 ± 12 ppm; the shielding constants calculated with respect to this value for $(NH_4)_2SO_4$ 4M and CS_2 are 249 and 581 ppm, respectively.

Recently, Jackowski et al.[95,120] have redetermined the absolute shielding constant for OCS, using the same value for the spin–rotation constant but a diamagnetic shielding calculated by CCSD(T) (coupled-cluster singles, doubles and triples) method. The new value is 817 ± 12 ppm. On this scale, the absolute shielding constants of the following references have been determined: SF_6 liquid (380.7 ppm), $(NH_4)_2SO_4$ in D_2O (204.0 ppm, at different concentrations), Cs_2SO_4 2M in H_2O (204.0 ppm), SO_2 liquid (-169.7 ppm at 300 K and -170.5 at 295 K) and CS_2 liquid (536.1 ppm).

5.2 Calculation of spin–spin coupling constants

Only two papers have been published on the theoretical calculations of spin–spin coupling constants involving the ^{33}S nucleus.[124] The single-bond coupling constants $^1J(^{33}S–^{15}N)$, $^1J(^{33}S–^{17}O)$, $^1J(^{33}S–^{31}P)$ and $^1J(^{33}S–^{33}S)$ have been calculated in the model compounds $H_2N–SH$, $HO–SH$, $H_2P–SH$, and $HS–SH$ by *ab initio* EOM–CCSD (equation of motion coupled-cluster singles and doubles) in the CI (configuration interaction) approximation. ^1J and its contributions (Fermi contribution FC, spin–orbit SO and spin–dipole SD contributions) have been calculated for different values of the dihedral angle H–S–Y–H. The results have demonstrated that, as expected, the J values are positive, with the sole exception of $^1J(^{33}S–^{31}P)$. The FC term gives a significant contribution to $^1J(^{33}S,Y)$, has the same sign as J, except for $^1J(^{33}S–^{33}S)$, and decreases in absolute value with increasing dihedral angle. The SO and SD terms have opposite signs from the FC contribution. In HS–SH and HO–SH, the competition of SD and SO with the FC term results in a relatively small coupling constant over the entire range of the dihedral. It has been demonstrated that ^1J depends strictly on the relative orientation of the lone pairs on the sulphur and Y atoms. Karplus-type equations

relating these coupling constants to the dihedral angle H–S–Y–H have been defined.

5.3 Calculation of ^{33}S nuclear quadrupole coupling constants

Quantum mechanical calculations of ^{33}S nuclear quadrupole coupling constants are not an easy matter (not only for the ^{33}S nucleus, but for all quadrupolar nuclei). Indeed, the electric field gradient is a typical core property, and it is difficult to find wave functions correctly describing the electronic distribution in close proximity to the nucleus. Moreover, in the case of ^{33}S, the real importance of the Sternheimer shielding contribution has not been completely assessed, and in any case the Sternheimer effect is difficult to calculate.

DFT methods give good results in the calculation of electric field gradients, provided that extended basis sets are used. Bailey et al.[125,126] have investigated the performances of different DFT and HF–DFT methods with different basis sets. For ^{33}S, they have found that the best results can be obtained by the B3LYP/ 6-311G(3df,3p) method. In the case of thiazole,[125] an excellent agreement between calculated and experimental values of ^{33}S nuclear quadrupole coupling tensor components has been obtained using the 6-31G(3df,3p) basis set with the B3PW91 functional. The calculated values are: $\chi_{aa} = 7.230$ MHz, $\chi_{bb} = -26.190$ MHz and $\chi_{cc} = 18.961$ MHz; the experimental values are: $\chi_{aa} = 7.171$ MHz, $\chi_{bb} = -26.175$ MHz and $\chi_{cc} = 19.004$ MHz.

In the literature, it is possible to find some interesting applications for the calculation of the ^{33}S nuclear quadrupole constant. In the following, some examples are described.

In the case of sulpholane,[76] it has been found by *ab initio* calculations that the principal component of the electric field gradient at the ^{33}S nucleus is perpendicular to the molecular plane containing the five ring moiety; the intermediate component lies along the C_2 axis.

Moreover, it has been possible to reproduce the substituent effect on the ^{33}S nuclear quadrupole coupling constant in 2-substituted ethanesulphonates[35] using the B3LYP functional. The correlation between experimental and calculated values can be considered satisfactory (corr. coeff. 0.98), but the calculated values tend to overestimate experimental values.

Bagno[116] has published the first systematic study on *ab initio* HF theoretical calculation of the ^{33}S electric field gradient. He examined a large series of compounds and found that in some cases, the calculation of the term $\chi^2(1+\eta^2/3)$ (Equation (3)) can help in predicting the possibility of observing ^{33}S NMR signals. For example, the impossibility of detecting ^{33}S signals for NaSCN and BuSCN could be due to the extremely large line width, since the calculated values of $\chi^2(1+\eta^2/3)$ are in the range 2,000–4,000 MHz^2. Moreover, the changes in the ^{33}S electric field gradient that occur during acid–base equilibria have been calculated for H_2S, CH_3SH, $CH_3SO_2NH_2$, CH_3SONH_2, H_2CS, $HCSNH_2$, $(CH_3)_2SO_2$ and $(CH_3)_2SO$.[98,127] These values have been used to predict changes in the ^{33}S NMR relaxation rate and line width. In the case of $CH_3SO_2NH_2$,

calculated line width values have been compared to the experimental ones, and good agreement has been found.

REFERENCES

1. S. S. Dharmatti and H. E. Weaver, *Phys. Rev.*, 1951, **83**, 845.
2. H. L. Retcofsky and R. A. Friedel, *Appl. Spectrosc.*, 1970, **24**, 379.
3. H. L. Retcofsky and R. A. Friedel, *J. Am. Chem. Soc.*, 1972, **94**, 6579.
4. O. Lutz, A. Nolle and A. Schwenk, *Z. Naturforsch. Teil A*, 1973, **28**, 1370.
5. O. Lutz, W. Nepple and A. Nolle, *Z. Naturforsch. Teil A*, 1976, **31**, 978.
6. R. Faure, E. J. Vincent, J. M. Ruiz and L. Léna, *Org. Magn. Reson.*, 1981, **15**, 401.
7. P. S. Belton, I. J. Cox and R. K. Harris, *J. Chem. Soc. Faraday Trans. 2*, 1985, **81**, 63.
8. J. F. Hinton, Sulfur-33 NMR spectroscopy, in: *Annual Reports on NMR Spectroscopy*, A. G. Webb, ed., Vol. 19, Academic Press, London, UK, 1987.
9. V. M. Bzhezovsky and G. A. Kalabin, ^{33}S NMR spectroscopy, in: *Chemistry of Organosulfur Compounds*, L. I. Belen'ki, ed., Horwood, Chichester, 1990.
10. G. Barbarella, *Prog. NMR Spectrosc.*, 1993, **25**, 317.
11. C. Rodger, N. Sheppard, H. C. E. McFarlane and W. McFarlane, Group VI — Oxygen, sulfur, selenium and tellurium, in: *NMR and the Periodic Table*, R. K. Harris and B. E. Mann, eds., Academic Press, London, 1978. O. Lutz, Group VI elements other than oxygen, in: *The Multinuclear Approach to NMR Spectroscopy*, J. B. Lambert and F. G. Riddell, eds., NATO ASI Series, D. Reidel Publishing Company, Dordrecht, 1982.; H. C. E. McFarlane and W. McFarlane, Sulfur, selenium, and tellurium, in: *Multinuclear NMR*, J. Mason, ed., Plenum Press, New York, 1987.
12. R. K. Harris, E. D. Becker, S. M. Cabral de Menezes, R. Goodfellow and P. Granger, *Pure Appl. Chem.*, 2001, **73**, 1795.
13. See for example: R. R. Ernst, G. Bodenhausen and A. Wokaun, *Principles of Nuclear Magnetic Resonance in One and Two Dimensions*, Oxford University Press, Oxford, 1988. A. G. Marshall and F. R. Verdun, *Fourier Transforms in NMR, Optical, and Mass Spectrometry — A User's Handbook*, Elsevier, Amsterdam, 1990. E. Fukushima and S. B. W. Roeder, *Experimental Pulse NMR. A Nuts and Bolts Approach*, Addison-Wesley Publishing Company, Reading, MA, 1981.
14. I. P. Gerothanassis, *Prog. NMR Spectrosc.*, 1987, **19**, 267.
15. D. Canet, J. Brondeau, J. P. Marchal and B. Robin-Lherbier, *Org. Magn. Reson.*, 1982, **20**, 51.
16. S. L. Patt, *J. Magn. Reson.*, 1982, **49**, 161.
17. C. Jameson, *Chem. Rev.*, 1991, **91**, 1375.
18. K. Jackowski, *J. Mol. Struct.*, 2001, **563–564**, 159.
19. W. Makulski and K. Jackowski, *J. Mol. Struct.*, 2004, **704**, 219.
20. J. C. Hoch and A. S. Stern, *NMR Data Processing*, Wiley, New York, 1996.
21. J. J. Led and H. Gesmar, *Chem. Rev.*, 1991, **91**, 1413; P. Koehl, *Prog. NMR Spectrosc.*, 1999, **34**, 257.
22. R. Musio and O. Sciacovelli, *J. Magn. Reson.*, 2001, **153**, 259.
23. T. A. Wagler, W. A. Daunch, P. L. Rinaldi and A. R. Palmer, *J. Magn. Reson.*, 2003, **161**, 191.
24. K. Jackowski, M. Wilczek, W. Makulski and W. Kozminski, *J. Phys. Chem. A*, 2002, **106**, 2829.
25. H. Tervonen, J. Saunavaara, L. P. Ingman and J. Jokisaari, *J. Phys. Chem. B*, 2006, **110**, 16232.
26. P. S. Belton, I. J. Cox and R. K. Harris, *Magn. Reson. Chem.*, 1986, **24**, 171.
27. H. Eckert and J. P. Yesinowsky, *J. Am. Chem. Soc.*, 1986, **108**, 2140.
28. R. E. Wasylishen, J. B. Macdonald and J. O. Friederich, *Can. J. Chem.*, 1983, **62**, 1181.
29. R. Annunziata and G. Barbarella, *Org. Magn. Reson.*, 1984, **22**, 250.
30. L. C. Dickinson, D. B. Chesnut and L. D. Quin, *Magn. Reson. Chem.*, 2004, **42**, 1037.
31. D. B. Chesnut and L. D. Quin, *Heteroat. Chem.*, 2004, **15**, 216.
32. N. F. Ramsey, *Phys. Rev.*, 1950, **78**, 699; A. Saika and C. P. Slichter, *J. Chem. Phys.*, 1954, **22**, 26.
33. R. Musio and O. Sciacovelli, *J. Org. Chem.*, 1997, **62**, 9031.
34. C. J. Jameson and H. S. Gutowsky, *J. Chem. Phys.*, 1964, **40**, 1714.
35. R. Musio and O. Sciacovelli, *Magn. Reson. Chem.*, 2006, **44**, 753.

36. R. E. Wasylishen, J. B. Macdonald and J. O. Friederich, *Can. J. Chem.*, 1983, **62**, 981.
37. (a) H. Duddeck, *Prog. NMR Spectrosc.*, 1995, **27**, 1. (b) *Phosphorous-31 NMR — Principles and Applications*, D. G. Gorenstein, ed., Academic Press, Orlando, 1984.
38. L. Cassidei and O. Sciacovelli, *J. Magn. Reson.*, 1985, **62**, 529.
39. J. Hoyle, J. S. Grossert, D. L. Hooper and S. Sotheeswaran, *Can. J. Chem.*, 1986, **64**, 1581.
40. R. A. Aitken, S. Arumugan, S. T. E. Mesher and F. G. Riddel, *J. Chem. Soc., Perkin Trans.*, 2002, **2**, 225.
41. T. Machiguchi, *Tetrahedron*, 1995, **51**, 1133.
42. T. Machiguchi, T. Hasegawa and H. Otani, *J. Am. Chem. Soc.*, 1994, **116**, 407.
43. D. W Boykin and A. L. Baumstark, ^{17}O NMR spectroscopic data for carbonyl compounds: I. Aldehydes and ketones II. Carboxylic acids and derivatives, in: *^{17}O NMR Spectroscopy in Organic Chemistry*, D. W. Boykin, ed., CRC Press, Boca Raton, 1991.
44. S. Chandrasekaran, ^{17}O NMR spectroscopy for single bonded oxygen: Alcohol, ethers and their derivatives, in: *^{17}O NMR Spectroscopy in Organic Chemistry*, D. W. Boykin, ed., CRC Press, Boca Raton, 1991.
45. D. B. Chesnut, L. D. Quin and P. J. Seaton, *Magn. Reson. Chem.*, 2004, **42**, S20.
46. A. B. Rozhenko, V. M. Bzhezovsky, V. V. Polovinko and A. G. Makarenko, *Magn. Reson. Chem.*, 1995, **33**, 853.
47. G. Barbarella, A. Bongini, C. Chatgilialoglu, S. Rossini and V. Tugnoli, *J. Org. Chem.*, 1987, **52**, 3857.
48. D. L. Harris and S. A. Evans Jr., *J. Org. Chem.*, 1982, **47**, 3355.
49. T. C. Farrar, B. M. Trost, S. L. Tang and S. E. Springer-Wilson, *J. Am. Chem. Soc.*, 1985, **107**, 262.
50. L. Cassidei, V. Fiandanese, G. Marchese and O. Sciacovelli, *Org. Magn. Reson.*, 1984, **22**, 486.
51. H. Duddeck, U. Korek, D. Rosenbaum and J. Drabowicz, *Magn. Reson. Chem.*, 1986, **24**, 792.
52. G. Barbarella, C. Chatgilialoglu, S. Rossini and V. Tugnoli, *J. Magn. Reson.*, 1986, **70**, 204.
53. G. Barbarella, C. Chatgilialoglu and V. Tugnoli, *J. Magn. Reson.*, 1990, **88**, 277.
54. V. M. Bzhezovsky, V. V. Penkovsky, A. B. Rozhenko, S. V. Iksanova, N. V. Kondratenko and L. M. Yagupolsky, *J. Fluor. Chem.*, 1994, **69**, 41.
55. J. B. Stothers, *Carbon-13 NMR Spectroscopy*, Academic press, London, 1972, p. 55.
56. G. J. Martin, M. L. Martin and J.-P. Gouesnard, ^{15}N-NMR spectroscopy NMR, in: *NMR Basic Principle and Progress*, P. Diehl, E. Fluck, H. Günther, R. Kosfeld and J. Seelig, eds., Vol. 18, Springer, Berlin, 1992.
57. J. F. Hinton and D. Buster, *J. Magn. Reson.*, 1984, **57**, 494.
58. D. S. Crumrine and B. Gillece-Castro, *J. Org. Chem.*, 1985, **50**, 4408.
59. D. S. Crumrine, J. M. Shankweiler and R. V. Hoffman, *J. Org. Chem.*, 1986, **51**, 5013.
60. Y. Kosugi, *Anal. Sci.*, 1989, **5**, 253.
61. D. C. French and D. S. Crumrine, *J. Org. Chem.*, 1990, **55**, 5494.
62. Y. Kosugi, *Anal. Sci.*, 1991, **7**, 209.
63. R. Musio and O. Sciacovelli, *J. Org. Chem.*, 1992, **57**, 1195.
64. A.-M. Häkkinen and P. Ruostesuo, *Magn. Reson. Chem.*, 1985, **23**, 424.
65. P. S. Belton and J. D. Woollins, *Magn. Reson. Chem.*, 1986, **24**, 1080.
66. T. T.-T. Nguyen, C. Deiseth, J.-P. Kintzinger, P.-A. Carrupt and P. Vogel, *Tetrahedron*, 1980, **36**, 2793.
67. P. S. Belton, I. J. Cox and R. K. Harris, *Magn. Reson. Chem.*, 1986, **24**, 1004.
68. W. A. Daunch and P. S. Rinaldi, *J. Magn. Reson. A*, 1996, **123**, 219.
69. T. A. Wagler, W. A. Daunch, M. Panzner, W. J. Youngs and P. L. Rinaldi, *J. Magn. Reson.*, 2004, **170**, 336.
70. P. Kroneck, O. Lutz and A. Nolle, *Z. Naturforsch Teil A*, 1980, **35**, 226.
71. P. S. Belton, I. J. Cox, R. K. Harris and M. J. O'Connor, *Aust. J. Chem.*, 1986, **39**, 943.
72. M. Kony, R. T. C. Brownlee and A. G. Wedd, *Inorg. Chem.*, 1992, **31**, 2281.
73. H. J. Jakobsen, A. R. Hove, H. Bildsøe, J. Skibsted and M. Brorson, *Chem. Commun.*, 2007, 1629.
74. Y. Kosugi and O. Okazaki, *Anal. Sci.*, 1991, **7**, 849.
75. J. F. Hinton, *J. Magn. Reson.*, 1984, **59**, 469.
76. B. H. Ruessink, W. J. van der Meer and C. MacLean, *J. Am. Chem. Soc.*, 1986, **108**, 192.
77. A. Abragam, *The Principles of Nuclear Magnetism*, Oxford University Press, London, 1961, p. 313.

78. J. F. Hinton and D. Shungu, *J. Magn. Reson.*, 1983, **54**, 309.
79. E. Haid, D. Köhnlein, G. Kössler, O. Lutz and W. Schich, *J. Magn. Reson.*, 1983, **55**, 145.
80. J. F. Hinton and D. Buster, *J. Magn. Reson.*, 1984, **58**, 324.
81. Y. Saito, *Can. J. Chem.*, 1965, **43**, 2530.
82. C. P. Slichter, *Principles of Magnetic Resonance*, Springer-Verlag, Berlin, 1980.
83. D. C. French and D. S. Crumrine, *J. Phys. Chem.*, 1993, **97**, 3371.
84. P. C. Schmidt, K. D. Sen, T. P. Das and A. Weiss, *Phys. Rev. B*, 1980, **22**, 4167.
85. M. J. Collins, C. I. Ratcliffe and J. A. Ripmeester, *J. Phys. Chem.*, 1989, **93**, 7495.
86. A. Lowenstein and D. Igner, *J. Phys. Chem.*, 1988, **92**, 2124.
87. G. Barbarella, *J. Mol. Struct. Theochem.*, 1989, **186**, 197.
88. M. Karplus and J. A. Pople, *J. Chem. Phys.*, 1963, **12**, 2803.
89. C. H. Townes and B. P. Dailey, *J. Chem. Phys.*, 1949, **17**, 782.
90. B. Berké, C. Chèze, J. Vercauteren and G. Deffieux, *Tetrahedron Lett.*, 1998, **39**, 5771.
91. A. A. M. Ali, R. K. Harris and P. S. Belton, *Magn. Reson. Chem.*, 1990, **28**, 318.
92. D. C. French and D. S. Crumrine, *J. Magn. Reson.*, 1989, **84**, 548.
93. T. M. Murray and D. S. Crumrine, *J. Magn. Reson.*, 1991, **91**, 573.
94. K. Jackowski, *J. Mol. Struct.*, 2006, **786**, 215.
95. K. Jackowski, W. Makulski and V. Koźmiński, *Magn. Reson. Chem.*, 2002, **40**, 563.
96. A. Antušek, K. Jackowski, W. Makulski, M. Jaszuński and V. Koźmiński, *Chem. Phys. Lett.*, 2005, **411**, 111.
97. R. Musio and O. Sciacovelli, unpublished results.
98. A. Bagno and C. Comuzzi, *Eur. J. Org. Chem.*, 1999, 287.
99. J.-M. Novelli, M. B. Ngassoum, R. Faure, J.-M. Ruiz, L. Lena, E.-J. Vincent and J. C. Escalier, *Am. Chem. Soc. Div. Pet. Chem. Prepr.*, 1985, **30**, 346.
100. S. A. Evans Jr., in: *Magnetic Resonance. Introduction, Advanced Topics and Applications to Fossil Energy*, L. Petrakis and J. Fraissurd, eds., Reidel, Dordrecht, 1984, p. 757.
101. M. B. Ngassoum, R. Faure, J. M. Ruiz, L. Lena, E. J. Vincent and B. Neff, *Fuel*, 1986, **65**, 142.
102. D. D. McIntyre and O. P. Strausz, *Magn. Reson. Chem.*, 1987, **25**, 36.
103. K. M. Eriksen, R. Fehrmann, G. Hatem, M-. Gaune-Escard, O. B. Lapina and V. M. Mastikhin, *J. Phys. Chem.*, 1996, **100**, 10771.
104. T. J. Bastow and S. N. Stuart, *Phys. Stat. Sol. (b)*, 1988, **145**, 719.
105. M. E. Smith and E. R. H. van Eck, *Prog. NMR Spectrosc.*, 1999, **34**, 159.
106. J. Jakobsen, A. R. Hoven, H. Bildsøe and J. Skibsted, *J. Magn. Reson.*, 2006, **180**, 170.
107. M. R. Hansen, M. Brorson, H. Bildsøe, J. Skibsted and H. J. Jakobsen, *J. Magn. Reson.*, 2008, **190**, 316.
108. J.-B. d'Espinose de Lacaillerie, F. Barberon, B. Bresson, P. Fonollosa, H. Zanni, V. E. Federov, N. G. Naumov and Z. Gan, *Cem. Concr. Res.*, 2006, **36**, 1781.
109. S. Couch, A. P. Howes, S. C. Kohn and M. E. Smith, *Solid State Nucl. Magn. Reson.*, 2004, **26**, 203.
110. C. J. Jameson, *Ann. Rev. Phys. Chem.*, 1996, **47**, 135; A. C. De Dios, *Prog. NMR Spectrosc.*, 1996, **29**, 229; C. J. Jameson, *Nucl. Magn. Reson.*, 1997, **26**, 46; H. Fukui, *Prog. NMR Spectrosc.*, 1997, **31**, 317; T. Helgaker, M. Jaszuński and K. Ruud, *Chem. Rev.*, 1999, **99**, 293. *Modelling NMR Chemical Shifts*. ACS Symposium Series 732, J. C. Facelli and A. C. de Dios, eds., American Chemical Society, Washington, DC, 1999.; *Calculation of NMR and EPR Parameters — Theory and Applications*, M. Kaupp, M. Bühl and V. G. Malkin, eds., Wiley-VCH, Weinheim, 2004.
111. S. Rothenberg, R. H. Young and H. F. Schaefer III, *J. Am. Chem. Soc.*, 1970, **92**, 3243.
112. J. Ridard, B. Levy and P. Millie, *Mol. Phys.*, 1978, **36**, 1025.
113. R. D. Amos and M. R. Battaglia, *Mol. Phys.*, 1978, **36**, 1517.
114. J. A. Tossell, P. Lazzeretti and D. J. Vaughan, *J. Magn. Reson.*, 1987, **73**, 334; J. A. Tossell and P. Lazzeretti, *J. Chem. Phys.*, 1988, **88**, 7251.
115. M. Schindler, *J. Chem. Phys.*, 1988, **88**, 7638; W. Kutzelnigg, U. Fleischer and M. Schindler, The IGLO method: Ab-initio calculation and interpretation of NMR chemical shifts and magnetic susceptibilities, in: *NMR Basic Principles and Progress*, P. Diehl, E. Fluck, H. Günther, R. Kosfeld and J. Seelig, eds., Vol. 23, Springer, Berlin, 1992.
116. A. Bagno, *J. Mol. Struct. Theochem.*, 1997, **418**, 243.

117. I. Alkorta and J. Elguero, *Struct. Chem.*, 1998, **9**, 187.
118. G. Malli and C. Froese, *Int. J. Quant. Chem.*, 1967, **1**, 95.
119. D. B. Chesnut, *Chem. Phys. Lett.*, 2003, **380**, 251.
120. K. Jackowski, M. Jaszuński, W. Makulski and J. Vaara, *J. Magn. Reson.*, 1998, **135**, 444.
121. D. Jiao, M. Barfield, J. E. Combariza and V. J. Hruby, *J. Am. Chem. Soc.*, 1992, **114**, 3639.
122. J. E. Combariza, M. Barfield and J. H. Enemark, *J. Phys. Chem.*, 1991, **95**, 5463.
123. G. Rasul, G. K. S. Prakash and G. A. Olah, *J. Org. Chem.*, 2000, **65**, 8786.
124. J. E. Del Bene and J. Elguero, *J. Phys. Chem A*, 2006, **110**, 12543; J. E. Del Bene and J. Elguero, *J. Phys. Chem A*, 2007, **111**, 2517.
125. W. C. Bailey, F. M. Gonzales and J. Castiglione, *Chem. Phys.*, 2000, **260**, 327.
126. W. C. Bailey, *J. Mol. Spectr.*, 2001, **209**, 57.
127. A. Bagno and G. Scorrano, *J. Phys. Chem.*, 1996, **100**, 1545.

APPENDIX

Table A.1. ^{33}S Larmor frequencies (ν_0 in MHz) at different magnetic field strengths B_0 (T); ^{1}H Larmor frequencies are reported for comparison

B_0	$\nu_0(^{33}\text{S})$	$\nu_0(^1\text{H})$
1.9	6.1	80
2.4	7.7	100
4.7	15.3	200
7.1	23.0	300
9.4	30.7	400
11.7	38.3	500
14.1	46.0	600
16.4	53.7	700
18.8	61.4	800

In the following tables ^{33}S NMR parameters of organic and inorganic compounds have been reported. Line width values, LW, are in hertz. Chemical shift values, δ, have been referred to SO_4^{2-}. Data in the literature referred to CS_2 and sulpholane have been converted in the SO_4^{2-} scale by the following relationships,[10] obtained from the chemical shift values reported by Belton et al.[7] (referred to Cs_2SO_4 2M in water):

$$\delta(SO_4^{2-}) = \delta(CS_2) - 333$$

$$\delta(SO_4^{2-}) = \delta(\text{sulpholane}) + 36.7$$

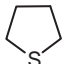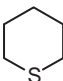**Table A.2.** ^{33}S NMR parameters of thiols, organic sulphides and thiophenes

	δ	LW	Experimental conditions	Original standard	Refs.
Thiols					
CH$_3$SH	−458	–	Neat, 8.5 T	(NH$_4$)$_2$SO$_4$ 4M (aq.)	36
CH$_3$(CH$_2$)$_3$SH	−415	2,100	Neat, 7.1 T	CsSO$_4$ 2M (aq.)	7
PhSH	−332	7,000	Neat, 11.7 T	Na$_2$SO$_4$ (aq.)	40
PhCH$_2$SH	−379	6,500	Neat, 11.7 T	Na$_2$SO$_4$ (aq.)	40
Organic sulphides					
(CH$_3$)$_2$S	−428	2,500	80% in CHCl$_3$, 30°C, 7.1 T	CS$_2$	47
PhSCH$_3$	−390	19,800	Neat, 11.7 T	Na$_2$SO$_4$ (aq.)	40
	−573	3,220	80% in CHCl$_3$, 30°C, 7.1 T	CS$_2$	47
	−302	4,000	80% in CHCl$_3$, 30°C, 7.1 T	CS$_2$	47
	−422	2,600	Neat, 1.4 T (CW)	CS$_2$	3
	−330	5,500	Neat, 35°C, 7.1 T	CS$_2$	29
	−354	4,800	Neat, 4.7–7.1 T	CsSO$_4$ 2M (aq.)	7
	−363	5,500	Neat, 35°C, 7.1 T	CS$_2$	29

Table A.2 *(Continued)*
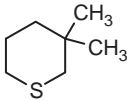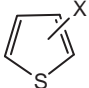
	δ	LW	Experimental conditions	Original standard	Refs.
	−366	2,500	Neat 35°C, 7.1 T	CS_2	29

Thiophenes

	δ	LW	Experimental conditions	Original standard	Refs.
X = H	−113	620	CS_2, 1.4 T	CS_2	3
	−119	1,450	Neat, 7.1 T	$CsSO_4$ 2M (aq.)	7
2-CH$_3$	−155	1,280	CS_2, 1.4 T	CS_2	3
3-CH$_3$	−136	1,600	CS_2, 1.4 T	CS_2	3
3-Br	−199	1,600	CS_2, 1.4 T	CS_2	3

Table A.3. ^{33}S NMR parameters of sulphoxides
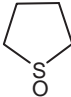
	δ	LW	Experimental conditions	Original reference	Refs.
(CH$_3$)$_2$SO	-20	4,900	Neat, 7.1 T	CsSO$_4$ 2M (aq.)	7
	-8	5,500	Neat, 35°C, 7.1 T	CS$_2$	29
	-100	2,600	Neat, 1.4 T (CW)	CS$_2$	3
	-213	4,950	2–3 M in CHCl$_3$, 30°C, 7.1 T	CS$_2$	47
	32	4,950	2–3 M in CHCl$_3$, 30°C, 7.1 T	CS$_2$	47
	27	2,990	2–3 M in CHCl$_3$, 30°C, 7.1 T	CS$_2$	47

Table A.4.1. ^{33}S NMR parameters of symmetric sulphones
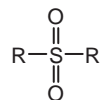
R	δ	LW	Experimental conditions	Original reference	Refs.
CH_3	−13	20	$CHCl_3$, 22°C, 4.7 T	CS_2	50
	−18	46	$CHCl_3$, 35°C, 7.1 T	CS_2	29
	−13.6	8.5	Acetone, 21°C, 7.1 T	$CsSO_4$ 2M (aq.)	7
	−13	50	$CHCl_3$, 22–25°C, 5.9 T	CS_2	48
	−1	275	TFA, 22–25°C, 5.9 T	CS_2	48
	−12	50	DMSO, 22–25°C, 5.9 T	CS_2	48
	−7	50	DMSO-d_6, 28°C, 1.9 T	$(NH_4)_2SO_4$ 4M (aq.)	6
	−12.8	15	$CDCl_3$, 20°C, 8.5 T	$(NH_4)_2SO_4$ 5M (aq.)	39
	−12.3	50	DMSO, 30–45°C, 4.7 T	Sulpholane	49
C_2H_5	1	70	$CHCl_3$, 22–25°C, 5.9 T	CS_2	48
	2	92	$CHCl_3$, 35°C, 7.1 T	CS_2	29
	4.9	50	$CDCl_3$, 20°C, 8.3 T	$(NH_4)_2SO_4$ 5M (aq.)	39
	1	100	$CHCl_3$, 22°C, 4.7 T	CS_2	50
n-C_3H_7	0	180	$CHCl_3$, 22–25°C, 5.9 T	CS_2	48
	2	130	DMSO, 22–25°C, 5.9 T	CS_2	48
	7	130	DMSO-d_6, 28°C, 1.9 T	$(NH_4)_2SO_4$ 4M (aq.)	6
	−2	92	$CHCl_3$, 35°C, 7.1 T	CS_2	29
i-C_3H_7	18	160	$CHCl_3$, 22–25°C, 5.9 T	CS_2	48
	18.1	120	$CDCl_3$, 20°C, 8.3 T	$(NH_4)_2SO_4$ 5M (aq.)	39
n-C_4H_9	3	180	$CHCl_3$, 22–25°C, 5.9 T	CS_2	48
	0.4	52	Acetone, 21°C, 7.1 T	$CsSO_4$ 2M (aq.)	7
	−7	92	$CHCl_3$, 35°C, 7.1 T	CS_2	29

t-C$_4$H$_9$	6	180	CHCl$_3$, 22°C, 4.7 T	CS$_2$	50
	33	160	CHCl$_3$, 22–25°C, 5.9 T	CS$_2$	48
	27.1	46	Acetone, 21°C, 7.1 T	CsSO$_4$ 2M (aq.)	7
n-C$_6$H$_{13}$	9	400	CDCl$_3$, 20°C, 4.7 T	SO$_4^{2-}$	101
CH$_2$=CH	−30	60	CHCl$_3$, 22°C, 4.7 T	CS$_2$	50
	−23	16	Aceton-d$_6$	CS$_2$	9
	−28	60	DMSO-d$_6$, 28°C, 1.9 T	(NH$_4$)$_2$SO$_4$ 4M (aq.)	6
CH$_2$=CHCH$_2$	1	80	DMSO-d$_6$/CDCl$_3$, 20°C, 4.7T	SO$_4^{2-}$	101
C$_6$H$_5$	−23	130	DMSO, 28°C, 1.9 T	(NH$_4$)$_2$SO$_4$ 4M (aq.)	8
	−23.3	48	DMSO, 30–45°C, 4.7 T	Sulpholane	49
	−21	120	CHCl$_3$, 22–25°C, 5.9 T	CS$_2$	48
	−28	130	DMSO-d$_6$, 22–25°C, 5.9 T	CS$_2$	48
	−23	70	CHCl$_3$, 22°C, 4.7 T	CS$_2$	50
	−25	161	CHCl$_3$, 35°C, 7.1 T	CS$_2$	29
	−24.5	42	Acetone, 21°C, 7.1 T	CsSO$_4$ 2M (aq.)	7
PhCH$_2$	−3	120	CHCl$_3$, 22–25°C, 5.9 T	CS$_2$	48
	−3.3	20	CDCl$_3$, 20°C	(NH$_4$)$_2$SO$_4$ 5M (aq.)	39
	−1	90	DMSO-d$_6$/CDCl$_3$, 20°C, 4.7 T	SO$_4^{2-}$	101
	−2	100	CHCl$_3$, 22°C, 4.7 T	CS$_2$	50
p-CH$_3$C$_6$H$_4$	−22	140	CHCl$_3$, 22–25°C, 5.9 T	CS$_2$	48
p-OHC$_6$H$_4$	−20	–	CHCl$_3$, 22–25°C, 5.9 T	CS$_2$	48

Table A.4.2. [33]S NMR parameters of asymmetric sulphones

$$R-\overset{\overset{\displaystyle O}{\|}}{\underset{\underset{\displaystyle O}{\|}}{S}}-R'$$
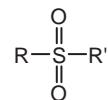
R	R′	δ	LW	Experimental conditions	Original reference	Refs.
CH$_3$	nPr	−7	92	CHCl$_3$, 35°C, 7.1 T	CS$_2$	29
	n-Bu	−7	92	CHCl$_3$, 35°C, 7.1 T	CS$_2$	29
	CH$_2$Cl	−7.2	90	CDCl$_3$, 20°C, 8.3 T	(NH$_4$)$_2$SO$_4$ 5M (aq.)	39
	CHCl$_2$	−0.2	280	CDCl$_3$, 20°C, 8.3 T	(NH$_4$)$_2$SO$_4$ 5M (aq.)	39
	CCl$_3$	4.5	300	CDCl$_3$, 20°C, 8.3 T	(NH$_4$)$_2$SO$_4$ 5M (aq.)	39
	CH$_2$Br	−10.3	95	CDCl$_3$, 20°C, 8.3 T	(NH$_4$)$_2$SO$_4$ 5M (aq.)	39
	CH$_2$Ph	−16.7	40	CDCl$_3$, 20°C, 8.3 T	(NH$_4$)$_2$SO$_4$ 5M (aq.)	39
		−3	10	Acetone-d$_6$	CS$_2$	9
		−19	40	CDCl$_3$	CS$_2$	9
	CHClCH$_3$	0.9	40	CDCl$_3$, 20°C, 8.3 T	(NH$_4$)$_2$SO$_4$ 5M (aq.)	39
	CH$_2$C(O)Ph	−12.1	215	CDCl$_3$, 20°C, 8.3 T	(NH$_4$)$_2$SO$_4$ 5M (aq.)	39
	CH(CH$_3$)C(O)Ph	−1.3	100	CDCl$_3$, 20°C, 8.3 T	(NH$_4$)$_2$SO$_4$ 5M (aq.)	39
	CHClC(O)Ph	−3.7	200	CDCl$_3$, 20°C, 8.3 T	(NH$_4$)$_2$SO$_4$ 5M (aq.)	39
	CHBrC(O)Ph	−5.0	400	CDCl$_3$, 20°C, 8.3 T	(NH$_4$)$_2$SO$_4$ 5M (aq.)	39
	CH$_2$COOCH$_3$	−12	78	CDCl$_3$, 35–45°C, 4.7 T	Sulpholane	49
	CH$_2$C(OCH$_2$)$_2$Ph	−11.7	100	CDCl$_3$, 20°C, 8.3 T	(NH$_4$)$_2$SO$_4$ 5M (aq.)	39
	CH(SCH$_3$)C(O)Ph	4.0	325	CDCl$_3$, 20°C, 8.3 T	(NH$_4$)$_2$SO$_4$ 5M (aq.)	39
	CH(SEt)C(O)Ph	5.9	120	CDCl$_3$, 20°C, 8.3 T	(NH$_4$)$_2$SO$_4$ 5M (aq.)	39
	CH(SPh)C(O)Ph	4.0	400	CDCl$_3$, 20°C, 8.3 T	(NH$_4$)$_2$SO$_4$ 5M (aq.)	39
	p-CH$_3$C$_6$H$_4$	−15	430	DMSO-d$_6$	CS$_2$	9
		−19.3	48	CDCl$_3$, 30–45°C, 4.7 T	Sulpholane	49

	p-CH$_3$OC$_6$H$_4$	-27	180	DMSO-d$_6$	CS$_2$	9
	p-FC$_6$H$_4$	-17	85	Acetone-d$_6$	CS$_2$	9
	m-FC$_6$H$_4$	-15	50	Acetone-d$_6$	CS$_2$	9
	p-ClC$_6$H$_4$	-20	350	DMSO-d$_6$	CS$_2$	9
		-14	85	Acetone-d$_6$	CS$_2$	9
		-19.4	87	Acetone, 21°C, 4.7 T	Cs$_2$SO$_4$ 0.2M (aq.)	7
	p-BrC$_6$H$_4$	-20	650	DMSO-d$_6$	CS$_2$	9
	m-BrC$_6$H$_4$	-15	30	Acetone-d$_6$	CS$_2$	9
	p-NH$_2$C$_6$H$_4$	-14	50	Acetone-d$_6$	CS$_2$	9
	p-NO$_2$C$_6$H$_4$	-11	122	DMSO-d$_6$	CS$_2$	9
	p-CH$_3$COC$_6$H$_4$	-14	85	Acetone-d$_6$	CS$_2$	9
	F	1	–	CHCl$_3$, 30°C, 7.1 T	CS$_2$	52
	Cl	2	1,500	CHCl$_3$, 30°C, 7.1 T	CS$_2$	52
	Br	-19	–	CHCl$_3$, 30°C, 7.1 T	CS$_2$	52
	I	-76	–	CHCl$_3$, 30°C, 7.1 T	CS$_2$	52
Ph	CH$_3$	-20	120	DMSO-d$_6$, 28°C, 1.9 T	(NH$_4$)$_2$SO$_4$ 4M	6
		-17	30	CHCl$_3$, 22°C, 4.7 T	CS$_2$	50
		-17	35	CDCl$_3$, 35–45°C, 4.7 T	Sulpholane	49
		-19	55	(CH$_2$Br)$_2$, 70°C, 9.4 T	(NH$_4$)$_2$SO$_4$	51
		-15	40	Acetone-d$_6$	CS$_2$	9
	CH$_2$CH$_3$	-7.0	125	CDCl$_3$, 20°C, 8.3 T	(NH$_4$)$_2$SO$_4$ 5M (aq.)	39, 29
		-9	160	CHCl$_3$, 35°C, 7.1 T	CS$_2$	50
		-9	100	CHCl$_3$, 22°C, 4.7 T	CS$_2$	51
		-9	90	(CH$_2$Br)$_2$, 70°C, 9.4 T	(NH$_4$)$_2$SO$_4$	9
		-5	80	Acetone-d$_6$	CS$_2$	9
	n-C$_3$H$_7$	-11	100	(CH$_2$Br)$_2$, 70°C, 9.4 T	(NH$_4$)$_2$SO$_4$	51
	i-C$_3$H$_7$	-2	160	(CH$_2$Br)$_2$, 70°C, 9.4 T	(NH$_4$)$_2$SO$_4$	51
		2	110	Acetone-d$_6$	CS$_2$	9
	n-C$_4$H$_9$	-11	100	(CH$_2$Br)$_2$, 70°C, 9.4 T	(NH$_4$)$_2$SO$_4$ (aq.)	51
	i-C$_4$H$_9$	-11	100	(CH$_2$Br)$_2$, 70°C, 9.4 T	(NH$_4$)$_2$SO$_4$ (aq.)	51

Table A.4.2 *(Continued)*

R	R′	δ	LW	Experimental conditions	Original reference	Refs.
	$t\text{-}C_4H_9$	5.9	144	Acetone, 21°C, 4.7 T	$CsSO_4$ 2M (aq.)	7
		6	180	$(CH_2Br)_2$, 70°C, 9.4 T	$(NH_4)_2SO_4$ (aq.)	51
		11	200	Acetone-d_6	CS_2	9
	$CH_2C(O)CH_3$	−20.0	150	$CDCl_3$, 20°C, 8.3 T	$(NH_4)_2SO_4$ 5M (aq.)	39
	$CH_2C(O)Ph$	−18.8	350	$CDCl_3$, 20°C, 8.3 T	$(NH_4)_2SO_4$ 5M (aq.)	39
		−17	440	DMSO-d_6	CS_2	9
	$CH_2C(O)NH_2$	−16	1,500	DMSO-d_6	CS_2	9
	CH_2COOCH_3	−13.3	78	$CDCl_3$, 30–45°C, 4.7 T	Sulpholane	49
	CH_2Ph	−13	92	$CHCl_3$, 35°C, 7.1 T	CS_2	29
		−11	100	$CHCl_3$, 22°C, 4.7 T	CS_2	50
	CH_2SCH_3	−4.3	39	$CDCl_3$, 30–45°C, 4.7 T	Sulpholane	49
	$CH_2CH{=}CH_2$	−11.3	50	$CDCl_3$, 30–45°C, 4.7 T	Sulpholane	49
	$CH_2CH{=}CCOOEt$	−15	207	$CHCl_3$, 35°C, 7.1 T	CS_2	29
	$CHClCH_3$	−6.6	50	$CDCl_3$, 20°C, 8.3 T	$(NH_4)_2SO_4$ 5M (aq.)	39
	CF_3	−25	1,000	Aceton-d_6 7.1 T	CS_2	9
	$CH(SPh)C(O)CH_3$	−17.0	350	$CDCl_3$, 20°C, 8.3 T	$(NH_4)_2SO_4$ 5M (aq.)	39
	$CH{=}CH_2$	−25	50	$CHCl_3$, 22°C, 4.7 T	CS_2	50
		−20	40	Aceton-d_6	CS_2	9
		−20	90	DMSO-d_6/$CDCl_3$, 4.7T	CS_2	101
	$CH{=}CHCH_3$	−28	115	$CHCl_3$, 35°C, 7.1 T	CS_2	29
		−23	50	$CDCl_3$, 30–45°C, 4.7 T	Sulpholane	49
	$CH{=}C(CH_3)_2$	−22	60	$CHCl_3$, 22°C, 4.7 T	CS_2	50
	(E)$CH{=}CHF$	−29	160	$CHCl_3$, 22°C, 4.7 T	CS_2	50
	(E)$CH{=}CHCl$	−26	200	$CHCl_3$, 22°C, 4.7 T	CS_2	50
	$CH{=}CCl_2$	−25	900	DMSO-d_6	CS_2	9
	(E)$CH{=}CHBr$	−27	110	$CHCl_3$, 22°C, 4.7 T	CS_2	50
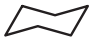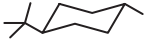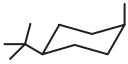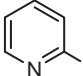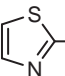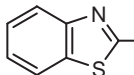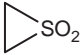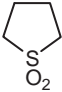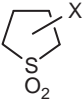
	(Z)CH=CHBr	−26	140	CHCl$_3$, 22°C, 4.7 T	CS$_2$	50
	(E)CH=CHPh	−24	80	CHCl$_3$, 22°C, 4.7 T	CS$_2$	50
		−3	40	(CH$_2$Br)$_2$, 70°C, 9.4 T	(NH$_4$)$_2$SO$_4$ (aq.)	51
		−3	410	(CH$_2$Br)$_2$, 70°C, 9.4 T	(NH$_4$)$_2$SO$_4$ (aq.)	51
		0	290	(CH$_2$Br)$_2$, 70°C, 9.4 T	(NH$_4$)$_2$SO$_4$ (aq.)	51
		−23	77	CHCl$_3$, 20°C, 4.7 T	Na$_2$SO$_4$ 0.2M (aq.)	97
		−32	360	CH$_3$OH, 50°C, 4.7 T	Na$_2$SO$_4$ 0.2M (aq.)	97
		−21	380	CH$_3$OH, 50°C, 4.7 T	Na$_2$SO$_4$ 0.2M (aq.)	97
C$_2$H$_5$	p-F-C$_6$H$_4$	−8	140	Acetone-d$_6$	CS$_2$	9
	m-F-C$_6$H$_4$	−4	60	Acetone-d$_6$	CS$_2$	9
	p-Cl-C$_6$H$_4$	−9	900	DMSO-d$_6$	CS$_2$	9
	CH$_2$SO$_2$C$_2$H$_5$	−10	>500	CDCl$_3$, 20°C, 8.3 T	(NH$_4$)$_2$SO$_4$ 5M (aq.)	39
n-C$_3$H$_7$	p-F-C$_6$H$_4$	−8	150	Acetone-d$_6$	CS$_2$	9

Table A.4.2 *(Continued)*

R	R′	δ	LW	Experimental conditions	Original reference	Refs.
i-C$_3$H$_7$	p-F-C$_6$H$_4$	0	180	Acetone-d$_6$	CS$_2$	9
	m-F-C$_6$H$_4$	5	120	Acetone-d$_6$	CS$_2$	9
	p-Cl-C$_6$H$_4$	3	1,000	DMSO-d$_6$	CS$_2$	9
n-C$_4$H$_9$	p-F-C$_6$H$_4$	−10	160	Acetone-d$_6$	CS$_2$	9
t-C$_4$H$_9$	p-F-C$_6$H$_4$	7	200	Acetone-d$_6$	CS$_2$	9
	p-Cl-C$_6$H$_4$	9	800	DMSO-d$_6$	CS$_2$	9
	m-F-C$_6$H$_4$	11	170	Acetone-d$_6$	CS$_2$	9
CH$_2$CH$_2$Cl	p-MeO-C$_6$H$_4$	−12	55	Acetone-d$_6$	CS$_2$	9
	p-NO$_2$-C$_6$H$_4$	−12	150	Acetone-d$_6$	CS$_2$	9
CH$_2$=CH	p-CH$_3$-C$_6$H$_4$	−21	35	Acetone-d$_6$	CS$_2$	9
	p-CH$_3$O-C$_6$H$_4$	−21	50	Acetone-d$_6$	CS$_2$	9
	p-Cl-C$_6$H$_4$	−22	130	Acetone-d$_6$	CS$_2$	9
	p-Br-C$_6$H$_4$	−22	90	Acetone-d$_6$	CS$_2$	9
	p-NO$_2$-C$_6$H$_4$	−23	210	Acetone-d$_6$	CS$_2$	9
	m-Br-C$_6$H$_4$	−22	120	Acetone-d$_6$	CS$_2$	9
PhCH$_2$	CH$_2$CH$_3$	2	20	Aceton-d$_6$	CS$_2$	9
	n-C$_3$H$_7$	3	40	Aceton-d$_6$	CS$_2$	9
	i-C$_3$H$_7$	8	120	Aceton-d$_6$	CS$_2$	9
	t-C$_4$H$_9$	15	200	Aceton-d$_6$	CS$_2$	9
	CHClCH$_3$	3.5	110	CDCl$_3$, 20°C, 8.3 T	(NH$_4$)$_2$SO$_4$ 5M (aq.)	39
	CHClPh	4.1	330	CDCl$_3$, 20°C, 8.3 T	(NH$_4$)$_2$SO$_4$ 5M (aq.)	39
	COOCH$_3$	−7.3	240	DMF, 30–45°C, 4.7 T	Sulpholane	49
Cl	Ph	−0.1	6,800	Neat, 11.7 T	Na$_2$SO$_4$	40
	CH$_2$Ph	23	5,600	CHCl$_3$, 11.7 T	Na$_2$SO$_4$	40

	CH$_2$CH$_3$	19	2,000	CHCl$_3$, 30°C, 7.1 T	CS$_2$	52
	OCH$_3$	−22	300	CHCl$_3$, 30°C, 7.1 T	CS$_2$	52
	OCH$_2$CH$_3$	−22	300	CHCl$_3$, 30°C, 7.1 T	CS$_2$	52
	CF$_3$	−21	300	CHCl$_3$, 30°C, 7.1 T	CS$_2$	52
F	CH$_2$CH$_3$	17	2,000	Neat, 11.7 T	Na$_2$SO$_4$	40
	OCH$_3$	−22	300	CHCl$_3$, 30°C, 7.1 T	CS$_2$	52
	Ph	4	6,400	Neat, 11.7 T	Na$_2$SO$_4$	40
	CH$_2$Ph	25	5,100	Neat, 11.7 T	Na$_2$SO$_4$	40

Table A.4.3. ^{33}S NMR parameters of cyclic sulphones

	δ	LW	Experimental conditions	Original standard	Refs.
▷SO$_2$	−88	300	CHCl$_3$, 0.1–0.5 M	CS$_2$	47
☐—SO$_2$	−2	230	CHCl$_3$, 0.1–0.5 M	CS$_2$	47
	−2.3	15	CHCl$_3$, 21°C, 7.1 T	CsSO$_4$ 2M (aq.)	7
(S O$_2$ ring)	35	69	CHCl$_3$, 35°C, 7.1 T	CS$_2$	29
	34.7	15	CHCl$_3$, 21°C, 7.1 T	CsSO$_4$ 2M (aq.)	7
	37	50	CHCl$_3$, 22–25°C, 5.9 T	CS$_2$	48
	36.7	50	CDCl$_3$, 30–45°C, 4.7 T	Sulpholane	49
	42	50	CDCl$_3$, 20°C, 4.7 T	SO$_4^{2-}$	101

(X–S O$_2$ ring structure)

	δ	LW	Experimental conditions	Original standard	Refs.
X = 2-CH$_3$	38	7	Acetone-d$_6$	CS$_2$	9
2-SO$_2$Cl	25	85	Acetone-d$_6$	CS$_2$	9
3-CH$_3$	35	60	DMSO, 28°C, 1.9 T	(NH$_4$)$_2$SO$_4$ 4M (aq.)	6
	37	60	DMSO-d$_6$/CHCl$_3$, 4.7 T	CS$_2$	101
3-CH$_2$NO$_2$	32	15	Acetone-d$_6$	CS$_2$	9
3-NH$_2$	33	80	DMSO, 28°C, 1.9 T	(NH$_4$)$_2$SO$_4$ 4M (aq.)	6
	32	10	Acetone-d$_6$	CS$_2$	9
3-NHPh	29	9	Acetone-d$_6$	CS$_2$	9
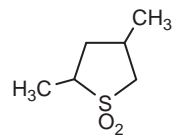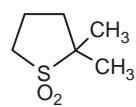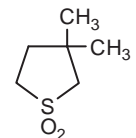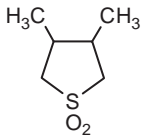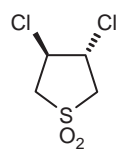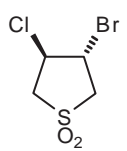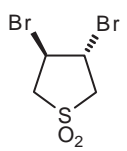
3-NO$_2$	27	40	Acetone-d$_6$	CS$_2$	9
3-OH	36	100	DMSO, 28°C, 1.9 T	(NH$_4$)$_2$SO$_4$ 4M (aq.)	6
	32	10	Acetone-d$_6$	CS$_2$	9
3-OCH$_3$	32	8	Acetone-d$_6$	CS$_2$	9
3-O(CH$_2$)$_2$CH$_3$	31	9	Acetone-d$_6$	CS$_2$	9
3-OPh	31	15	Acetone-d$_6$	CS$_2$	9
3-Ph	33	4	Acetone-d$_6$	CS$_2$	9
3-SCSNCH$_2$CH$_3$	30	20	Acetone-d$_6$	CS$_2$	9
3-SO$_2$NCH$_2$CH$_3$	30	100	Acetone-d$_6$	CS$_2$	9
3-SO$_2$OPh	29	120	Acetone-d$_6$	CS$_2$	9
3-SO$_3$H	33	120	Acetone-d$_6$	CS$_2$	9
3-Cl	28.5	10	Acetone-d$_6$ 20–22°C, 7.1 T	CS$_2$	46
	29	10	Acetone-d$_6$	CS$_2$	46,9

	37	90	DMSO, 28°C, 1.9 T	(NH$_4$)$_2$SO$_4$ 4M (aq.)	6
	38	40	Acetone-d$_6$	CS$_2$	11

	32	207	CHCl$_3$, 35°C, 7.1 T	CS$_2$	29

	29	69	CHCl$_3$, 35°C, 7.1 T	CS$_2$	29

Table A.4.3 *(Continued)*

	δ	LW	Experimental conditions	Original standard	Refs.
	25	115	CHCl$_3$, 35°C, 7.1 T	CS$_2$	29
	16.8	50	Acetone-d$_6$, 20–22°C, 7.1 T	CS$_2$	46
	18.4	15	Acetone-d$_6$, 20–22°C, 7.1 T	CS$_2$	46
	18.5	15	Acetone-d$_6$, 20–22°C, 7.1 T	CS$_2$	46
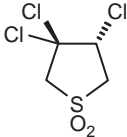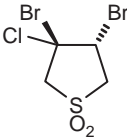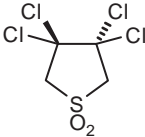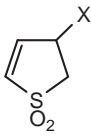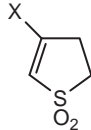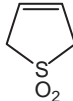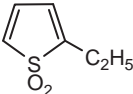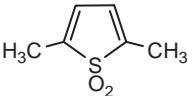
Structure	δ	Δν	Conditions	Ref. compound	Ref.
3,3,4-trichlorotetrahydrothiophene 1,1-dioxide (Cl, Cl / Cl) S O₂	4.0	210	Acetone-d₆, 20–22°C, 7.1 T	CS₂	46
(Cl, Br / Br) S O₂	7.2	105	Acetone-d₆, 20–22°C, 7.1 T	CS₂	46
(Cl, Cl / Cl, Cl) S O₂	−1.2	210	Acetone-d₆, 20–22°C, 7.1 T	CS₂	46

X-substituted 2,5-dihydrothiophene 1,1-dioxide (X) S O₂

X	δ	Δν	Conditions	Ref. compound	Ref.
X = Cl	28	40	Acetone-d₆	CS₂	9
OH	30	30	Acetone-d₆	CS₂	9
OCH₃	29	45	Acetone-d₆	CS₂	9

Table A.4.3 *(Continued)*

	δ	LW	Experimental conditions	Original standard	Refs.

	δ	LW	Experimental conditions	Original standard	Refs.
X = H	39	8	Acetone-d_6	CS_2	9
CH$_3$	38	8	Acetone-d_6	CS_2	9
Cl	25	50	Acetone-d_6	CS_2	9

	δ	LW	Experimental conditions	Original standard	Refs.
	28	50	CHCl$_3$, 22–25°C, 5.9 T	CS_2	48
	27	50	DMSO, 28°C, 1.9 T	(NH$_4$)$_2$SO$_4$ 4M (aq.)	6
	27.7	14	CDCl$_3$, 35–45°C, 4.7 T	Sulpholane	49
	27–31	5–18	Acetone-d_6	CS_2	9
	26.5	18	Acetone, 21°C, 7.1 T	CsSO$_4$ 2M (aq.)	7
	31	310	DMSO-d_6/CDCl$_3$, 20°C, 4.7 T	SO_4^{2-}	101

	δ	LW	Experimental conditions	Original standard	Refs.
	26	50	DMSO-d_6/CDCl$_3$, 20°C, 4.7 T	SO_4^{2-}	101
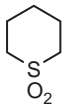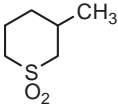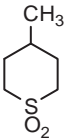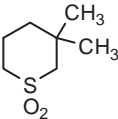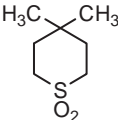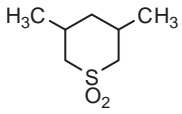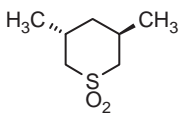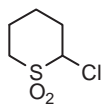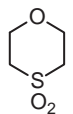
	−12	92	CHCl₃, 35°C, 7.1 T	CS₂	47
	−11.4	44	CHCl₃, 21°C, 7.1 T	CsSO₄ 2M (aq.)	7
	−11	50	CHCl₃, 22–25°C, 5.9 T	CS₂	48
	−9.8	45	CDCl₃, 8.3 T	(NH₄)₂SO₄ 4M (aq.)	39
	−11	92	CHCl₃, 35°C, 7.1 T	CS₂	29
	−12	69	CHCl₃, 35°C, 7.1 T	CS₂	29
	−13	115	CHCl₃, 35°C, 7.1 T	CS₂	29
	−11	138	CHCl₃, 35°C, 7.1T	CS₂	29

Table A.4.3 *(Continued)*

	δ	LW	Experimental conditions	Original standard	Refs.
	−11	92	$CHCl_3$, 35°C, 7.1 T	CS_2	29
	−12	69	$CHCl_3$, 35°C, 7.1 T	CS_2	29
	−9.6	100	$CDCl_3$	$(NH_4)_2SO_4$ 4M (aq.)	39
	−18	100	$CHCl_3$, 22–25°C, 5.9 T	CS_2	48
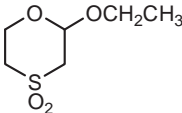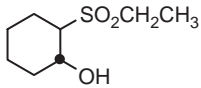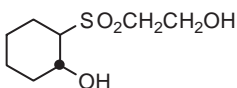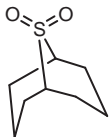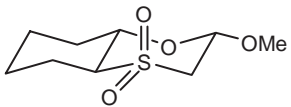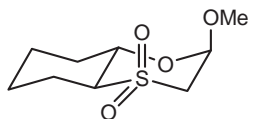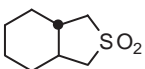
	−18	100	CHCl₃, 22–25°C, 5.9 T	CS₂	48
	10	250	CH₃OH, 22–25°C, 5.9 T	CS₂	48
	7	600	DMSO, 22–25°C, 5.9 T	CS₂	48
	7	1,000	CHCl₃, 22–25°C, 5.9 T	CS₂	48
	5	150	Acetone, 22–25°C, 5.9 T	CS₂	48
	4	225	CH₃OH, 22–25°C, 5.9 T	CS₂	48
	−8	190	CHCl₃, 22–25°C, 5.9 T	CS₂	48

Table A.4.3 *(Continued)*

	δ	LW	Experimental conditions	Original standard	Refs.
	-10	200	CHCl$_3$, 22–25°C, 5.9 T	CS$_2$	48
	-20	200	CHCl$_3$, 22–25°C, 5.9 T	CS$_2$	48
	25	92	CHCl$_3$, 35°C, 7.1 T	CS$_2$	29
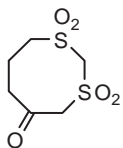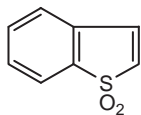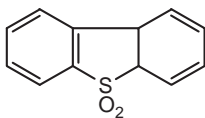
(structure: 1,3-dithiepane-type ring with O₂, S, SO₂ and ketone)	35	645	CHCl₃, 35°C, 7.1 T	CS₂	29
(structure: benzothiophene S,S-dioxide)	17	430	DMSO-d₆/CDCl₃, 20°C, 4.7 T	SO_4^{2-}	101
(structure: dibenzothiophene S,S-dioxide)	4	330	DMSO-d₆/CDCl₃, 20°C, 4.7 T	SO_4^{2-}	101

Table A.5. ^{33}S NMR parameters of sulphonates $R - SO_3^-$

R	δ	LW	Experimental conditions	Original standard	Refs.
CH$_3$	−5.6	28	H$_2$O, 21°C, 4.7 T	Na$_2$SO$_4$ 0.2M (aq.)	38
	−4.8	30	H$_2$O, 37°C, pH = 14, 1.9 T	(NH$_4$)$_2$SO$_4$ 4M (aq.)	58
	−5.2	22	H$_2$O, 37°C, pH = 14, dec., 1.9 T	(NH$_4$)$_2$SO$_4$ 4M (aq.)	58
	−5.6	30	H$_2$O, 37°C, pH = 1, 1.9 T	(NH$_4$)$_2$SO$_4$ 4M (aq.)	58
	−5	150	D$_2$O, 28°C, 1.9 T	(NH$_4$)$_2$SO$_4$ 4M (aq.)	6
n-C$_3$H$_7$	2.2	200	H$_2$O, 21°C, 4.7 T	Na$_2$SO$_4$ 0.2M (aq.)	38
n-C$_4$H$_9$	3.4	350	H$_2$O, 21°C, 4.7 T	Na$_2$SO$_4$ 0.2M (aq.)	38
NaOOCCH$_2$	−9.6	10	H$_2$O, 21°C, 4.7 T	Na$_2$SO$_4$ 0.2M (aq.)	38
NH$_2$CH$_2$	−2.3	80	H$_2$O, 21°C, 4.7 T	Na$_2$SO$_4$ 0.2M (aq.)	38
XCH$_2$CH$_2$SO$_3^-$					
X = H	3.5	134	H$_2$O/D$_2$O (1:1), 22°C, 11.7 T	Na$_2$SO$_4$ 1M (aq.)	35
	4.2	160	H$_2$O, 21°C, 4.7 T	Na$_2$SO$_4$ 0.2M (aq.)	38
CH$_3$	1.7	222	H$_2$O/D$_2$O (1:1), 22°C, 11.7 T	Na$_2$SO$_4$ 1M (aq.)	35
	2.2	200	H$_2$O, 21°C, 4.7 T	Na$_2$SO$_4$ 0.2M (aq.)	38
NH$_2$	−1.3	90	H$_2$O/D$_2$O (1:1), 22°C, 11.7 T	Na$_2$SO$_4$ 1M (aq.)	35
SH	−3.14	78	H$_2$O/D$_2$O (1:1), 22°C, 11.7 T	Na$_2$SO$_4$ 1M (aq.)	35
OH	−3.8	57	H$_2$O/D$_2$O (1:1), 22°C, 11.7 T	Na$_2$SO$_4$ 1M (aq.)	35
Br	−5.5	28	H$_2$O/D$_2$O (1:1), 22°C, 11.7 T	Na$_2$SO$_4$ 1M (aq.)	35
	−6.0	33	H$_2$O, 42°C, pH = 14, 1.9 T	(NH$_4$)$_2$SO$_4$ 4M (aq.)	58
	−6.3	38	H$_2$O, 42°C, pH = 1, 1.9 T	(NH$_4$)$_2$SO$_4$ 4M (aq.)	58
Cl	−6.2	23	H$_2$O/D$_2$O (1:1), 22°C, 11.7 T	Na$_2$SO$_4$ 1M (aq.)	35
NH$_3^+$	−6.6	11	H$_2$O/D$_2$O (1:1), 22°C, 11.7 T	Na$_2$SO$_4$ 1M (aq.)	35
NH$_2$NH	0	33	H$_2$O, 37°C, pH = 14, 1.9 T	(NH$_4$)$_2$SO$_4$ 4M (aq.)	58
CH$_2$=CH	−13.4	35	H$_2$O, 21°C, 4.7 T	Na$_2$SO$_4$ 0.2M (aq.)	38
	−11	70	D$_2$O, 28°C, 1.9 T	(NH$_4$)$_2$SO$_4$ 4M (aq.)	6
CH$_2$=CHCH$_2$	−0.4	74	H$_2$O, 37°C, pH = 1, 1.9 T	(NH$_4$)$_2$SO$_4$ 4M (aq.)	58
NH$_2$CH(COOH)CH$_2$	−9.0	80	D$_2$O, 28°C, 1.9 T	(NH$_4$)$_2$SO$_4$ 4M (aq.)	6
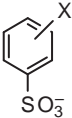
X = H	−11.4	8.8	H$_2$O/D$_2$O (1:1), 22°C, 4.7 T	Na$_2$SO$_4$ 1M (aq.)	63
	−12.1	27	H$_2$O, 41°C, pH = 14, 1.9 T	(NH$_4$)$_2$SO$_4$ 4M (aq.)	58
	−11.8	24	H$_2$O, 35°C, pH = 1, 1.9 T	(NH$_4$)$_2$SO$_4$ 4M (aq.)	58
	−11.7	19	H$_2$O, 38°C, dec. pH = 1, 1.9 T	(NH$_4$)$_2$SO$_4$ 4M (aq.)	58
	−12.2	31	H$_2$O, 41°C, pH = 1, 1.9 T	(NH$_4$)$_2$SO$_4$ 4M (aq.)	58
	−11.1	410	HCl conc., 41°C, pH < 0, 1.9 T	(NH$_4$)$_2$SO$_4$ 4M (aq.)	58
	−12.0	–	H$_2$O, 36°C, 1.9T	(NH$_4$)$_2$SO$_4$ 4M (aq.)	59
	−11.3	8.8	H$_2$O, 20°C, pH = 2, 7.1 T	(NH$_4$)$_2$SO$_4$ 0.1M (aq.)	61
	−11.7	6.5	H$_2$O, 39°C, pH = 2, 7.1 T	(NH$_4$)$_2$SO$_4$ 0.1M (aq.)	61
4-NO$_2$	−15.7	60	H$_2$O/D$_2$O (1:1), 22°C, 4.7 T	Na$_2$SO$_4$ 1M (aq.)	63
	−19.1	–	H$_2$O, 36°C, 1.9 T	(NH$_4$)$_2$SO$_4$ 4M (aq.)	59
	−15.7	58.8	H$_2$O, 20°C, pH = 5, 7.1 T	(NH$_4$)$_2$SO$_4$ 0.12M (aq.)	61
	−15.7	47.5	H$_2$O, 39°C, pH = 5, 7.1 T	(NH$_4$)$_2$SO$_4$ 0.12M (aq.)	61
4-COCH$_3$	−13.9	18	H$_2$O/D$_2$O (1:1), 22°C, 4.7 T	Na$_2$SO$_4$ 1M (aq.)	63
	−13.6	13.8	H$_2$O, 20°C, pH = 4, 7.1 T	(NH$_4$)$_2$SO$_4$ 0.12M (aq.)	61
	−13.9	12.5	H$_2$O, 39°C, pH = 4, 7.1 T	(NH$_4$)$_2$SO$_4$ 0.12M (aq.)	61
4-Cl	−13.2	5.3	H$_2$O/D$_2$O (1:1), 22°C, 4.7 T	Na$_2$SO$_4$ 1M (aq.)	63
	−13.0	9.0	H$_2$O, 20°C, pH = 2, 7.1 T	(NH$_4$)$_2$SO$_4$ 0.12M (aq.)	61
	−13.3	6.2	H$_2$O, 39°C, pH = 2, 7.1 T	(NH$_4$)$_2$SO$_4$ 0.12M (aq.)	61

Table A.5 *(Continued)*

R	δ	LW	Experimental conditions	Original standard	Refs.
4-F	−13.1	4.9	H_2O/D_2O (1:1), 22°C, 4.7 T	Na_2SO_4 1M (aq.)	63
4-Br	−13.3	–	H_2O, 36°C, 1.9 T	$(NH_4)_2SO_4$ 4M (aq.)	59
	−12.8	9.0	H_2O, 20°C, pH = 2, 7.1 T	$(NH_4)_2SO_4$ 0.12M (aq.)	61
	−13.2	7.5	H_2O, 39°C, pH = 2, 7.1 T	$(NH_4)_2SO_4$ 0.12M (aq.)	61
4-CH_3	−11.0	21	H_2O/D_2O (1:1), 22°C, 4.7 T	Na_2SO_4 1M (aq.)	63
	−10.9	35	H_2O, 38°C, pH = 1, 1.9 T	$(NH_4)_2SO_4$ 4M (aq.)	58
	−11.3	–	H_2O, 36°C, 1.9 T	$(NH_4)_2SO_4$ 4M (aq.)	59
	−10.6	21.2	H_2O, 20°C, pH = 2, 7.1 T	$(NH_4)_2SO_4$ 0.12M (aq.)	61
	−11.1	11.5	H_2O, 39°C, pH = 2, 7.1 T	$(NH_4)_2SO_4$ 0.12M (aq.)	61
	−10	90	D_2O, 28°C, 1.9 T	$(NH_4)_2SO_4$ 4M (aq.)	6
4-OH	−10.8	30	H_2O/D_2O (1:1), 22°C, 4.7 T	Na_2SO_4 1M (aq.)	63
4-O^-	−8.1	140	H_2O/D_2O (1:1), 22°C, 4.7 T	Na_2SO_4 1M (aq.)	33
4-NH_2	−9.9	58	H_2O/D_2O (1:1), 22°C, 4.7 T	Na_2SO_4 1M (aq.)	63
	−9.8	51.5	H_2O, 20°C, pH = 11, 7.1 T	$(NH_4)_2SO_4$ 0.12M (aq.)	61
	−10.0	23.8	H_2O, 39°C, pH = 11, 7.1 T	$(NH_4)_2SO_4$ 0.12M (aq.)	61
4-NH_3^+	−14.3	22	H_2O/D_2O (1:1), 22°C, 4.7 T	Na_2SO_4 1M (aq.)	63
	−14.2	18.1	H_2O, 20°C, pH = 1, 7.1 T	$(NH_4)_2SO_4$ 0.12M (aq.)	61
	−14.4	15.6	H_2O, 39°C, pH = 1, 7.1 T	$(NH_4)_2SO_4$ 0.12M (aq.)	61
4-$N(CH_3)_2$	−9.2	79	H_2O/D_2O (1:1), 22°C, 4.7 T	Na_2SO_4 1M (aq.)	63
	−9.6	75.6	H_2O, 20°C, pH = 8, 7.1 T	$(NH_4)_2SO_4$ 0.12M (aq.)	61
	−9.6	45.0	H_2O, 39°C, pH = 8, 7.1 T	$(NH_4)_2SO_4$ 0.12M (aq.)	61
4-$NH(CH_3)_2^+$	−15.3	55	H_2O/D_2O (1:1), 22°C, 4.7 T	Na_2SO_4 1M (aq.)	33
	−15.3	55	H_2O, 20°C, pH = 2, 7.1 T	$(NH_4)_2SO_4$ 0.12M (aq.)	61
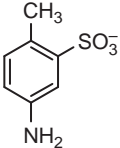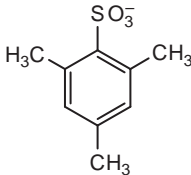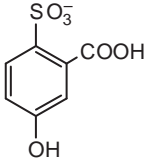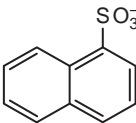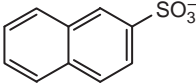
	−15.2	34.5	H_2O, 39°C, pH = 2, 7.1 T	$(NH_4)_2SO_4$ 0.12M (aq.)	61
4-SO_3^-	−13.8	19	H_2O/D_2O (1:1), 22°C, 4.7 T	Na_2SO_4 1M (aq.)	33
	−13.8	18.8	H_2O, 20°C, pH = 8, 7.1 T	$(NH_4)_2SO_4$ 0.12M (aq.)	61
	−14.1	14.2	H_2O, 39°C, pH = 8, 7.1 T	$(NH_4)_2SO_4$ 0.12M (aq.)	61
3-NO_2	−15.9	100	H_2O/D_2O (1:1), 22°C, 4.7 T	Na_2SO_4 1M (aq.)	33
	−17.9	–	H_2O, 36°C, 1.9 T	$(NH_4)_2SO_4$ 4M (aq.)	59
	−15.9	49.0	H_2O, 20°C, pH = 2, 7.1 T	$(NH_4)_2SO_4$ 0.12M (aq.)	61
	−16.2	42.5	H_2O, 39°C, pH = 2, 7.1 T	$(NH_4)_2SO_4$ 0.12M (aq.)	61
3-CH_3	−10.7	–	H_2O, 36°C, 1.9 T	$(NH_4)_2SO_4$ 4M (aq.)	59
	−10.9	18.8	H_2O, 20°C, pH = 2, 7.1 T	$(NH_4)_2SO_4$ 0.12M (aq.)	61
	−11.2	8.8	H_2O, 39°C, pH = 2, 7.1 T	$(NH_4)_2SO_4$ 0.12M (aq.)	61
3-OH	−12.3	15	H_2O/D_2O (1:1), 22°C, 4.7 T	Na_2SO_4 1M (aq.)	33
3-O^-	−9.5	70	H_2O/D_2O (1:1), 22°C, 4.7 T	Na_2SO_4 1M (aq.)	33
3-NH_2	−11.1	19	H_2O/D_2O (1:1), 22°C, 4.7 T	Na_2SO_4 1M (aq.)	33
3-NH_3^+	−15.1	37	H_2O/D_2O (1:1), 22°C, 4.7 T	Na_2SO_4 1M (aq.)	33
3-CF_3	−15.3	–	H_2O, 36°C, 1.9 T	$(NH_4)_2SO_4$ 4M (aq.)	59
	−14.2	19.5	H_2O, 20°C, pH = 2, 7.1 T	$(NH_4)_2SO_4$ 0.12M (aq.)	61
	−14.4	18.2	H_2O, 39°C, pH = 2, 7.1 T	$(NH_4)_2SO_4$ 0.12M (aq.)	61
3-SO_3^-	−13.9	22	H_2O/D_2O (1:1), 22°C, 4.7 T	Na_2SO_4 1M (aq.)	33
	−14	51	H_2O, 37°C, pH = 1, 1.9 T	$(NH_4)_2SO_4$ 4M (aq.)	58
	−13.9	21.5	H_2O, 20°C, pH = 4, 7.1 T	$(NH_4)_2SO_4$ 0.12M (aq.)	61
	−14.2	16.0	H_2O, 39°C, pH = 4, 7.1 T	$(NH_4)_2SO_4$ 0.12M (aq.)	61
2-SO_3^-	−19	240	H_2O, 37°C, pH = 1, 1.9 T	$(NH_4)_2SO_4$ 4M (aq.)	58
2-CHO	−18	99	H_2O, 37°C, pH = 1, 1.9 T	$(NH_4)_2SO_4$ 4M (aq.)	58

	−14	27	H_2O, 37°C, pH = 1, 1.9 T	$(NH_4)_2SO_4$ 4M (aq.)	58

Table A.5 *(Continued)*

R	δ	LW	Experimental conditions	Original standard	Refs.
	−16	38	H_2O, 37°C, pH = 1, 1.9 T	$(NH_4)_2SO_4$ 4M (aq.)	58
	−10	80	H_2O, 37°C, pH = 1, 1.9 T	$(NH_4)_2SO_4$ 4M (aq.)	58
	−15.2 −11 −15.2	12 46 –	H_2O, 21°C, 4.7 T H_2O, 37°C, pH = 1, 1.9 T D_2O, pH 11–14, 5.9 T	Na_2SO_4 0.2M (aq.) $(NH_4)_2SO_4$ 4M (aq.) $(NH_4)_2SO_4$ (aq.)	38 58 62
	−11.5 −11.6	15 –	H_2O, 21°C, 4.7 T D_2O, pH 11–14, 5.9 T	Na_2SO_4 0.2M (aq.) $(NH_4)_2SO_4$ (aq.)	38 62
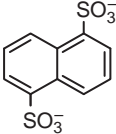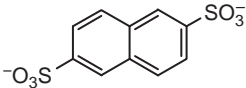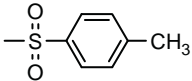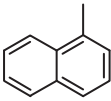
	−16.1	–	D_2O, pH 11–14, 5.9 T	$(NH_4)_2SO_4$ (aq.)	62
	−12.7	–	D_2O, pH 11–14, 5.9 T	$(NH_4)_2SO_4$ (aq.)	62
d-canfor-10-sulphonic acid	−0.3	113	H_2O, 37°C, pH<1, 1.9 T	$(NH_4)_2SO_4$ 4M (aq.)	58

Table A.6. ^{33}S NMR parameters of sulphur–nitrogen compounds
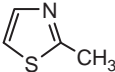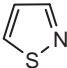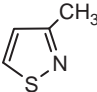
		δ	LW	Experimental conditions	Original reference	Refs.
Sulphimides						
R, R′	**R″**					
p-CH$_3$C$_6$H$_4$, CH$_3$	p-CH$_3$C$_6$H$_4$SO$_2$	−18	1,200	CHCl$_3$, 35°C, 7.1 T	CS$_2$	29
p-CH$_3$OC$_6$H$_4$, CH$_3$	p-CH$_3$C$_6$H$_4$SO$_2$	2	1,100	CHCl$_3$, 35°C, 7.1 T	CS$_2$	29
C$_6$H$_5$CH$_2$, CH$_3$	p-CH$_3$C$_6$H$_4$SO$_2$	−10	1,500	CHCl$_3$, 35°C, 7.1 T	CS$_2$	29
C$_6$H$_5$CH$_2$, CH$_3$	p-CH$_3$C$_6$H$_4$SO$_2$	−13	2,500	CHCl$_3$, 35°C, 7.1 T	CS$_2$	29
Sulphoximides						
R, R′	**R″**					
Ph, CH$_3$	CH$_3$	−31	1,200	CHCl$_3$, 35°C, 7.1 T	CS$_2$	29
p-CH$_3$C$_6$H$_4$, CH$_3$	H	−28	1,200	CHCl$_3$, 35°C, 7.1 T	CS$_2$	29
Ph, CH$_3$		−39	700	CHCl$_3$, 35°C, 7.1 T	CS$_2$	29
p-CH$_3$C$_6$H$_4$, CH$_3$	Phtalimido	−23	1,100	CHCl$_3$, 35°C, 7.1 T	CS$_2$	29
	Phtalimido	−29	1,500	CHCl$_3$, 35°C, 7.1 T	CS$_2$	29
CH$_2$ = CH,						

Sulphonamides

R—S(=O)(=O)—N(R')(R'')
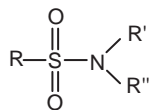
R	R', R''					
CH$_3$	CH$_3$, CH$_3$	-10.2	50–200	CHCl$_3$, 2.4 T	CS$_2$	64
Ph	H, H	-25	980	Acetone, 11.7 T	CsSO$_4$	40
Ph	CH$_3$, CH$_3$	-2.2	50–200	CHCl$_3$, 2.4 T	CS$_2$	64
Ph	H, NH$_2$	-7	2,300	Acetone, 11.7 T	CsSO$_4$	40
p-CH$_3$C$_6$H$_4$	H, H	-30	1,380	CHCl$_3$, 35°C, 7.1 T	CS$_2$	29
p-CH$_3$C$_6$H$_4$	CH$_3$, NO	-18	5,000	CHCl$_3$, 11.7 T	CsSO$_4$	40
NH$_2$	H, H	-15	256	D$_2$O, 7.1 T	CsSO$_4$	65

Table A.7. ^{33}S NMR parameters of miscellaneous organic compounds

	δ	LW	Experimental conditions	Original reference	Refs.
CS_2	-333	350	Neat, 7.1 T	Cs_2SO_4 2M (aq.)	7
$(CH_3CH_2)_2S_2$	-168	5,120	Neat, CW	CS_2	3
	-297	10,600	Neat, 11.7 T	Na_2SO_4	40
CH_3CH_2NCS	-340	4,300	Neat, 7.1 T	Cs_2SO_4 2M (aq.)	7
$PhNCS$	-570	23,000	Neat, 11.7 T	Na_2SO_4	40
CH_3SCN	-369	450	Neat, 11.7 T	Na_2SO_4	40
$PhN{=}S{=}O$	261	6,800	Neat, 7.1 T	Cs_2SO_4 2M (aq.)	65
$(CH_3)_3CN{=}S{=}O$	257	1,460	Neat, 7.1 T	Cs_2SO_4 2M (aq.)	65
$(CH_3)_3SiN{=}S{=}NSi(CH_3)_3$	299	3,406	Neat, 7.1 T	Cs_2SO_4 2M (aq.)	65
$(CH_3)_3SiN{=}S{=}NC(CH_3)_3$	272	4,270	Neat, 7.1 T	Cs_2SO_4 2M (aq.)	65
	-72	4,200	Neat, 11.7 T	Na_2SO_4	40
	53.7	–	Neat, 8.5 T	$(NH_4)_2SO_4$ 4M (aq.)	36
	51	7,700	Neat, 11.7 T	Na_2SO_4	40
$PhSO_2H$	-20	610	$CHCl_3$, 11.7 T	Na_2SO_4	40
$PhSO_2Na$	-13	640	NaOH aq., 11.7 T	Na_2SO_4	40
$p\text{-}CH_3C_6H_5SO_2Na$	-11	$>10,000$	H_2O, 11.7 T	Na_2SO_4	40
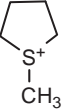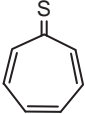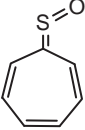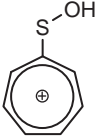
CH$_3$CH$_2$SOCl	218	6,200	Neat, 11.7 T	Na$_2$SO$_4$	40
HOCH$_2$SO$_2$Na	−5	500	H$_2$O, 7.1 T	Na$_2$SO$_4$	40
CH$_3$OSO$_3$Na	−10	700	H$_2$O, 7.1 T	Cs$_2$SO$_4$ 2M (aq.)	7
(CH$_3$O)$_2$SO$_2$	−12.6	1,400	Neat, 7.1 T	Cs$_2$SO$_4$ 2M (aq.)	7
(CH$_3$)$_2$S$^+$I$^-$	−285	5,400	D$_2$O, 45°C, 14.1 T	CS$_2$	30
	−238	5,600	D$_2$O, 45°C, 14.1 T	CS$_2$	30

	−287	11,500	CDCl$_3$, −40°C, 9.4 T	(NH$_4$)$_2$SO$_4$	41

	−6	–	CDCl$_3$, 9.4 T	(NH$_4$)$_2$SO$_4$	41

	−85	–	CF$_3$COOH	(NH$_4$)$_2$SO$_4$	42

(CH$_3$)$_3$PS	−536	–	CDCl$_3$, 22°C, 9.4 T	CS$_2$	45

Table A.7 *(Continued)*

	δ	LW	Experimental conditions	Original reference	Refs.
$(C_6H_5)_3PS$	-408	$>3,000$	$CDCl_3$ 20°C, 9.4 T	CS_2	45
Cl_3PS	-105	$>3,000$	10% C_6D_6, 45°C, 9.4 T	CS_2	45
$S_4N_4O_2$	-35	1,400	THF, 7.1 T	Cs_2SO_4 2M (aq.)	65

Table A.8. ^{33}S NMR parameters of some inorganic sulphides

	δ	LW	Experimental conditions	Original reference	Refs.
Li$_2$S	−680	1,380	Solid, 11.7 T	CS$_2$	27
Na$_2$S	−592	500	Solid, 11.7 T	CS$_2$	27
	−594	1,600	Solid, CW	CS$_2$	3
	−580	3,200	H$_2$O, 7.1 T	Cs$_2$SO$_4$ 2M (aq.)	67
	−588	3,700	In NaOH 0.1 M, 7.1 T	CsSO$_4$ 2M (aq.)	67
	−583	2,700	In NaOH 1 M, 7.1 T	CsSO$_4$ 2M (aq.)	67
MgS	−507	300	Solid, 11.7 T	CS$_2$	27
CaS	−362	100	Solid, 11.7 T	CS$_2$	27
SrS	−290.2	100	Solid, 11.7 T	CS$_2$	27
BaS	− 42	250	Solid, 11.7 T	CS$_2$	27
PbS	−626, -630	300, 580	Solid, 11.7 T	CS$_2$	27
CdS	−617	–	Solid, 11.7 T	CS$_2$	27
ZnS	−560	–	Solid, 11.7 T	CS$_2$	27
ZnS (sphalerite)	−563	65	Solid	CS$_2$	3
(NH$_4$)$_2$S$_n$	−584	2,200	In H$_2$O, 7.1 T	Cs$_2$SO$_4$ 2M (aq.)	7

Table A.9. ^{33}S NMR parameters of some inorganic sulphates

	δ	LW	Experimental conditions	Original reference	Refs.
Na_2SO_4	-3	2,300	Solid, 11.7 T	CS_2	27
	0.06	6.1	1.4 M in H_2O, 5.9 T	$(NH_4)_2SO_4$ (aq.)	74
	-0.55	9.5	1 M in H_2O, pH = 6.4, 7.1 T	Cs_2SO_4 2M (aq.)	26
K_2SO_4	1	4,300	Solid, 11.7 T	CS_2	27
Rb_2SO_4	-4	3,500	Solid, 11.7 T	CS_2	27
Cs_2SO_4	2	3,200	Solid, 11.7 T	CS_2	27
$MgSO_4$	-1.2	7.0	0.1 M in H_2O, pH = 6.8, 7.1 T	Cs_2SO_4 2M (aq.)	26
	-1.4	12.0	1.0 M in H_2O, pH = 8.2, 7.1 T	Cs_2SO_4 2M (aq.)	26
	-1.45	18.0	2.0 M in H_2O, pH = 7.8, 7.1 T	Cs_2SO_4 2M (aq.)	26
	-1.6	37.0	4.0 M in H_2O, pH = 7.5, 7.1 T	Cs_2SO_4 2M (aq.)	26
$CaSO_4$	-7	3,500	Solid, 11.7 T	CS_2	27
$CaSO_4 \cdot 2H_2O$	4	2,000	Solid, 11.7 T	CS_2	27
$(NH_4)_2SO_4$	-1.0	3.3	2 M in H_2O, pH = 5.7, 7.1 T	Cs_2SO_4 2M (aq.)	26
$Al_2(SO_4)_3$	-1.6	46.0	0.4 M in H_2O, pH = 2.9, 7.1 T	Cs_2SO_4 2M (aq.)	26
Tl_2SO_4	-13	3,600	Solid, 11.7 T	CS_2	27
$CuSO_4$	58.4	167	0.4 M in H_2O, 5.9 T	$(NH_4)_2SO_4$ (aq.)	74
	67.0	135	0.8 M in H_2O, 5.9 T	$(NH_4)_2SO_4$ (aq.)	74
$CdSO_4$	-0.8	38	0.8 M in H_2O, 5.9 T	$(NH_4)_2SO_4$ (aq.)	74
Ce_2SO_4	1.1	6.3	0.7 M in H_2O, 5.9 T	$(NH_4)_2SO_4$ (aq.)	74
$Na_2Ca(SO_4)_2$	5	1,700	Solid, 11.7 T	CS_2	27
$Na_2Mg(SO_4)_2 \cdot 4H_2O$	-12	16,000	Solid, 11.7 T	CS_2	27
$KAl(SO_4) \cdot 12H_2O$	-6	2,100	Solid, 11.7 T	CS_2	27
$RbAl(SO_4)_2 \cdot 12H_2O$	1	1,050	Solid, 11.7 T	CS_2	27
$CsAl(SO_4)_2 \cdot 12H_2O$	-2	950	Solid, 11.7 T	CS_2	27
$NH_4Al(SO_4)_2 \cdot 12H_2O$	0	950	Solid, 11.7 T	CS_2	27
$TlAl(SO_4)_2 \cdot 12H_2O$	-1	1,050	Solid, 11.7 T	CS_2	27

Table A.10. ^{33}S NMR parameters of miscellaneous inorganic compounds

	δ	LW	Experimental conditions	Original reference	Refs.
$(NH_4)_2[WS_nO_{4-n}]$ (liquid)					
$n = 4$	159	13	0.3–0.4 M in H_2O, 7.1 T	Cs_2SO_4 2M (aq.)	7,71,72
$n = 3$	57	140	0.3–0.4 M in H_2O, 7.1 T	Cs_2SO_4 2M (aq.)	7,71
$n = 2$	−56	220	0.3–0.4 M in H_2O, 7.1 T	Cs_2SO_4 2M (aq.)	7,71
$n = 1$	−186	300	0.3–0.4 M in H_2O, 7.1 T	Cs_2SO_4 2M (aq.)	7,71
$(NH_4)_2[WS_4]$ (solid)			Solid state, 14.1 T	Cs_2SO_4 1M (aq.)	73
S(1), S(2)	389	–			
S(3)	396	–			
S(4)	380	–			
$(Et_4N)_2[WS_4]$	373	45	0.4 M in MeCN, 4.7 T	Cs_2SO_4 2M (aq.)	72
$(NH_4)_2[MoS_nO_{4-n}]$ liquid					
$n = 4$	344	38	0.4 M in H_2O, 4.7 T	Cs_2SO_4 2M (aq.)	72
	345	38	0.3–0.4 M in H_2O, 7.1 T	Cs_2SO_4 2M (aq.)	7,71
$n = 3$	240	170	0.3–0.4 M in H_2O, 7.1 T	Cs_2SO_4 2M (aq.)	7,71
$n = 2$	123	250	0.3–0.4 M in H_2O, 7.1 T	Cs_2SO_4 2M (aq.)	7,71
$n = 1$	−25	200	0.3–0.4 M in H_2O, 7.1 T	Cs_2SO_4 2M (aq.)	7,71
$(NH_4)_2[MoS_4]$ (solid)	347	–	Solid state, 14.1 T	Cs_2SO_4 1M (aq.)	73
$(Et_4N)_2[MoS_4]$	183	24	0.4 M in MeCN, 4.7 T	Cs_2SO_4 2M (aq.)	72
$(nPr_4N)_2[(CN)CuS_2WS_2]$	248	404	0.4 M in MeCN, 4.7 T	Cs_2SO_4 2M (aq.)	72
$(nPr_4N)_2[(CN)AgS_2WS_2]$	106	974	0.4 M in MeCN, 4.7 T	Cs_2SO_4 2M (aq.)	72
$(nPr_4N)_2[(CN)_2Cu_2S_2WS_2]$	16	959	0.4 M in MeCN, 4.7 T	Cs_2SO_4 2M (aq.)	72
$(nPr_4N)_2[(CN)CuS_2MoS_2]$	445	257	0.4 M in MeCN, 4.7 T	Cs_2SO_4 2M (aq.)	72
$(nPr_4N)_2[(PhS)CuS_2MoS_2]$	436	383	0.4 M in MeCN, 4.7 T	Cs_2SO_4 2M (aq.)	72
$(nPr_4N)_2[(CN)AgS_2MoS_2]$	257	830	0.4 M in MeCN, 4.7 T	Cs_2SO_4 2M (aq.)	72
$(nPr_4N)_2[(CN)_2Cu_2S_2MoS_2]$	139	835	0.4 M in MeCN, 4.7 T	Cs_2SO_4 2M (aq.)	72
CS_2	−333	375	Neat, 8.5 T	$(NH_4)_2SO_4$ 4M (aq.)	36
	−333	350	Neat, 7.1 T	Cs_2SO_4 2M (aq.)	7

Table A.10 *(Continued)*

	δ	LW	Experimental conditions	Original reference	Refs.
OCS	−594	–	Neat, 8.5 T	$(NH_4)_2SO_4$ 4M (aq.)	36
H_2S	−503	–	Neat, 22°C, 8.5 T	$(NH_4)_2SO_4$ 4M (aq.)	36
$HFSO_3$	−22.4	–	Neat, 22°C, 8.5 T	$(NH_4)_2SO_4$ 4M (aq.)	36
SO_2	374.9	315	Liq., 8.5 T	$(NH_4)_2SO_4$ 4M (aq.)	28,36
$SOCl_2$	224	–	Liq., 8.5 T	$(NH_4)_2SO_4$ 4M (aq.)	36
SO_2Cl_2	−44.7	–	Neat, 22°C, 8.5 T	$(NH_4)_2SO_4$ 4M (aq.)	36
SO_2F_2	−40.8	–	Neat, −50°C, 8.5 T	$(NH_4)_2SO_4$ 4M (aq.)	36
SF_6	−176.6	–	Neat, 22°C, 8.5 T	$(NH_4)_2SO_4$ 4M (aq.)	36
$Na_2S_2O_3$	36.3	37	In D_2O, 2.1 T	SO_4^{2-}	80
	33.5	30	In H_2O, 5.9 T	$(NH_4)_2SO_4$ (aq.)	74
$(NH_4)_2S_2O_3$	34.5	36	4 M in H_2O, 6.91 MHz	Na_2SO_4 4M (aq.)	5,36
$K_2S_2O_8$	−23	3,000	H_2O sat., 11.7 T	Na_2SO_4 sat (aq.)	40
H_2SO_4	108	2,300	Conc., CW	CS_2	3
	−6.2	1,650	In H_2O 1:1, 5.9 T	$(NH_4)_2SO_4$ (aq.)	74
	−9.9	830	In H_2O 1:2, 5.9 T	$(NH_4)_2SO_4$ (aq.)	74
	−10.8	660	In H_2O 1:5, 5.9 T	$(NH_4)_2SO_4$ (aq.)	74
	−8.8	–	5 M in H_2O, 8.3 T	$(NH_4)_2SO_4$ 4M (aq.)	36

CHAPTER 2

NMR of Peptide Toxins

K. Johan Rosengren, Norelle L. Daly and **David J. Craik**

Contents

Abstract   This article gives an overview of the use of NMR to determine the structures of peptide-based toxins, with 'toxin' loosely defined as a peptide that has a harmful effect on any organism. We focus on peptides up to 100 amino acids as these are particularly amenable to NMR structural analysis. Typically these peptides are soluble, stable, synthetically accessible and give well-defined NMR spectra. The coverage includes toxins produced by bacteria, plants and animals, and there is a particular emphasis on disulphide-rich peptides. An analysis of the Protein Data Bank (PDB) shows that NMR has played an important role in determining the structures of a wide range of toxins and has provided insights into their structure–function relationships. Examples of classes of peptides covered include antimicrobial peptides,

Division of Chemistry and Structural Biology, Institute for Molecular Bioscience, The University of Queensland, Brisbane, Qld 4072, Australia

defensins, cyclotides and conotoxins. A number of these have applications in drug design, and selected examples are described.

1. INTRODUCTION

NMR has played an important role in the delineation of the three-dimensional (3D) structures of a wide range of peptide-based toxins. The aim of this review is to give an overall perspective of the range of structures that are seen in these toxins and to highlight how NMR has been particularly useful in their determination. We broadly classify toxins as any molecule that has a toxic effect on an organism but here we restrict our coverage to peptide-based toxins. They range from classic protein toxins present in the venoms of a wide range of animals, including scorpions, spiders and snakes, to a range of antimicrobial peptides.

Our coverage includes bacterial, plant and animal toxins and we focus mainly on the period from approximately 2003 onwards, with some early examples also included for historical perspective, or for completeness in defining the scope of structures determined. For the examples we describe in more depth, there is an emphasis on studies from our laboratory, but these are illustrative of a wide range of studies from other laboratories. Our laboratory has had a particular interest in peptides that have head-to-tail cyclised backbones and so a number of the examples fit this theme.

In this article, we do not cover the methodological aspects of NMR structure determination of peptides. The reader is referred to a recent article and review on this topic.[1,2] Rather, our focus is describing the structures themselves and the role that NMR has played in providing insights into the biology and structure–activity relationships of toxins.

2. NMR AS A TOOL FOR DETERMINING THE STRUCTURES OF TOXINS

NMR is particularly suitable for the study of peptidic toxins because these molecules are typically small in size (less than ~ 50 amino acids), are usually highly soluble and very often have well-defined structures stabilised by disulphide bonds, which predispose them to have excellent dispersion in their NMR spectra. Indeed, small disulphide-rich peptides are perhaps the one area of structural biology where NMR dominates over X-ray crystallography as the preferred structural technique. The Protein Data Bank (PDB), for example, shows that of the approximately 50,000 structures deposited, less than 20% have been determined by NMR, but if the analysis is done over peptides smaller than 50 amino acids then the proportion of NMR structures is approximately 90%. An example of the important role of NMR in structure determination of peptide toxins involves those from marine cone snails known as conotoxins. Of the 125 conotoxin structures

reported in the PDB, 115 have been determined using NMR methods.[3] Figure 1 summarises the features of peptide-based toxins that make them particularly suitable for NMR analysis.

Due to the small size of peptide toxins, there is usually no need to undertake isotopic labelling for structural analysis, and most NMR structures of toxins deposited in the PDB have been derived exclusively using two-dimensional homonuclear NMR methods. The relatively large amounts of sample required for NMR studies (typically >1 mg), and the fact that, in general, only microgram quantities can be conveniently obtained from native sources, often dictate the use of synthetic samples for structural studies. This trend is changing with the development of improved sensitivity, arising from a combination of higher field magnets, nano- and cryoprobes, and the generally increasing sensitivity of NMR spectrometers.

The majority of structures have been done on peptides made using solid-phase peptide synthesis. The assembly and folding of peptides of up to 50 amino acids is relatively straightforward using this approach.[4] There are some instances where peptides for structure determination were prepared using recombinant expression in bacterial systems, but this is atypical. First, because there is no need to do this if the sample is not required to be isotopically labelled, and second, because toxin molecules are often difficult to express in bacterial cells as they are toxic to cells by nature. Nevertheless, there are some cases where it is advantageous to incorporate labels into peptide toxins. NMR methods have been used to take advantage of these isotope labels, for example, to study complexes between toxins and target molecules, resolve complex post-translational modifications, define hydrogen bonds or characterise relaxation parameters. The introduction of labels is not strictly limited to peptides produced recombinantly in bacteria. For example, a recent study showed that it is possible to ^{15}N label peptides in whole plants to facilitate HSQC studies.[5]
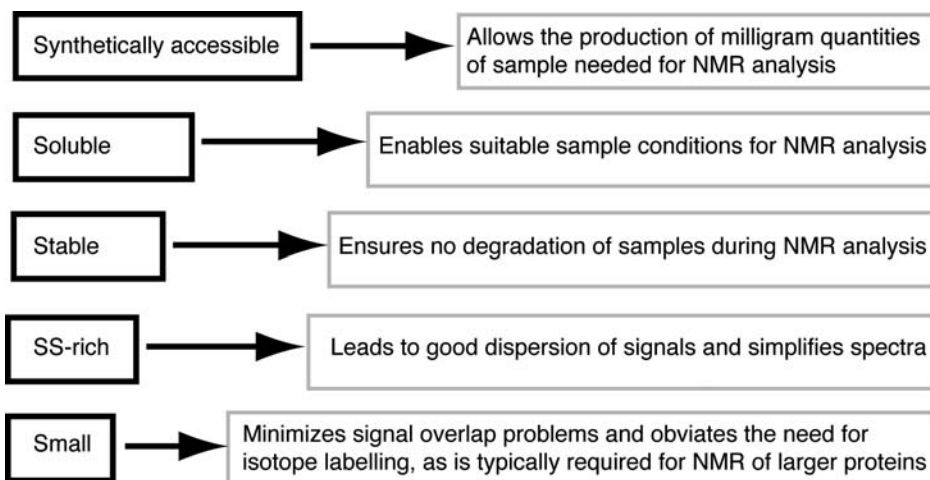

Figure 1 Overview of factors that make NMR a particularly useful tool for the structural characterisation of peptide toxins.

Table 1 gives a list of the toxins that have been structurally characterised by NMR in the period of coverage of this review. The sequences were selected from entries deposited in the PDB from January 2003 onwards, which contained the keywords 'toxin' and 'NMR', along with a few additional entries where the molecules are toxic but this keyword was not used in the original PDB descriptor. We include only entries with an arbitrary cut-off of <100 amino acid residues. The length of the table highlights the significant contribution that NMR has made to the structural biology of peptide toxins. We broadly grouped the entries under the headings bacterial, plant and animal toxins and now describe some illustrative examples in more detail.

3. MICROBIAL TOXINS

3.1 Bacterial toxins

Bacteria have developed methods for generating peptide toxins that are secreted into the surrounding media and that, by interacting with or inhibiting organisms in their proximity, provide the producing strain with a competitive advantage. Among these molecules are several potent bacterial toxins that are well known because of their influence on human health, including botulinum toxin, tetanus toxin and diphtheria toxin. However, these molecules are very large proteins or protein complexes that are not amenable to NMR studies, and thus not within the scope of this review. Instead, in the following section, we focus on the many classes of microbial peptide toxins of <100 residues, for which NMR is often the method of choice for structural studies. The majority of these peptides are antimicrobial and their bioactivity is directed towards organisms closely related to the producing ones.[6,7] The production of these compounds requires sophisticated mechanisms to ensure self-immunity and these peptides are often produced as inactive precursors that are subsequently activated by proteolytic digestion by specific proteases and/or by post-translational modifications.[8] These activation events are generally performed by helper proteins that are encoded together with the precursor gene and exporter/self-immunity genes in gene clusters,[8,9] and in many cases, due to the potential toxic effects on the producer organisms, activation is often linked to efficient export.[9] Alternatively, specific self-immunity proteins are produced that bind to and inhibit the effect of the toxin prior to its secretion.[10]

Microbial and fungal peptide toxins vary greatly in size, structure and consequently mechanism of action and NMR has, in many cases, proven to be the key technique for characterising their structures. This, in turn, has provided important insights into their biological function.

3.2 Microcins

Microcins are peptides that are produced by Gram-negative bacteria, including *Escherichia coli*, that inhibit the growth of competing related genera, thereby

Table 1 Structures of peptide toxins solved by solution NMR techniques from 2003 onwards and submitted to the PDB

PDB ID	Sequence[a]	Chain length[b]	Descriptor[c]	Source[d]
Microbial and fungal toxins				
1S7P	GGAGHVPEYF	10	Thermolysin-digested microcin J25	*Escherichia coli*
1S7P	VGIGTPISFYG	11	Thermolysin-digested microcin J25	*E. coli*
1VM2	GLFDKLKSLVSDFX[d]	14	Anticancer peptide design based on the N-terminal sequence of *E. coli* enzyme IIA (glucose)	
1VM3	GLFDIVKSLVSDFX	14	Membrane-targeting peptide design based on the N-terminal sequence of *E. coli* enzyme IIA (glucose)	
1VM4	GLFDIVKKLVSDFX	14	Antibacterial and antitumour peptide design based on the N-terminal membrane anchor of *E. coli* enzyme IIA (glucose)	
1P0J	AKKVFKRLEKLFSKIQNWKX	20	HP (2-20), Asp to Trp modification in sds-d25 micelles	
1P0L	AKKVFKRLEKLFSKIWNDKX	20	HP (2-20), Gln to Trp modification in sds-d25 micelles	
1P0O	AKKVFKRLEKLFSKIWNWKX	20	HP (2-20), substitution of Trp for Gln and Asp at position 17 and 19 modification in sds-d25 micelles	
1P5K	AKKVFKRLEKSFSKIQNDKX	20	HP (2-20), Ser to Leu11 modification in sds-d25 micelles	
1P5L	AKKVSKRLEKLFSKIQNDKX	20	HP (2-20), Phe5 to Ser modification in sds-d25 micelles	
1MQX	CAFALPGGGGVCALAAECIX	20	Type-B lantibiotics mersacidin in meoh/H_2O Mixture	*Bacillus* sp. HIL-Y85/54728
1MQY	CAFALPGGGGVCALAAECIX	20	Type-B lantibiotics mersacidin in DPC micelles	*Bacillus* sp. HIL-Y85/54728

Table 1 *(Continued)*

PDB ID	Sequence[a]	Chain length[b]	Descriptor[c]	Source[d]
1MQZ	CAFALPGGGGVCALAAECIX	20	Type-B lantibiotics mersacidin bound to lipid II in DPC micelles	*Bacillus* sp. HIL-Y85/ 54728
1OT0	AKKVFKRLEKLFSKIQNWKX	20	HP (2-20), AMP and its analogues	*Helicobacter pylori*
1P0G	AKKVFKRLEKLFSKIQNDKX	20	HP (2-20), AMP and its analogues	*H. pylori*
1Q71	GGAGHVPEYFVGIGTPISFYG	21	Microcin J25, a threaded sidechain-to-backbone ring structure	*E. coli*
2KAM	MAQDIISTIGDLVKWIIDTVNKFTKK	26	δ-Toxin	*Staphylococcus aureus*
1YTR	KSSAYSLQMGATAIKQVKKLFKKWGW	26	Plantaricin a in DPC micelles	*Lactobacillus plantarum*
1Z64	GWGSFFKKAAHVGKHVGKAALTHYLX	26	Pleurocidin in DPC micelles	*Pseudopleuronectes americanus*
2HGO	ETCVSCVNFGNGFCGDNCGNSWACSGC	27	Cassiicolin	*Corynespora cassiicola*
2IT7	GCPRILMRCKQDSDCLAGCVCGPNGFCG	28	Squash trypsin inhibitor EETI-II	*Ecballium elaterium*
1W9N	XAAIVKAAIKAAKKLCRGFALACGCHFAGKK	31	Epilancin 15x, novel antibiotic	*Staphylococcus epidermidis*
2AB9	GYKTSISTITIEDNGRCTKSIPPICFPDGRP	31	Precursor protein that produces the cyclic trypsin inhibitor SFTI-1	*Helianthus annuus*
2JUI	FNRGGYNFGKSVRHVVDAIGSVAGIRGILKSIR	33	Two-peptide bacteriocin plantaracin EF	*L. plantarum*
2DDL	AFCNLRMCQLSCRKSLGCLLGKCIGDKCKCYGC	33	Lei4P	*Leiurus quinquestriatus hebraeus*
2RLW	VFHAYSARGVRNNYKSAVGPADWVISAVRGFIHG	34	Two-peptide bacteriocin plantaracin EF	*L. plantarum*
1PXQ	NKGCATCSIGAACLVDGPIPDFEIAGATGLFGLWG	35	Subtilosin A	*Bacillus subtilis*
2JPK	KKWGWLAWVDPAYEFIKGFGKG AIKEGNKDKWKNI	35	Lactococcin G-b in DPC	*Lactococcus lactis*
2JPM	KKWGWLAWVDPAYEFIKGFGK GAIKEGNKDKWKNI	35	Lactococcin G-b in TFE	*L. lactis*
2KC8	GSHKQTLLSDEDAELVEIVKERLRNPKPVRVTLDEL	36	RelE (R81A/R83A) mutant in complex with antitoxin relbc (K47-L79) peptide	*E. coli*

2JPJ	GTWDDIGQGIGRVAYWVGKALGNLSD VNQASRINRKKKH	39	Lactococcin G-a in DPC	*L. lactis*
2JPL	GTWDDIGQGIGRVAYWVGKALGNLSDVN QASRINRKKKH	39	Lactococcin G-a in TFE	*L. lactis*
1ZFU	GFGCNGPWDEDDMQCHNHCKSIK GYKGGYCAKGGFVCKCY	40	Plectasin, peptide antibiotic with therapeutic potential from a saprophytic fungus	*Pseudoplectania nigrella*
2A2B	ARSYGNGVYCNNKKCWVNRGEA TQSIIGGMISGWASGLAGM	41	Curvacin A	*Lactobacillus curvatus*
1OG7	KYYGNGVHCGKHSCTVDWGTAIGNI GNNAAANWATGGNAGWNK	43	Sakacin P, pediocin-like AMP in lipid micelles	*Lactobacillus sake*
1OHN	KYYGNGVHCGKHSCTVDWGTAIGNI GNNAAANWATGGNAGWNK	43	Sakacin P, pediocin-like AMP in lipid micelles	*L. sake*
1OHM	KYYGNGVHCGKHSCTVDWGTAIG CIGNNAAANWATGGNAGWNKC	44	Sakacin P variant, stabilised by inserted C-terminal disulphide bridge	*L. sake*
2B9K	AIKLVQSPNGNFAASFVLDGTKWIF KSKYYDSSKGYWVGIYEVWDRK	47	LCI, an AMP from *B. subtilis*	*B. subtilis*
2K29	GSHMGSINLRIDDELKARSYAALEKM GVTPSEALRLMLEYIADNERLPFKQTL	53	DBD domain of *E. coli* antitoxin relb	*E. coli*
1KG1	DRCRYTLCCDGALKAVSACLHESESCLVPGD CCRGKSRLTLCSYGEGGNGFQCPTGYRQC	60	NIP1 elicitor protein	*Rhynchosporium secalis*
1RY3	MNSVKELNVKEMKQLHGGVNYGNGVSC SKTKCSVNWGQAFQERYTAGINSF VSGVASGAGSIGR	64	The precursor for carnobacteriocin B2, an AMP from *Carnobacterium piscicola*	*Carnobacterium maltaromaticum*
2ADL	MKQRITVTVDSDSYQLLKAYD VNISGLVSTTMQNEARRLRAERWKVENQE GMVEVARFIEMNGSFADENKDW	72	CcdA, bacterial antitoxin, implications for DNA and toxin binding	*E. coli*
2ADN	MKQRITVTVDSDSYQLLKAYDVNISGLV STTMQNEARRLRAERWKVENQEGM VEVARFIEMNGSFADENKDW	72	CcdA, bacterial antitoxin, implications for DNA and toxin binding	*E. coli*
1OF9	GEILCNLCTGLINTLENLLTTKGADKVK DYISSLCNKASGFIATLCTKVLDFGIDKL IQLIEDKVDANAICAKIHAC	77	Amoebapore A, pore forming toxin	*Entamoeba histolytica*
1QVP	GSHMDAAAPGTRVIDAATSMPRKVR IVQINEIFQVETDQFTQLLDADIRVGSE VEIVDRDGHITLSHNGKDVELLDDLAHTIRIEEL	87	DtxR, C-terminal SH3-like domain from diphtheria toxin repressor, residues 144–226	*Corynebacterium diphtheriae*
2JSO	MEWLVKKSCCNKQDNRHVLMLCDAGGAIKMIA EVKSDFAVKVGDLLSPLQNALYCINREKLHTV KVLSASSYSPDEWERQCKVAGKTQ	88	Antimicrobial resistance protein	*E. coli K12*

Table 1 *(Continued)*

PDB ID	Sequence[a]	Chain length[b]	Descriptor[c]	Source[d]
2K19	MGKLKWFSGGKERSNQAENIITDLLDD LKTDLDNESLKKVLENYLEELKQKSASVPLI LSRMNLDISKAIRNDGVTLSDYQSKKLKE LTSISNIRYGY	98	PisI	*C. maltaromaticum*
2KC8	GSHMAYFLDFDERALKEWRKLGS TVREQLKKKLVEVLESPRIEANKLRGMPDC YKIKLRSSGYRLVYQVIDEKVVVFVISVGK AEASEVYSEAVKRIL	98	RelE (R81A/R83A) mutant in complex with antitoxin relbc (K47-L79) peptide	*E. coli*
2KC9	GSHMAYFLDFDERALKEWRKL GSTVREQLKKKLVEVLESPRIEANKLRG MPDCYKIKLRSSGYRLVYQVIDEKVVVF VISVGKAEASEVYSEAVKRIL	98	RelE (R81A/R83A) mutant in the free state	*E. coli*
Plant toxins				
1O8Y	GRCTKSIPPICFPD	14	SFTI-1(6, 5), an acyclic permutant of the proteinase inhibitor SFTI-1, *trans–trans–trans* conformer (tt-a)	
1O8Z	GRCTKSIPPICFPD	14	SFTI-1(6, 5), an acyclic permutant of the proteinase inhibitor SFTI-1, *cis–trans–trans* conformer (ct-a)	
1T9E	GRATKSIPPIAFPD	14	Disulphide analogue of the cyclic sunflower trypsin inhibitor SFTI-1	
2BEY	CTKSIPPICTKSIPPI	16	c2 symmetrical bifunctional bicyclic inhibitor based on SFTI-1	
1WN8	GVKSSETTLTMFLKEMQLKGLP	22	OaNTR	*Oldenlandia affinis*
2FQA	SAISCGETCFKFKCYTPRCSCSYPVCK	27	Violacin A	*Viola odorata*
1WN4	ALETQKPNHLLEEALVAFAKKGNLGGLP	28	VoNTR	*V. odorata*
2F2I	CGETCVGGTCNTPGCTCSWDKCTRNGLPV	29	[P20D,V21K]-kalata B1	
2F2J	CGETCVGGTCNTPGCTCSKNKCTRNGLPV	29	[W19K, P20N, V21K]-kalata B1	
2V1V	RVCPRILLECKKDSDCLAECVCLEHGYCG	29	M8l mutant of squash trypsin inhibitor cmti-i	

1ZNU	CGETCVGGTCNTPGCTCSWPVCTRNGLPV	29	Cyclotide kalata B1 in DPC micelles solution	*O. affinis*
1NB1	CGETCVGGTCNTPGCTCSWPVCTRNGLPV	29	High-resolution kalata B1	*O. affinis*
1PT4	CGETCFGGTCNTPGCSCTWPICTRDGLPV	29	Möbius cyclotide kalata B2	*O. affinis*
1ZNU	CGETCVGGTCNTPGCTCSWPVCTRNGLPV	29	Cyclotide kalata B1 in DPC micelles solution	*O. affinis*
2JUE	CGETCVGGTCNTPGCTCSWPVCTRNGLPV	29	All-D kalata B1	
2JWM	CGETCTLGTCYTQGCTCSWPICKRNGLPV	29	Ternary complex kalata B7/Mn^{2+}/ DPC micelle	*O. affinis*
2K7G	GVPICGETCTLGTCYTAGCSCSWPVCTRN	29	Cyclotide varv F	*Viola arvensis*
1ZUV	VGECVRGRCPSGMCCSQWGYCGKGPKYCGR	30	AcAMP2-like peptide with phenylalanine 18 mutated to tryptophan	
1ZWU	VGECVRGRCPSGMCCSQAGYCGKGPKYCGR	30	AcAMP2-like peptide with β-(2-naphthyl)-alanine residue	
1ZNT	VGECVRGRCPSGMCCSQFGFCGKGPKYCGRX	31	AcAMP2-like peptide with non-natural fluoroaromatic residue (acamp2f18pff/Y20Pff) complex with *N,N,N*-triacetylchitotriose	
2IT8	GVCPKILKKCRRDSDCPGACICRGNGYCGX	30	Linear analogue of the cyclic squash trypsin inhibitor mcoti-II	
1NBJ	CAESCVYIPCTVTALLGCSCSNRVCYNGIP	30	High-resolution solution structure of cycloviolacin O1	*V. odorata*
1VB8	CAESCVWIPCTVTALLGCSCSNKVCYNGIP	30	Solution structure of vhr1, the first cyclotide from root tissue	*Viola hederacea*
2ERI	CGESCVFIPCISTLLGCSCKNKVCYRNGVIP	31	Circulin B	*Chassalia parviflora*
1ZA8	CGESCAMISFCFTEVIGCSCKNKVCYLNSIS	31	Leaf-specific cyclotide vhl-1	*V. hederacea*
2GJ0	GSIPACGESCFKGKCYTPGCSCSKYPLCAKN	31	Cycloviolacin O14	*V. odorata*
1T0W	EQCGRQAGGKLCPNNLCCSQWGWCGSTDEYCSX	33	Truncated hevein of 32 aa (hevein-32) complex with *N,N,N*-triacetylglucosamina	
1YP8	CGESCFLGTCYTKGCSCGEWKLCYGTNGGTIFD	33	Solution structure of the cyclotide tricyclon A	*Viola tricolor*
2PO8	CPKILKKCRRDSDCPGACICRGNGYCGSGSDGGV	34	Two-disulphide intermediate of MCoTI-II	
1WO9	AGECTPGQTKKQDCNTCTCTPTGI WGCTRKACRTT	35	Selective inhibition of trypsins by insect peptides: role of P6–P10 loop	

Table 1 *(Continued)*

PDB ID	Sequence[a]	Chain length[b]	Descriptor[c]	Source[d]
1R1F	TFCGETCRVIPVCTYSAALGCTCDDR SDGLCKRNGDP	37	Cyclotide palicourein: implications for the development of pharmaceutical and agricultural applications	*Palicourea condensate*
1JMN	KSCCPNTTGRNIYNTCRFGGGS RQVCASLSGCKIISASTCPSDYPK	46	Viscotoxin A2	*Viscum album*
1JMP	KSCCPNTTGRNIYNTCRLGGGSRER CASLSGCKIISASTCPSDYPK	46	Viscotoxin B	*V. album*
1ORL	KSCCPNTTGRNIYNTCRFAGGSRE RCAKLSGCKIISASTCPSDYPK	46	Viscotoxin C1	*V. album*
1NBL	KSCCRNTLARNCYNACRFTGGSQPT CGILCDCIHVTTTTCPSSHPS	46	Hellethionin D	*Helleborus purpurascens*
2GL1	KTCENLANTYRGPCFTTGSCDDHCKNKEHL RSGRCRDDFRCWCTRNC	47	*Vigna radiata* defensin 2 (vrd2)	*V. radiata*
2JYY	DRICTNCAAGTKGCKYFSDDGTFVC EGESDPRNPKAAPRNCDPRIAYGICPLA	53	C8A/C37A-T1 from *Nicotiana alata*	
2AIH	GDDVKSACCDTCLCTRSQPPTCRCVD VRESCHSACDKCVCAYSNPPQCQCYD THKFCYKACHNSEIE	67	Trypsin/chymotrypsin Bowman– Birk inhibitor from *Lens culinaris*	*L. culinaris*
1JXC	CPEIEAQGNECLKEYGGDVGFG FCAPRIFPTICYTRCRENKGAKGGRCRW GQGSNVKCLCDFCGDTPQ	68	ATT, an *Arabidopsis* trypsin/ chymotrypsin inhibitor	*Arabidopsis thaliana*
Animal toxins				
1DG0	CPWQPWC	7	Des[gly1]-contryphan-r cyclic peptide (major form)	
1NXN	GDCPWKPWCX	10	Contryphan-vn	*Conus ventricosus*
1SBU	GFASLPILKNG	11	Peptide containing a dimetylthiazolidine: an analogue of δ-conotoxin EVIA loop 2	
2B5Q	VCCGYKLCHPC	11	CMrVIA, λ-conotoxin (globular conformation)	
2IH6	VCCGYPLCHPC	11	Pro6 variant of CMrVIA conotoxin	

2B5P	VCCGYKLCHPC	11	CMrVIA, λ-conotoxin (ribbon isoform)	*Conus marmoreus*
2BC7	GACSDPRAAWRC	12	[Sec2,8]-ImI	
2BC8	GAASDPRAAWRA	12	[Sec2,3,8,12]-ImI	
2IFJ	GCCSDKRCAWRC	12	Lys6 deamidated variant of ImI conotoxin	
2IGU	GCCSDPRCAWRC	12	Deamidated analogue of ImI conotoxin	
2IH7	VCCGYPLCHPCX	12	Amidated Pro6 analogue of CMrVIA conotoxin	
2IHA	VCCGYKLCHPCX	12	Amidated variant of CMrVIA conotoxin	
1U62	FQWQRNIRKVRX	12	Lactoferrin-based peptide FQWQRNIRKVR in complex with lipopolysaccharide	
1XV4	FQWQRNIRKVRX	12	Antimicrobial, endotoxin-neutralising peptide LF11 in SDS micelles	
1XV7	FQWQRNIRKVRX	12	Antimicrobial, endotoxin-neutralising peptide LF11 in DPC micelles	
2FBU	LLGDFFRKSKEK	12	N-terminal fragment of human LL-37	
2GMC	FQWQRNIRKVRX	12	C12-LF11 bound to DPC micelles	
2GMD	FQWQRNIRKVRX	12	C12-LF11 bound to SDS micelles	
2FR9	ECCNPACGRHYFC	13	α-Conotoxin GI (Ser12)-benzoylphenylalanine derivative	
2FRB	ECCFPACGRHYSC	13	α-Conotoxin GI (Asn4)-benzoylphenylalanine derivative	
2IFI	GCCSDARCAWRCX	13	Ala6 variant of ImI conotoxin	
2IFZ	GCCSDKRCAWRCX	13	Lys6 variant of ImI conotoxin	
1RGJ	FRYYESSLEPWDD	13	Complex between α-bungarotoxin and mimotope of the nicotinic acetylcholine receptor with enhanced activity	*Bungarus multicinctus*
2NS3	GCCSTPPCAVLYCX	14	Ribbon BuIA	

Table 1 *(Continued)*

PDB ID	Sequence[a]	Chain length[b]	Descriptor[c]	Source[d]
1QXQ	ILKKWPWWPWRRKX	14	Cyclic indolicidin peptide derivative with higher charge	
2DCX	ALWKTLLKKVLKAX	14	NC12-K4S4(1-13)a, dermaseptin AMP analogue	
2DD6	ALWKTLLKKVLKAX	14	K4-S4(1-13)a, dermaseptin truncated antimicrobial analogue	
2F3A	RLFDKIRQVIRKFX	14	LL-37-derived aurein 1.2 analogue (LLAA)	
2FBS	FKRIVQRIKDFLRX	14	LL-37 core peptide bound to detergent micelles	
2I1D	VRRFPWWWPFLRRX	14	Tritrp 1, DPC micelle-bound	
2I1E	VKKFPWWWPFLKKX	14	Tritrp 2, DPC micelle-bound	
2I1F	VRRFAWWWAFLRRX	14	Tritrp 3, DPC micelle-bound	
2I1G	VRRYPWWWPYLRRX	14	Tritrp 5, DPC micelle-bound	
2I1H	VRRFAWWWPFLRRX	14	Tritrp 7, DPC micelle-bound	
2I1I	VRRFPWWWAFLRRX	14	Tritrp 8, DPC micelle-bound	
2I28	GCCSTPPCAVLYCX	14	α-Conotoxin BuIA	*Conus bullatus*
2EW4	NGVCCGYKLCHPCX	14	MrIA	*C. marmoreus*
1VM5	GLFDIIKKIAESFX	14	Micelle-bound aurein 1.2, antimicrobial frog peptide	*Litoria raniformis*
1T51	ILGKIWEGIKSLFX	14	IsCT, scorpion-derived AMP and its analogues	*Opisthacanthus madagascariensis*
1T52	ILGKIWKGIKSLFX	14	IsCT, scorpion-derived AMP and its analogues	*O. madagascariensis*
1T54	ILGKIAEGIKSLFX	14	IsCT, scorpion-derived AMP and its analogues	*O. madagascariensis*
1T55	ILGKIWKPIKKLFX	14	IsCT, scorpion-derived AMP and its analogues	*O. madagascariensis*
2J15	NGVCCGYKLCHPCAG	15	Cyclic MrIA, an exceptionally stable and potent cyclic conotoxin with a novel topological fold that targets the norepinephrine transporter	

2JQC	DWEYHAHPKPNSFWT	15	L-Amino acid mutant of a D-amino acid containing conopeptide	
2JMY	KWKLFKKIGAVLKVL	15	CM15 in DPC micelles	
2JQB	DWEYHAHPKPNSXWT	15	Conomarphin, a D-amino acid containing conopeptide at pH 5	*C. marmoreus*
2YYF	DWEYHAHPKPNSXWT	15	Conomarphin a D-amino acid containing conopeptide	*C. marmoreus*
2EFZ	VCCPFGGCHELCYCCD	16	M-1 conotoxin with a novel disulphide linkage	
1QX9	ICLKKWPWWPWRRCKX	16	Cyclic indolicidin peptide derivative with higher charge	
2H8S	GCCSDPRCNYDHPEICX	17	α-Conotoxin Vc1.1	*Conus victoriae*
1UL2	GCCSHPACAGNNQHICX	17	α-Conotoxin GIC	*Conus geographus*
2RLG	ALYKKFKKKLLKSLKRLG	18	AMP RP-1 bound to SDS micelles	
2RLH	ALYKKFKKKLLKSLKRLG	18	AMP RP-1 bound to DPC micelles	
2GCZ	GCCSHPACNVNNPHICGX	18	α-Conotoxin OmIA	*Conus omaria*
1WO0	KWCFRVCYRGICYRRCRX	18	Tachyplesin I in H2O	*Tachypleus tridentatus*
1WO1	KWCFRVCYRGICYRRCRX	18	Tachyplesin I in dodecylphosphocholine micelles	*T. tridentatus*
1MTQ	IRDECCSNPACRVNNPHVC	19	α-Conotoxin GID	*C. geographus*
1ZLC	RDPCCSNPVCTVHNPQICX	19	α-Conotoxin PIA	*Conus purpurascens*
1K64	RDPCCYHPTCNMSNPQICX	19	α-Conotoxin EI	*Conus spurius*
1RKK	RRWCFRVCYRGFCYRKCRX	19	Polyphemusin I	*Limulus polyphemus*
1X7K	RRWCFRVCYRGRFCYRKCR	19	PV5	*L. polyphemus*
2B5K	RRWCFRVCYRGRFCYRKCRX	20	PV5 in DPC micelles	*L. polyphemus*
2JPY	FLSLIPHAINAVSTLVHHFX	20	Phylloseptin-2	*Phyllomedusa hypochondrialis*
2JQ0	FLSLIPHAINAVSAIAKHNX	20	Phylloseptin-1	*P. hypochondrialis*
2JQ1	FLSLIPHAINAVSALANHGX	20	Phylloseptin-3	*P. hypochondrialis*
1S6W	GCRFCCNCCPNMSGCGVCCRF	21	Hybrid white striped bass hepcidin	
2JNI	RWCVYAYVRIRGVLVRYRRCW	21	AMP arenicin-2 in aqueous solution	*Arenicola marina*
2JSB	RWCVYAYVRVRGVLVRYRRCW	21	Arenicin-1	*A. marina*
2AJW	GCCSNPVCHLEHSNLCGGAAGG	22	MII-6, cyclic conotoxin	
2JOS	FFHHIFRGIVHVGKTIHRLVTG	22	Piscidin in presence of DPC micelles	

Table 1 *(Continued)*

PDB ID	Sequence[a]	Chain length[b]	Descriptor[c]	Source[d]
2OJN	FFHHIFRPIVHVGKTIHRLVTG	22	Piscidin 1 and its analogues	
2OJO	FFHHIFRAIVHVAKTIHRLVTG	22	Piscidin 1 and its analogues	
1R9I	ERLCCGFPKSCRSRQCKPHRCC	22	PIIIA toxin	*C. purpurascens*
1Q2J	ERCCNGRRGCSSRWCRDHSRCC	22	Tetrodotoxin-resistant Na$^+$ channel binding by μ-conotoxin smIIIA	*Conus stercusmuscarum*
2OJM	FFHHIFRGIVHVGKTIHRLVTG	22	Piscidin 1 and its analogues	*Morone*
1XKM	ENREVPPGFTALIKTLRKCKII	22	AMP distinctin in water	*Phyllomedusa distincta*
2AK0	GCCSNPVCHLEHSNLCGAGGAAG	23	MII-7, cyclic conotoxin	
1V28	ENFAGGCATGFMRTADGRCKPTF	23	Paralytic peptide of the wild silkmoth, *Antheraea yamamai*	*A. yamamai*
1WQE	NDPCEEVCIQHTGDVKACEEACQ	23	OmTx3, toxin from the scorpion *O. madagascariensis*	*O. madagascariensis*
2K98	GIGKFLKKAKKGIGAVLKVLTTGL	24	MSI-594, potent AMP in presence of lipopolysaccharide micelle	
1G92	FLPLLILGSLLMTPPVIQAIHDAQR	25	Poneratoxin	*Paraponera clavata*
2FCG	IGKEFKRIVQRIKDFLRNLVPRTES	25	C-terminal fragment of human LL-37	
1JLO	HPPCCLYGKCRRYP GCSSASCCQRX	25	psi-Conotoxin PIIIE	*C. purpurascens*
1JLP	GPPCCLYGSCRPFP GCYNALCCRKX	25	psi-Conotoxin PIIIF	*C. purpurascens*
1XKM	NLVSGLIEARKYLEQLHRKLKNCKV	25	AMP distinctin in water	*P. distincta*
1ZRV	HVDKKVADKVLLLKQLRIMRLLTRL	25	Spinigerin in H20/TFE 50%	*Pseudacanthotermes spiniger*
1ZRW	HVDKKVADKVLLLKQLRIMRLLTRL	25	Spinigerin in H20/TFE 10%	*P. spiniger*
1TT3	CKGKGAKCSKLMYDCCTGSCRSGKCX	26	ω-Conotoxin [K10]MVIIA	
2AMN	RVKRVWPLVIRTVIAGYNLYRAIKKK	26	Fowlicidin-1, a novel cathelicidin AMP from chicken	
2G9P	GLFGKLIKKFGRKAISYAVKKARGKH	26	Latarcin 2A, AMP from spider (*Lachesana tarabaevi*) venom	*L. tarabaevi*
1TTK	CKGKGAKCSRLMYDCC TGSCRSGKCX	26	ω-Conotoxin MVIIA, an N-type calcium channel blocker	*Conus magus*

2FQC	FPRPRICNLACRAGIGHK YPFCHCRX	26	Conotoxin pl14a	*Conus planorbis*
2PCO	SMWSGMWRRKLKKLR NALKKKLKGEK	26	Latarcin-1, spider AMP	*L. tarabaevi*
1WQC	DPCYEVCLQQHGNV KECEEACKHPVE	26	OmTx1, toxin from the scorpion *O. madagascariensis*	*O. madagascariensis*
1V4Q	CKGKGAPCRKTMYDCCKGRC GRRGRCX	27	Analogue peptide of ω-conotoxin MVIIC	
2HFR	KRFWPLVPVAINTVAAGINLYKAIRRK	27	Fowlicidin-3, AMP	*Gallus*
1YZ2	CKQAGESCDIFSQNCCVGTCAFICIEX	27	Am2766	*Conus amadis*
1IXT	SCNNSCQSHSDCASHCI CTFRGCGAVN	27	Gm9a, novel P-superfamily spasmodic conotoxin	*Conus gloriamaris*
1WQD	DPCYEVCLQQHGNV KECEEACKHPVEY	27	OmTx2, toxin from the scorpion *O. madagascariensis*	*O. madagascariensis*
1TR6	CKSPGSSCSKTSYNCCR SCNPYTKRCYX	28	ω-Conotoxin [K10]GVIA, a cyclic cysteine knot peptide	
1TTL	CKSPGSSCSPTSYNCCRSC NPYTKRCYX	28	ω-Conotoxin GVIA, an N-type calcium channel blocker	*C. geographus*
1V5A	RCLPSGKACAGVTQKIP CCGSCVRGKCS	28	Covalitoxin I	*Corecnemius validus*
1WM8	VGCEECPMHCKGKNANPT CDDGVCNCNV	28	BmP03, from venom of scorpion *Buthus martensii* Karsch	*Mesobuthus martensii*
1Y29	KCLPPGKPCYGATQKIPC CGVCSHNKCT	28	Huwentoxin-x	*Ornithoctonus huwena*
2GX1	GCKLTFWKCKNKKECCGWN ACALGICMPR	29	Spider toxin that affects the activation of mammalian Na$^+$ channels	*Macrothele gigas*
1WM7	ATCEDCPEHCATQNARAK CDNDKCVCEPK	29	BmP01, from venom of scorpion *B. martensii* Karsch	*M. martensii*
1V7F	YCQKWMWTCDSARKCCEGLVC RLWCKKIIX	30	Phrixotoxin 1	*Phrixotrichus auratus*
2CK5	CKISRQCLKPCKDAGMRFG KCMNGKCHCTPK	31	δ 1-7 Aosk1	
1PQR	GCCGPYPNAACHPCGCKV GRPPYCDRPSGGX	31	α-Conotoxin EIVA	*Conus ermineus*
1RMK	ACSKKWEYCIVPILGFVYCCPGLIC GPFVCV	31	MrVIB, conotoxin	*C. marmoreus*
2GDL	LVQRGRFGRFLRKIRRFRPKVTI TIQGSARF	31	Fowlicidin-2, AMP	*L. tarabaevi*

Table 1 *(Continued)*

PDB ID	Sequence[a]	Chain length[b]	Descriptor[c]	Source[d]
1PVZ	TPFAIKCATDADCSRKCP GNPPCRNGFCACT	31	BmP07, K$^+$ channel blocker from scorpion *B. martensii* Karsch	*M. martensii*
1Q2K	AACYSSDCRVKCVAMGFS SGKCINSKCKCYK	31	BmBKTx1, K$^+$ channel blocker from *B. martensii* Karsch	*M. martensii*
1RJI	TPYPVNCKTDRDCVMCGLGIS CKNGYCQGCT	31	BmKX, K$^+$ channel blocker from *B. martensii* Karsch	*M. martensii*
1S8K	ETQCQSVRDCQQYCLTPD RCSYGTCYCKTTX	31	BmKK4, K$^+$ channel blocker from scorpion *B. martensii* Karsch	*M. martensii*
1WT8	TPYPVNCKTDRDCVM CGLGISCKNGYCQGCT	31	BmP08, from venom of scorpion *B. martensii* Karsch	*M. martensii*
1WQB	WLGCARVKEACGPWEWPCCSGL KCDGSECHPQ	32	Aptotoxin VII, from venom of a trap-door spider	*Aptostichus schlingeri*
2K10	GILSSFKGVAKGVAKDLAGKLL ETLKCKITGC	32	Rantuerin-2csa, broad-spectrum antibacterial peptide, identification of a full-length helix–turn–helix motif	*Rana cascadae*
2K1I	RRTCHCRSRCLRRESNS GSCNINGRIFSLCCR	32	Oral mucosal α-defensin from Rhesus macaque	
1PJV	AVCVYRTCDKDCKRRGYRSGKCINN ACKCYPY	32	Cobatoxin 1, scorpion venom	*Centruroides noxius*
1TV0	GLLCYCRKGHCKRGERVR GTCGIRFLYCCPRR	32	Cryptdin-4, the most potent α-defensin from mouse Paneth cells	*Mus musculus*
2JTB	GCKGFGDSCTPGKNECCPNY ACSSKHKWCKVYL	33	Hainantoxin-III	*Ornithoctonus hainana*
1IE6	GDCLPHLKRCKADNDCCGKK CKRRGTNAEKRCR	33	Imperatoxin a	*Pandinus imperator*
1Y2P	ASCRTPKDCADPCRKETGCPYGK CMNRKCKCNRC	34	Hstx3P	*Heterometrus spinifer*
2IGR	KWKVFKKIEKKWKVFKKIEKAGP KWKVFKKIEKX	34	CB1a, novel anticancer peptide derived from natural AMP cecropin B	
1ZJQ	GCGGLMAGCDGKSTFCCSGYNCSP TWKWCVYARP	34	Jingzhaotoxin-VII	*Chilobrachys jingzhao*

2A2V	ECRKMFGGCSVDSDCCAHLGCKPTLKYCAWDGTF	34	Jingzhaotoxin-XI	*C. jingzhao*
2AAP	GCGGLMAGCDGKSTFCCSGYNCSPT WKWCVYARP	34	Jingzhaotoxin-VII	*C. jingzhao*
1TYK	GCLEFWWKCNPNDDKCCRPKLKCSKLFKLCNFSF	34	GsMTx-4, toxin from the tarantula, *Grammostola spatulata*, which inhibits mechanosensitive ion channels	*Grammostola rosea*
1S6X	ECGKFMWKCKNSNDCCKDLVCSS RWKWCVLASPF	34	VSTx	*G. spatulata*
1NIX	ECKGFGKSCVPGKNECCSGYACNSRDKWCKVLLX	34	Hainantoxin-I	*O. hainana*
2JX6	GLWSKIKAAGKEAAKAAAKAAGKAA LNAVSEAVX	34	Antibiotic peptide dermadistinctin K	*P. distincta*
2K9B	GLWSKIKAAGKEAAKAAAKAAGKA ALNAVSEAVX	34	Dermadistinctin K, antibiotic peptide	*P. distincta*
1X5V	ACGILHDNCVYVPAQNPCCRGLQCRYGKCLVQVS	34	PcFK1	*Psalmopoeus cambridgei*
1LA4	TCRYLFGGCKTTADCCKHLACRSDGKYCAWDGTF	34	SGTx1	*Scodra griseipes*
1WPD	VSCTGSKDCYAPCRKQTGCPYGKCM NRKCKCNRC	34	Evidence for domain-specific recognition of SK and Kv channels by MTX and HsTx1 scorpion toxins	*Scorpio maurus palmatus, H. spinifer*
1LMR	ADDDCLPRGSKCLGENKQCCKGTTCMF YANRCVGV	35	ADO1, voltage-sensitive calcium channel L-type blocker	*Agriosphodrus dohrni*
1LU8	GCLEFWWKCNPNDDKCCRPKLKC SKLFKLCNFSFX	35	GsMTx-4	*G. spatulata*
1V56	IRCSGSRDCYSPCMKQTGCPNAKCINKSCKCYGCX	35	Spinoxin, a K^+ channel blocker	*H. spinifer*
1WZ5	LVKCRGTSDCGRPCQQQTGAPNSKC INRMCKCYGA	35	Pi1-3p	*P. imperator*
1RYG	ECLGFGKGCNPSNDQCCKSSNLVC SRKHAWCKYEIX	36	R29A mutant of Na^+ channel inhibitor hainantoxin-IV	*O. hainana*
1RYV	ECLGFGKGCNPSNDQCCKSSNLVCS RAHRWCKYEIX	36	K27A mutant of Na^+ channel inhibitor hainantoxin-IV	*O. hainana*
2E2S	GGCLPHNRFCNALSGPRCCSGLKCK ELSIWDSRCLX	36	Agelenin, insecticidal peptide	*Allagelena opulenta*
2I1T	DGECGGFWWKCGRGKPPCCK GYACSKTWGWCAVEAP	36	Jingzhaotoxin-III, novel toxin inhibiting both Nav and Kv channels	*C. jingzhao*
2K38	GFGALFKFLAKKVAKTVAKQAAKQGA KYVVNKQMEX	36	Cupiennin 1A	*Cupiennius salei*

Table 1 *(Continued)*

PDB ID	Sequence[a]	Chain length[b]	Descriptor[c]	Source[d]
1NIY	ECLGFGKGCNPSNDQCCKSSNLV CSRKHRWCKYEIX	36	Hainantoxin-IV by 2d	*O. hainana*
1IYC	ELPKLPDDKVLIRSRSNCPKGKVWN GFDCKSPFAFS	36	Scarabaecin, antifungal peptide	*Oryctes rhinoceros*
1MM0	ACNFQSCWATCQAQHSIYFRRAFCDRS QCKCVFVRG	36	Termicin, AMP from termite	*P. spiniger*
2K9E	XRSCIDTIPKSRCTAFQCKHSLKYRLS FCRKTCGTCX	37	Shk-192, potent Kv1.3-specific immunosuppressive polypeptide	
2G9L	GILDTLKQFAKGVGKDLVKGAA QGVLSTVSCKLAKTC	37	Gaegurin 4, AMP and its mode of membrane interaction	*Rana rugosa*
2K6O	LLGDFFRKSKEKIGKEFKRIVQRIKDFLRNLVPRTES	37	Human ll-37	*Homo sapiens*
1M2S	FGLIDVKCFASSECWTACKKVTGSGQG KCQNNQCRCY	37	BmTx3B, K$^+$ channel blocker from *B. martensii* Karsch venom	*M. martensii*
2K4U	VGINVKCKHSRQCLKPCKDAGMRFGK CTNGKCHCTPK	37	ADWX-1, scorpion toxin	*M. martensii*
2JP6	GSTGPQTTCQAAMCEAGCKGLGK SMESCQGDTCKCKA	37	Recombinant form of the Kv1.3 channel blocker Tc32	*Tityus cambridgei*
1UT3	SFGLCRLRRGFCARGRCRFPSIPI GRCSRFVQCCRRVW	38	Spheniscin-2, a β-defensin from penguin stomach preserving food	*Aptenodytes patagonicus*
2JTU	GPSFCKADEKPCEYHADCCNCC LSGICAPSTNWILPGC	38	Iota-RXIA(38)	*Conus radiatus*
2CK4	GVIINVKCKISRQCLKPCKDAGMRFGKCM NGKCHCTPK	38	Aosk1	*Orthochirus scrobiculosus*
1N8M	IEAIRCGGSRDCYRPCQKRTGCPNAKC INKTCKCYGCS	38	Pi4, a four disulphide bridged scorpion toxin active on K$^+$ channels	*P. imperator*
1V90	GCLGEGEKCADWSGPSCCDGFYCSCRS MPYCRCRNNSX	38	δ-Paluit1-NH$_2$	*Paracoelotes luctuosus*
1V91	ACVGDGQRCASWSGPYCCDGYY CSCRSMPYCRCRNNSX	38	δ-Paluit2-NH$_2$	*P. luctuosus*

2AXK	EIDTNVKCSGSSKCVKICIDRYNT RGAKCINGRCTCYP	38	Discrepin, a scorpion venom toxin blocking K$^+$ channels	*Tityus discrepans*
2Z3S	GVPINVSCTGSKDCYAPCRKQT GCPNAKCINKSCKCYGC	39	AgTx2-MTX	
1HLY	TVIDVKCTSPKQCLPPCKAQFG IRAGAKCMNGKCKCYPH	39	Hongotoxin 1	*Centruroides limbatus*
2H1Z	GSCVPVDQPCSLNTQPCCDDATCTQ ERNENGHTVYYCRA	39	Dual-target spider toxin	*Hadronyche versuta*
2E3G	ATCDLASKWNWNHTLCAAHCIARRYRGG YCNSKAVCVCRN	40	DEF-DAA, a mutant of anopheles defensin DEF-AAA	*Anopheles gambiae*
2NY8	ATCDLASGFGVGSSLCAAHCIARR YRGGYCNSKAVCVCRN	40	Antibacterial defensin DEF-AAA	*A. gambiae*
2NZ3	ATCDLASIFNVNHALCAAHCIARR YRGGYCNSKAVCVCRN	40	DEF-acaa, a mutant of anopheles defensin DEF-AAA	*A. gambiae*
1LMM	EDCIPKWKGCVNRHGDCCEGLEC WKRRRSFEVCVPKTPKT	40	OLE_LINK1Psalmotoxin 1OLE_LINK1$^+$ channel	*P. cambridgei*
1WMT	VHTNIPCRGTSDCYEPCEKKYNCA RAKCMNRHCNCYNNCPW	41	Istx, scorpion toxin from *O. madagascariensis*	*O. madagascariensis*
1WT7	WCSTCLDLACTGSKDCYAPCRK QTGCPNAKCINKSCKCYGC	41	BuTX-MTX: a butantoxin– maurotoxin chimera	
2NY9	ATCDLASGFGVGSSLCAAHCLVKG YRGGYCKNKICHCRDKF	41	DEF-ABB, a mutant of anopheles defensin DEF-AAA	*A. gambiae*
1WQK	GTTCYCGKTIGIYWFGTKTCPSNR GYTGSCGYFLGICCYPVD	42	APETx1, specific peptide inhibitor of human ether-a-go-go-related gene K$^+$ channels from the venom of the sea anemone *Anthopleura elegantissima*: a new fold for an HERG toxin	*A. elegantissima*
1WXN	GTACSCGNSKGIYWFYRPSCPTD RGYTGSCRYFLGTCCTPAD	42	APETx2, specific peptide inhibitor of ASIC3 proton-gated channels	*A. elegantissima*
1NE5	DRDSCVDKSRCAKYGYYQECQDCC KNAGHNGGTCMFFKCKCA	42	CnErg1, a HERG-specific scorpion toxin	*C. noxius*
1PX9	DRDSCVDKSRCAKYGYYQECQDC CKNAGHNGGTCMFFKCKCA	42	Native cnErg1 Ergtoxin, a highly specific inhibitor of HERG channel	*C. noxius*
1H5O	YKQCHKKGGHCFPKEKICLPPS SDFGKMDCRWRWKCCKKGSG	42	Crotamine, a neurotoxin from *Crotalus durissus terrificus*	*C. durissus terrificus*
1Z99	YKQCHKKGGHCFPKEKICLPP SSDFGKMDCRWRWKCCKKGSG	42	Crotamine, a myotoxin	*C. durissus terrificus*

Table 1 *(Continued)*

PDB ID	Sequence[a]	Chain length[b]	Descriptor[c]	Source[d]
2JR8	GKIPVKAIKQAGKVIGKGLRAIN IAGTTHDVVSFFRPKKKKH	42	*Manduca sexta* moricin	*M. sexta*
1ZUE	IMFFEMQACWSHSGVCRDKSERNC KPMAWTYCENRNQKCCEY	42	DLP-2	*Ornithorynchus anatinus*
1ZUF	IMFFEMQACWSHSGVCRDKSERN CKPMAWTYCENRNQKCCEY	42	DLP-4	*O. anatinus*
2JR3	DDTPSSRCGSGGWGPCLPI VDLLCIVHVTVGCSGGFGCCRIG	42	Antibacterial peptide from eggshell matrix	*Pelodiscus sinensis*
1ZRX	RGFRKHFNKLVKKVKHTISETAHVAKD TAVIAGSGAAVVAAT	42	Stomoxyn in H20/TFE 50%	*Stomoxys calcitrans*
2DCV	YVSCLFRGARCRVYSGRSCCFGYYCR RDFPGSIFGTCSRRNF	42	Tachystatin b, horseshoe crab AMP with the cystine-knot motif	*T. tridentatus*
2DCW	YITCLFRGARCRVYSGRSCCFGYYCRRDFP GSIFGTCSRRNF	42	Tachystatin b, horseshoe crab AMP with the cystine-knot motif	*T. tridentatus*
2E3F	ATCDLASFSSQWVTPNDSLCAAHC IARRYRGGYCNGKRVCVCR	43	DEF-BAT, a mutant of anopheles defensin DEF-AAA	*A. gambiae*
2B68	GFGCPGNQLKCNNHCKSISCRAG YCDAATLWLRCTCTDCNGKK	43	Recombinant *Crassostrea gigas* defensin	*C. gigas*
2ROO	CGSKRAWCKEKKDCCCGYNCVYAW YNQQSSCERKWKYLFTGEC	43	Magi4, spider toxin	*M. gigas*
2E3E	ATCDLASFSSQWVTPNDSLCAAHCLVK GYRGGYCKNKICHCRDKF	45	DEF-BBB, a mutant of anopheles defensin DEF-AAA	*A. gambiae*
2JRY	GPSFCKADEKPCEYHADCCNCCLS GICAPSTNWILPGCSTSSFXKI	46	Excitatory I1-superfamily conotoxin	*C. radiatus*
2P4L	GPSFCKADEKPCEYHADCCNC CLSGICAPSTNWILPGCSTSSFFKI	46	Excitatory I1-superfamily conotoxin	*C. radiatus*
2H9X	GVPCRCDSDGPSVHGNTLSGTV WVGSCASGWHKCNDEYNIAYECCKQ	47	CgNa toxin	*Condylactis gigantea*
1XV3	HSSGYTRPLRKPSRPIFIRPIGCDVCY GIPSSTARLCCFRYGDCCHL	47	Synthetic penaeidin 4	*Litopenaeus setiferus*
1Z6V	GRRRRSVQWCAVSQPEATKCFQWQR NMRKVRGPPVSCIKRDSPIQCIQA	49	Human lactoferricin	*H. sapiens*

1Z6W	GRRRRSVQWCAVSQPEATKCF QWQRNMRKVRGPPVSCIKRDSPIQCIQA	49	Human lactoferricin	*H. sapiens*
2JOT	IDTCRLPSDRGRCKASFERWYFN GRTCAKFIYGGCGGNGNKFPTQEAC MKRCAKA	55	Huwentoxin-XI	*O. huwena*
1NH5	KDGYPVDSKGCKLSCVANNYCDN QCKMKKASGGHCYAMSCYCEG LPENAKVSDSATNICG	60	CsE-v5, a new world scorpion neurotoxin	*Centruroides exilicauda*
2CA7	KDRPSLCDLPADSGSGTKAE KRIYYNSARKQCLRFDYTGQGG NENNFRRTYDCQRTCLYT	60	Conkunitzin-s1, first member of a new kunitz-type neurotoxin family	*Conus striatus*
2K35	QIVDCWETWSRCTKWSQGGTGT LWKSCNDRCKELGRKRGQCEEKPSRCPL SKKAWTCICY	60	Hydramacin-1, peptide from the basal metazoan hydra	*Hydra*
1RL5	LKCNKLVPIAYKTCPEGKNLCYK MFMMSDLTIPVKRGCIDVCPKNS LLVKYVCCNTDRCN	60	Cytotoxin I (major form)	*Naja oxiana*
1ZAD	LKCNKLVPIAYKTCPEG KNLCYKMFMMSDLTIPVKRGCIDV CPKNSLLVKYVCCNTDRCN	60	CTI, cytotoxin I from *N. oxiana* in complex with DPC micelle	*N. oxiana*
1UEO	QVYKGGYARPIPRPPPFVR PLPGGPIGPYNGCPVSCRGISFSQARSCCS RLGRCCHVGKGYSG	63	[T8A]-penaeidin-3	*Litopenaeus vannamei*
1T1T	KIDGYPVDYWNCKRICWYNNKYCNDLC KGLKADSGYCWGWTLSCYCQGLPD NARIKRSGRCRA	63	Kurtoxin	*Parabuthus transvaalicus*
2E0H	VRDAYIAQNYNCVYHCARDAYCNELC TKNGAKSGSCPYLGEHKFACYCK DLPDNVPIRVPGKCH	64	BmKαIT01, α-insect toxin from venom of the Chinese scorpion *B. martensii* Karsch	*M. martensii*
2J6D	ARPKDRPSYCNLPADSGSGTKPEQRIY YNSAKKQCVTFTYNGKGGNGNN FSRTNDCRQTCQYPVG	65	Conkunitzin-s2, cone snail neurotoxin	*C. striatus*
1VYC	RKCLIKYSQANESSKTCPSGQLLCLK KWEIGNPSGKEVKRGCVATCPK PWKNEIIQCCAKDKCNA	65	Neurotoxin from *Bungarus candidus*	*B. candidus*
2JQP	LTCLICPEKDCQKVHTCRNEE KICVKRFYDKNQLGWRAQRGCAVS CPKAKPNETVQCCSTDKCNK	65	Bungatoxin from Malayan krait	*B. candidus*

Table 1 *(Continued)*

PDB ID	Sequence[a]	Chain length[b]	Descriptor[c]	Source[d]
1JC6	KNRPTFCNLLPETGRCNALIPA FYYNSHLHKCQKFNYGGCGGNANN FKTIDECQRTCAAKYGRSS	65	*Bungarus fasciatus* IX, a kunitz-type chymotrypsin inhibitor	*B. fasciatus*
1PE4	RDGYPLASNGCKFGCSGLGE NNPTCNHVCEKKAGSDYGYCYAW TCYCEHVAEGTVLWGDSGTGPCRS	67	Cn12, α scorpion toxin acting on Na$^+$ channels	*C. noxius*
1MR6	MQCKTCSFYTCPNSETCPDGKNI CVKRSWTAVRGDGPKREIRR ECAATCPPSKLGLTVFCCTTDNCNH	68	γ-Bungarotoxin, implication for the role of the residues adjacent to RGD in integrin binding	*B. multicinctus*
1WWN	KKNGYAVDSSGKVSECLLNNYCNN ICTKVYYATSGYCCLLSCYCFGL DDDKAVLKIKDATKSYCDVQII	69	BmK-βIT, an excitatory scorpion toxin from *B. martensii* Karsch	*M. martensii*
2JYO	ASNFDCCLGYTDRILHPKFIVG FTRQLANEGCDINAIIFHTKKKLSVCAN PKQTWVKYIVRLLSKKVKNM	70	Human MIP-3α/CCL20	
1W6B	ITCYKTPIPITSETCAPGQNLCYTKTWC DAWCGSRGKVIELGCAATCPTVESYQDI KCCSTDDCNPHPKQKRP	73	Long neurotoxin from the venom of the Asian cobra	*N. oxiana*
1RGJ	IVCHTTATSPISAVTCPPGENLCYRK MWCDAFCSSRGKVVELGCAATCPSKKPYEEVT CCSTDKCNPHPKQRPG	74	Complex between α-bungarotoxin and mimotope of the nicotinic acetylcholine receptor with enhanced activity	*B. multicinctus*
2RNG	NPLIPAIYIGATVGPSVWAYLV ALVGAAAVTAANIRRASSDNHSCAGNRGW CRSKCFRHEYVDTYYSAVCGRYFCCRSR	79	Big defensin	*T. tridentatus*
2JVE	MGSSHHHHHHSSGLVPRGSHMALKC FTRNGDDRTVTTCAEEQTRCLFVQLPY SEIQECKTVQQCAEVLEEVTAIGYPAK CCCEDLCNRSEQ	91	Extracellular domain of Prod1, a protein implicated in proximodistal identity during amphibian limb regeneration	*Notophthalmus viridescens*
2JS9	MSGSHHHHHHSSGIEGRGRSALSCQMCELVVK KYEGSADKDANVIKKDFDAECKK LFHTIPFGTRECDHYVNSKVDPIIHELE GGTAPKDVCTKLNECP	99	Caenopore-5 (81 Pro *cis* conformer)	*Caenorhabditis elegans*

2JSA	MSGSHHHHHHSSGIEGRGRSALSCQMC ELVVKKYEGSADKDANVIKKDFDAECKK LFHTIPFGTRECDHYVNSKVDPIIHE LEGGTAPKDVCTKLNECP	99	Caenopore-5 (81 Pro *trans* conformer)	*C. elegans*
Designed toxins				
2OTQ	RRWFWR	6	Cyclo(RRWFWR) bound to DPC micelles	Synthetic combinatorial library
2OX2	RRWWFR	6	Cantionic, cyclo(RRWWFR) bound to DPC-micelles	Synthetic combinatorial library
1QVK	RRWWRF	6	cyc-(RRWWRF) bound to DPC micelles	Synthetic combinatorial library
1QVL	RRWWRF	6	cyc-(RRWWRF) bound to SDS micelles	Synthetic combinatorial library
1SKI	RRYYRF	6	cyc-(RRYYRF) bound to DPC micelles	Synthetic combinatorial library
1SKK	KKWWKF	6	cyc-(KKWWKF) bound to DPC micelles	Synthetic combinatorial library
1SKL	RRAARF	6	cyc-(RRNALNALRF) bound to DPC micelles	Synthetic combinatorial library
2JQ2	HPLKQYWWRPSI	12	Anticoccidial peptide PW2 in DPC micelles	Phage display

Note: AMP, antimicrobial peptide.

[a]One letter codes are used throughout; X refers to post-translational modifications.

[b]Only proteins <100 amino acid residues have been included.

[c]All peptides listed were identified through one of the following keyword phrases — toxin, antimicrobial peptide or protease inhibitor. Some entries corresponding solely to immunity proteins, or where large toxins in complex with small peptides or nucleic acid, were manually removed.

[d]The source organism is given for naturally occurring peptides only, not modified analogues.

controlling the local microbial flora.[11,12] This phenomenon is sometimes referred to as bacterial-antagonism and the existence of such compounds has been long recognised, and has been a major inspiration in the search for naturally occurring novel antibiotics. Microcins are diverse in sequence, structure and mode of antimicrobial action,[12] with examples targeting membranes,[13] DNA gyrase,[14,15] RNA polymerase[16,17] and protein translation.[18] Recently they have been divided into class I and class II microcins, referring to post-translationally modified and unmodified peptides, respectively.[19]

Solution-state NMR has played a major role in the structural characterisation of two microcins in particular, microcin B17 and microcin J25 (MccJ25), for which a key issue has been resolving the nature of their respective post-translational modifications. Microcin B17 contains thiazole and oxazole rings created by modification of Cys and Ser residues. The nature of these modifications was confirmed during the mid-1990s by extensive use of triple-resonance experiments identifying the covalent connections through scalar couplings.[20] The more recent identification of the unusual post-translational modification of MccJ25 together with the determination of its 3D structure is described in detail below.

3.2.1 Microcin J25

MccJ25 was first identified as an antimicrobial compound produced by an *E. coli* strain isolated from human faeces in the early 1990s.[21] It was found to have potent antimicrobial activity in the submicromolar range against several Gram-negative strains, including some pathogenic *Salmonella* and *Shigella* species.[21] Around a decade later, the primary and 3D structures of this molecule were reported through extensive NMR and biochemical analysis.[22] At that time, it was reported that MccJ25 is a highly hydrophobic peptide of 21 amino acid residues that carries a single post-translational modification, resulting from a cyclisation event.[22] The primary sequence was independently confirmed when it was established that MccJ25 is encoded as a 57 amino acid precursor (McJA), as part of a plasmid-borne gene cluster also comprising two processing enzymes, McJB and McJC, as well an ABC transporter-like export protein McJD.[9] McJB and McJC are involved in the proteolytic processing as well as the cyclisation of McJA into mature MccJ25, whereas McJD is responsible for efficient export and thereby self-immunity.[9,23]

In the initial reports on the structure determination, the cyclisation event was deduced, based on several observations, to involve the N- and C-termini, resulting in a head-to-tail macrocyclic peptide. First, the N-terminus was not susceptible to Edman degradation and the C-terminus could not be processed by carboxypeptidase Y cleavage.[22] Second, although MccJ25 was highly resistant to proteolysis, it could be digested by thermolysin to yield a single product with a mass increase of 18 Da, consistent with the termini being cross-linked. Third, Edman sequencing of the thermolysin-digested fragment suggested the continuation of the sequence after the C-terminal Gly residue with additional Gly residues, consistent with residues 1 and 2 both being Gly.[22] Finally, from NMR studies of MccJ25, which were performed in methanol due to the poor solubility in water, structural restraints broadly consistent with a head-to-tail cyclisation were derived.[24] The NMR data revealed that the peptide was highly folded with

excellent signal dispersion, and were used to deduce a 3D structure with a compact fold, which was characterised by a small β-sheet that twisted and folded back onto itself.[24]

Figure 2 shows the fingerprint region of the NOESY spectrum of MccJ25 in methanol, illustrating the signal dispersion and high quality of the data. NMR studies were subsequently performed on the thermolysin-digested analogue (t-MccJ25), revealing that although digestion partly destroyed the structure, half of the molecule remained highly folded.[25] Remarkably, both the native MccJ25 peptide and t-MccJ25 were found to be uniquely stable, retaining their ordered structures at temperatures >100°C and at highly denaturing conditions, as evident from NMR studies in DMSO or urea/guanidinium chloride solutions.[25] Although similar stability has been reported for other macrocyclic peptides from plants (i.e. cyclotides described later in this article), unlike MccJ25, cyclotides contain disulphide bonds and it was difficult to understand how simple cyclisation alone could explain the stability of MccJ25. Particularly puzzling was the behaviour of t-MccJ25, as this peptide was described as a linear unmodified peptide lacking any cross-bracing features that could account for its structured core.[25]
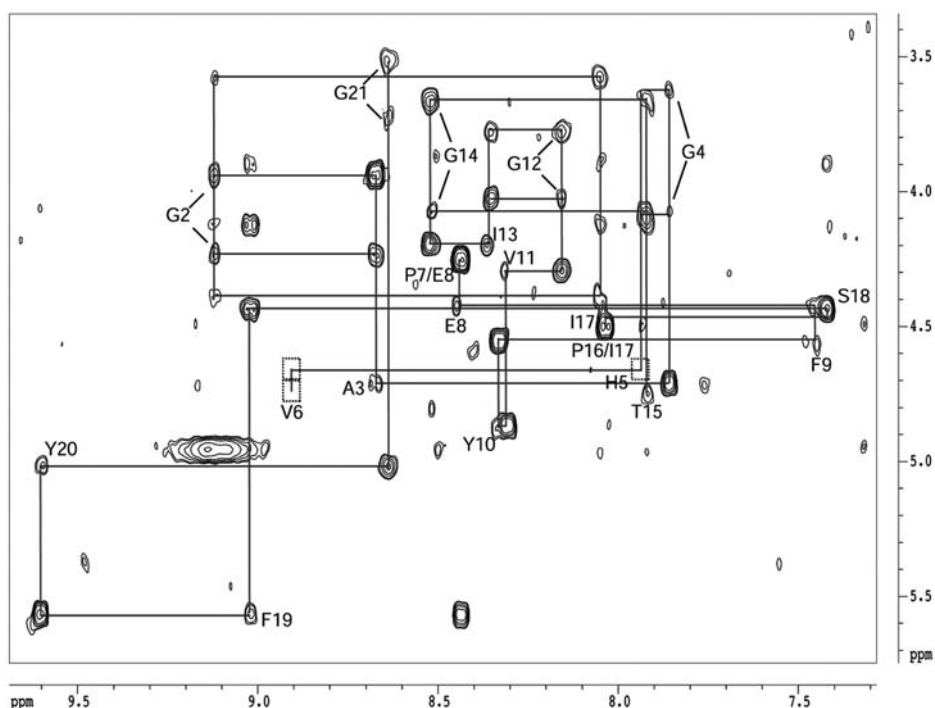
Figure 2 NOESY spectrum of MccJ25 in methanol recorded at 750 MHz. Sequential connections are indicated with lines and residue numbers. The excellent signal dispersion with amide shifts ranging from 9.5 to 7.5 ppm and Hα shifts from 5.5 to 3.5 ppm is indicative of the highly ordered structure.

The unusual structural features of MccJ25 and the identification of its unique mode of action, RNA polymerase inhibition,[26] sparked considerable further interest in the peptide, and during later studies, inconsistencies with the previously published data were observed. In particular, the native peptide produced by *E. coli* appeared to behave very differently to a synthetic head-to-tail cyclic peptide that was supposedly identical. Consequently, in a 2003 issue of the *Journal of the American Chemical Society*, three research teams independently, and in parallel, reported, based on NMR and MS analyses, that the proposed macrocyclic structure was incorrect.[27–29] In fact, MccJ25 has an N-terminus to Glu8 carboxyl sidechain lactam link, resulting in the formation of an octa-peptide ring. This ring is wrapped around the C-terminal segment, creating a noose-like motif, and it is this noose-like motif that is responsible for the well-ordered and stable structure of MccJ25.[27–29] The evidence for the Gly1–Glu8 link was based primarily on MS data but it was supported by strong NOE contacts between Gly1 and Glu8. In contrast, no 'sequential' NOEs were seen between Gly21 and Gly1. The new structure was also more consistent with the NMR data in general and finally in one of the studies, doubly labelled ^{13}C/^{15}N MccJ25 was produced and the lactam bridge was confirmed by triple-resonance experiments.[27]

Figure 3 shows the corrected NMR structures of MccJ25 and t-MccJ25. It is evident that the native structure is well defined throughout the sequence, with possibly a flexible region around the turn involving residues 13–14.[28] The structure is characterised by two small antiparallel β-sheets, one creating a hairpin extending away from the threaded core and the second being formed by interactions between the N-terminal ring and its threaded segment.[28] Digestion with thermolysin disrupts the hairpin segment but the threaded region remains fully structured,[30] despite the molecule now being a two-chain peptide lacking covalent links between the chains. The reason that this stable non-covalent entity is possible is evident from a space-filling model of the threaded structure. The octa-peptide ring wraps very tightly around the penetrating peptide chain and the positioning of two bulky amino acid sidechains, Phe19 and Tyr20, on either side of the ring prevents the tail from slipping out.[27–29] The structure simply cannot unfold without breakage of bonds and it is this feature that gives MccJ25 its unique stability.

It can also be concluded from the structure that the maturation involves the peptide folding before the covalent link between Gly1 and Glu8 is made so that the ring is formed around the peptide chain rather than the tail being threaded through the ring after it is created. Structure–activity studies on MccJ25 and t-MccJ25 have identified that although t-MccJ25 lacks antimicrobial activity against most strains, this is not due to impaired RNA polymerase inhibition, as this peptide inhibits transcription *in vitro*.[31] Rather, it is due to disrupted bacterial uptake of t-MccJ25.[31] Thus, it appears that the threaded region is responsible for interaction with the intracellular target, whereas the hairpin region is functionally important for interactions with the active import machinery.[32]

The studies on MccJ25 illustrate the unique strengths and weaknesses of NMR spectroscopy for structure determination of biomolecules. The determination of 3D structure through collection of NMR-based structural information in the form
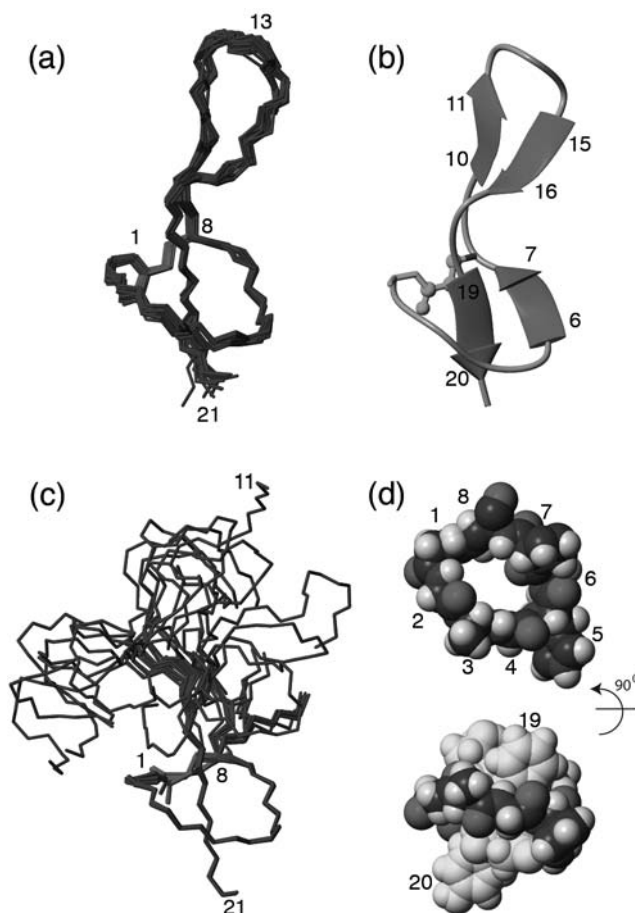
Figure 3   Structural features of MccJ25: (a) structural ensemble representing the solution structure of MccJ25 (PDB code 1Q71); (b) ribbon diagram of the lowest energy structure, illustrating the key element of secondary structure; (c) structural ensemble representing the solution structure of t-MccJ25 (PDB code 1S7P); and (d) space-filling model of the octa-peptide ring formed by the Gly1–Glu8 lactam cross-link. Selected amino acids are labelled with residue numbers.

of distance restraints and dihedral angles together with computational modelling is a powerful technique, evident from the rapidly rising number of NMR structures determined. However, it is an indirect strategy, and the information available may not always be sufficient to identify unusual covalent structures correctly, such as post-translational modifications or the connectivities of multiple disulphide bonds. Strikingly for MccJ25, the assumption of a head-to-tail cyclisation based on biochemical analysis could not be ruled out by an NMR analysis, as the set of NOEs initially identified was later found to be roughly consistent with both head-to-tail and sidechain-to-tail cyclisation arrangements.[24] Similarly, there are several examples of disulphide-rich proteins where the NMR restraints have been found to be consistent with what was later identified as an

erroneous structure,[33,34] as discussed later in this review. Particular strengths of NMR include powerful triple-resonance experiments, which can be used to resolve complex structural features if isotopically labelled material is available, and the ability to deduce high-resolution 3D structures of biomolecules once the covalent geometry is known, without the need for crystals. Furthermore, the ability of NMR to generate data for samples in different solvents and conditions allows for the study of highly hydrophobic peptides such as MccJ25, and also allows the analysis of the thermal and chemical stability of proteins.[25]

3.3 Bacteriocins

Most antimicrobial peptides produced by Gram-positive bacteria are classified as bacteriocins, and like microcins they are diverse in size and structure.[35,36] Recent classification schemes divide bacteriocins into three classes: lantibiotics (class I), heat-stable non-lantibiotics (class II) and heat-labile antimicrobial proteins (class III), of which the majority of bacteriocins belong either to class I or class II. NMR spectroscopy has been applied in numerous studies of bacteriocins and an overview of the range of diversity in the 3D structures that have been determined by NMR spectroscopy is provided in Figure 4.

3.3.1 Class I bacteriocins: lantibiotics
Lanthionine-containing antibiotics (lantibiotics) are ribosomally synthesised peptides that undergo a range of post-translational modifications, including the
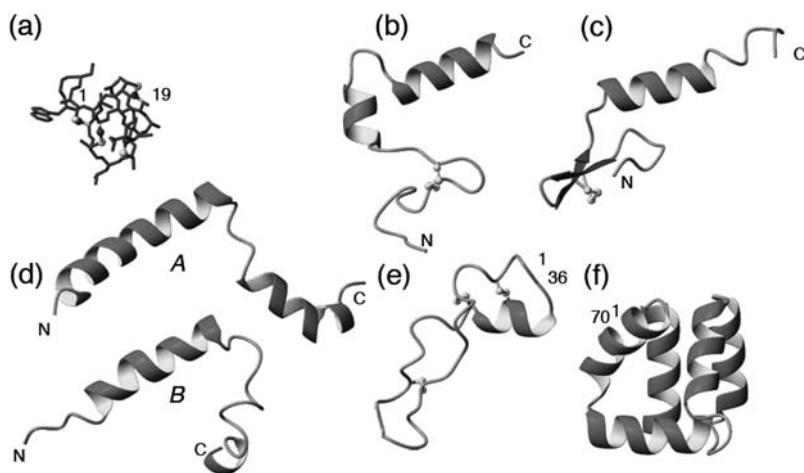
Figure 4 Structural features and diversity of bacteriocins. Solution NMR structures are shown for (a) the lantibiotic actagardine (PDB code 1AJ1); the pedocin-like bacteriocins (b) curvacin A (PDB code 2A2B) and (c) leucocin A (PDB code 1CW6); (d) the A and B chain of the two-chain bacteriocin lactococcin G in DPC micelles (PDB codes 2JPJ and 2JPK); and the cyclic bacteriocins (e) subtilosin (PDB code 1AJ1) and (f) AS-48 (PDB code 1E68). Disulphide bonds and lanthionine linkages are shown in ball-and-stick. Chain termini are labelled N and C and the cyclisation points on the cyclic peptides are labelled with residue numbers.

cross-linking of serine, threonine and cysteine residues to form intramolecular lanthionine ring systems.[35] Lantibiotics are generally divided into type A and type B peptides, with the former being more elongated and flexible in solution, with ordered structure only being associated with the intramolecular ring systems, and the latter being more globular and conformationally restrained.[35] Lantibiotics are active against Gram-positive strains and exert their action at the plasma membrane.[37] In contrast, they are inactive against Gram-negative strains as a result of an inability to penetrate the outer membrane.

NMR studies have been used to resolve the structures of several lantibiotics.[38] Cinnamycin and duramycin have been shown to adopt U-shaped globular structures, resulting from their intertwined lanthionine cross-links, which include a head-to-tail thioether.[38] The structures are amphipathic, with hydrophobic residues clustered around the bend of the U-shaped and hydrophilic residues located around the termini. Likewise, the type B peptides mersacidin and actagardine adopt well-defined globular folds in methanol and water:acetonitrile mixtures.[39,40]

The most famous lantibiotic is the class A peptide nisin, which is produced by *Lactococcus lactis* and has been used as a food preservative for more than half a century. The widespread interest in nisin has led to considerable efforts in characterising its structure–activity relationships. NMR structural studies of nisin in the presence of micelles and using ^{31}P NMR suggest that it remains associated with the membrane surface during the formation of pores and does not insert into the hydrophobic bilayer.[41,42] It has been shown recently that nisin has a second mode of action, explaining its nanomolar antibacterial activity. Nisin binds to the membrane-bound peptidoglycan precursor lipid II, preventing its incorporation into the cell wall. The nature of the interaction has been characterised in detail by the structure determination of the nisin lipid II complex. Heteronuclear studies using ^{15}N-labelled nisin, together with unlabelled lipid II, were performed in DMSO.[43] The formation of the 1:1 ratio complex was easily confirmed by significant chemical shift changes in nisin as a result of the interaction with the negatively charged pyrophosphate group. Furthermore, ^{15}N relaxation studies revealed a distinct increase in order parameters in the N-terminal region of nisin on addition of lipid II.[43] The N-terminus of nisin forms a cage-like structure that surrounds lipid II, forming up to five intermolecular hydrogen bonds between backbone amide protons and the pyrophosphate linking-group of lipid II.[43] Two of these hydrogen bonds were directly confirmed by hydrogen bond scalar couplings using ^{31}P-edited ^{1}H–^{15}N HSQC experiments.[43] The geometry of the complex was further determined by 36 intermolecular NOEs between residues 1–10 of nisin and the ligand. Interestingly, although the N-terminal part of nisin is exclusively responsible for the interaction with lipid II, a hinge region and the more flexible C-terminal domain are also required for the formation of membrane pores. The suggested mechanism is that the N-terminal region binds to lipid II and remains at the surface while the C-terminal domain inserts into the membrane and induces the pore.[44] The importance of lipid II for the nisin pore is evident from studies showing that the lifetime and diameter of the pore in membranes containing lipid II are 6 s and 2 nm, respectively, whereas in membranes lacking lipid II, the

diameter is reduced to 1 nm and the lifetime of the pore is in the millisecond range.[45]

3.3.2 Class II bacteriocins: heat stable non-lantibiotic peptides

Class II bacteriocins can be further divided into four groups based on structural features: pediocin-like bacteriocins, two-peptide bacteriocins, cyclic bacteriocins and linear non-pediocin-like one-peptide bacteriocins. NMR has been used to characterise examples from each of these subgroups.

3.3.2.1 Pediocin-like bacteriocins.   The pediocin-like bacteriocins are the most homogenous and perhaps the most studied group, and are produced by a number of strains of lactic acid bacteria.[36] Pediocin-like peptides are between 37 and 48 amino acids in length, cationic and exert activity by disrupting bacterial membranes. Five members of the family (leucocin A,[46] carnobacteriocin B2,[47] curvacin A,[48] sakacin P[49] and a mutated analogue of sakacin P[49] with an artificial disulphide bond) have been studied by NMR. Pediocin-like peptides are unfolded in solution but become structured when associated with membrane mimics, making them ideal for NMR studies using micelle solution. A small antiparallel β-sheet in the conserved N-terminal region, which is stabilised by one disulphide bond, characterises their structure. This domain is the more polar region, comprising a number of positive charges. A flexible hinge region precedes the C-terminal domain, which is more hydrophobic and is characterised by an amphipathic α-helix, or in the case of curvacin A, two helical regions with a second hinge between the two.[48] The mechanism of action involves interaction between negative membranes and the cationic N-terminal region followed by insertion of the C-terminal domain into the membrane. The latter is also, at least in some cases, believed to participate in stereo-specific interactions with a membrane component, possibly mannose phosphotransferase system permease.[50] Structural analysis indicates that pediocin-like peptides have two distinct domains with independent specific functions, which is supported by studies on synthetic chimeric peptides. Such peptides retain target selectivity of the parent peptide of the C-terminal domain, suggesting that this region is responsible for target selection.[51]

3.3.2.2 Two-peptide bacteriocins.   The two-peptide bacteriocins are unique antibiotics in that they require two separate peptides, without cross-links, for optimal antimicrobial activity.[36] The two peptides share features with other bacteriocins, including positive charge and amphipathicity. Additionally, they are both gene encoded together on the same operon and are associated with only one immunity protein.[52] The chains of some two-peptide bacteriocins show mild antimicrobial activity independent of one another, whereas for others such as lactococcin G individual α- and β-chains have no activity at 50 μM despite lactococcin G being active at 50 pM.[53] Thus, the two chains should be considered one antimicrobial entity rather than two individual peptides with a synergistic effect.[36,52]

Recently the structures of the two individual peptides of lactococcin G[54] and plantaricin E/F[55] have been studied in DPS micelles and TFE solutions using NMR. All peptides form predominantly helical structures. The structure of lactococcin G was analysed by ^{15}N-edited 3D HSQC–TOCSY and HSQC–NOESY analysis.[54] The α-chain, which is 39 residues long, comprises two helical regions (residues 3–21 and 24–34) while the β-chain, which is 35 residues long, comprises one helical region (residues 6–19). Similar structural features were seen for plantaricin.[55] All two-peptide bacteriocins have a Gly–X–X–X–Gly motif, which is a helix–helix interaction motif. A proposed mechanism of action for the two-peptide bacteriocins is that they insert their helices in the membrane independently, before interacting with each other through these motifs.[54,55]

3.3.2.3 Cyclic bacteriocins.

At least seven bacteriocins discovered over recent years have been shown to have the unusual feature of a head-to-tail circular backbone.[56] This post-translational modification is believed to stabilise the 3D structures of the peptides in a conformation needed for their membrane-disrupting function.

Enterocin AS-48 is the best characterised head-to-tail cyclic bacteriocin and is isolated from *Enterococcus faecalis* S-48.[57] It consists of 70 amino acids, with a large proportion of cationic residues, and possesses potent bactericidal activity against both Gram-positive and Gram-negative strains.[58] It was one of the first confirmed cases of a head-to-tail post-translational cyclisation of a translated gene product.[59] The elucidation of this unique structural feature involved enzymatic cleavage studies and mass spectrometry analysis, as well as characterisation of the AS-48 genomic structure. The AS-48 gene cluster is plasmid encoded and includes helper molecules for both production and self-immunity.[60] The mode of action of AS-48, like most positively charged antimicrobial peptides, involves formation of pores in the plasma membrane, which causes a loss of the proton-motive force and subsequently cell death.[61]

NMR solution studies on a sample of unlabelled purified AS-48 allowed complete proton NMR assignments based on homonuclear two-dimensional experiments, including COSY, TOCSY and NOESY, and standard sequential assignment strategies.[62] Despite its large size for exclusively homonuclear studies, the signal dispersion resulting from its highly ordered structure allowed collection of considerable amounts of structural data, including close to 800 interproton distances derived from NOE correlations, resulting in a well-defined 3D structural ensemble, as shown in Figure 5.[63]

The structure is characterised by a tightly packed five-helix bundle with short loops linking the helical segments.[63] Regular hydrogen bonding patterns are seen throughout the helical regions, with some additional hydrogen bonds stabilising the loops. The helices embed a hydrophobic core that likely greatly contributes to the stability of the fold.[63] Strikingly, the head-to-tail linkage between Met1 and Trp70, the original termini of the precursor protein, is found in the middle of helix 5, suggesting the cyclisation is crucial for the fold itself. This was confirmed to be the case by experiments on the linear precursor produced by recombinant
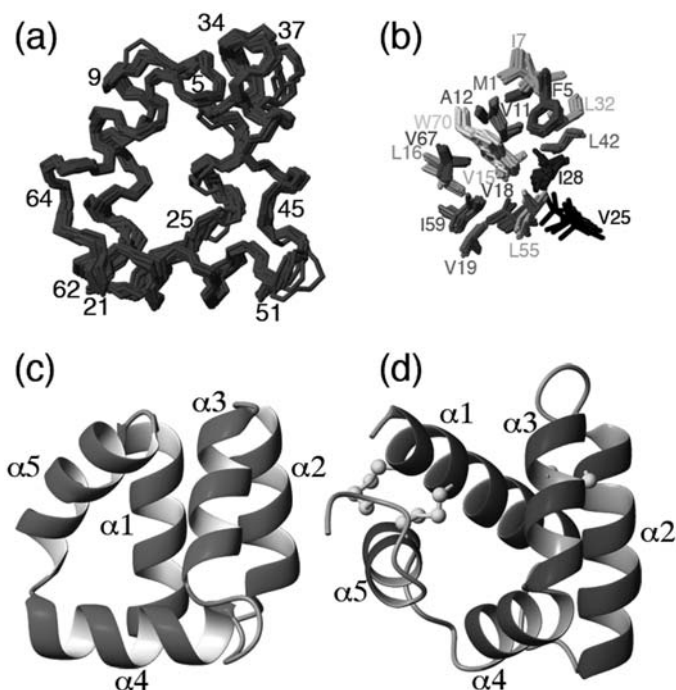
Figure 5 Structural features of bacteriocin AS-48. (a) Structural ensemble representing the solution structure of AS-48 (PDB code 1E68). (b) Packing of hydrophobic sidechains in the core of AS-48. Residues with less than 20% surface exposure are shown and labelled with residue numbers. (c) Ribbon diagram illustrating the orientation of the five helices and comparison to the saposin fold represented by (d) the solution structure of NK-lysin (PDB code 1NKL).

overexpression, which does not appear to be able to adopt a native-like fold.[63] This is not surprising, as linearisation would be expected to disrupt the helix and prevent important interactions of the sidechains of Val67, Met1 and Phe5 with the hydrophobic core. An amphipathic nature is a common feature of antimicrobial peptides, but the amphipathic character of the individual helices in AS-48 is low. Nonetheless, the 10 positive charges in the sequence are clustered in a segment of only 26 residues, resulting in a strongly polarised molecule.[63] The region carrying the positive charges is located in helix 4, the loop between helices 4 and 5 and the N-terminal part of helix 5, and this region is likely to initiate the contact with negatively charged bacterial membranes.

Database searches aimed at identifying related proteins found that the closest structural relative to bacteriocin AS-48 is the effector polypeptide from porcine lymphocytes, NK-lysin.[63] Similar to AS-48, this 76-residue protein adopts a globular fold with five helices surrounding a hydrophobic core but lacks a circular backbone.[64] Instead, NK-lysin comprises three cross-bracing disulphide bonds that stabilise the structure. Despite the linear backbone of NK-lysin creating differences in the orientation of helix 5 in relation to the one in AS-48, and despite no significant sequence homology between them, the backbone

atoms of 55 out of 70 residues in AS-48 can be superimposed on NK-lysin with an RMSD of 3.6 Å.[63]

The NK-lysin fold is also found in several other proteins, including the saposin polypeptides, which solubilise lipids and activate lysosomal hydrolases, and is generally referred to as a 'saposin fold'.[64] All saposins are highly resistant to thermal degradation, withstanding temperatures in the range 90–100°C.[65] Although in the saposins this stability can be accounted for by the three disulphide bonds, it is interesting to note that a circular backbone together with an optimised packing of the hydrophobic core can achieve a similar stabilisation, as the thermal denaturing temperature of AS-48 is 93°C.[58]

The identification of the structural similarity of AS-48 to NK-lysin provides functional clues to the action of AS-48. NK-lysin, like AS-48, carries a net charge of +6 but has a completely different charge distribution, with the charges being distributed in a belt around the molecule.[64] Although both peptides have been shown to interact with the plasma membrane of sensitive cells, their different charge distribution suggests that the orientation in which they approach the membrane may differ. NK-lysin is believed to disrupt membrane by 'molecular electroporation', that is, the formation of pores due to an electric field caused by binding of charged molecules to the membrane.[66] This mode of action relies on the accumulation of sufficient charge density at the membrane. Given that AS-48 carries the same net charge and an even more non-symmetrical charge distribution than NK-lysin, a similar mechanism of membrane disruption is likely. Recent crystallographic and ultracentrifugation experiments have confirmed that bacteriocin AS-48 aggregates into dimers, further supporting the idea of accumulation in the bacterial membrane.[67]

4. PLANT TOXINS

It can be argued that because plants, like bacteria, are limited in their defence capabilities relative to animals, that is, they cannot run or fight if attacked by a predator, their chemical armoury must be particularly potent. Indeed ricin, a plant protein from the castor bean plant, is one of the most toxic substances known to date, with a lethal dose (LD_{50}) of 3–5 μg/kg.[68] Rather than describing the structures of large proteins such as ricin, which are beyond the scope of NMR analysis, here we focus on the structures of smaller peptidic toxins produced by plants for defence against pathogen or predator attack. These molecules are of interest for a number of reasons, including their potential applications as new pesticides, typically via the transfer of their genes to non-producer crop species for the protection of those crops against pests, or in the discovery of new drugs. They also have applications as structural scaffolds for protein engineering studies.

4.1 Thionins

Thionins are cystine-rich, cationic peptides and are ~5 kDa in size.[69] They are subdivided into α/β-thionins and γ-thionins. The γ-thionins are now generally

referred to as plant defensins because they are structurally more closely related to mammalian and insect defensins than to α/β-thionins.[70] There are four classes of α/β-thionins: type I α/β-thionins contain 45 amino acids and have four disulphide bonds; type II thionins are of similar size and also have four disulphide bonds; type III thionins contain 45–46 amino acids and have three disulphide bonds; and type IV thionins are ~46 amino acids long, have three disulphide bonds and are of neutral charge. The type I and II thionins differ in the number of basic residues in their sequences, typically 10 for type I and 7 for type II.[69,71]

Although the different types of thionins have different numbers of disulphide bridges and variations in their residue types, their overall structure is similar, as revealed from NMR and X-ray structures.[69] Their structures comprise an N-terminal β-strand linked to two antiparallel α-helices connected by a short coil motif, followed by another β-strand forming an antiparallel β-sheet and a C-terminal coiled region. Figure 6 highlights the two-helical nature of plant thionins with the NMR-derived structure of viscotoxin B,[72,73] a type III thionin that occurs in the mistletoe plant *Viscum album*. Along with viscotoxins A2 and A3, it is among the most abundant thionins that occur in mistletoe-derived medicines used in anticancer remedies. The structures of various analogues have been useful in rationalising the variations in cytotoxic activity of the different viscotoxins.

Thionins are thought to exert their toxic effects through interactions with membranes.[69,71,74] In the 'carpet' model, peptides accumulate on the membrane surface, resulting in changes in membrane fluidity, and ultimately disruption of the membrane.[75] An alternative mechanism for loss of membrane integrity by thionins is via the solubilisation of phospholipids.[76] This variation of the carpet model is based on the observation of a conserved binding site for phospholipid head groups in thionins and their tendency to form oligomers. It has been
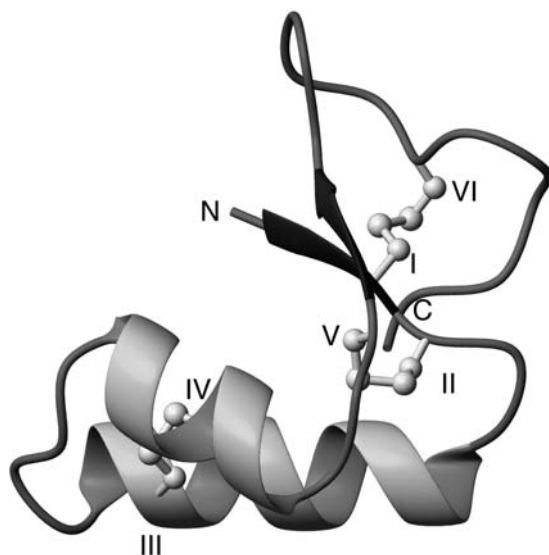
Figure 6   Three-dimensional structure of viscotoxin B (1JMP) from mistletoe (*Viscum album*).

proposed that after an electrostatically driven approach to the membrane, the hydrophobic α-helical face of the thionin inserts into the membrane, leading to the formation of patches of negatively charged lipids close to the positively charged thionin.[69,76] The reduced activity of viscotoxin B over viscotoxins A2 and A3 is thought to be related to the positioning of an Arg residue protruding outside the hydrophobic plane formed by the two amphipathic helices through which the viscotoxins bind to membranes.

4.2 Plant defensins

Plant defensins are cystine-rich, cationic peptides, which range in size from 45 to 54 amino acids and generally include eight cysteine residues involved in four disulphide bonds. They were first discovered in wheat and barley[77] and it is now thought that most plants express defensins in a wide range of tissues.[78–80] Their biological activities are targeted at many plant pests, including fungi, bacteria and insects. The 3D structure of plant defensins comprises an N-terminal β-strand followed by an α-helix and two more β-strands. Together the β-strands form a triple-stranded antiparallel β-sheet. The structure is stabilised by disulphide bonds, two of which connect the α-helix and the central β-strand. A third disulphide bond stabilises the structure by linking the β-strand after the helix to the coiled part after the α-helix. This motif is referred to as the cysteine-stabilised αβ-motif (CSαβ)[75,81,82] and also occurs in toxins isolated from insects, spiders and scorpions.[83–87] The fourth disulphide bond links the C-terminus with the N-terminal β-strand. Two plant defensins, PhD1 and PhD2, feature a fifth disulphide bond and have been proposed to be the prototypes of a new subclass of defensins.[75,82]

The global structure of plant defensins is notably different from α/β-thionins, which is one of the reasons for the different nomenclature, but defensin structures have some parallels with toxins seen in animals. The structures of the antifungal plant defensins Rs-AFP[81] and NaD1[88] from radish and tobacco, respectively, are shown in Figure 7, where they are compared to the thionin β-purothionin,[89] the structurally related antimicrobial toxin drosomycin, isolated from fruit flies[90] and the ion-channel blocking toxin charybdotoxin from scorpions.[84] This comparison highlights the common structural scaffold that has been adopted by plants and insects as part of their defence strategies, and incidentally also highlights the valuable contribution that NMR spectroscopy has played in delineating the structures of these scaffolds.

4.3 Plant proteinase inhibitors

Plants express a variety of typically very stable proteinase inhibitors in a range of tissues, from seeds to leaves to flowers, which are toxic to microbes and predatory insects. These peptide-based inhibitors come in a range of sizes, from the smallest gene-encoded cyclic peptide known to date, sunflower trypsin inhibitor 1 (SFTI-1),[91,92] a 14-residue cyclic peptide with a single disulphide bond, to squash inhibitors[93] that are approximately 30 residues in size and feature a cystine-knot motif, to ∼50-residue proteinase inhibitors found in the stigmas of the ornamental
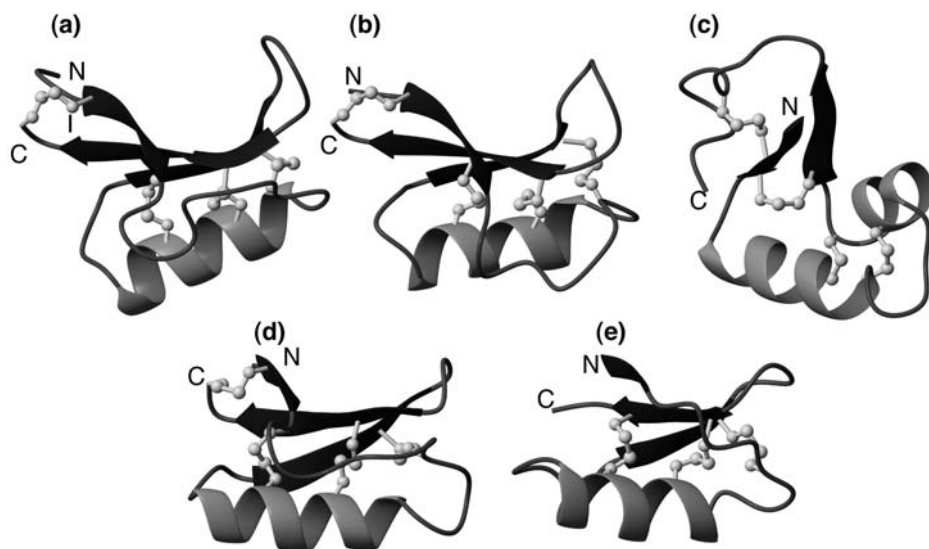
Figure 7 Comparison of the plant defensin structures (a) Rs-AFP (PDB code 1AYJ) and (b) NaD1 (PDB code 1MR4) with (c) β-purothionin (PDB code 1BHP) reveals the structural differences between plant defensins and α/β-thionins. The plant defensin architecture resembles that of insect defensins, for example, (d) drosomycin (PDB code 1MYN) or (e) the scorpion toxin charybdotoxin (PDB code 2CRD).

tobacco *Nicotiana alata*.[94] NMR has been used extensively in the characterisation of these and other classes of protease inhibitors but for illustrative purposes, here we focus on SFTI-1 and the squash inhibitors, both of which have some similarities to another large family of defence molecules called cyclotides that we describe in some detail later in this article.

4.3.1 SFTI

SFTI-1 is a 14 amino acid cyclic peptide expressed in the seeds of sunflowers.[91] As its name suggests, it is a potent trypsin inhibitor, and indeed is the most potent Bowman–Birk inhibitor (BBI) known, with a subnanomolar inhibition constant for trypsin. Although not strictly a toxin, since its natural function is not yet known, we include it here because of our focus on cyclic peptides from plants, and because other trypsin inhibitors from plants are regarded as toxins because of their toxic effects on insect pests.

   The structure of SFTI-1 was first reported in complex with trypsin, with the X-ray structure revealing the head-to-tail cyclic peptide backbone braced with a single disulphide bond.[91] The complex with trypsin is very well defined and characterised by a series of strong hydrogen bonding interactions between the β-hairpin structure of the peptide and trypsin, accounting for the exceptional potency of SFTI-1 as an inhibitor. The NMR solution structure shown in Figure 8[95] is very similar to the crystal structure, confirming that SFTI-1 is a rigid molecule and that its conformation does not change on binding. The rigidity derives from a
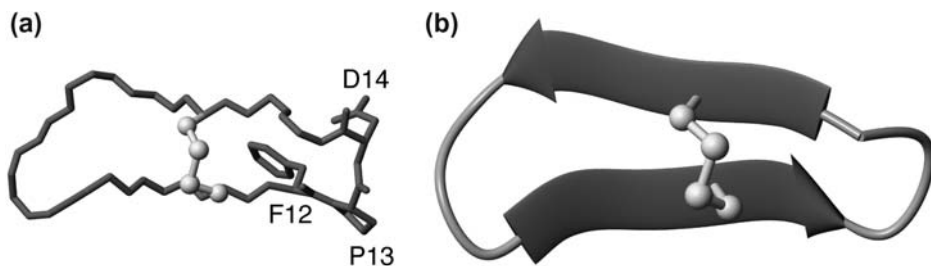
Figure 8 Structural data on SFTI-1. The three-dimensional structure is shown in stick format in (a), with the secondary structure shown in (b).
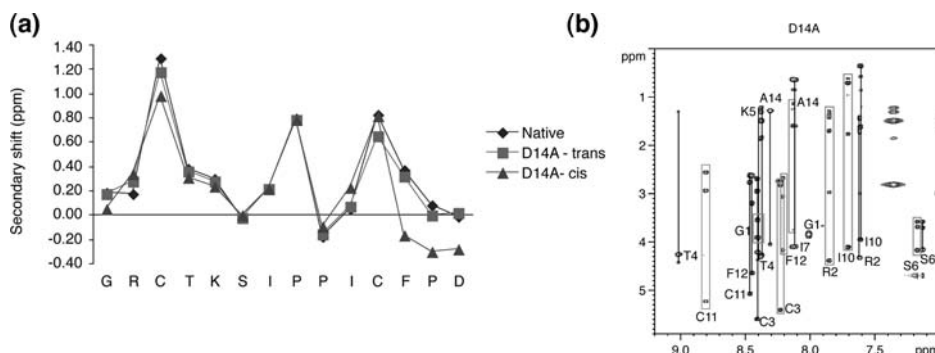
Figure 9 NMR data showing the *cis/trans* isomerisation of an alanine mutant of SFTI-1. (a) A comparison of the secondary shifts of native SFTI-1 with the mutant in which Asp14 is replaced with an Ala. The *trans* isomer is very similar to the native peptide, whereas the *cis* isomer has differences around Pro13. (b) TOCSY spectra of the Asp14 mutant highlighting the second conformation that occurs as a result of *cis/trans* isomerisation around Pro13. The *cis* conformation is not observed in the native peptide.[96]

combination of the cyclic backbone, bracing disulphide bond and internal hydrogen bonding network across the strands of the hairpin structure.

Recently, NMR has been invaluable in defining structure–activity relationships of SFTI-1. An Ala scan of SFTI-1 showed that mutations of single residues did not perturb the overall fold.[96] A full 3D structure determination of all of the Ala mutants was not necessary to come to this conclusion, which was achieved by noting the similarity of the αH chemical shifts of the mutants. The most significant structural change occurred when Asp14 was mutated to Ala and in this case two conformations were present in the spectra as a result of *cis/trans* isomerisation of Pro13, as shown in Figure 9b. It appears that Asp14 is important in stabilising the *trans* peptide bond preceding Pro13 and is therefore a key residue in maintaining the highly constrained structure of SFTI-1. This stabilisation is related to a hydrogen bond between the sidechain of Asp14 and the amide proton of Arg2 that is lost on Ala substitution. This study also revealed that a conserved *cis*-proline bond in BBIs is not critical for a well-defined structure or nanomolar inhibitory activity of trypsin. In full-length BBIs, this *cis*-proline appears to be

critical for structure and activity, and therefore it appears that the tightly folded SFTI-1 scaffold overcomes the need for this residue.[96]

4.3.2 Squash inhibitors

The seeds of squash plants are rich in a family of trypsin and chymotrypsin inhibitors that are approximately 35 amino acids in size and have been extensively investigated not only for their enzyme inhibitory activity, but also because they are very stable mini-protein scaffolds with applications in protein engineering. The best studied examples are *Ecballium elaterium* trypsin inhibitor (EETI-II) and *Cucurbita maxima* trypsin inhibitor (CMTI). Both X-ray and NMR have been used to characterise their structures, which incorporate a cystine-knot motif formed by three conserved disulphide bonds.[93] We will describe this motif in more detail in a later section describing the plant cyclotides.

Although the majority of squash trypsin inhibitors are conventional peptides with free N- and C-termini, two examples, MCoTI-I and MCoTI-II, from the seeds of the tropical vine *Momordica cochinchinensis*, have a head-to-tail cyclised backbone, and on this basis form part of the cyclotide family of plant proteins. As with SFTI-1, the cyclic backbone is assumed to have evolved to confer advantages on these molecules over their linear counterparts. To test this hypothesis, a recent study on EETI-II and MCoTI-II used NMR to monitor thermal unfolding to determine the differences in intrinsic structural stability of linear versus cyclic homologues. Interestingly, little difference was observed, suggesting that cyclisation may have evolved for reasons other than just improved structural integrity. For example, this could include reducing susceptibility to chemical denaturation, or to proteolysis, or providing an additional loop for conferring affinity and specificity on binding interactions.[97] Consistent with the first of these suggestions, the studies suggested that the cyclic form is more stable to denaturants, a property that may prove useful in the use of these molecules as drug design candidates.[97]

4.4 Cyclotides

Cyclotides are a family of disulphide-rich plant peptides that are characterised by their unique topology comprising a head-to-tail cyclised backbone and a knotted arrangement of three disulphide bonds that cross-link their six conserved Cys residues.[98,99] Their characteristic cystine-knot motif comprises a ring formed by two disulphide bonds (Cys^I–Cys^{IV} and Cys^{II}–Cys^V) and their connecting backbone segments that is penetrated by a third disulphide bond (Cys^{III} and Cys^{VI}). The structural features of the cyclic cystine-knot motif are highlighted for the prototypic cyclotide, kalata B1, in Figure 10, which also shows the location of six loops that comprise the backbone segments between successive cysteine residues.

Cyclotides have a range of biological activities, with several fitting into the 'toxic' category, including haemolytic,[100] insecticidal,[101,102] nematocidal[103] and cytotoxic activities.[104] They were originally discovered based on the use of the African plant *Oldenlandia affinis* as a uterotonic agent in indigenous medicine.[105]
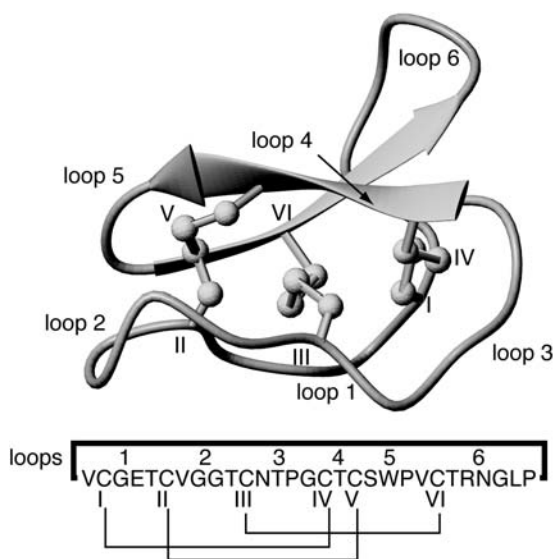
Figure 10 Three-dimensional structure and sequence of the cyclotide kalata B1 (PDB code 1NB1). The cysteine residues are labelled with Roman numerals and the intercysteine loops are labelled 1–6.

The plant was traditionally boiled in water to produce a medicinal tea that was used to accelerate childbirth. Reports of this use stimulated interest in characterising the bioactive component, which was subsequently found to be a 29 amino acid peptide referred to as kalata B1.[105] Cyclotides have also been reported to possess antimicrobial activity,[106] and, for example, synthetic versions of the cyclotides circulin B and cyclopsychotride A are active against both Gram-positive and Gram-negative bacteria.[106] Impaired antimicrobial activity of cyclotides is observed at high salt concentration in the assay buffer and the phenomenon of activity linked to ionic strength has also been described for thionins and plant defensins and is an indicator of activity at membranes.

It appears that the main functional role of cyclotides in plants is as defence agents against insect pests. Jennings et al.[101] showed that cyclotides are toxic to the caterpillars *Helicoverpa punctigera* and *H. armigera*. After consuming a diet containing kalata B1 or kalata B2, these insects are stunted in their growth and development.[101]

In addition to the interest associated with the biological activities of cyclotides, their unusual structures have attracted interest from structural biologists and drug designers. Together, the backbone cyclisation and cystine-knot motif render cyclotides as a class of structurally unique peptides that show exceptionally high stability against chemical, thermal or enzymatic degradation.[107–112] Because of this stability, cyclotides have been proposed to have applications as protein engineering templates.[113]

Elucidation of the structures of cyclotides has relied heavily on NMR studies, which were, for instance, pivotal in defining that kalata B1 had a cyclic peptide

backbone.[114] Initial studies aimed at defining the disulphide connectivity suggested the cyclic cystine knot as a signature motif for cyclotides.[98,99,114] However, as in many disulphide-rich peptides, alternative disulphide connectivities are theoretically possible, and in some cases are energetically similar to the native connectivity. After the original structure of kalata B1 was published, a study by a different group suggested an alternative laddered, rather than a knotted, disulphide connectivity.[33] Subsequent chemical reduction studies[115] and NMR studies identifying the configuration of the cystine sidechains through careful measurements of $^3J_{H\alpha-H\beta}$ coupling constants[34] showed that the original knotted topology was, in fact, correct. Figure 11 shows some of the NMR data that were valuable in reaffirming the knotted disulphide connectivity.

The controversy over the connectivity does highlight the fact that the determination of disulphide connectivities in disulphide-rich peptides is notoriously difficult and caution needs to be exercised in using solely NMR methods to determine disulphide connectivity. Isotopic labelling approaches[116] have been recently used for conotoxins, a disulphide-rich class of animal toxins that are described in more detail later in this article.

So far, cyclotides have been discovered in plants from the Violaceae (violet), Rubiaceae (coffee) and Cucurbitaceae (cucumber) families[110] and have been divided mainly into two structural subfamilies called the Möbius and bracelet cyclotides. These two subfamilies are distinguished by the presence of a *cis*-proline residue in loop 5 for the Möbius subfamily.[34,98,102,117,118] On the basis of their trypsin inhibitory activity, the two cyclotides MCoTI-I and MCoTI-II[93,119,120] form a third subfamily, referred to as the trypsin inhibitor cyclotides. As noted earlier, these peptides are homologous to linear cystine knot containing trypsin inhibitors from squash plants. By contrast, it is rare to find non-cyclic analogues of cyclotides from the two main subfamilies, and indeed the only example for which a structure is reported is violacin A.[121]

Figure 12 shows an overview of the structural features of the three subfamilies of cyclotides, as exemplified by kalata B2 (Möbius subfamily),[102] cycloviolacin O1 (bracelet subfamily)[34] and MCoTI-II (trypsin inhibitor subfamily).[119] In addition to the cyclic backbone and knotted topology, all cyclotides are stabilised by a network of hydrogen bonds. This network has been particularly well studied for the two major subfamilies, Möbius and bracelet, where a conserved glutamic acid residue in loop 1 of the structures forms hydrogen bonds with the backbone amides of two residues in loop 3. The pK_a of the glutamic acid residue was measured by recording spectra at different pH values and plotting the change in chemical shift of residues proximal to the glutamic acid. Figure 13 shows the pH titration for Asn15 and Thr16 for kalata B1 and highlights the hydrogen bonds involving these residues. Low pK_a values were observed for the conserved glutamic acid in kalata B1 and cycloviolacin O1 (3.5 and 3.0, respectively), indicating that the deprotonated state is stabilised.

The mechanism of action of cyclotides is thought to involve membrane binding. This suggestion is supported by recent surface plasmon resonance studies showing that the cyclotides kalata B1 and B6 bind to lipids.[122] The structure of kalata B1 in contact with DPC micelles, used as an NMR-friendly model
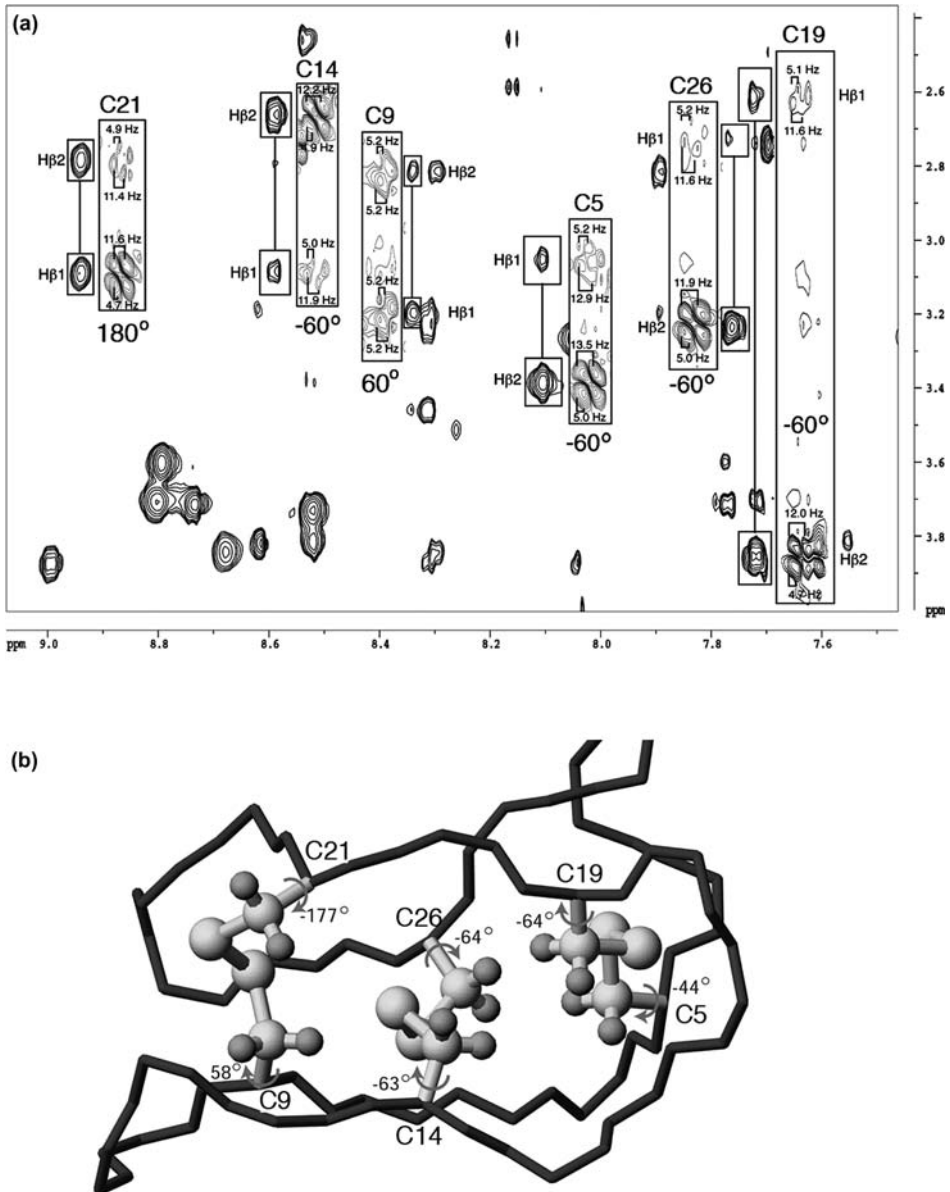
Figure 11 Cysteine conformations in kalata B1. (a) ECOSY spectrum of kalata B1 with the HαHβ cross-peaks for the cysteine residues shown. The intensities of the respective NOESY are shown beside the ECOSY peaks. (b) Average χ1 dihedral angles in the NMR ensembles, consistent with the dihedral angles determined experimentally by NOE and coupling constants.
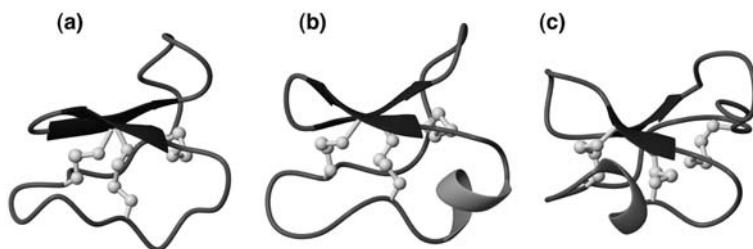
Figure 12 Three-dimensional structures of kalata B2 (a), cycloviolacin O1 (b) and MCoTI-II (c) (PDB codes 1PT4, 1NBJ and 1IB9, respectively), shown as representatives of the Möbius, bracelet and trypsin inhibitor subfamilies of cyclotides.
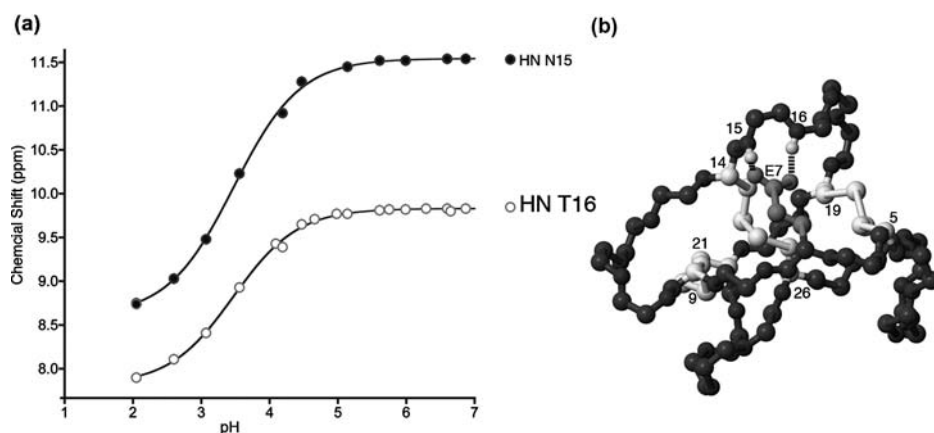
Figure 13 NMR and structural data supporting a hydrogen bonding network in cyclotides linking a conserved Glu residue in loop 1 (Glu7) with backbone amides of loop 3. (a) pH titration of selected residues in kalata B1. Proton chemical shifts for the amide protons of Asn15 and Thr16 are plottted as a function of pH. These residues display a marked pH dependence as a result of the protonation of Glu7. (b) The hydrogen bond network is highlighted in the NMR structure of kalata B1.

membrane system, was reported recently.[123] The proposed interface of the Möbius cyclotide kalata B1 with a DPC micelle is shown in Figure 14, and coincides with a surface-exposed patch of hydrophobic residues that is observed in all cyclotides studied so far. Consistent with membrane binding being a general mechanism for the activity of cyclotides, Svangard et al. demonstrated that the bracelet cyclotide cycloviolacin O2 is capable of disrupting lipid membranes.[124] NMR studies have also demonstrated that kalata B1 and kalata B7 can coordinate Mn^{2+} ions, as evident from specific line broadening of protons near the conserved Glu residue, due to the paramagnetic relaxation effect of the metal ion.[33,125] The affinity of this interaction appears to be weak and its biological significance is not clear, although it has been suggested as one mechanism to enhance the positive charge on cyclotides so as to facilitate binding to anionic membrane components.[33,125]
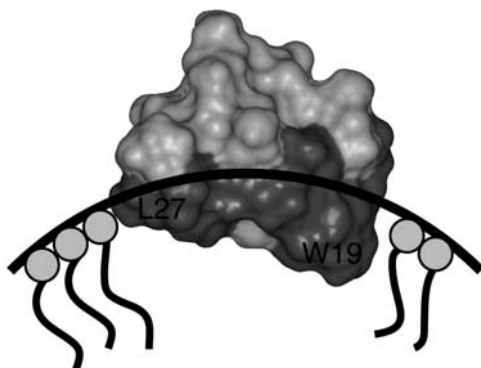
Figure 14   Proposed interaction of kalata B1 with dodecylphosphocholine membranes.[123] A schematic representation of DPC micelles is shown with a surface representation of kalata B1. The hydrophobic face of the cyclotide associates with the surface of the micelle.

Interaction with cell membranes as the primary mechanism of action of cyclotides is supported by recent microscopy studies on the guts of larvae that had ingested cyclotides.[126] Analysis of the mid-gut of kalata B1-fed *H. armigera* larvae revealed a pronounced effect on the gut diameter, which was three times bigger than that of larvae on a control diet. Light and electron microscopy showed that the epithelial cells were no longer present, columnar cells had lysed and the morphology of the peritropic membrane had changed.[126] In the same study, it was also found that the cyclic backbone of cyclotides is essential for insecticidal activity. The guts of larvae on a diet of an acyclic mutant of kalata B1 showed only minor damage compared to the effect of the cyclic peptide.[126] These observations make a strong case for the interaction of cyclotides with cell membranes, particularly in the insect gut, as the basis for their biological activity *in vivo*.

There have been a number of structure–activity studies on cyclotides and a recent alanine scan, in which every individual non-cysteine residue was successively mutated to alanine, showed that there is a patch of surface-exposed residues essential for insecticidal activity.[127] Interestingly, these bioactive residues all cluster on one face of the molecule and do not correspond to the hydrophobic patch on the surface that is thought to be involved in membrane binding. This duality of a membrane-binding patch and a bioactive patch is puzzling at first but it is thought to reflect a self-association phenomenon for cyclotides in which the bioactive patch mediates self-association, which is required as well as membrane binding for bioactivity.[127] NMR studies were crucial in these mutagenesis studies and were used to confirm that alanine mutagenesis did not disrupt the fold of cyclotides, thus eliminating the possibility that structural variations might have confounded the interpretation of the bioassay data.

The biosynthesis of cyclotides involves precursor proteins that contain one, two or three copies of a single mature peptide domain (e.g. the Oak1 precursor encodes one copy of kalata B1 and the Oak4 precursor encodes three copies of kalata B2[101]), or domains corresponding to different cyclotides (e.g. Oak2 encodes one copy each of kalata B3 and kalata B6[128]). The precursors also contain an

endoplasmic reticulum (ER) signal sequence, a pro-region, one or more copies of a highly conserved N-terminal repeat (NTR) region just upstream of the mature peptide domain and a C-terminal tail.[128] NMR studies have shown that the NTR sequence, when synthesised as an isolated peptide fragment, adopts an α-helical structure, which suggests that it may play a structural role in folding or processing but no structures of any intact cyclotide precursor protein have yet been reported.[128]

In vivo, formation of the disulphide bridges in cyclotides might be facilitated by a protein disulphide isomerase (PDI) recently isolated from O. affinis,[129] whereas backbone cyclisation is mediated by an asparaginyl endopepti- dase.[130,131] Support for the latter proposal comes from the fact that a C-terminal Asn residue is essential for cyclisation of the peptide backbone.[101,130,132] Violacin A, a recently discovered cyclotide derivative from the plant Viola odorata, has a point mutation at the C-terminal residue of the mature peptide (Lys instead of Asn) and is a linear peptide as a result. NMR studies show that its lack of a circular backbone leads to flexibility at the N-terminus, although it features a cystine-knot motif and is otherwise structurally similar to cyclotides.[121]

5. ANIMAL TOXINS

Many animal peptide toxins have been characterised by NMR spectroscopy, including examples from species as diverse as marine sponges to mammals. Although these peptides vary significantly in their sequence, structure and function, they do share common features, such as the structural motifs present and their activities. For example, many toxins target ion channels or have antimicrobial activity. In this section, we have chosen examples from the vast array of available peptide toxin structures to illustrate this structural and functional diversity and similarity.

5.1 Invertebrate toxins

5.1.1 Marine sponges

Marine sponges contain a host of bioactive compounds, particularly small molecules, and also contain a range of peptides that are non-ribosomally synthesised, often containing non-native amino acids. However, there are examples of peptides of ribosomal origin, including, for example, asteropine A isolated from the sponge Asteropus simplex.[133] This peptide comprises 36 residues and three disulphide bonds. It has potent sialidase inhibitory activity and thus has applications in the design of novel viral inhibitors. Structural analysis of asteropine A with NMR spectroscopy revealed a cystine-knot motif, similar to that already described for plant toxins. This observation emphasises the fact that the cystine-knot motif is extremely prevalent in disulphide-rich peptides.[134] Asteropine A, discovered in 2006, was the first reported cystine-knot peptide isolated from marine invertebrates other than from cone snails, which are described in more detail below.
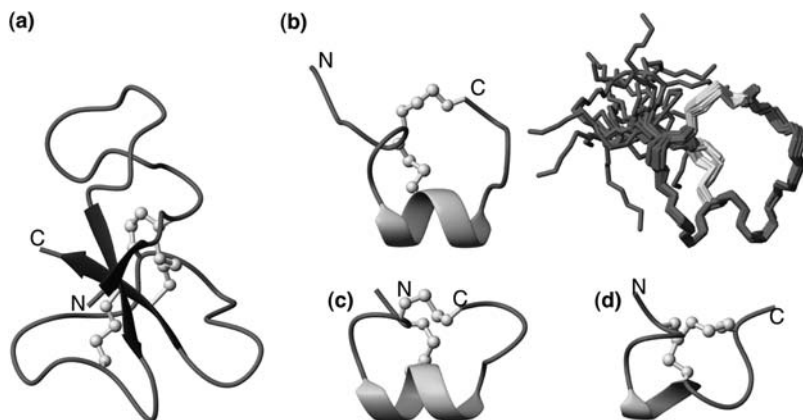
Figure 15 Three-dimensional structures of selected marine toxins. (a) CgNa from sea anemone (PDB code 2H9X); (b) GID from *Conus geographus* (an ensemble of the lowest energy structures is shown to the right to highlight the disordered N-terminal tail (PDB code 1MTQ)); (c) Vc1.1 from *Conus victoriae* (PDB code 2H8S); and (d) RgIA from *Conus regius*.[139] The β-strands are shown as arrows and the helical regions as thickened ribbons.

5.1.2 Sea anemones

In contrast to studies of marine sponges, where the majority of research efforts have focused on small molecule toxins, for sea anemones the majority of characterised toxins are peptidic in nature. Sea anemones release a range of peptide toxins as a protection strategy against predators. These toxins mainly affect ion-channel activity, and the sodium channel toxins from sea anemone have been broadly classified into type I and type II toxins based on sequence homology. Several comprehensive reviews have been published on this family of toxins.[135–137] A recent example, CgNa, was isolated from the Caribbean sea anemone *Condylactis gigantea* and contains 47 amino acids.[138] The structure contains an antiparallel β-sheet and three disulphide bonds that brace the structure, as shown in Figure 15a. Interestingly, the structure contains elements that are similar to the type I and type II toxins, as well as elements that are different to other known toxins. In particular, a surface-exposed patch of hydrophobic residues, which is present in all anemone-derived peptide toxins, is disrupted by negatively charged surface patches. This difference confers unique functional properties to this toxin in terms of action at voltage-gated sodium channels.[138]

5.1.3 Cone snails

One of the most extensively studied families of peptide toxins, the conotoxins, is isolated from marine cone snails.[140,141] Each snail produces a suite of 100–200 peptides in its venom, which is used for the capture of prey, and given that more than 500 species of cone snails are thought to exist, conotoxins represent an enormous diversity of peptide toxins. They have been classified into families, based on their target receptor specificity, and superfamilies, according to their

precursor signal sequences, and we will refer to these families and superfamilies later in this article. As well as being vital for the natural physiological functions of their host species, conotoxins have exciting potential therapeutic applications based on their potent activity and selectivity for a range of ion channels, transporters and receptors. One conotoxin, MVIIA (with the trade name Prialt), is already marketed in Europe and the US as a treatment for chronic intractable pain[142,143] and other conotoxins are in various stages of pre-clinical and clinical trials.

The majority of conotoxin structures (115 of 125 structures in the PDB) have been determined by NMR spectroscopy as opposed to X-ray crystallography. They have significant structural diversity as a result of their diverse sequences and disulphide connectivities. Furthermore, conotoxins also have a large number of post-translational modifications, including the presence of hydroxyproline, γ-carboxyglutamic acid and bromotryptophan residues, epimerisation, glycosylation and amidation,[144,145] that enhance their structural diversity. A recent analysis of NMR data for the unusual amino acids present in conotoxins[3] provides a reference source for chemical shifts of post-translationally modified amino acids.

Recent structures in the conotoxin field include those of the conotoxins GID, Vc1.1, RgIA, SIIIA, TxIIIA and conomarphin. These peptides belong to different superfamilies and vary in terms of their structures and biological targets. GID, Vc1.1 and RgIA belong to the α-conotoxin family, which comprises peptides that are generally 12–19 amino acids in length[146,147] and are competitive antagonists of neuronal nicotinic acetylcholine receptor (nAChR) subtypes.[148] α-Conotoxins contain two disulphide bonds with a Cys^I–Cys^{III}, Cys^{II}–Cys^{IV} connectivity, and their 3D structure is characterised by an α-helix centred around Cys^{III}.[149] nAChRs are pentameric membrane receptors and the α-conotoxins act by binding at the interface between two of the subunits.[150–152] There is significant interest in the study of various neuronal nAChR receptor subtypes because they have been implicated in disorders such as pain, Alzheimer's disease, epilepsy[153,154] and small-cell lung carcinoma.[155,156]

α-Conotoxin GID is a 19-residue peptide isolated from the venom of *Conus geographus*.[157] It has two post-translationally modified residues, γ-carboxyglutamic acid and hydroxyproline, but does not have the amidated C-terminus that is typically present in the majority of α-conotoxins. In addition, GID has an unusual N-terminal tail (i.e. it has a few residues N-terminal of the first cysteine residue) that was unprecedented in the α-conotoxin family at the time of its discovery. Analysis of the activity of this peptide against nAChR subtypes expressed in oocytes revealed that it selectively and potently inhibits the α7, α3β2 and α4β2 subtypes of the neuronal nAChR, with high potency, with IC_{50} of 4.5, 3.1 and 152 nM, respectively.[157]

There are limited peptidic inhibitors of the α4β2 subtype, and given its wide distribution in the brain, the discovery of novel inhibitors for this subtype is of significant interest.[158] The unusual N-terminal tail of GID was shown to be important for activity at the α4β2 subtype and prompted NMR studies of structure–activity relationships of GID.[157,159] The NMR structure of GID[157] shows the characteristic fold of the α-conotoxins but the N-terminal tail is disordered in

solution (Figure 15b). Interestingly, removal of the N-terminal tail results in a less well-defined structure despite the fact that the majority of α-conotoxins do not contain this tail. Notwithstanding the structural influence of the tail, an analysis of ^{1}H chemical shifts of a suite of alanine mutants of GID indicated that the majority of residues can be mutated without significant structural perturbations.[159] Combining the structure and activity data showed that a limited number of residues appear to be important for binding of α-conotoxins to neuronal nAChRs, with the α4β2 nAChR subtype being particularly stringent in its binding requirements.

The α9α10 nAChR subtype has also received attention in the recent literature as an important target for therapeutic applications. The α-conotoxins Vc1.1[160] and RgIA[161] are specific antagonists of the α9α10 subtype of the nAChR and have significant analgesic activity in rat models of neuropathic pain.[162,163] Although these peptides target the same nAChR subtype, they belong to different structural subclasses, which are defined by the number of residues between Cys^{II} and Cys^{III} (loop 1), and Cys^{III} and Cys^{IV} (loop 2). Specifically, Vc1.1 and RgIA belong to the 4/7 and 4/3 classes, respectively. Despite the potent activity of these conotoxins at the α9α10 nAChR subtype, it is not currently certain that this is the receptor by which the analgesic activity is mediated. Very recent studies have suggested that the analgesic activity shown by these two peptides might not involve the α9α10 nAChR because some mutants of Vc1.1 maintain activity at the α9α10 nAChR but do not have analgesic activity.[164] It has been suggested that these peptides are also agonists of the G-protein-coupled GABA (B) receptor and that this might be the mechanism of their analgesic activity.[165]

As a result of the different number of residues in the intercysteine loops for Vc1.1 and RgIA, their 3D structures differ. Vc1.1 adopts a well-defined structure[166] as indicated in Figure 15c, but the NMR spectra recorded on RgIA reveal several residues (Asp^5, Tyr^{10} and Cys^{12}) with broadened resonances, indicating localised conformational exchange.[139] The main element of secondary structure of RgIA is a 3_{10} helix (Figure 15d) rather than an α-helix observed in most of the α-conotoxins. Further studies are underway to determine the utility of these peptides as drug leads.

Several other conotoxins have also been shown to have analgesic activity, including SIIIA, which is a potent sodium channel blocker, and therefore belongs to the μ-conotoxin family. The structure of SIIIA has recently been determined,[167] and although it does not target the nAChR it has a similar overall fold to the α-conotoxins, with a helical region centred around a cysteine residue. Despite the overall fold being similar, there is no sequence similarity to the α-conotoxins, and indeed SIIIA contains three disulphide bonds rather than the characteristic two of the α-conotoxins. The structural study on SIIIA included a dynamics analysis, which showed that the N-terminus and Ser^9 have more flexibility than the rigid C-terminal. The ability to elucidate dynamic properties such as these from NMR relaxation measurements is one of the advantages of NMR spectroscopy compared to X-ray crystallography in the study of peptide structures.

Conotoxins belonging to the same superfamily have, by definition, highly similar precursor signal sequences, and are thought to have evolved from a

common ancestral gene. An intensively structurally studied superfamily, the M-superfamily, comprises conotoxins with three disulphides, and has been divided into different branches based on the number of residues between the cysteine residues. The different branches have different disulphide connectivities. Conotoxin TxIIIA is a member of the m-1 branch of the M-superfamily, and contains 15 residues. Analysis of the structure with NMR spectroscopy revealed a 'triple-turn' motif similar to an m-2 branch member, MrIIIA, despite the different sequences and disulphide connectivity.[168] Elucidation of the structure–activity relationships for these peptides awaits the discovery of their receptors.[168]

Another member of the M-superfamily, conomarphin also contains 15 residues but is devoid of disulphide bonds and contains a d-amino acid.[169] Although the mature toxin has no sequence similarity to other M-superfamily peptides, its signal sequence suggests it is part of the M-superfamily. Despite the lack of disulphide bonds, the peptide still has a well-defined structure characterised by a loop region in the middle of the peptide and a 3_{10} helix at the C-terminus. Mutation of the d-Phe residue and subsequent structural analysis suggests that this residue is important in stabilising its well-defined structure. Conomarphin represents a new family of conotoxins, the biological activity of which remains to be determined.[169]

5.1.4 Aracnids and insects

Aracnids are equipped with a sophisticated arsenal of peptide-based toxins used in hunting their prey. As with the toxins described above, these peptides are generally <100 amino acids in size and are amenable to structural analysis with NMR spectroscopy, with some structures shown in Figure 16. Again, this field is dominated by disulphide-rich peptides, some of which contain cystine-knot motifs. For instance, jingzhaotoxin III (JZTX-III) from the Chinese spider *Chilobrachys jingzhao* is a sodium channel inhibitor that contains a cystine-knot motif.[170] This motif is apparent in the 3D structure shown in Figure 16a and an examination of a surface representation of the structure reveals a hydrophobic patch surrounded by charged residues, similar to the tarantula toxin, hanatoxin 1, which blocks potassium channels. Consequently, Liao et al.[170] tested the JZTX-III toxin against potassium channels, and significant inhibitory activity was observed. This study highlights the value of structures for providing insights into biological activities, and is a prime example of where peptides with very different sequences can present similar biological activities.

Another example of a cystine knot containing spider toxin is agelenin, isolated from *Agelena opulenta*.[171] Agelenin also has activity against ion channels but in this case has calcium, rather than sodium or potassium, channel inhibitory activity. By contrast, there are other spider venom peptides with quite different structures and biological activities. The latarcins, from the venom of the *Lachesana tarabaevi* spider, are non-cysteine-containing peptides with antimicrobial activity.[172] Generally, they are thought to be unstructured in solution but form helical structures in membrane environments. The structure of Ltc1 was determined using NMR spectroscopy in SDS micelles and revealed an amphiphilic helix, as shown in Figure 16.[173] Dye-leakage fluorescent assays and ^{31}P NMR spectroscopy
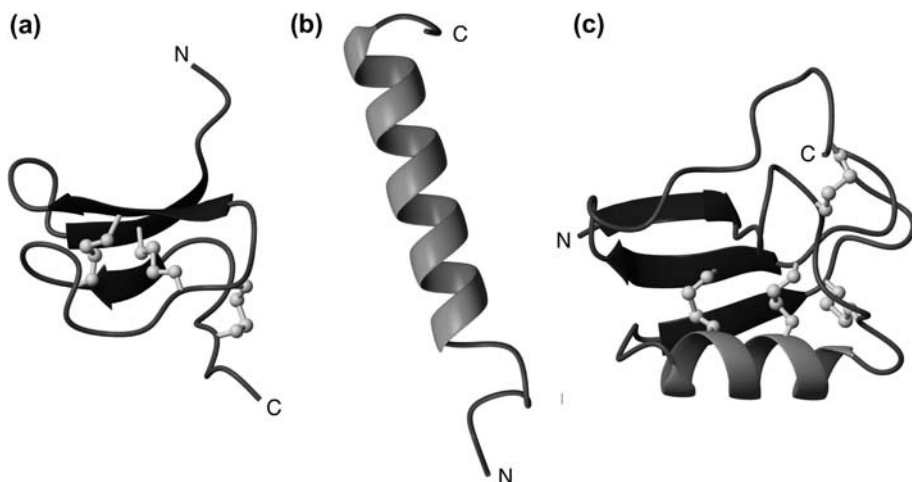
Figure 16 Three-dimensional structures of selected aracnid toxins. (a) Jingzhaotoxin-III from the Chinese spider *Chilobrachys jingzhao* (PDB code 2I1T); (b) BmKalphaIT01 from the scorpion *Buthus martensii* Karsch (PDB code 2E0H); and (c) latarcin-1 from the *Lachesana tarabaevi* spider venom (PDB code 2PCO).

provided evidence that the mechanism of action of these peptides can vary depending on the pattern of hydrophobic residues.[173]

Scorpion toxins display a range of different topologies. For example, BmK αIT01, from *Buthus martensii*, has activity against both insects and mammals.[174] Its structure was analysed by X-ray crystallography and NMR spectroscopy, and interestingly, slight differences were observed. The crystal structure was published in 2003[175] and revealed a non-proline *cis* peptide bond between residues 9 and 10. However, a recent study has shown that in solution, both *cis* and *trans* forms are present; the structure of the *cis* form is shown in Figure 16. It is yet to be proven, but it has been suggested that this conformational flexibility might be responsible for the dual insect/animal activity.[174]

One of the most well-known examples of insect toxins is melittin, a bee venom peptide with potent haemolytic activity. Melittin adopts an α-helical conformation, and has been extensively characterised using a range of techniques, including both solution- and solid-state NMR spectroscopy.[176] Some helical peptides with antimicrobial activity have also been found in wasps, such as eumenine mastroparan-AF (EMP-AF-NH₂) from the venom of the solitary wasp *Anterhynchium flavormarginatum micado*,[177] and the cecropins found in the haemolymph of *Hyalophora cecropia*.[178] Several of these peptides have cytotoxic activity and are potential anticancer agents.[179]

5.2 Vertebrate toxins

In addition to the vast array of toxins isolated from invertebrates, many toxins have been characterised from vertebrates. They include both disulphide-rich
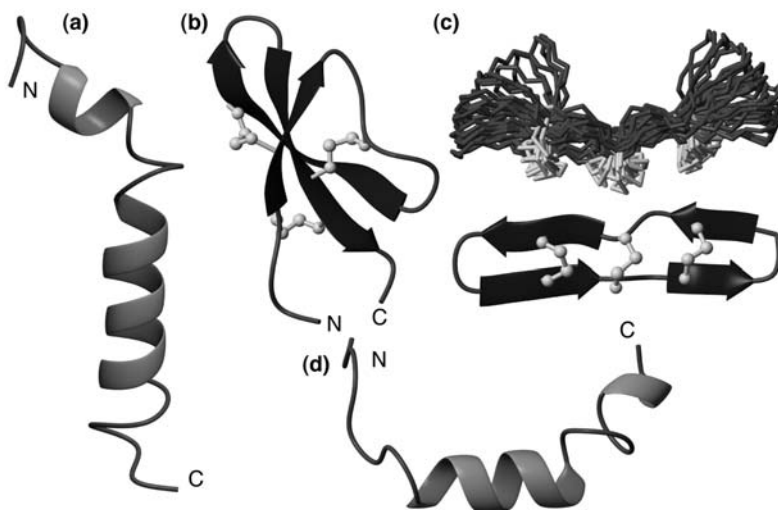
Figure 17 Three-dimensional structures of vertebrate antimicrobial peptides. (a) pardaxin from fish mucous glands (PDB code 1XC0); (b) cryptdin-4 from mouse Paneth cells (PDB code 2GW9); (c) retrocyclin-2, a synthetic peptide based on a human genome sequence (PDB code 2ATG) (an overlay of the 20 lowest energy structures is given to highlight the structural disorder associated with this laddered arrangment of the three disulphide bonds); and (d) fowlicidin-1 from chickens (PDB code 2AMN).

toxins and those without disulphide bonds. To date, the majority of vertebrate toxins examined have involved those with antimicrobial activity but the diversity of their structure suggests that they act via varying mechanisms. Examples are discussed below and their structures are shown in Figure 17.

5.2.1 Pardaxins and temporins

Pardaxins and temporins are antimicrobial peptides isolated from fish mucous and frog skin, respectively. The pardaxins are thought to repel sharks and are toxic to a range of organisms. They are ~ 30 residues in length and NMR studies have shown that pardaxin Pa4 adopts a bend–helix–bend–helix motif in SDS micelles.[180] Solid-state NMR studies have helped to elucidate how the peptide interacts with lipids.[180] The temporins contain only 10–13 residues, making them some of the smallest naturally occurring antimicrobial peptides.[181] Given their small size, it has been suggested that they might be useful templates for the design of novel antimicrobial agents. Similar to other antimicrobial peptides, these peptides adopt helical conformations and their net charges appear to have a significant influence on their membrane-damaging potential.[182]

5.2.2 Animal defensins

In addition to the plant defensins mentioned in Section 4, defensins are also widespread in vertebrates. These antimicrobial peptides are involved in the innate immune response, and are classified into three subfamilies that present

different disulphide connectivities of their three disulphide bonds. The α- and β-defensins share a similar overall fold, which comprises a triple-stranded β-sheet cross-braced by disulphide bonds. The θ-defensins include fewer examples to date, most likely because they have been discovered relatively recently.[183] The α-defensins have a Cys^{I}–Cys^{VI}, Cys^{II}–Cys^{IV} and Cys^{III}–Cys^{V} arrangement of their disulphide bonds (4), whereas the β-defensins have a Cys^{I}–Cys^{V}, Cys^{II}–Cys^{IV} and Cys^{III}–Cys^{VI} connectivity (3). By contrast, the θ-defensins have a laddered arrangement of their disulphide bonds (Cys^{I}–Cys^{VI}, Cys^{II}–Cys^{V} and Cys^{III}–Cys^{IV}). Other features of the θ-defensins are that they are significantly smaller, with only 18 residues compared to more than 30 residues for the α- and β-defensins, and have a head-to-tail cyclic peptide backbone.

Examples of the α-defensins include the mouse Paneth cell α-defensins, termed cryptdins.[184,185] These peptides display antimicrobial activity against both Gram-positive and Gram-negative bacteria, with cryptdin4 (Crp4) displaying the greatest mouse α-defensin bactericidal activity in *in vitro* assays. The mechanism of action of these peptides involves disruption of membranes, which is dependent on the surface positive charge and amphipathicity of the peptide.[184,185] Recently the structure and roles of the invariant disulphide array and of a salt-bridge that is highly conserved throughout the α-defensin peptide family have been studied.[186,187] Crp4 adopts a characteristic α-defensin fold with a triple-stranded β-sheet. Removal of any of the three disulphide bonds has a detrimental effect on the stability of peptide fold as judged by NMR chemical shift analysis. Interestingly, an all Cys-to-Ala mutant completely loses its structure but retains high antimicrobial activity.[186] However, this mutant is highly susceptible to proteolysis.[186] By contrast, mutation of the glutamic acid residue involved in the conserved salt-bridge to aspartic acid only induces local structural changes, mostly involving conformational changes of sidechains, which do not affect the biological activity. The results suggest that the primary role of the conserved salt-bridge in α-defensins is likely to be in *in vivo* biosynthesis and folding rather than in the function of the final folded product.[187]

The 'original' θ-defensin, RTD-1, was discovered in rhesus monkey leukocytes on the basis of its activity against bacteria and fungi.[183] Despite having three disulphide bonds and a circular backbone in common with the cyclotides (Section 4), RTD-1 does not display a well-defined structure in solution, presumably because the disulphide bonds are in a laddered arrangement rather than the knotted arrangement of the cyclotides. Corresponding peptides have not been found in humans, but an analysis of human bone marrow revealed that mRNA homologous to that of the precursors of the RTD-1 is present. However, a premature stop codon within the signal sequence domain of the human mRNA transcripts prevents translation.[188] Synthetic versions of several peptides encoded by these nucleic acid sequences have been made using solid-phase peptide synthesis and were named retrocyclins, reflecting their 'out-of-date' and cyclic nature.[189] Interestingly, these peptides have broad-spectrum antimicrobial activity that can protect human cells from infection by HIV-1, herpes simplex[190] and influenza A[191] viruses. It has been reported that they are also effective against *Bacillus anthracis*.[192] These synthetic peptides essentially represent potent antiviral

agents that humans once probably expressed but no longer do because of a premature stop codon in the corresponding genes.

The tertiary structure of retrocyclin-2 in a membrane-mimicking environment was determined recently and consists of a well-defined β-hairpin braced by the three laddered disulphide bonds.[193] Analytical ultracentrifugation and NMR diffusion experiments indicated that retrocyclin-2 self-associates to form a trimer. Self-association is an important feature of some antimicrobial peptides but the role of this self-association in the mechanism of action of the retrocyclins is yet to be determined.

It has been suggested that retrocyclins might be useful as topical agents for antiviral therapies[194] and so the structural information derived from NMR studies has provided valuable information for the further development of these molecules. A recent study proposing the use of aminoglycosides to essentially make human cells ignore the premature stop codon and produce retrocyclins opens up an alternative approach to antiviral therapy. Although there are several issues yet to be explored with this approach, including potential toxicity problems, it is interesting to speculate that it might one day be possible to switch on the production of retrocyclins in humans to protect against viruses such as HIV.[195] The premature stop codon ironically inactivated in our genome may be reawakened.

5.2.3 Cathelicidins
Cathelicidins are antimicrobial properties that generally lack disulphide bonds. They were originally identified in mammals and later identified in fish, chicken and snake.[192] Snake cathelicidin was shown to have a close evolutionary relationship with platypus cathelicidin, providing support for the notion of the reptilian characteristics of platypus. The 3D structure of chicken cathelicidin (fowlicidin-1) has been determined using NMR spectroscopy and reveals an α-helical structure with a slight kink (Figure 17).[196] This peptide is potent against a range of bacteria and it can also suppress lipopolysaccharide-induced expression of proinflammatory genes in macrophages. Furthermore, it retains activity in high salt concentrations and thus it has been suggested to be useful in the design of novel antimicrobial agents.[196] Fragments of fowlicidin-1 have also been studied with NMR spectroscopy when bound to lipopolysaccharides by using transferred nuclear Overhauser effect spectroscopy and saturation transfer difference NMR studies.[197]

6. CONCLUSIONS AND OUTLOOK

From the examples described in this article, it can be seen that NMR has played an important role in the structural and dynamic characterisation of a wide range of peptide toxins. Most of the focus has been on 3D structural characterisation, but NMR can also provide dynamic information, a feature that distinguishes it from X-ray crystallography. Although there have been relatively few NMR relaxation studies of toxins, we expect that there will be an increasing emphasis

on exploring dynamic aspects of toxins and their interactions with target macromolecules in the future. With increasing advances in NMR technology, and with improvements in peptide synthesis and recombinant technologies for producing toxin peptides, it is anticipated that NMR will continue to play a vital role in the determination of the structure–activity relationships of toxins.

ACKNOWLEDGEMENTS

REFERENCES

1. P. Guntert, *Eur. Biophys. J.*, 2009, **38**, 129.
2. M. Billeter, G. Wagner and K. Wuthrich, *J. Biomol. NMR*, 2008, **42**, 155.
3. U. C. Marx, N. L. Daly and D. J. Craik, *Magn. Reson. Chem.*, 2006, **44(Spec. No.)**, S41.
4. S. B. Kent, *Chem. Soc. Rev.*, 2009, **38**, 338.
5. J. S. Mylne and D. J. Craik, *Biopolym.: Pept. Sci.*, 2008, **90**, 575.
6. O. Gillor, A. Etzion and M. A. Riley, *Appl. Microbiol. Biotechnol.*, 2008, **81**, 591.
7. S. Duquesne, V. Petit, J. Peduzzi and S. Rebuffat, *J. Mol. Microbiol. Biotechnol.*, 2007, **13**, 200.
8. L. A. Draper, R. P. Ross, C. Hill and P. D. Cotter, *Curr. Protein Pept. Sci.*, 2008, **9**, 39.
9. J. O. Solbiati, M. Ciaccio, R. N. Farias, J. E. Gonzalez-Pastor, F. Moreno and R. A. Salomon, *J. Bacteriol.*, 1999, **181**, 2659.
10. L. A. Draper, K. Grainger, L. H. Deegan, P. D. Cotter, C. Hill and R. P. Ross, *Mol. Microbiol.*, 2009, **71**, 1043.
11. F. Baquero and F. Moreno, *FEMS Microbiol. Lett.*, 1984, **23**, 117.
12. S. Duquesne, D. Destoumieux-Garzon, J. Peduzzi and S. Rebuffat, *Nat. Prod. Rep.*, 2007, **24**, 708.
13. M. R. Rintoul, B. F. de Arcuri, R. A. Salomon, R. N. Farias and R. D. Morero, *FEMS Microbiol. Lett.*, 2001, **204**, 265.
14. J. L. Vizan, C. Hernandez-Chico, I. del Castillo and F. Moreno, *EMBO J.*, 1991, **10**, 467.
15. J. G. Heddle, S. J. Blance, D. B. Zamble, F. Hollfelder, D. A. Miller, L. M. Wentzell, C. T. Walsh and A. Maxwell, *J. Mol. Biol.*, 2001, **307**, 1223.
16. J. Mukhopadhyay, E. Sineva, J. Knight, R. M. Levy and R. H. Ebright, *Mol. Cell*, 2004, **14**, 739.
17. K. Adelman, J. Yuzenkova, A. La Porta, N. Zenkin, J. Lee, J. T. Lis, S. Borukhov, M. D. Wang and K. Severinov, *Mol. Cell*, 2004, **14**, 753.
18. J. I. Guijarro, J. E. Gonzalez-Pastor, F. Baleux, J. L. San Millan, M. A. Castilla, M. Rico, F. Moreno and M. Delepierre, *J. Biol. Chem.*, 1995, **270**, 23520.
19. A. M. Pons, I. Lanneluc, G. Cottenceau and S. Sable, *Biochimie*, 2002, **84**, 531.
20. A. Bayer, S. Freund and G. Jung, *Eur. J. Biochem.*, 1995, **234**, 414.
21. R. A. Salomon and R. N. Farias, *J. Bacteriol.*, 1992, **174**, 7428.
22. A. Blond, J. Peduzzi, C. Goulard, M. J. Chiuchiolo, M. Barthelemy, Y. Prigent, R. A. Salomon, R. N. Farias, F. Moreno and S. Rebuffat, *Eur. J. Biochem.*, 1999, **259**, 747.
23. S. Duquesne, D. Destoumieux-Garzon, S. Zirah, C. Goulard, J. Peduzzi and S. Rebuffat, *Chem. Biol.*, 2007, **14**, 793.
24. A. Blond, M. Cheminant, I. Segalas-Milazzo, J. Peduzzi, M. Barthelemy, C. Goulard, R. Salomon, F. Moreno, R. Farias and S. Rebuffat, *Eur. J. Biochem.*, 2001, **268**, 2124.
25. A. Blond, M. Cheminant, D. Destoumieux-Garzon, I. Segalas-Milazzo, J. Peduzzi, C. Goulard and S. Rebuffat, *Eur. J. Biochem.*, 2002, **269**, 6212.

26. J. Yuzenkova, M. Delgado, S. Nechaev, D. Savalia, V. Epshtein, I. Artsimovitch, R. A. Mooney, R. Landick, R. N. Farias, R. Salomon and K. Severinov, *J. Biol. Chem.*, 2002, **277**, 50867.

27. M. J. Bayro, J. Mukhopadhyay, G. V. Swapna, J. Y. Huang, L. C. Ma, E. Sineva, P. E. Dawson, G. T. Montelione and R. H. Ebright, *J. Am. Chem. Soc.*, 2003, **125**, 12382.

28. K. J. Rosengren, R. J. Clark, N. L. Daly, U. Göransson, A. Jones and D. J. Craik, *J. Am. Chem. Soc.*, 2003, **125**, 12464.

29. K. A. Wilson, M. Kalkum, J. Ottesen, J. Yuzenkova, B. T. Chait, R. Landick, T. Muir, K. Severinov and S. A. Darst, *J. Am. Chem. Soc.*, 2003, **125**, 12475.

30. K. J. Rosengren, A. Blond, C. Afonso, J. C. Tabet, S. Rebuffat and D. J. Craik, *Biochemistry*, 2004, **43**, 4696.

31. E. Semenova, Y. Yuzenkova, J. Peduzzi, S. Rebuffat and K. Severinov, *J. Bacteriol.*, 2005, **187**, 3859.

32. O. Pavlova, J. Mukhopadhyay, E. Sineva, R. H. Ebright and K. Severinov, *J. Biol. Chem.*, 2008, **283**, 25589.

33. L. Skjeldal, L. Gran, K. Sletten and B. F. Volkman, *Arch. Biochem. Biophys.*, 2002, **399**, 142.

34. K. J. Rosengren, N. L. Daly, M. R. Plan, C. Waine and D. J. Craik, *J. Biol. Chem.*, 2003, **278**, 8606.

35. S. M. Asaduzzaman and K. Sonomoto, *J. Biosci. Bioeng.*, 2009, **107**, 475.

36. J. Nissen-Meyer, P. Rogne, C. Oppegard, H. S. Haugen and P. E. Kristiansen, *Curr. Pharm. Biotechnol.*, 2009, **10**, 19.

37. Y. Hechard and H. G. Sahl, *Biochimie*, 2002, **84**, 545.

38. F. J. van De Ven and G. Jung, *Antonie van Leeuwenhoek*, 1996, **69**, 99.

39. T. Prasch, T. Naumann, R. L. Markert, M. Sattler, W. Schubert, S. Schaal, M. Bauch, H. Kogler and C. Griesinger, *Eur. J. Biochem.*, 1997, **244**, 501.

40. N. Zimmermann and G. Jung, *Eur. J. Biochem.*, 1997, **246**, 809.

41. A. J. Driessen, H. W. van den Hooven, W. Kuiper, M. van de Kamp, H. G. Sahl, R. N. Konings and W. N. Konings, *Biochemistry*, 1995, **34**, 1606.

42. H. W. Van Den Hooven, C. A. Spronk, M. Van De Kamp, R. N. Konings, C. W. Hilbers and F. J. Van De Van, *Eur. J. Biochem.*, 1996, **235**, 394.

43. S. T. Hsu, E. Breukink, E. Tischenko, M. A. Lutters, B. de Kruijff, R. Kaptein, A. M. Bonvin and N. A. van Nuland, *Nat. Struct. Mol. Biol.*, 2004, **11**, 963.

44. H. E. Hasper, B. de Kruijff and E. Breukink, *Biochemistry*, 2004, **43**, 11567.

45. I. Wiedemann, R. Benz and H. G. Sahl, *J. Bacteriol.*, 2004, **186**, 3259.

46. N. L. Fregeau Gallagher, M. Sailer, W. P. Niemczura, T. T. Nakashima, M. E. Stiles and J. C. Vederas, *Biochemistry*, 1997, **36**, 15062.

47. Y. Wang, M. E. Henz, N. L. Gallagher, S. Chai, A. C. Gibbs, L. Z. Yan, M. E. Stiles, D. S. Wishart and J. C. Vederas, *Biochemistry*, 1999, **38**, 15438.

48. H. S. Haugen, G. Fimland, J. Nissen-Meyer and P. E. Kristiansen, *Biochemistry*, 2005, **44**, 16149.

49. M. Uteng, H. H. Hauge, P. R. Markwick, G. Fimland, D. Mantzilas, J. Nissen-Meyer and C. Muhle-Goll, *Biochemistry*, 2003, **42**, 11417.

50. D. B. Diep, M. Skaugen, Z. Salehian, H. Holo and I. F. Nes, *Proc. Natl. Acad. Sci. U.S.A.*, 2007, **104**, 2384.

51. L. Johnsen, G. Fimland and J. Nissen-Meyer, *J. Biol. Chem.*, 2005, **280**, 9243.

52. C. Oppegard, P. Rogne, L. Emanuelsen, P. E. Kristiansen, G. Fimland and J. Nissen-Meyer, *J. Mol. Microbiol. Biotechnol.*, 2007, **13**, 210.

53. G. Moll, T. Ubbink-Kok, H. Hildeng-Hauge, J. Nissen-Meyer, I. F. Nes, W. N. Konings and A. J. Driessen, *J. Bacteriol.*, 1996, **178**, 600.

54. P. Rogne, G. Fimland, J. Nissen-Meyer and P. E. Kristiansen, *Biochim. Biophys. Acta*, 2008, **1784**, 543.

55. N. Fimland, P. Rogne, G. Fimland, J. Nissen-Meyer and P. E. Kristiansen, *Biochim. Biophys. Acta*, 2008, **1784**, 1711.

56. M. Maqueda, M. Sanchez-Hidalgo, M. Fernandez, M. Montalban-Lopez, E. Valdivia and M. Martinez-Bueno, *FEMS Microbiol. Rev.*, 2008, **32**, 2.

57. A. Galvez, M. Maqueda, E. Valdivia, A. Quesada and E. Montoya, *Can. J. Microbiol.*, 1986, **32**, 765.

58. A. Gálvez, G. GimÅnez-Gallego, M. Maqueda and E. Valdivia, *Antimicrob. Agents Chemother.*, 1989, **33**, 437.

59. B. Samyn, M. Martinez-Bueno, B. Devreese, M. Maqueda, A. Galvez, E. Valdivia, J. Coyette and J. Van Beeumen, *FEBS Lett.*, 1994, **352**, 87.

60. M. Martinez-Bueno, E. Valdivia, A. Galvez, J. Coyette and M. Maqueda, *Mol. Microbiol.*, 1998, **27**, 347.

61. A. Galvez, M. Maqueda, M. Martinez-Bueno and E. Valdivia, *J. Bacteriol.*, 1991, **173**, 886.

62. K. Wüthrich, *NMR of Proteins and Nucleic Acids*, Wiley-Interscience, New York, 1986.

63. C. Gonzalez, G. M. Langdon, M. Bruix, A. Galvez, E. Valdivia, M. Maqueda and M. Rico, *Proc. Natl. Acad. Sci. U.S.A.*, 2000, **97**, 11221.

64. E. Liepinsh, M. Andersson, J. M. Ruysschaert and G. Otting, *Nat. Struct. Biol.*, 1997, **4**, 793.

65. M. Andersson, T. Curstedt, H. Jornvall and J. Johansson, *FEBS Lett.*, 1995, **362**, 328.

66. M. Miteva, M. Andersson, A. Karshikoff and G. Otting, *FEBS Lett.*, 1999, **462**, 155.

67. M. J. Sanchez-Barrena, M. Martinez-Ripoll, A. Galvez, E. Valdivia, M. Maqueda, V. Cruz and A. Albert, *J. Mol. Biol.*, 2003, **334**, 541.

68. J. Audi, M. Belson, M. Patel, J. Schier and J. Osterloh, *JAMA*, 2005, **294**, 2342.

69. B. Stec, *Cell. Mol. Life Sci.*, 2006, **63**, 1370.

70. F. R. Terras, K. Eggermont, V. Kovaleva, N. V. Raikhel, R. W. Osborn, A. Kester, S. B. Rees, S. Torrekens, F. Van Leuven J. Vanderleyden, et al., *Plant Cell*, 1995, **7**, 573.

71. F. Garcia-Olmedo, A. Molina, J. M. Alamillo and P. Rodriguez-Palenzuela, *Biopolymers*, 1998, **47**, 479.

72. A. Coulon, A. Mosbah, A. Lopez, A. M. Sautereau, G. Schaller, K. Urech, P. Rouge and H. Darbon, *Biochem. J.*, 2003, **374**, 71.

73. A. Coulon, E. Berkane, A. M. Sautereau, K. Urech, P. Rouge and A. Lopez, *Biochim. Biophys. Acta*, 2002, **1559**, 145.

74. D. E. A. Florack and W. J. Stiekema, *Plant Mol. Biol.*, 1994, **26**, 25.

75. M. Giudici, R. Pascual, L. de la Canal, K. Pfuller, U. Pfuller and J. Villalain, *Biophys. J.*, 2003, **85**, 971.

76. B. Stec, O. Markman, U. Rao, G. Heffron, S. Henderson, L. P. Vernon, V. Brumfeld and M. M. Teeter, *J. Pept. Res.*, 2004, **64**, 210.

77. F. J. Colilla, A. Rocher and E. Mendez, *FEBS Lett.*, 1990, **270**, 191.

78. W. F. Broekaert, B. P. A. Cammue, M. F. C. De Bolle, K. Thevissen, G. W. De Samblanx and R. W. Osborn, *Crit. Rev. Plant Sci.*, 1997, **16**, 297.

79. W. F. Broekaert, F. R. G. Terras, B. P. A. Cammue and R. W. Osborn, *Plant Physiol.*, 1995, **108**, 1353.

80. R. W. Osborn, G. W. De Samblanx, K. Thevissen, I. Goderis, S. Torrekens, F. Van Leuven, S. Attenborough, S. B. Rees and W. F. Broekaert, *FEBS Lett.*, 1995, **368**, 257.

81. F. Fant, W. Vranken, W. Broekaert and F. Borremans, *J. Mol. Biol.*, 1998, **279**, 257.

82. B. J. Janssen, H. J. Schirra, F. T. Lay, M. A. Anderson and D. J. Craik, *Biochemistry*, 2003, **42**, 8214.

83. J. H. Pease and D. E. Wemmer, *Biochemistry*, 1988, **27**, 8491.

84. F. Bontems, B. Gilquin, C. Roumestand, A. Menez and F. Toma, *Biochemistry*, 1992, **31**, 7756.

85. Y. Kobayashi, H. Takashima, H. Tamaoki, Y. Kyogoku, P. Lambert, H. Kuroda, N. Chino, T. X. Watanabe, T. Kimura S. Sakakibara, et al., *Biopolymers*, 1991, **31**, 1213.

86. F. Bontems, C. Roumestand, B. Gilquin, A. Menez and F. Toma, *Science*, 1991, **254**, 1521.

87. B. Cornet, J. M. Bonmatin, C. Hetru, J. A. Hoffmann, M. Ptak and F. Vovelle, *Structure*, 1995, **3**, 435.

88. F. T. Lay, F. Brugliera and M. A. Anderson, *Plant Physiol.*, 2003, **131**, 1283.

89. B. Stec, U. Rao and M. M. Teeter, *Acta Crystallogr. D Biol. Crystallogr.*, 1995, **51**, 914.

90. C. Landon, P. Sodano, C. Hetru, J. Hoffmann and M. Ptak, *Protein Sci.*, 1997, **6**, 1878.

91. S. Luckett, R. S. Garcia, J. J. Barker, A. V. Konarev, P. R. Shewry, A. R. Clarke and R. L. Brady, *J. Mol. Biol.*, 1999, **290**, 525.

92. M. L. Korsinczky, H. J. Schirra and D. J. Craik, *Curr. Protein Pept. Sci.*, 2004, **5**, 351.

93. L. Chiche, A. Heitz, J. C. Gelly, J. Gracy, P. T. Chau, P. T. Ha, J. F. Hernandez and D. Le-Nguyen, *Curr. Protein Pept. Sci.*, 2004, **5**, 341.

94. A. H. Atkinson, R. L. Heath, R. J. Simpson, A. E. Clarke and M. A. Anderson, *Plant Cell*, 1993, **5**, 203.

95. M. L. Korsinczky, H. J. Schirra, K. J. Rosengren, J. West, B. A. Condie, L. Otvos, M. A. Anderson and D. J. Craik, *J. Mol. Biol.*, 2001, **311**, 579.

96. N. L. Daly, Y.-K. Chen, F. M. Foley, P. S. Bansal, R. Bharathi, R. J. Clark, C. P. Sommerhoff and D. J. Craik, *J. Biol. Chem.*, 2006, **281**, 23668.

97. A. Heitz, O. Avrutina, D. Le-Nguyen, U. Diederichsen, J. F. Hernandez, J. Gracy, H. Kolmar and L. Chiche, *BMC Struct. Biol.*, 2008, **8**, 54.

98. D. J. Craik, N. L. Daly, T. Bond and C. Waine, *J. Mol. Biol.*, 1999, **294**, 1327.

99. C. K. Wang, Q. Kaas, L. Chiche and D. J. Craik, *Nucleic Acids Res.*, 2008, **36**, D206.

100. T. Schöpke, M. I. Hasan Agha, R. Kraft, A. Otto and K. Hiller, *Sci. Pharm.*, 1993, **61**, 145.

101. C. Jennings, J. West, C. Waine, D. Craik and M. Anderson, *Proc. Natl. Acad. Sci. U.S.A.*, 2001, **98**, 10614.

102. C. V. Jennings, K. J. Rosengren, N. L. Daly, M. Plan, J. Stevens, M. J. Scanlon, C. Waine, D. G. Norman, M. A. Anderson and D. J. Craik, *Biochemistry*, 2005, **44**, 851.

103. M. L. Colgrave, A. C. Kotze, Y. H. Huang, J. O'Grady, S. M. Simonsen and D. J. Craik, *Biochemistry*, 2008, **47**, 5581.

104. E. Svangard, U. Göransson, Z. Hocaoglu, J. Gullbo, R. Larsson, P. Claeson and L. Bohlin, *J. Nat. Prod.*, 2004, **67**, 144.

105. L. Gran, *Medd. Nor. Farm. Selsk.*, 1970, **12**, 173.

106. J. P. Tam, Y. A. Lu, J. L. Yang and K. W. Chiu, *Proc. Natl. Acad. Sci. U.S.A.*, 1999, **96**, 8913.

107. M. L. Colgrave and D. J. Craik, *Biochemistry*, 2004, **43**, 5965.

108. D. J. Craik, *Science*, 2006, **311**, 1563.

109. S. S. Nair, J. Romanuka, M. Billeter, L. Skjeldal, M. R. Emmett, C. L. Nilsson and A. G. Marshall, *Biochim. Biophys. Acta*, 2006, **1764**, 1568.

110. D. J. Craik, M. Cĕmažar and N. L. Daly, *Curr. Protein Pept. Sci.*, 2007, **10**, 176.

111. C. W. Gruber, M. Cemazar, M. A. Anderson and D. J. Craik, *Toxicon*, 2007, **49**, 561.

112. P. B. Pelegrini, B. F. Quirino and O. L. Franco, *Peptides*, 2007, **28**, 1475.

113. D. J. Craik, R. J. Clark and N. L. Daly, *Expert Opin. Investig. Drugs*, 2007, **16**, 595.

114. O. Saether, D. J. Craik, I. D. Campbell, K. Sletten, J. Juul and D. G. Norman, *Biochemistry*, 1995, **34**, 4147.

115. U. Göransson and D. J. Craik, *J. Biol. Chem.*, 2003, **278**, 48188.

116. A. Walewska, J. J. Skalicky, D. R. Davis, M. M. Zhang, E. Lopez-Vera, M. Watkins, T. S. Han, D. Yoshikami, B. M. Olivera and G. Bulaj, *J. Am. Chem. Soc.*, 2008, **130**, 14280.

117. R. J. Clark, N. L. Daly and D. J. Craik, *Biochem. J.*, 2006, **394**, 85.

118. D. J. Craik, N. L. Daly, J. Mulvenna, M. R. Plan and M. Trabi, *Curr. Protein Pept. Sci.*, 2004, **5**, 297.

119. A. Heitz, J. F. Hernandez, J. Gagnon, T. T. Hong, T. T. Pham, T. M. Nguyen, D. Le-Nguyen and L. Chiche, *Biochemistry*, 2001, **40**, 7973.

120. J. F. Hernandez, J. Gagnon, L. Chiche, T. M. Nguyen, J. P. Andrieu, A. Heitz, T. Trinh Hong, T. T. Pham and D. Le Nguyen, *Biochemistry*, 2000, **39**, 5722.

121. D. C. Ireland, M. L. Colgrave, P. Nguyencong, N. L. Daly and D. J. Craik, *J. Mol. Biol.*, 2006, **357**, 1522.

122. H. Kamimori, K. Hall, D. J. Craik and M. I. Aguilar, *Anal. Biochem.*, 2005, **337**, 149.

123. Z. O. Shenkarev, K. D. Nadezhdin, V. A. Sobol, A. G. Sobol, L. Skjeldal and A. S. Arseniev, *FEBS J.*, 2006, **273**, 2658.

124. E. Svangard, R. Burman, S. Gunasekera, H. Lovborg, J. Gullbo and U. Goransson, *J. Nat. Prod.*, 2007, **70**, 643.

125. Z. O. Shenkarev, K. D. Nadezhdin, E. N. Lyukmanova, V. A. Sobol, L. Skjeldal and A. S. Arseniev, *J. Inorg. Biochem.*, 2008, **102**, 1246.

126. B. L. Barbeta, A. T. Marshall, A. D. Gillon, D. J. Craik and M. A. Anderson, *Proc. Natl. Acad. Sci. U.S.A.*, 2008, **105**, 1221.

127. S. M. Simonsen, L. Sando, K. J. Rosengren, C. K. Wang, M. L. Colgrave, N. L. Daly and D. J. Craik, *J. Biol. Chem.*, 2008, **283**, 9805.

128. J. L. Dutton, R. F. Renda, C. Waine, R. J. Clark, N. L. Daly, C. V. Jennings, M. A. Anderson and D. J. Craik, *J. Biol. Chem.*, 2004, **279**, 46858.

129. C. W. Gruber, M. Cemazar, R. J. Clark, T. Horibe, R. F. Renda, M. A. Anderson and D. J. Craik, *J. Biol. Chem.*, 2007, **282**, 20435.

130. I. Saska, A. D. Gillon, N. Hatsugai, R. G. Dietzgen, I. Hara-Nishimura, M. A. Anderson and D. J. Craik, *J. Biol. Chem.*, 2007, **282**, 29721.

131. A. D. Gillon, I. Saska, C. V. Jennings, R. F. Guarino, D. J. Craik and M. A. Anderson, *Plant J.*, 2008, **53**, 505.

132. J. P. Mulvenna, L. Sando and D. J. Craik, *Structure*, 2005, **13**, 691.

133. K. Takada, T. Hamada, H. Hirota, Y. Nakao, S. Matsunaga, R. W. van Soest and N. Fusetani, *Chem. Biol.*, 2006, **13**, 569.

134. S. Cheek, S. S. Krishna and N. V. Grishin, *J. Mol. Biol.*, 2006, **359**, 215.

135. K. Shiomi, *Toxicon*, 2009.

136. Y. Moran, D. Gordon and M. Gurevitz, *Toxicon*, 2009.

137. S. Diochot and M. Lazdunski, *Prog. Mol. Subcell. Biol.*, 2009, **46**, 99.

138. E. Salceda, J. Perez-Castells, B. Lopez-Mendez, A. Garateix, H. Salazar, O. Lopez, A. Aneiros, L. Standker, L. Beress, W. G. Forssmann, E. Soto, J. Jimenez-Barbero and G. Gimenez-Gallego, *Biochem. J.*, 2007, **406**, 67.

140. B. M. Olivera, J. Rivier, J. K. Scott, D. R. Hillyard and L. J. Cruz, *J. Biol. Chem.*, 1991, **266**, 22067.

141. B. M. Olivera and L. J. Cruz, *Toxicon*, 2001, **39**, 7.

142. U. Klotz, *Int. J. Clin. Pharmacol. Ther.*, 2006, **44**, 478.

143. J. A. Williams, M. Day and J. E. Heavner, *Expert Opin. Pharmacother.*, 2008, **9**, 1575.

144. A. C. Rigby, E. Lucas-Meunier, D. E. Kalume, E. Czerwiec, B. Hambe, I. Dahlqvist, P. Fossier, G. Baux, P. Roepstorff, J. D. Baleja, B. C. Furie, B. Furie and J. Stenflo, *Proc. Natl. Acad. Sci. U.S.A.*, 1999, **96**, 5758.

145. J. Kang, W. Low, T. Norberg, J. Meisenhelder, K. Hansson, J. Stenflo, G. P. Zhou, J. Imperial, B. M. Olivera, A. C. Rigby and A. G. Craig, *Eur. J. Biochem.*, 2004, **271**, 4939.

146. J. L. Dutton and D. J. Craik, *Curr. Med. Chem.*, 2001, **8**, 327.

147. J. M. McIntosh, A. D. Santos and B. M. Olivera, *Annu. Rev. Biochem.*, 1999, **68**, 59.

148. L. P. Dwoskin and P. A. Crooks, *J. Pharmacol. Exp. Ther.*, 2001, **298**, 395.

149. E. L. Millard, N. L. Daly and D. J. Craik, *Eur. J. Biochem.*, 2004, **271**, 2320.

150. P. H. Celie, I. E. Kasheverov, D. Y. Mordvintsev, R. C. Hogg, P. van Nierop, R. van Elk, S. E. van Rossum-Fikkert, M. N. Zhmak, D. Bertrand, V. Tsetlin, T. K. Sixma and A. B. Smit, *Nat. Struct. Mol. Biol.*, 2005, **12**, 582.

151. S. B. Hansen, G. Sulzenbacher, T. Huxford, P. Marchot, P. Taylor and Y. Bourne, *EMBO J.*, 2005, **24**, 3635.

152. C. Ulens, R. C. Hogg, P. H. Celie, D. Bertrand, V. Tsetlin, A. B. Smit and T. K. Sixma, *Proc. Natl. Acad. Sci. U.S.A.*, 2006, **103**, 3615.

153. M. J. O'Neill, T. K. Murray, V. Lakics, N. P. Visanji and S. Duty, *Curr. Drug Targets CNS Neurol. Disord.*, 2002, **1**, 399.

154. H. Geerts, L. Finkel, R. Carr and A. Spiros, *J. Neural Transm.*, 2002, Suppl. 203.

155. M. A. Sciamanna, G. E. Griesmann, C. L. Williams and V. A. Lennon, *J. Neurochem.*, 1997, **69**, 2302.

156. A. Codignola, J. M. McIntosh, M. G. Cattaneo, L. M. Vicentini, F. Clementi and E. Sher, *Neurosci. Lett.*, 1996, **206**, 53.

157. A. Nicke, M. L. Loughnan, E. L. Millard, P. F. Alewood, D. J. Adams, N. L. Daly, D. J. Craik and R. J. Lewis, *J. Biol. Chem.*, 2003, **278**, 3137.

158. D. C. Lam, L. Girard, R. Ramirez, W. S. Chau, W. S. Suen, S. Sheridan, V. P. Tin, L. P. Chung, M. P. Wong, J. W. Shay, A. F. Gazdar, W. K. Lam and J. D. Minna, *Cancer Res.*, 2007, **67**, 4638.

159. E. L. Millard, S. T. Nevin, M. L. Loughnan, A. Nicke, R. J. Clark, P. F. Alewood, R. J. Lewis, D. J. Adams, D. J. Craik and N. L. Daly, *J. Biol. Chem.*, 2009, **284**, 4944.

160. D. W. Sandall, N. Satkunanathan, D. A. Keays, M. A. Polidano, X. Liping, V. Pham, J. G. Down, Z. Khalil, B. G. Livett and K. R. Gayler, *Biochemistry*, 2003, **42**, 6904.

161. M. Ellison, C. Haberlandt, M. E. Gomez-Casati, M. Watkins, A. B. Elgoyhen, J. M. McIntosh and B. M. Olivera, *Biochemistry*, 2006, **45**, 1511.

162. N. Satkunanathan, B. Livett, K. Gayler, D. Sandall, J. Down and Z. Khalil, *Brain Res.*, 2005, **1059**, 149.

163. M. Vincler, S. Wittenauer, R. Parker, M. Ellison, B. M. Olivera and J. M. McIntosh, *Proc. Natl. Acad. Sci. U.S.A.*, 2006, **103**, 17880.
164. S. T. Nevin, R. J. Clark, H. Klimis, M. J. Christie, D. J. Craik and D. J. Adams, *Mol. Pharmacol.*, 2007, **72**, 1406.
165. B. Callaghan, A. Haythornthwaite, G. Berecki, R. J. Clark, D. J. Craik and D. J. Adams, *J. Neurosci.*, 2008, **28**, 10943.
166. R. J. Clark, H. Fischer, S. T. Nevin, D. J. Adams and D. J. Craik, *J. Biol. Chem.*, 2006, **281**, 23254.
139. R. J. Clark, N. L. Daly, R. Halai, S. T. Nevin, D. J. Adams and D. J. Craik, *FEBS Lett.*, 2008, **582**, 597.
167. S. Yao, M. M. Zhang, D. Yoshikami, L. Azam, B. M. Olivera, G. Bulaj and R. S. Norton, *Biochemistry*, 2008, **47**, 10940.
168. O. M. McDougal, M. W. Turner, A. J. Ormond and C. D. Poulter, *Biochemistry*, 2008, **47**, 2826.
169. Y. Han, F. Huang, H. Jiang, L. Liu, Q. Wang, Y. Wang, X. Shao, C. Chi, W. Du and C. Wang, *FEBS J.*, 2008, **275**, 1976.
170. Z. Liao, C. Yuan, K. Peng, Y. Xiao and S. Liang, *Toxicon*, 2007, **50**, 135.
171. N. Yamaji, K. Sugase, T. Nakajima, T. Miki, M. Wakamori, Y. Mori and T. Iwashita, *FEBS Lett.*, 2007, **581**, 3789.
172. S. A. Kozlov, A. A. Vassilevski, A. V. Feofanov, A. Y. Surovoy, D. V. Karpunin and E. V. Grishin, *J. Biol. Chem.*, 2006, **281**, 20983.
173. P. V. Dubovskii, P. E. Volynsky, A. A. Polyansky, D. V. Karpunin, V. V. Chupin, R. G. Efremov and A. S. Arseniev, *Biochemistry*, 2008, **47**, 3525.
174. X. Tong, J. Zhu, Y. Ma, X. Chen, G. Wu, F. He, C. Cao and H. Wu, *Biochemistry*, 2007, **46**, 11322.
175. Y. Huang, Q. Huang, H. Chen, Y. Tang, H. Miyake and M. Kusunoki, *Acta Crystallogr. D Biol. Crystallogr.*, 2003, **59**, 1635.
176. H. Raghuraman and A. Chattopadhyay, *Biosci. Rep.*, 2007, **27**, 189.
177. K. Konno, M. Hisada, H. Naoki, Y. Itagaki, N. Kawai, A. Miwa, T. Yasuhara, Y. Morimoto and Y. Nakata, *Toxicon*, 2000, **38**, 1505.
178. D. Hultmark, H. Steiner, T. Rasmuson and H. G. Boman, *Eur. J. Biochem.*, 1980, **106**, 7.
179. J. M. Wu, P. S. Jan, H. C. Yu, H. Y. Haung, H. J. Fang, Y. I. Chang, J. W. Cheng and H. M. Chen, *Peptides*, 2009, **30**, 839.
180. F. Porcelli, B. Buck, D. K. Lee, K. J. Hallock, A. Ramamoorthy and G. Veglia, *J. Biol. Chem.*, 2004, **279**, 45815.
181. M. L. Mangoni, *Cell. Mol. Life Sci.*, 2006, **63**, 1060.
182. F. Abbassi, C. Galanth, M. Amiche, K. Saito, C. Piesse, L. Zargarian, K. Hani, P. Nicolas, O. Lequin and A. Ladram, *Biochemistry*, 2008, **47**, 10513.
183. Y.-Q. Tang, J. Yuan, G. Ösapay, K. Ösapay, D. Tran, C. J. Miller, A. J. Ouellette and M. E. Selsted, *Science*, 1999, **286**, 498.
184. A. J. Ouellette, M. M. Hsieh, M. T. Nosek, D. F. Cano-Gauci, K. M. Huttner, R. N. Buick and M. E. Selsted, *Infect. Immun.*, 1994, **62**, 5040.
185. T. Ayabe, D. P. Satchell, C. L. Wilson, W. C. Parks, M. E. Selsted and A. J. Ouellette, *Nat. Immunol.*, 2000, **1**, 113.
186. A. Maemoto, X. Qu, K. J. Rosengren, H. Tanabe, A. Henschen-Edman, D. J. Craik and A. J. Ouellette, *J. Biol. Chem.*, 2004, **279**, 44188.
187. K. J. Rosengren, N. L. Daly, L. M. Fornander, L. M. Jonsson, Y. Shirafuji, X. Qu, H. J. Vogel, A. J. Ouellette and D. J. Craik, *J. Biol. Chem.*, 2006, **281**, 28068.
188. A. M. Cole, T. Hong, L. M. Boo, T. Nguyen, C. Zhao, G. Bristol, J. A. Zack, A. J. Waring, O. O. Yang and R. I. Lehrer, *Proc. Natl. Acad. Sci. U.S.A.*, 2002, **99**, 1813.
189. R. I. Lehrer and A. Cole, *Curr. Protein Pept. Sci.*, 2004.
190. B. Yasin, W. Wang, M. Pang, N. Cheshenko, T. Hong, A. J. Waring, B. C. Herold, E. A. Wagar and R. I. Lehrer, *J. Virol.*, 2004, **78**, 5147.
191. E. Leikina, H. Delanoe-Ayari, K. Melikov, M.-S. Cho, A. Chen, A. J. Waring, W. Wang, Y. Xie, J. A. Loo, R. I. Lehrer and L. V. Chernomordik, *Nat. Immunol.*, 2005, in press.
192. W. Wang, C. Mulakala, S. C. Ward, G. Jung, H. Luong, D. Pham, A. J. Waring, Y. Kaznessis, W. Lu, K. A. Bradley and R. I. Lehrer, *J. Biol. Chem.*, 2006, **281**, 32755.

193. N. L. Daly, Y. K. Chen, K. J. Rosengren, U. C. Marx, M. L. Phillips, A. J. Waring, W. Wang, R. I. Lehrer and D. J. Craik, *Biochemistry*, 2007, **46**, 9920.
194. A. M. Cole and A. L. Cole, *Am. J. Reprod. Immunol.*, 2008, **59**, 27.
195. N. Venkataraman, A. L. Cole, P. Ruchala, A. J. Waring, R. I. Lehrer, O. Stuchlik, J. Pohl and A. M. Cole, *PLoS Biol.*, 2009, **7**, e95.
196. Y. Xiao, H. Dai, Y. R. Bommineni, J. L. Soulages, Y. X. Gong, O. Prakash and G. Zhang, *FEBS J.*, 2006, **273**, 2581.
197. A. Bhunia, H. Mohanram and S. Bhattacharjya, *Biopolymers*, 2009, **92**, 9.

CHAPTER 3

Application of NMR Spectroscopy in Isotope Effects Studies

Stefan Jankowski

Contents

Abstract Isotope effects on chemical shifts are versatile tools in structure elucidation, particularly useful for the intra- and intermolecular hydrogen bounded systems in the liquid and solid state. Isotope effects on coupling constants are more important theoretically and are applied in examination of calculation methods. This review is dedicated to application of kinetic isotope effects, measured by means of NMR spectroscopy at natural abundance and combine with theoretical calculations, in reaction mechanisms studies. Reaction mechanisms studied by means of NMR are described on the basis of quantitative analysis of experimental isotope effects.

Institute of Organic Chemistry, Faculty of Chemistry, Technical University of Lodz, Zeromskiego 116, 90-924 Lodz, Poland

Theoretical calculations for alternative mechanisms are not discussed in detail but final conclusions are reported only.

1. INTRODUCTION

First publications on nuclear magnetic resonance and isotope effects appeared almost at the same time. The first NMR spectra, independently recorded in two laboratories by Bloch and Purcell groups, were published in the same issue of *Physical Review* in 1946.[1,2] One year later the idea of isotope effects was introduced by Bigeleisen.[3] Isotope shifts on shielding were first discussed by Gutovsky 12 years later.[4]

Isotope effects are divided into kinetic, thermodynamic (equilibrium) and intrinsic isotope effects. Kinetic isotope effects (KIEs) on chemical reactions and thermodynamic isotope effects on equilibriums result from changes in vibrational force constants and zero point energies between the initial and transition or final state, respectively. Isotope effects based on direct or indirect comparison of the reaction rates of isotopologues are called intermolecular. The isotope effect is considered as intramolecular when substrate, in which isotopic atoms occupy equivalent reactive positions, reacts to produce non-statistical distribution of isotopomeric product molecules.[5] The NMR isotope effects of static molecules are single-state physical properties, intrinsic to that molecule and its particular set of vibrational force constants. The differences of chemical shifts and coupling constants originated from substitution of lighter by heavier isotopomer are called chemical shift and coupling constant isotope effects, respectively.

2. ISOTOPE EFFECTS ON CHEMICAL SHIFTS AND SPIN–SPIN COUPLING CONSTANTS

Isotope effect on chemical shift is observed after the substitution of neighbouring ^mX isotope in the molecule with the heavier $^{m'}X$ isotope. According to notation proposed by Gombler[6] isotope shift is given by formula:

$$^n\Delta A(^{m'/m}X) = \frac{\nu_A(A^{m'}X) - \nu_A(A^mX)}{\nu(A^mX)} \quad (m') \tag{1}$$

In terms of the nuclear shielding difference the isotope shift is equal to:

$$^n\Delta A(^{m'/m}X) = \sigma^A(A^mX) - \sigma^A(A^{m'}X) = \sigma - \sigma^* \tag{2}$$

where the asterisk represents the heavy isotopomer.

The effects of intramolecular dynamics (vibration and rotation) on nuclear shielding have been observed as temperature dependence of resonance

frequency of isolated molecule and isotope shift upon isotopic substitution of neighbouring nuclei. The temperature dependence of nuclear shielding written as a virial expansion in the gas density ρ is as follows:

$$\sigma(T,\rho) = \sigma_0(T) + \sigma_1(T)\rho + \sigma_2(T)\rho^2 + \ldots \tag{3}$$

The first term, $\sigma_0(T)$, is a statistical average of the nuclear magnetic shielding tensor over all possible orientation of the molecule in the magnetic field and is different for the isotopomers. Theoretical aspects of isotope shifts were covered by Jameson and Osten.[7]

There are several general observations about magnitudes and signs of isotope shift:

1. Upon substitution with heavier isotope NMR signal is usually shifted towards lower frequency (higher shielding).
2. The magnitude of the isotope shift reflects the range of observed nuclei chemical shifts, decreases with increasing number of bonds between isotopic substitution and observed nuclei and is related to the fractional change in mass upon isotopic substitution.
3. Isotope shift exhibit additivity (is proportional to the number of substituted equivalent atoms).

Primary isotope effects are defined as the difference in magnetic shielding of the isotopes of nuclei of the same element. Secondary isotope effect on nuclear shielding are considered as intrinsic isotope effects and equilibrium isotope effects. The former effects are caused by isotopic substitution, the later by conformational changes or shifts in equilibria as a consequence of isotopic substitution.

Review covering all aspects of isotope shifts appeared first in 1967[8] and later one for the period 1965–1982.[9] The majority of publications were dedicated to secondary isotope effects, only few were dealing with the primary isotope effects. A combination of equilibrium isotope effects and NMR spectroscopy as a mechanistic tool in physical organic chemistry was covered by Siehl.[10]

Next reviews were dedicated to problems of hydrogen-bonded systems. Hydrogen/deuterium isotope effects on NMR parameters in liquids and solids have been reviewed by Limbach et al.[11] Review covers period to 2004 and illustrates the correlation of intermolecular hydrogen-bonded systems geometry and H/D isotope shifts and coupling constants, particularly measured in the solid state and in liquids at low temperature. Several reviews concern the isotope effects on intramolecular hydrogen-bonded systems.[12–17] Since that time several new papers dedicated to hydrogen-bonded systems were published, mostly on intramolecular systems.[18–24]

Isotope effects on coupling constants are more difficult to recognize than isotope effects on chemical shielding. The difference of chemical shifts between isotopomers is easier to determine than slightly differences in signals splitting. The primary isotope effect on coupling constant defined as:

$$\Delta_p{}^nJ(A^{2/1}H) = |{}^nJ(AD)|^*(\gamma_H/\gamma_D) - |{}^nJ(AH)| \tag{4}$$

correspond to the effect of replacement of hydrogen by deuterium on coupling between separated by n bonds nuclei A and H. The reduced coupling constant is equal to:

$$^{n}K(AH) = \frac{4\pi^2[^{n}J(AH)]}{(h\gamma_A\gamma_H)} \tag{5}$$

The secondary isotope effect on the n-bond coupling constant between nuclei A and B originated from substitution in the molecule of ^{m}X by the heavier isotope $^{m'}X$ is equal to:

$$\Delta_s{}^{n}J(AB)[^{m'/m}X] = |^{n}J(AB)|^* - |^{n}J(AB)| \tag{6}$$

Analogously to isotope shift asterisk * denotes heavier isotopomer. The absolute signs of coupling constants are usually unknown and absolute values are compared.

For a diatomic molecule the isotope effect on coupling constant J is given in the following equation:

$$\langle J\rangle^* - \langle J\rangle = \left(\frac{\partial J}{\partial r}\right)_e (\langle \Delta r\rangle^* - \langle \Delta r\rangle) + \frac{1}{2}\left(\frac{\partial^2 J}{\partial r^2}\right)[(\langle(\Delta r)^2\rangle^* - \langle(\Delta r)^2\rangle)] + \dots \tag{7}$$

where,

$$\left(\frac{\partial J}{\partial r}\right)_e = \frac{h\gamma_N\gamma_{N'}}{4\pi^2}\left(\frac{\partial K}{\partial r}\right)_e \tag{8}$$

In polyatomic molecules several electronic factors contribute to the isotope effect on J. The primary isotope effect involves largely the primary derivative of the coupling constant, the secondary isotope effect on the coupling involves largely the secondary derivative of the coupling constant with respect to the stretching of a remote bond.

Similarly to isotope effects on chemical shifts the magnitude of isotope effect on coupling constant are proportional to the fractional changes in masses and mostly are observed for deuterium or tritium. The general trends observed for isotope effects on coupling constants with their theoretical explanations have been presented by Jameson and Osten.[25,26] The largest observed primary effects are ^{1}J $(^{31}P,H) = +12.19$ Hz for PH_3[27] and $^{1}J(^{119}Sn,H) = +10.5$ Hz[28] in SnH_3^-. For nitrous oxide in acetonitrile the ^{1}J $(^{14}N-^{14}N)$ equal to 4.233 ± 0.006 Hz was measured.[29] In comparison with $^{1}J(^{15}N-^{15}N)$ equal to -9.16 ± 0.30 Hz, the double primary isotope effect $\Delta_p{}^{1}J(N,N)$ is equal to 0.42 Hz. $^{16}O/^{18}O$ induced proton isotope shift for H_2O is equal to 0.86 Hz at 80°C and 1.1 Hz for HDO at the same temperature. Authors suggest anomalously strong (0.32 ppb) nonadditivity effect.[30] Secondary isotope effects as large as $\Delta_s{}^{1}J(^{29}Si,F)$ $[^{2/1}H] = -2.0$ Hz[31] for $HSiF_3$ and $\Delta_s{}^{1}J(^{119}Sn,H)$ $[^{2/1}H] = +3.0$ Hz[28] for SnH_3^- have been determined.

Theoretical calculations of isotope effects on chemical shifts and coupling constants and comparison with experimental values were used as a method of the calculation methods verification. Several papers were dedicated to this topic, mostly the review articles.[32–35]

The first paper dealing with the NMR determination of non-random distribution of deuterium appeared in 1981 and the *site-specific natural isotope fractionation studied by nuclear magnetic resonance* (SNIF-NMR) terminology was proposed.[36] Since this time several review articles on application of deuterium and ^{13}C NMR natural abundance spectroscopy were published.[37–41]

3. KINETIC ISOTOPE EFFECTS MEASURED AT NATURAL ABUNDANCE

Among different methods for the reaction mechanisms elucidation, KIEs are considered as the very sensitive tool for determining the structure of transition states in chemical and enzymatic reactions. Values of isotope effects compared with theoretical predictions for different mechanisms allow selection of the most probable mechanism. Isotope effects can be determined by different methods, using enriched or natural abundance samples.[42] In the beginning for many years high precision mass spectrometry and radiochemical measurements were applied for isotope effects determination. The application of mass spectrometry requires selective sample degradations without isotopic fractionation into small molecules suitable (mostly CO_2) for analysis. NMR spectroscopy allows avoiding such degradation and analysis at natural abundance. Initially this technique was applied for determination of relatively large ^2H KIEs over 20 years ago[43,44] and 10 years later for ^{13}C KIEs.[45] High precision quantitative measurements of ^{13}C at natural abundance (1.1%) are easier with developing of NMR spectrometers, nuclear magnetic resonance became competitive with mass spectrometry.[46]

3.1 Theory and practice of kinetic isotope effect measurements

The isotope ratio is a ratio of the numbers of heavy and light isotopes and changes for substrate or product as any reaction proceeds. Substrate enriches in slower-reacting component and product enriches in faster reacting component. Thus, the isotope ratio R compared to the isotope ratio of starting material R_0 is related to the extent of reaction F and KIE by the equation:

$$\frac{R}{R_0} = (1 - F)^{(1/\text{KIE})-1} \tag{9}$$

KIE is defined as k_L/k_H ratio, where k_L and k_H are rate constants of reaction with light (L) and heavy (H) isotopomer, respectively.[47]

KIE can be calculated from the equation:

$$\text{KIE} = \frac{\log(1 - F)}{\log[(1 - F)R/R_0]} \tag{10}$$

or

$$\text{KIE} = \frac{\log(1 - F)}{\log[1 - (FR_p/R_0)]} \tag{11}$$

where R_p — the isotope ratio of product.

The uncertainties in calculated KIE according to Equation (10) are:[47]

$$\Delta KIE_R = \frac{\partial KIE}{\partial (R/R_0)} \Delta F = -\frac{1}{R/R_0} \times \frac{\ln(1-F)}{\ln^2[(1-F)R/R_0]} \times \Delta F \qquad (12)$$

$$\Delta KIE_F = \frac{\partial KIE}{\partial F} \Delta F = \frac{1}{1-F} \times \frac{\ln(R/R_0)}{\ln^2[(1-F)R/R_0]} \times \Delta F \qquad (13)$$

For KIE determined from analysis of the product isotope ratio (Equation (11)) the uncertainties are:

$$\Delta KIE_R = \frac{\partial KIE}{\Delta (R_p/R_0)} \Delta F = \frac{F}{1-(FR_p/R_0)} \times \frac{\ln(1-F)}{\ln^2[1-(FR_p/R_0)]} \Delta F \qquad (14)$$

$$\Delta KIE_F = \frac{\partial KIE}{\partial F} \Delta F$$
$$= \frac{(R_p/R_0)/(1-(FR_p/R_0))\ln(1-F) - (1/(1-F))\ln[1-(FR_p/R_0)]}{\ln^2[1-(FR_p/R_0)]} \Delta F \qquad (15)$$

When unreacted starting material is analysed, the uncertainty of KIE is decreasing with increasing extent of reaction. For KIE derived from analysis of product isotope ratios the smallest errors in KIE are for the low conversion. Precision of NMR measurements is relatively low and the uncertainty of the KIE is dominated by ΔKIE_R. Usually two–three samples of substrate are analysed over 70% conversion or product up to 20% conversion.

To minimize both random and systematical errors of NMR analysis the following methodology for acquisition and processing was used. Prepared identically samples are verified by T_1 measured for each sample and samples with significantly different T_1 should not be analysed. At least two independent samples should be measured several times. Calibrated pulses $\pi/2$ or shorter, long relaxation delays ($>8T_1$ for $\pi/2$) and inverse-gated acquisition are used for acquisition of spectra with resolution over 10 points/Hz. Zero-filling can be applied when necessary. Signals of interest should be centred in spectral window. Processing procedures: baseline corrections (usually a zero-order correction), phasing and integrations were carried out consistently for all samples. Integration ranges should be at least $10\times$ multiple of the peak width at half-height and signal to noise at least 500 is necessary. As internal standard for integration signal of atom or group is used with assumption that its isotope composition is constant during the reaction course since it is not involved in bond formation or bond breakage. The signal of 'internal standard' cannot overlap with other signals of material or impurities. The limitation of this method is necessity of isolation of reactants in adequate amounts for NMR measurements, which can be difficult for substrate at high extent of reaction. The simple test was proposed by Singleton and Szymanski[48] for examination of different NMR parameters on accurate ^{13}C integrations. ^{13}C NMR spectrum of 4-acetoxy-1-butanol **2** obtained by acylation of 1,4-butanediol **1** contains four signals.

$$(16)$$
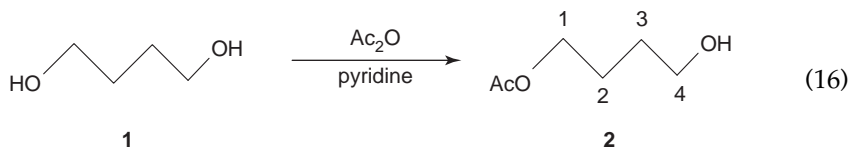
Integrations of two pairs of signal: C1/C4 and C2/C3 should be equal due to the symmetry of the substrate and negligible isotope effect of acylation.

The procedure of isotope effect studies will be illustrated on several examples. First one concerns studies of phosphonate–phosphate rearrangement (Scheme 1). Phosphite **3** reacts in the presence of triethylamine with *o*-nitrobenzaldehyde (Pudovik reaction) to form 1-hydroxyphosphonate **4** as mixture of two diastereo-isomers, 1:1. Amine also catalyses the reverse *retro*-phospho-aldol (*retro*-Abramov) reaction of 1-hydroxyphosphonate to phosphite and aldehyde and rearrangement to phosphate **5**. In acetonitrile at 65°C Pudovik reaction is much faster than of *retro*-Abramov reaction and phosphonate–phosphate rearrangement, which rates are comparable. Important fact for the mechanism elucidation was experimental evidence that rearrangement occurs with retention of configuration at phosphorus atom.[49]

Because the phosphonate–phosphate rearrangement requires P–C bond break-age and formation of the P–O bond kinetic isotope studies by means of ^{13}C NMR were chosen.[50] ^{13}C KIEs were derived from NMR analysis of substrate-*o*-nitro-benzaldehyde or product–phosphate. Samples of aldehyde were prepared using the 'dead-end' method. To the solution of phosphite **3** and triethylamine in acetonitrile an excess of aldehyde was added and solution was heated at 65°C to complete conversion of phosphonate **4** to phosphate **5** monitored by ^{31}P NMR. The aldehyde conversions 0.2–0.8 were calculated from the balance of concentrations. The changes of ^{13}C composition were determined for carbonyl carbon atom using signal of *meta* aryl carbon as an internal standard. KIE 1.0223(14) was calculated from the slope of linear relationship of isotopic ratio R and fraction of reaction,
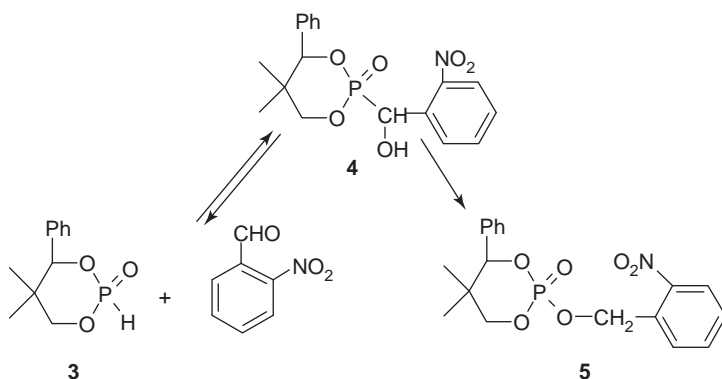
Scheme 1.

derived from Equation (17):

$$\log R = \log R_0 + \left(\frac{1}{\text{KIE}} - 1\right)\log(1 - F) \tag{17}$$

For product, phosphate **5**, changes of ^{13}C content were analysed for acyclic methylene carbon with signal of one methyl group as a reference. Samples were prepared for low conversion (0.1–0.2) and full conversion. For low conversion of product ($F < 0.3$) the isotope effect can be calculated from the formula:[42]

$$\text{KIE} = \frac{R_\infty}{R_p} \tag{18}$$

where R_∞ is product isotopic ratio at full conversion. The ^{13}C KIE was found to be equal to 1.0295(10), higher in comparison with the isotope effect determined from substrate analysis. Such difference can originate from intramolecular isotope effect (*vide infra*) or from product side reaction. In the presence of triethylamine, used as catalyst, phosphoric acid anion (Equation (19)) ($<10\%$) was formed via amine nucleophilic attack on methylene carbon:

$$\tag{19}$$
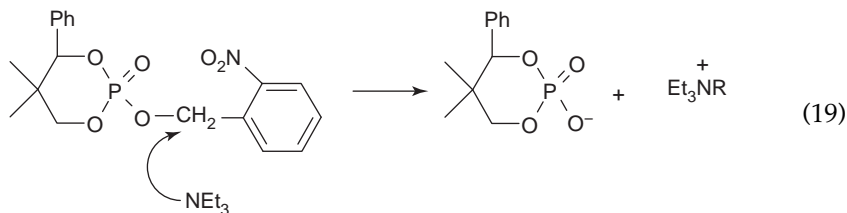
Reaction (19) causes larger isotope effect determined for product than effect for substrate due to additional fractionation of analysed carbon atom in the side reaction. For mechanistic analysis ^{13}C KIE based on the substrate analysis was used. DFT calculations of isotope effects for each step of the reaction led to conclusion that the rate-determining step involves breaking of the P–C bond in the tetragonal pyramidal intermediate.

Different isotope effects from substrate and product analysis originate not only by the side-reactions, but also can be observed when the partially labelled molecule passed the rate-determining step and can react with different distribution of isotopes in the product-determining step. Changes of the substrate isotopic constitution provide the intermolecular isotope effect on the rate-determined step, whereas the analysis of product can inform about the intramolecular isotope effect.

Illustration of the simultaneous determination of intermolecular and intramolecular ^{13}C and ^{2}H KIEs at natural abundance are studies of the Baeyer–Villiger (B–V) oxidation of cyclohexanone to ε-caprolactone.[48]

$$\tag{20}$$

6
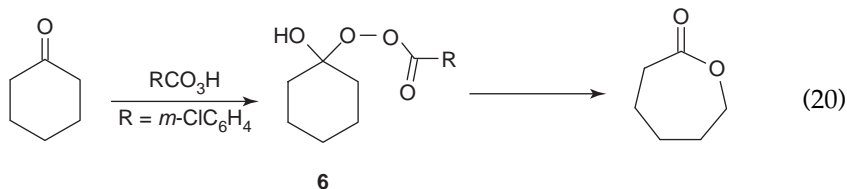
It is known, that the B–V reaction follows two-step mechanism with formation of the Criegee intermediate and reaction conditions determine which step is the rate determining.[51]

Changes of ^{2}H and ^{13}C isotopic composition were determined for recovered at high conversion cyclohexanone and for caprolactone isolated at low conversion. Calculated isotope effects are summarized in Figure 1.

The very large ^{13}C intermolecular isotope effect at the carbonyl carbon indicates that formation of Criegee intermediate is rate-determining step. The difference of intermolecular (negligible) and intramolecular (large) KIEs for α-methylene group is strong evidence that the migration step occurs after the rate-determining step. Concerted migration of α-methylene group from carbon atom to oxygen atom was confirmed by Becke3LYP/6-31G* calculations (Equation (21)).

$$ \text{(21)} $$
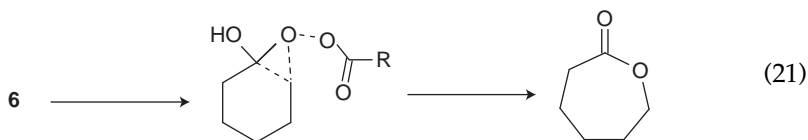
Probing mechanism of the reaction involving intramolecular competition between different isotopic species at several chemically equivalent positions, the number of equivalent sites must be taken into consideration. In the case of deuterium content at natural abundance the concentration of multiply labelled molecule is negligible and not-deuterated molecules are invisible in the ^{2}H NMR. When reaction is taken to the completion the retained and transferred deuterium can be calculated from the ^{2}H spectra of substrate and product. The KIE is given by:

$$ \frac{k_H}{k_D} = \frac{D_{retained}}{D_{transfered}} \times \frac{1}{n-1} \tag{22} $$

where n is the number of chemically equivalent site in the reactant.[43]

KIE calculated from this equation corresponds to the overall effect including primary and secondary isotope effects. For reaction with a C–H bond breakage in a methyl or methylene group the primary isotope effect (KIE$_{1°}$) is observed for
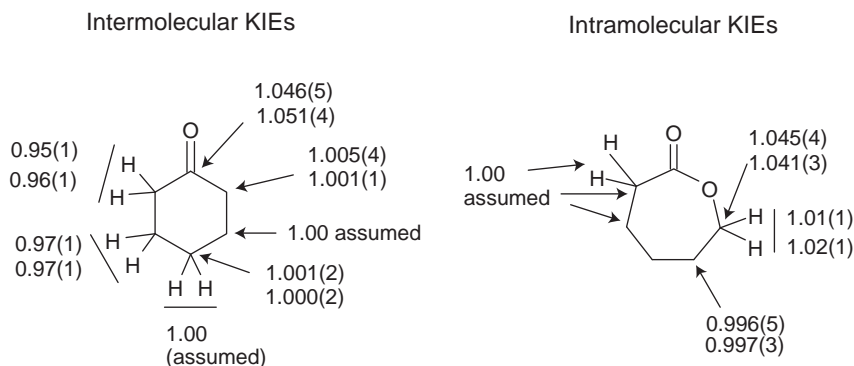
Figure 1 Intermolecular and intramolecular ^{2}H and ^{13}C isotope effects for the Baeyer–Villiger oxidation of cyclohexanone (standard deviations in parentheses).

broken C–H bond and the secondary effect (KIE_{2°) for the C–H bonds left behind. A general methodology for the determination of both the primary and secondary KIEs was elaborated in Singleton's laboratory.[52] In the $FeCl_3$ catalysed reaction of *tert*-butyl hydroperoxide with ethylbenzene (k_{HH}), 1-deuterioethylbenzene (k_{HD}) and 1,1-dideuterioethylbenzene (k_{DD}) all afford the same product, acetophenone:

$$(23)$$
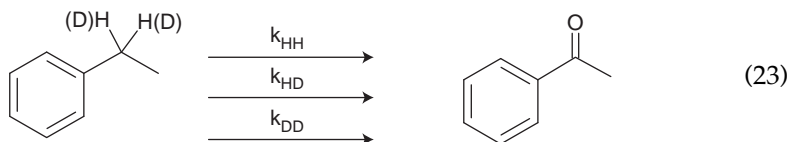
The overall observed isotope effect k_{HH}/k_{HD} is given by Equation (24), where statistical factor of 2 is introduced because of the presence of two hydrogens in ethylbenzene:

$$\frac{k_{HH}}{k_{HD}} = \frac{2}{1/KIE_{1^0} + 1/KIE_{2^0}} \tag{24}$$

and k_{HH}/k_{DD} is given by Equation (25):

$$\frac{k_{HH}}{k_{DD}} = KIE_{1^0} \times KIE_{2^0} \tag{25}$$

Combination of Equations (24) and (25) gives formulas for primary and secondary isotope effects:

$$KIE_1 = \frac{(k_{HH}/k_{DD}) + \Delta}{k_{HH}/k_{HD}} \quad KIE_{1^0} = \frac{(k_{HH}/k_{DD}) - \Delta}{k_{HH}/k_{HD}} \tag{26}$$

where

$$\Delta = \sqrt{\frac{k_{HH}}{k_{DD}} \left[\frac{k_{HH}}{k_{DD}} - \left(\frac{k_{HH}}{k_{HD}} \right)^2 \right]}$$

Precision of determination of k_{HH}/k_{HD} and k_{HH}/k_{DD} is crucial for applicability of KIE_{1° and KIE_{2° in mechanistic analysis.

For oxidation of ethylbenzene in $FeCl_3$-catalysed reaction with *tert*-butyl hydroxyperoxide isotope effect $k_{HH}/k_{HD} = 2.02(4)$ was found in analysis of deuterium content in ethylbenzene at natural abundance. Mixture of ethylbenzene and 1,1-dideuteroethylbenzene (45:55) was used for the determination of $k_{HH}/k_{DD} = 5.0(1)$. Isotope effects $KIE_{1^\circ} = 3.5(2)$ and $KIE_{2^\circ} = 1.41(6)$ were calculated from formulas (26). The value of primary isotope effect is consistent with a C–H bond breakage in the rate-limiting step, but its value does not allow distinguishing among a hydrogen radical abstraction, C–H insertion or a hydride abstraction processes. Secondary isotope effect is consistent with formation of benzylic radical.

3.2 Experimental versus theoretical isotope effects

For the elementary reaction:

$$A \xrightarrow{k} P \tag{27}$$

the KIE is given by the rate constants ratio $\alpha = k_L/k_H$, where L and H corresponds to light and heavy isotopes, respectively. In the case of the complex reactions the relationship between experimentally determined the overall isotope effect and intrinsic isotope effects is more complex.[53] Assuming the steady-state approximation for the intermediate B concentration in the multistep reaction

$$A \underset{k_{-1}}{\overset{k_1}{\rightleftarrows}} B \overset{k_2}{\rightarrow} P \tag{28}$$

the experimental rate is equal to:

$$k_{exp} = \frac{k_1 k_2}{k_{-1} + k_2} \tag{29}$$

and the experimental isotope effect is given by

$$\alpha_{exp} = \frac{\alpha_1}{\alpha_{-1}} \frac{\alpha_2 + x\alpha_{-1}}{1 + x} \tag{30}$$

where $x = k_{2L}/k_{-1L}$ is called the partitionic factor or the commitment to catalysis.

According to the Equation (30) the experimental isotope effect depends not only on the intrinsic isotope effects α_i, but also on the rate constants k_2 and k_{-1}. The intrinsic isotope effects describe the structure of the transition states and the commitment reflects the relative heights of energetic barriers of competitive reactions. If $k_{2L} \gg k_{-1L}(x \gg 1)$, the formation of intermediate **B** is the rate-limiting step and experimental isotope effect is equal to $\alpha_1(\alpha_{exp} = \alpha_1)$. When intermediate **B** returns to substrate much faster than forms the product: $k_{2L} \ll k_{-1L}(x \ll 1)$, the experimental isotope effect is $\alpha_{exp} = (\alpha_1\alpha_2)/\alpha_{-1}$. For more complex multistep reactions the analysis of isotope effects is analogous, however the commitment factor become a complex collection of kinetic terms.[54]

The application of isotope effects studies of reaction mechanism includes comparison of experimental values of isotope effects and predicted isotope effects computed for alternative reaction pathways. On the basis of such analysis some of the pathways may be excluded. Theoretical KIEs are calculated using the method of Bigeleisen and Mayer.[1,55] KIEs are a function of transition state and substrate vibrational frequencies. Equilibrium isotope effects are calculated from substrate and product data. Different functionals and data sets are used in these calculations. Implementation of a one-dimensional tunnelling correction into conventional transition-state theory significantly improved the prediction of heavy-atom isotope effects.[56] Uncertainty of predicted isotope effect can be assessed from the relationship between KIEs and the distances of formed or broken bonds in the transition states, calculated for different optimized structures.[57] Calculations of isotope effects from sets of frequencies for optimized structures of reactants and transition states are facilitated by adequate software: QUIVER[58] and ISOEFF.[59]

Verification of different theoretical methods used in calculations of transition states was thoroughly discussed by Singleton et al.[60] on the basis of their own and published by others studies of Claisen rearrangement. The rearrangements of allyl vinyl ether (Equation (31)) and allyl phenyl ether (Equation (32)) were chosen for by the combined ^{2}H, ^{13}C and ^{17}O isotope effects and calculation studies.

(31)

(32)
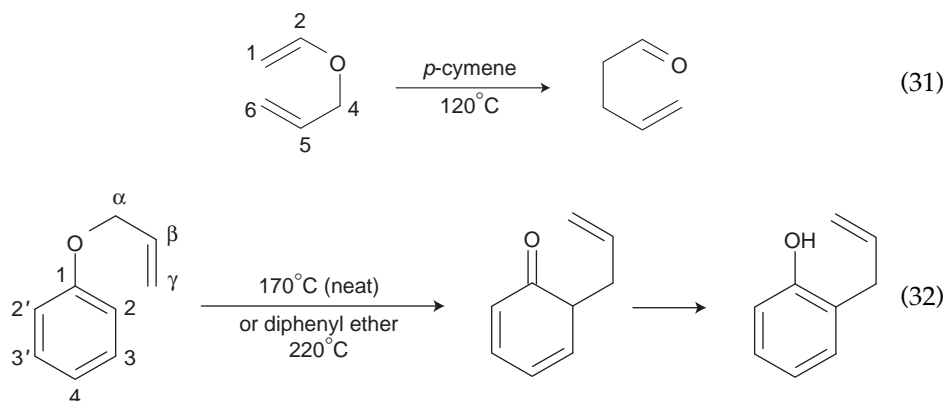
The experimental KIEs were determined for the aliphatic Claisen rearrangement in *p*-cymene at 120°C and for the aromatic Claisen rearrangement either neat at 170°C or in diphenyl ether at 220°C. Changes in ^{2}H, ^{13}C or ^{17}O composition were determined for unreacted substrates. For carbon analysis of allyl vinyl ether the C5 carbon was used as an internal standard. The C4 atom and *meta* aryl protons were used as references in analysis of allyl phenyl ether. The ^{17}O analysis was based on a new methodology. The results are summarized in Table 1, along with predicted isotope effects calculated for experimental temperatures by means of different computational methods. The absolute values of predicted isotope effects for C4 and C5 atoms varied with theoretical level and all isotope effects were rescaled to get reference effects equal to 1.000.

Taking into consideration the agreement between experimental and predicted isotope effects, in the case of the aliphatic Claisen the best transition state is represented by the MP4/6-31G* structure. For both aliphatic and aromatic rearrangements the transition states are intermediate between the B3LYP/6-31G* and the MP2/6-31G* structures. This publication is a valuable guide in application of KIEs in mechanistic studies.

4. KINETIC ISOTOPE EFFECT STUDIES OF REACTION MECHANISMS BY NMR SPECTROSCOPY

4.1 Cycloadditions

Determination of ^{13}C KIEs on natural abundance was introduced by Singleton. The reaction of isoprene with maleic anhydride was selected to examine the synchronity of the Diels–Alder reaction.[45]

(33)
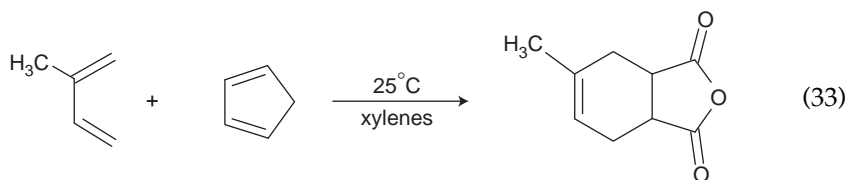
Table 1 Experimental and calculated ^{2}H, ^{13}C and ^{17}O kinetic isotope effects for the Claisen rearrangement[60]

	Expt. 1	Expt. 2	AM1	MP2 6-31G*	MP4(SDQ) 6-31G*	RHF 6-31G*	Becke3LYP/		CASSCF 6-31G*-6d7a
							6-31G*	6-311+G**	
^{13}C and ^{17}O KIEs for the aliphatic Claisen rearrangement (120°)									
C1	1.014(2)	1.013(1)	1.030	1.013	1.012	1.011	1.012	1.012	1.007
C2	1.000(2)	1.001(1)	1.000	1.000	1.000	0.996	0.999	1.000	1.003
O	1.017(5)	1.021(5)	1.013	1.019	1.019	1.015	1.017	1.018	1.020
C4	1.035(2)	1.033(2)	1.026	1.033	1.035	1.032	1.029	1.029	1.037
C5	1.0 (assumed)				1.000 (relative)				
C6	1.015(1)	1.015(1)	1.030	1.016	1.015	1.014	1.014	1.014	1.007
^{2}H, ^{13}C and ^{17}O KIEs for the aromatic Claisen rearrangement (170°)									
Cα	1.027(3)	1.025(2)	–	1.029	–	1.026	1.023	1.022	–
Cβ	1.002(4)	1.002(2)	–	1.001	–	1.006	1.002	1.002	–
Cγ	1.020(5)	1.018(2)	–	1.018	–	1.020	1.020	1.020	–
C1	1.001(3)	1.000(2)	–	1.000	–	0.998	1.000	1.000	–
C2,C2′	1.008(3)	1.007(2)	–	1.006	–	1.008	1.009	1.009	–
C3,C3′	1.003(3)	1.002(2)	–	1.000	–	1.000	1.001	1.001	–
C4	1.0 (assumed)	1.000 (relative)							
O	1.012(4)	1.010(5)	–	1.017	–	1.015	1.013	1.013	–
α-d	1.071(10)	1.074(7)	–	1.067	–	1.053	1.061	1.057	–
β-d	0.985(13)	0.971(11)	–	0.981	–	0.991	0.986	0.984	–
γ$_{cis}$-d	0.978(7)	0.972(8)	–	0.972	–	0.961	0.967	0.970	–
Expt. 3 at 220°C in diphenyl ether									
Cα	1.020(5)	–	–	1.025	–	1.023	1.020	1.020	–
Cβ	1.002(6)	–	–	1.001	–	1.005	1.002	1.001	–
Cγ	1.020(6)	–	–	1.017	–	1.019	1.019	1.019	–
C2,C2′	1.006(4)	–	–	1.006	–	1.007	1.008	1.008	–
C3,C3′	0.999(6)	–	–	1.000	–	1.000	1.001	1.001	–
C4	1.0 (assumed)				1.000 (relative)				
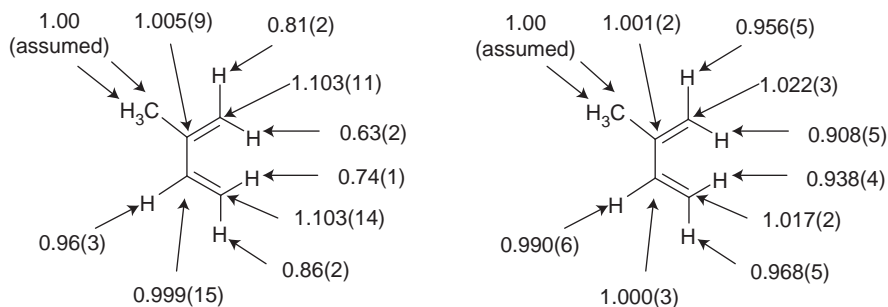
Figure 2 The relative ^{2}H and ^{13}C isotopic composition of recovered isoprene relative to starting isoprene with standard deviations in parentheses (left). Calculated ^{2}H and ^{13}C KIEs (right).

The remaining isoprene was distilled off from a reaction taken to $98.9 \pm 0.1\%$ completion, determined by means of GC. For ^{2}H and ^{13}C NMR analysis the methyl group was used as 'internal standard' (Figure 2).

Isotope effects for C2, C3 and H3 are small as can be expected for no reacting atoms. Differences between ^{2}H and ^{13}C kinetic isotopes for C1 and C4 atoms are outside of experimental errors and verify the earlier theoretical predictions of reaction asynchrony. Secondary deuterium KIEs were within experimental error of the unsymmetrical and symmetrical transition states.[61]

The reaction of hexachlorocyclopentadiene with electron-rich alkenes is classified as 'inverse electron demand' Diels–Alder reaction, but its reaction with electron-poor alkenes is considered as a stepwise process based on a lack of stereospecificity. The cycloaddition of **7** with ethyl vinyl ether:

(34)
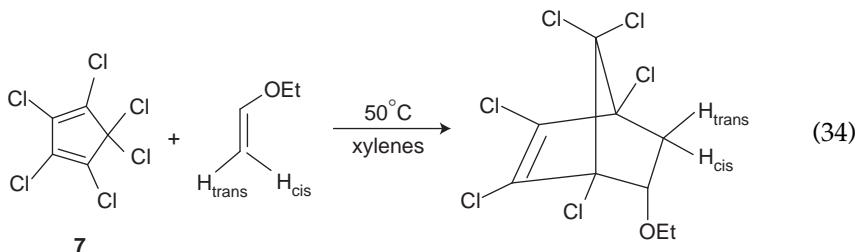
affords the *endo* adduct in quantitative yield. Such stereochemistry can be achieved from both concerted and stepwise process. In the later case the ring closure of biradical intermediate should be faster than the loss of stereochemistry. For reaction (Equation (34)) in xylene at 50°C changes in ^{13}C and ^{2}H isotopic composition in recovered, unreacted ethyl vinyl ether were calculated relatively to the methyl ^{13}C peak and ^{2}H methylene peak.[62]

Theoretical KIEs were predicted in (U)Becke3LYP/6-31G* calculations for a concerted and stepwise Diels–Alder reaction as shown in Figure 3. Any of predicted KIEs is not in good agreement with experimental data. The ^{13}C KIEs calculated for concerted mechanism match with experiment, but the ^{2}H KIEs are lower by few percent. The great difference between the theoretical and
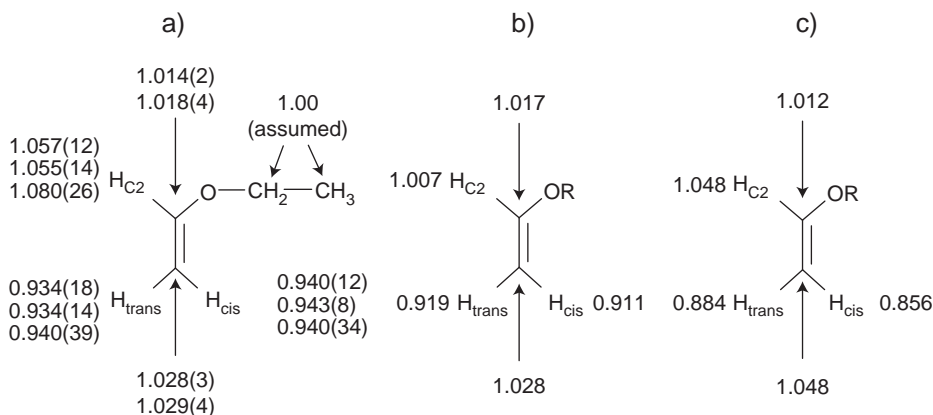
Figure 3 ^{2}H and ^{13}C kinetic isotope effects: experimental (a), calculated for concerted (b) and stepwise (c) mechanisms.

experimental KIEs speaks against the stepwise mechanism. However, the H_{C2} KIE ≈ 1.06 cannot be assigned to any of these border mechanisms and suggests very asynchronous but concerted process. In additional experiment was found that the rate of reaction was not changed when xylene was replaced by polar acetonitrile. Overall, the best explanation of experimental results is a concerted reaction with asynchronous transition state.

The asynchronous concerted [2+4] cycloaddition was also proposed from ^{2}H and ^{13}C KIEs for reaction of isoprene with methyl vinyl ketone, ethyl acrylate and acrolein catalysed by Et_2AlCl.[63]

(35)
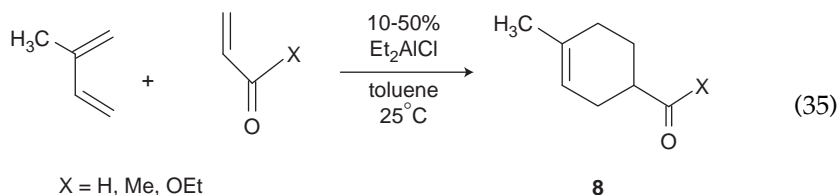
At room temperature the non-catalysed reactions were very slow. In the presence of catalyst the yields of *para* cycloadducts **8** were $>90\%$. The ^{2}H and ^{13}C KIEs, determined from the analysis of recovered isoprene after 65–95% conversion, are presented in Table 2.

Two mechanistic pathways are presented as Scheme 2.

The selection between concerted and stepwise mechanism on the basis of qualitative analysis of ^{13}C KIEs (Table 2) do not allow to select dominating mechanism. The large carbon isotope effect on C1 and small effects on other carbons suggest the stepwise mechanism or highly asynchronous concerted mechanism. The deuterium KIEs are consistent with a concerted mechanism. The inverse KIEs in the $H4_{out}$ and $H4_{in}$ positions are indicative for the bond formation to C4 in the transition state and are not expected for the stepwise mechanism.

Table 2 Experimental and theoretical ^2H and ^{13}C KIEs for the Lewis acid catalyzed Diels-Alder reaction of isoprene with acrolein, methyl vinyl ketone and ethyl acrylate in toluene at 25°C

	Acrolein X = H		Methyl vinyl ketone X = Me		Ethyl acrylate X = Oet		Calc. KIE
	Expt. 1[a]	Expt. 2[a]	Expt. 1[a]	Expt. 2[a]	Expt. 1[a]	Expt. 2[a]	
C1	1.030(3)	1.026(10)	1.028(3)	1.030(6)	1.026(4)	1.029(4)	1.031
C2	1.004(3)	1.006(9)	1.007(4)	1.002(6)	0.999(3)	1.002(4)	1.004
C3	1.001(2)	1.001(10)	1.003(4)	1.003(5)	1.002(4)	1.001(5)	1.000
C4	1.000(3)	1.001(10)	1.006(4)	1.005(5)	1.003(3)	1.005(4)	1.002
$H1_{in}+H1_{out}$	0.915(6)	0,916(7)	0.919(4)	0.919(3)	0.916(3)	0.915(3)	0.910
H3	0.965(5)	0.967(13)	0.970(7)	0.964(3)	0.970(6)	0.973(3)	0.934
$H4_{out}$	0.978(6)	0.979(18)	0.979(9)	0.983(4)	0.978(9)	0.993(4)	0.986
$H4_{in}$	0.951(4)	0.947(8)	0.972(5)	0.963(6)	0.950(6)	0.958(3)	0.968

[a]Errors are given in parentheses.
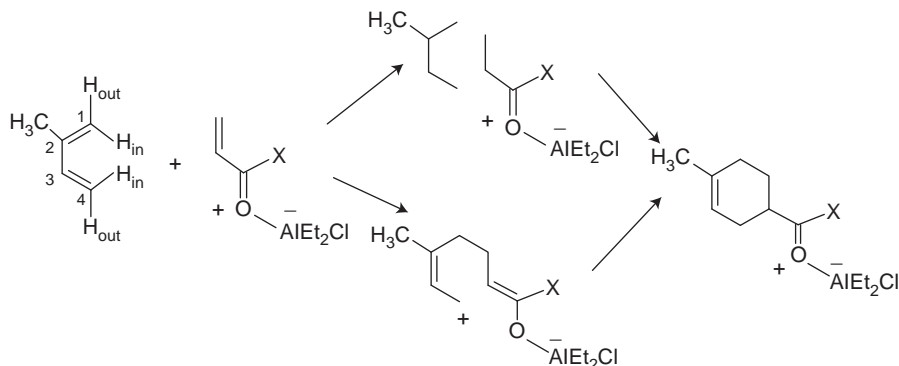
Scheme 2.

Theoretical Becke3LYP/6-31G* calculations for the reaction of isoprene with acrolein evidenced the *endo* s-*cis* transition structure for a highly asynchronous but concerted mechanism. Theoretical KIEs presented in Table 2 show excellent agreement with experimental data except effect for H3. For this atom predicted inverse KIE is larger than experimental value. The explanation of this discrepancy is the short distance of 2.7 Å between the chlorine atom and H3 in modelled molecule. This crowding substantially changes the predicted C–H stretching frequency compared to that in starting isoprene and this change is reflected in large inverse isotope effect.

Sterically hindered or electronically disfavoured reactions as well as thermally forbidden cycloadditions are possible in the radical–cation-mediated cycloadditions. Generally, this type of reaction starts with electron transfer from one of the reagents to a one-electron oxidant (Equation (36)):

$$X + Y \xrightarrow{-e^-} X^{+\bullet} + Y \rightarrow XY^{+\bullet} \xrightarrow{+e^-} XY \qquad (36)$$
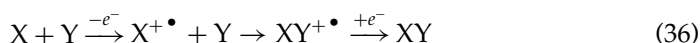
The electron transfer activates molecule and enables the cycloaddition process. The kinetics of these reactions is well documented; much less information is on the nature of regio- and stereoselectivity. The stepwise mechanism was proposed for the electron-transfer-catalysed Diels–Alder reaction of indole and 1,3-cyclohexadiene catalysed by *tris*(4-bromophenyl)aminium hexachloroantimonate in dichloromethane at 0°C in the presence of $NaHCO_3$ and CH_3COCl (Scheme 3).[64]

Unreacted indol was used for ^{13}C composition analysis with C-4 atom as an internal standard for ^{13}C KIEs determination (Figure 4).

The significant ^{13}C KIE at C3 and the low effect at C2 suggest a new bond formation to C3 and ruling out attack or ring closure at C2 in the rate-limiting step of the cycloaddition. However, the low ^{13}C KIE at C2 can be also attributed to a highly asynchronous concerted cycloaddition process.

By theoretical calculations (B3LYP/6-31G*) four reaction pathways were investigated: formation of *endo* or *egzo* product with initial bond formation to C2 or C3 in indole. For each mechanism theoretical ^{13}C KIE were analysed and the best agreement of theoretical and experimental KIEs was found for the reaction involving the intermediacy of the radical cation **11**, resulting from electrophilic aromatic substitution of indole at C3 by cyclohexadiene in the rate-limiting step:
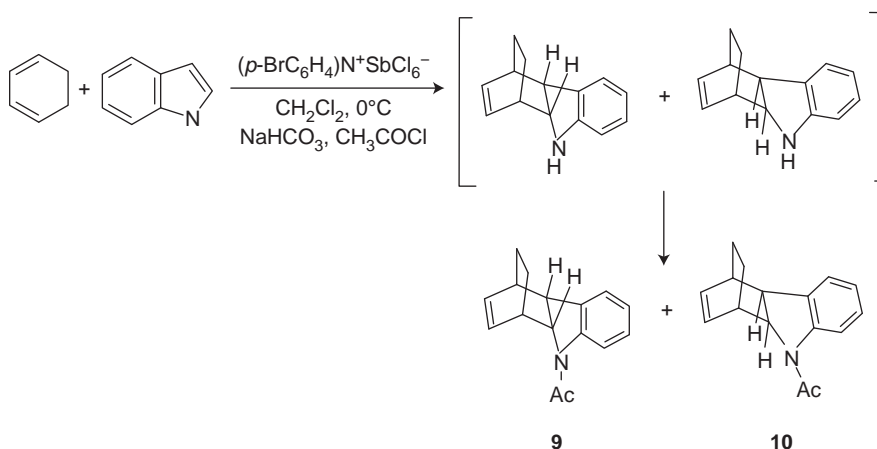
Scheme 3.
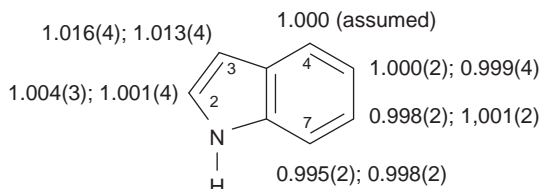
Figure 4 ^{13}C KIEs for the radical–cation catalysed Diels–Alder reaction of indole with cyclohexadiene.
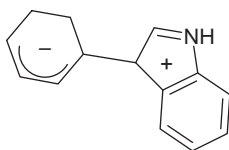
11

The intermediate collapses in the next step to *endo* or *exo* final products **9** and **10** (Scheme 3). The calculated *exo* barrier is 0.8 kcal/mol higher in energy and corresponds to experimentally observed *endo/exo* ratio 3:1.

Another example of cycloaddition selectivity was observed for the reaction of cyclopentadiene with diphenylketene (Equation (37)). Originally only products of [2+2] cycloaddition were observed and these reactions were considered as highly periselective.

$$(37)$$
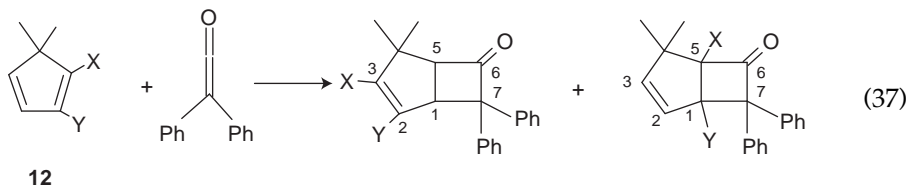
12

The reaction was carried in boiling benzene with 5,5-dimethylcyclopentadiene **12** selectively deuterated (X = D, Y = H or X = H, Y = D). The secondary deuterium isotope effects were measured by means of ^{1}H and ^{2}H NMR.[65] The large and inverse (0.84) isotope effect for C5–C6 bond formation and no effect (1.00) for C1–C7 bond formation corresponds to extensive $sp^2 \rightarrow sp^3$ rehybridization[66] of C1 atom and no rehybridization at C2 atom. At the rate-determining transition state only formation of one carbon–carbon bond is advanced in formation of [2+2] cycloadduct.

The metastable byproduct of [4+2] cycloaddition was detected when the reaction of cyclopentadiene with diphenylketene was (Equation (38)) was examined by low-temperature NMR experiment at $-30°C$.[67] The [4+2] cycloadduct was not observed at elevated temperature because easily isomerizes to [2+2] cycloaddition product via [3,3] sigmatropic (Claisen) rearrangement. This observation was supported by kinetic measurements (^{1}H NMR) and isolation of [4+2] cycloadduct.[68] Mechanism proposed by Machiguchi and Yamabe was re-examined by Singleton.[69]
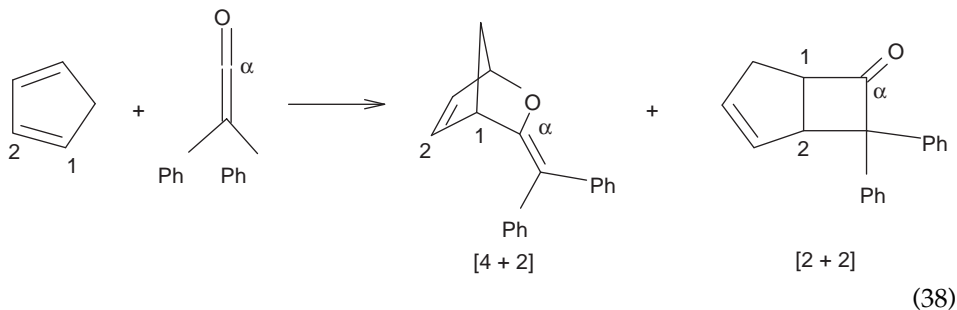
$$(38)$$

Contrary to earlier findings Singleton and co-workers proved that [2+2] cycloadduct can be formed directly, without intermediacy of [4+2] cycloadduct. The conclusion from the qualitative analysis of ^{13}C KIE shown in Figure 5 is that C1–Cα bond was fully formed before the rate-determining step is in accordance with earlier deuterium KIE measurements for the reaction of diphenylketene with 5,5-dimethylcyclopentadiene.[65]

The detailed analysis of kinetic measurements, KIEs and theoretical calculations for different mechanisms led to conclusion that a single transition state can afford dynamically both [4+2] and [2+2] products.[69]

The fumurate ester amide was applied as a probe of synchrony of alkene cycloaddition in reaction with palladium trimethylenemethane (Scheme 4).[70] The choice of an alkene was important because symmetrical alkenes would show very likely symmetrical KIEs independently on concerted or stepwise mechanism due to averaging. On the other side, highly unsymmetrical alkene may favour stepwise mechanism or highly asynchronous cycloaddition, difficult to distinguish from the stepwise mechanism. ^{13}C Analysis of product **13** at low ($\sim$20%) conversion gave changes of ^{13}C integrations relative to C12 (assigned as
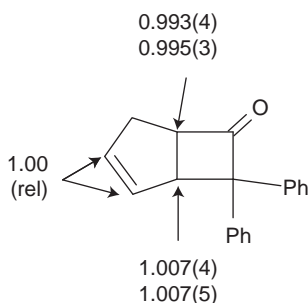
Figure 5 Intramolecular ^{13}C KIEs for the reaction of cyclopentadiene with diphenylketene at 25°C.
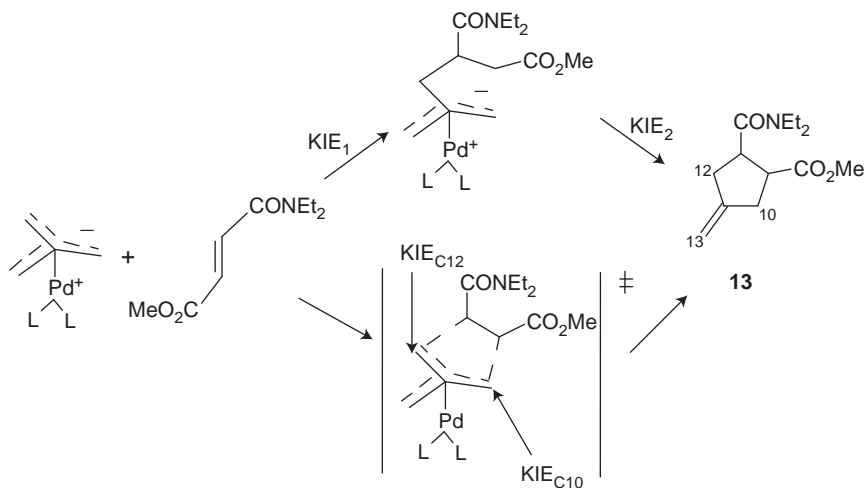
Scheme 4.

1.000) equal to 1.000(4) for C10 and 1.029(6) for C13. For stepwise mechanism calculated from NMR data isotope effects KIE_1 and KIE_2 were found equal to 1.015 ± 0.005 and 1.029 ± 0.007, respectively. For concerted mechanism of cycloaddition KIE_{C10} and KIE_{C12} would be 1.029 ± 0.006 and 1.029 ± 0.007, respectively. These results strongly support a concerted mechanism for the Pd-TMM cycloaddition with the fumurate ester amide.

[2+2] Cycloaddition of ketenes with aldehydes is frequently used in synthesis of β-lactones. To study synchronicity of this process BF_3-catalysed reaction of cyclohexanecarboxaldehyde with *tert*-butyldimethylsilylketene **14** (TBS-*tert*-butyldimethylsilyl) was chosen.[71]

(39)
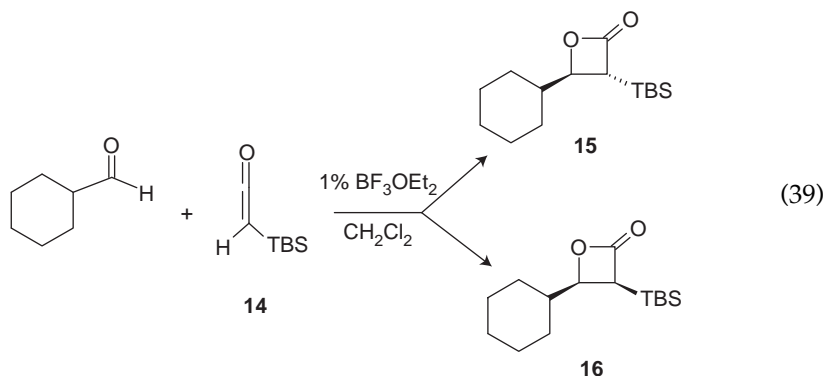
^{13}C KIE were determined for products — diastereoisomers **15** and **16**, and collected in Figure 6.

The substantial differences of isotope effects in diastereoisomers **15** and **16** indicate differences in mechanisms or rate-determining steps in the formation of these products. Significant ^{13}C isotope effect at α and β carbon atoms and no effect at carbonyl atom suggest rate limiting of the Cα–Cβ bond in *trans*-β-lactone **15**. The formation of *cis*-β-lactone **16** is accompanied by substantial isotope effects at all carbons, what can be associated with concerted cycloaddition or ^{13}C KIE at the
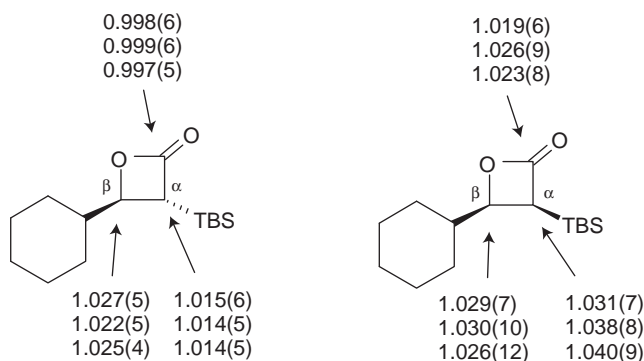
Figure 6 ^{13}C KIEs for BF_3OEt_2 catalysed cycloaddition of cyclohexanecarboxaldehyde with **13** at 0°C.

carbonyl atom can originate from a rate-limiting second step for a stepwise mechanism. This quantitative analysis was verified by B3LYP/6-31+G* calculations and led to conclusion that reaction follows a stepwise cycloaddition mechanism.

4.2 Addition to the multiple bonds

Bromination of alkenes belongs to the most important and comprehensively studied reaction in organic synthesis. ^{2}H and ^{13}C isotope effects were measured for bromination of 1-pentene **17** in CCl$_4$ at 25°C.[72] Unreacted 1-pentane was recovered from reactions taken to 88–95% and then brominated. The resulting 1,2-dibromopentane **18** was analysed by ^{2}H and ^{13}C NMR in comparison to 1,2-dibromopentane obtained from original 1-pentene. Experimental isotope effects are summarized in Figure 7.

    Isotope effects on both olefinic carbon atoms are similar, small but significant. Both secondary deuterium isotope effects are inverse, as should be expected[66] for the reaction proceeding with change **17** of hybridization from sp^2 to sp^3. For the hydrogen on C2 atom isotope effect is smaller. Theoretical Becke3LYP calculations with Ahlrichs SVP basis set for the bromine atoms and 6-31G* basis set for other atoms gave predicted isotope effects for the Br$_2$–propene complex, the propene bromonium ion and for the transfer of Br$^+$ between propene molecules. The best agreement of experimental and predicted isotope effects was found for the rate-limiting formation of a bromonium ion. The difference of deuterium isotope effects suggests an asynchronous transition state with greater bond formation to the terminal carbon. ^{13}C KIEs are less sensitive to asynchrony of the transition state.

$$\textbf{17} \xrightarrow[\substack{\text{(from HCCl}_3\text{/NaOH} \\ \text{/BnN}^+\text{Et3Cl}^-)}]{:CCl_2}$$

(40)
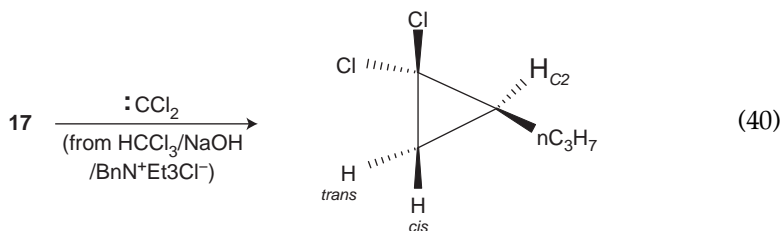
    1-Pentene **17** was also used in mechanistic studies of cycloaddition of carbenes to alkenes.[73]
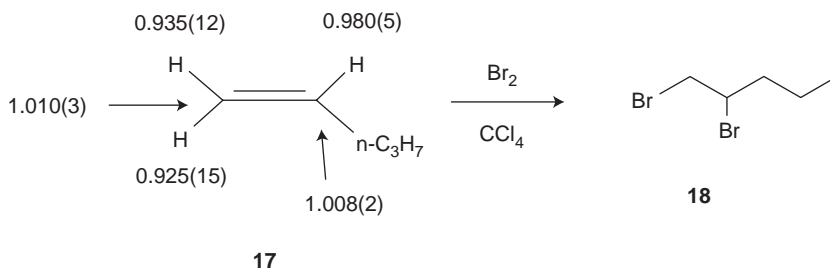
Figure 7 ^{2}H and ^{13}C kinetic isotope effects for bromination of 1-pentene **17**.

Procedure of ^{13}C NMR analysis was identical like in the case of 1-pentene bromination.[72] Calculated ^{2}H and ^{13}C isotope effects are summarized in Figure 8.

The differences in deuterium and carbon isotope effects indicate the asymmetric transition state with more advanced carbon–carbon bond formation to the terminal C1 atom. The difference between deuterium isotope effects for H_{cis} and H_{trans} hydrogens probably originates from experimental uncertainty. Theoretical calculations (B3LYP/6-31G*, B3LYP/6-311+G*) for carbene addition to 1-butene were carried out for two modes with carbene approaching carbon atom C1 or C2. The best agreement for experimental isotope effects is for carbene attack on terminal carbon atom and the carbene–alkene separation in the transition state of 2.5 Å.

Mechanism of Shi epoxidation was probed for synthesis of (+)-(R,R) epoxide **20** in the reaction of *trans*-2-methylstyrene **18** with peroxymonosulphate (Oxone) in the presence of catalyst **19**, chiral ketone derived from fructose (Scheme 5).[74]

^{13}C NMR analysis was applied for unreacted styrene **18** from two reactions taken to 83% and 93% conversion. Experimental and predicted isotope effects are shown in Figure 9.
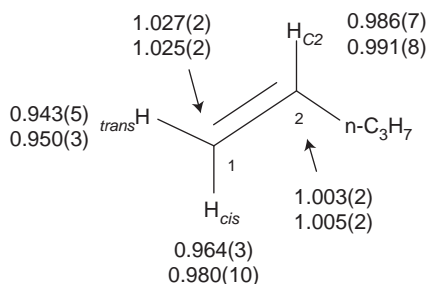
Figure 8 Experimental ^{2}H and ^{13}C KIEs for cyclopropanation of **17** with dichlorocarbene at 25°C.

Scheme 5.

0.998(2)
1.001(1)
[1.000]

1.001(1)
1.001(2)
[1.000]

1.005(1)
1.006(2)
[1.006]

1.002(2)
1.001(2)
[0.998]

1.000
assumed
[1.000]

0.999(2)
1.001(2)
[1.001]

1.022(2)
1.020(2)
[1.022]
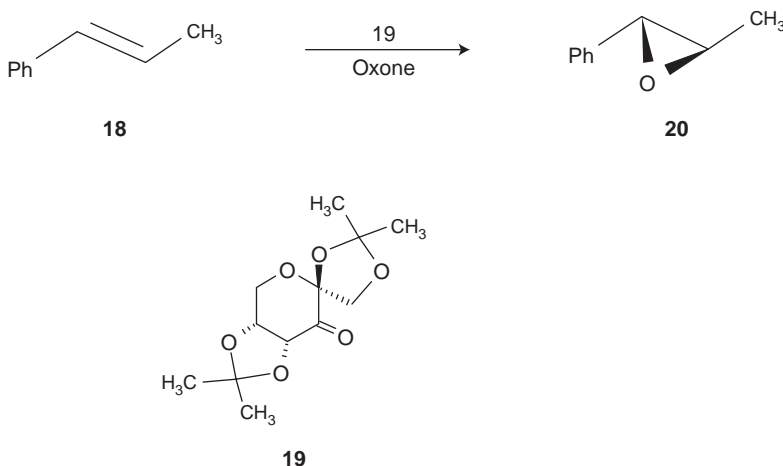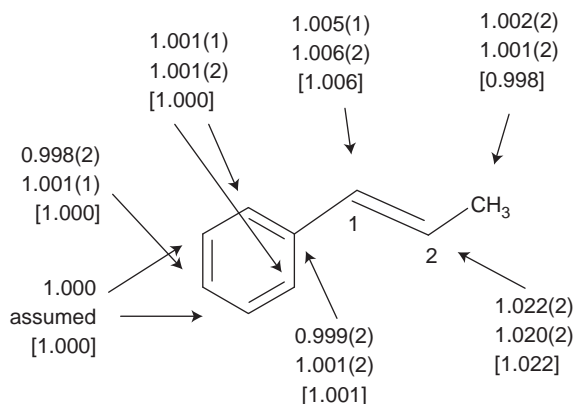
Figure 9 Experimental and predicted (in brackets) ^{13}C KIEs for Shi epoxidation of *trans*-2-methylstyrene **18**.

In theoretical calculations (B3LYP/6-31G*) different catalyst conformations and alkene orientation were taken into consideration. The best agreement of experimental and predicted isotope effects were achieved for asynchronous transition state with oxygen atom distances of 2.32 and 1.99 Å to carbon atoms 1 and 2, respectively.

The Weitz–Scheffer reaction, the epoxidation of α,β-unsaturated carbonyls, is valuable transformation in organic chemistry.[75] The accepted two-step mechanism involves the addition of peroxy anion and formation of peroxyenolate, which undergoes a ring-closing intramolecular nucleophilic substitution of C2 carbon atom.

$$(41)$$
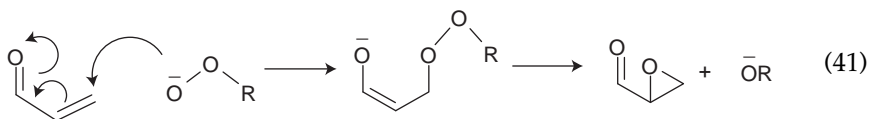
For isotope effect studies epoxidation of cyclohexanone with *tert*-butyl hydroperoxide in the presence of DBU in 1,2-dichloroethane (DCE) at 22°C was chosen (Equation (42)).[76]

$$(42)$$
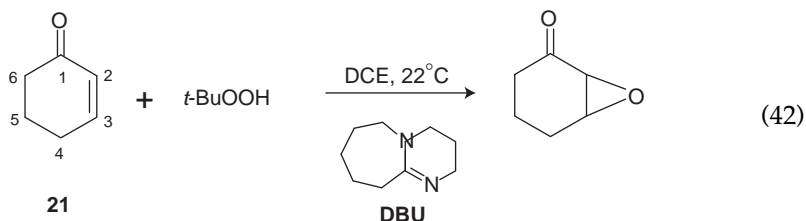
Unreacted cyclohexanone, isolated from reactions taken to 83% and 89% conversion was analysed by ^{13}C NMR and experimental isotope effects were calculated. For theoretical calculations (B3LYP/6-31+G**/PCM) DBU was replaced

by 1,2-dimethyl-1,4,5,6-tetrahydropyrimidine. Considered reaction pathways included axial or equatorial attack on cyclohexanone, different orientation of base and an *anti* (O–O–C=C dihedral angle of approximately 180°) or *gauche* (O–O–C=C dihedral angle of approximately 75°) orientation of the attacking oxygen atom versus the carbon–carbon double bond. Experimental and predicted isotope effects are collected in Table 3.

The predicted isotope effects for the addition transition states are of about 1.030 at C3 and 1.008 at C2 and small KIEs for remaining carbons, as can be expected for a major bonding change at C3 and minor at C2. Predicted isotope effects for the ring-closure step are 1.012 at C2 near unity at C3. The value of 1.012 is near the low end of primary ^{13}C KIEs, but consistent with relatively low isotope effects observed in other epoxidation reactions (*vide infra*). Overall, KIEs support the addition of a peroxy anion to the enone as the rate-limiting step.

The addition of anilines to vinylarenes is catalysed by a combination of Pd(OCOCF$_3$)$_2$, a chelating *bis*-phosphine such as DPPF and TfOH as a source of triflate anion.[77]

Ph-NH$_2$ + [structure 22] → [structure 23]   (43)

2% Pd(TFA)$_2$
3% DPPF
20% TfOH
benzene, 100°C

22   **23**
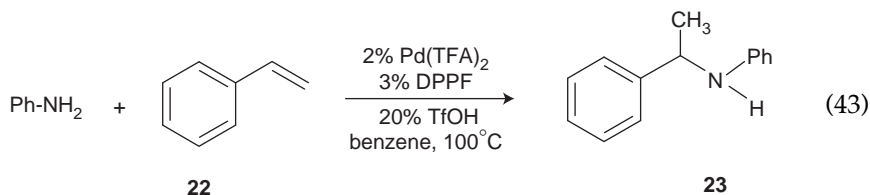
Under applied conditions (Equation (43)) the Markovnikov hydroamination product **23** was formed in 92% isolated yield.[78] Changes in ^{13}C composition were calculated using the aromatic *para* carbon atom as reference and the experimental KIEs are summarized in Figure 10.

Mechanism proposed by Hartwig[77] assumes the formation of η^3-benzyl complex **24** and the product formation via nucleophilic attack of aniline on complex **24** (Equation (44)).

Table 3 Experimental and predicted ^{13}C kinetic isotope effects for the epoxidation of cyclohexanone in the presence of DBU

Cyclohexanone carbon	C$_1$	C$_2$	C$_3$	C$_4$	C$_5$
	Experimental KIEs				
	1.001	1.010	1.032(4)	1.004(3)	0.998(4)
	Predicted KIEs				
Axial addition	1.004	1.008	1.027	0.997	0.999
Equatorial addition	1.004	1.007	1.031	1.001	1.001
Axial ring-closure	1.006	1.012	0.997	0.996	0.999
Equatorial ring-closure	1.005	1.012	1.000	0.999	1.001
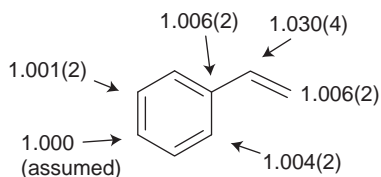
Figure 10 ^{13}C KIEs for catalysed hydroamination of styrene with aniline in benzene at 80°C.
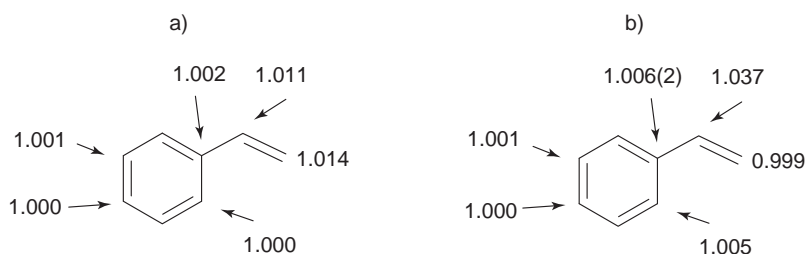
Figure 11 Predicted ^{13}C KIEs for alternative mechanisms of catalysed hydroamination of styrene with aniline in benzene at 80°C (see text).

(44)
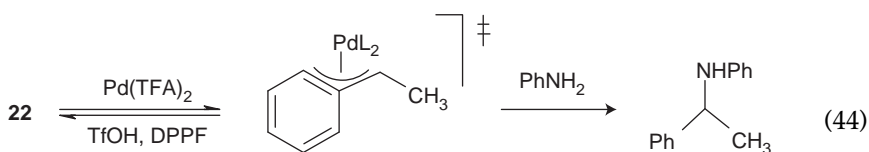
24

The observed KIEs support the rate-determining nucleophilic attack on π-complex, because its formation should be accompanied with small and approximately equal ^{13}C KIE at the olefinic carbons.[79] The reversibility of π-complex formation was proofed by employing partially deuterated (65%) aniline. From ^{2}H NMR was found, that recovered styrene contains approximately 25% deuterium in each olefinic positions and no deuterium in the aromatic ring. Theoretical calculations (B3LYP with SDD basis set on Pd and 6-31+G** on all other atoms) were carried for alternative mechanisms assuming that hydropalladation is irreversible (Figure 11a) or that hydropalladation is reversible and the aniline attack is the rate-determining step (Figure 11b).

Overall, from experimental and calculated isotope effects combined with deuterium exchange experiment was concluded that the key selectivity-determining step is a nucleophilic displacement on a η^3-benzyl complex.

Mechanistic picture of the conjugate addition of lithium dialkylcuprates to enones is not clearly delineated, despite essential meaning of this reaction in organic synthesis. ^{13}C KIE studies were used in order to determine the rate-limiting step for the reaction of Bu$_2$CuLi with cyclohexanone (Equation (45)).[80]

(45)
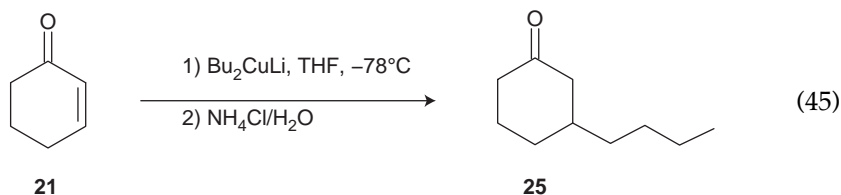
The mean values of ^{13}C isotope effects determined in three independent experiments for unreacted substrate (81–92% completion) and product (10% completion) are summarized in Figure 12.

^{13}C isotope effect at C3 (1.025) corresponds to the bonding change at this atom in the rate-determining step. Smaller but significant ^{13}C KIE at Ca atom is indicative for the butyl group transfer in the same step. Such results are consistent with reductive elimination process in the rate-determining step.

Further ^{13}C and ^{17}O KIE experiments were performed in order to determine role of solvent in chlorotrimethylsilane-mediated addition of organocuprates to cyclohexanone in THF or ethyl ether (Scheme 6).[79]

3-Butylcyclohexanone 25 in ether and 3-butyl-1-(trimethylsilyloxy)cyclohexene 26 in THF were formed almost quantitatively. Similarly to previous work isotope effects were measured for substrate and product. For the reaction in THF a substantial ^{17}O effect (1.018–1.019) was measured, as should be expected for change of bonding at oxygen atom. Small normal ^{13}C effects were found for C1 (1.000–1.005), C2 (1.003–1.007), C3 (1.004–1.008) and no effect (0.996–1.002) for Ca carbon of the butyl group. When THF was replaced by ethyl ether the most notable observation were significant ^{13}C isotope effects at C3 (1.014–1.018) of the enone and Ca atom of the alkyl substituent. These values are similar to those observed previously for the reaction without TMSCl.[80] Thus, the presence of TMSCl does not change the rate-determining step in ether. However, in the more basic THF the lithium coordination is attenuated and dominates irreversible silylation of enone-cuprate π-complex. This observation is consistent with predicted isotope effects.

Reaction of styrene with phenyldiazoacetate was chosen to study mechanistic differences between unstabilized and stabilized carbenoids in cyclopropanation of alkenes (Equation (46)).[81] As catalyst were used Rh$_2$(octanoate)$_4$ or Rh$_2$(S-DOSP)$_4$ [bisrhodium tetrakis[(S)-N-(dodecylbenzenesulphonyl)prolinate].
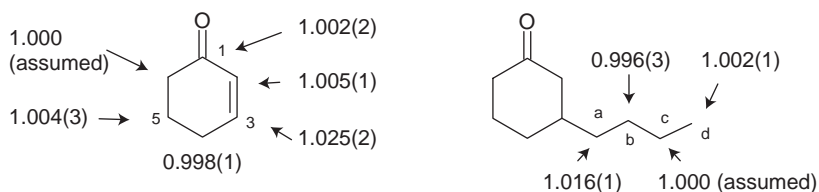
Figure 12   Experimental ^{13}C KIEs for substrate and product of the addition of Bu$_2$CuLi to cyclohexanone (−78°C).
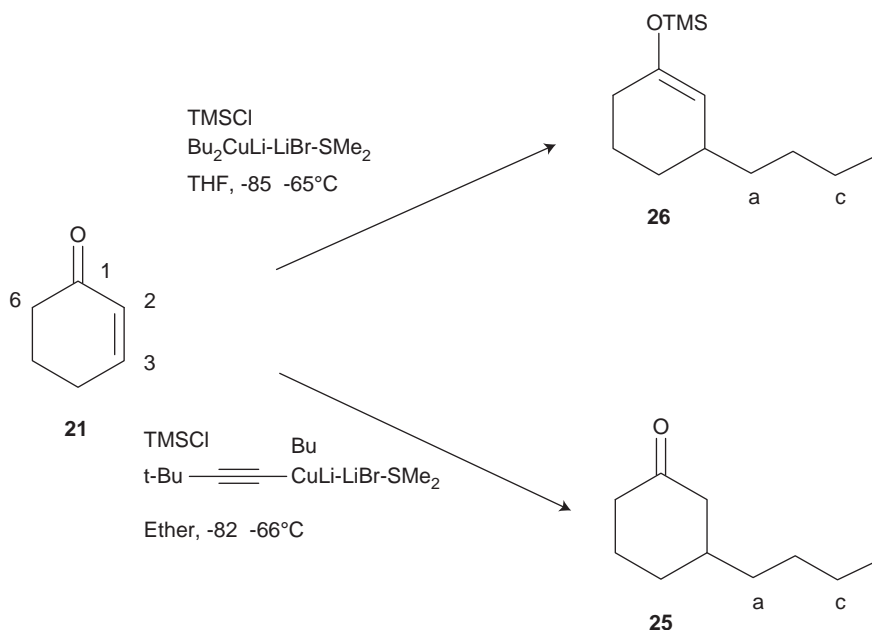
Scheme 6.

(46)
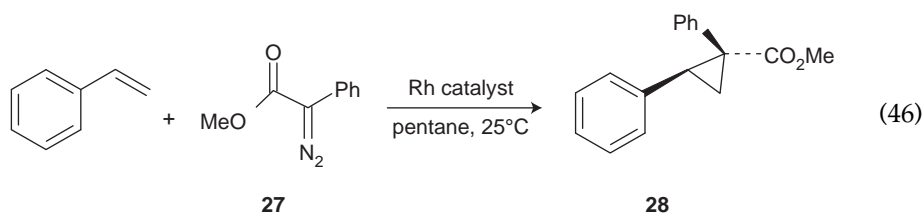
The resulting isotope effects determined relative to the *para* carbon are summarized in Figure 13. Independently of used catalyst similar ^{13}C isotope effects were observed for olefinic carbons. This fact suggests that in the presence of the bulky chiral catalyst as Rh_2(S-DOSP)$_4$ the geometry of the cyclopropanation transition state was not change.

Theoretical calculations (B3LYP) gave predicted isotope effects consistent with experimental effects. Modelled reaction pathway involves complexation of the diazoesters to rhodium, loss of N_2 and rhodium carbenoid formation and formation of asynchronous but concerted cyclopropanation transition state.

Reaction of osmium tetraoxide dihydroxylation of alkenes was studied by means of ^{2}H and ^{13}C KIEs in order to find arguments for '(3+2)' cycloaddition mechanism.[82] Dihydroxylation of *tert*-butylethylene **29** was carried out in a *t*-BuOH/water biphase at 3°C:
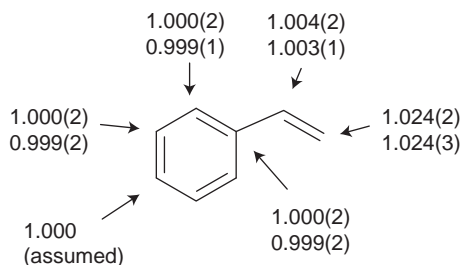
Figure 13 ^{13}C KIEs for the catalytic reaction of styrene with **27**.
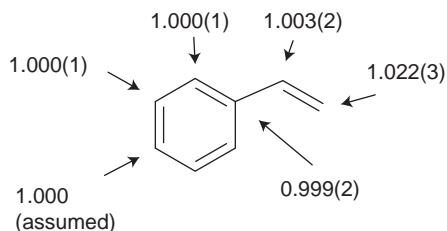
Figure 13 (*Continued*).
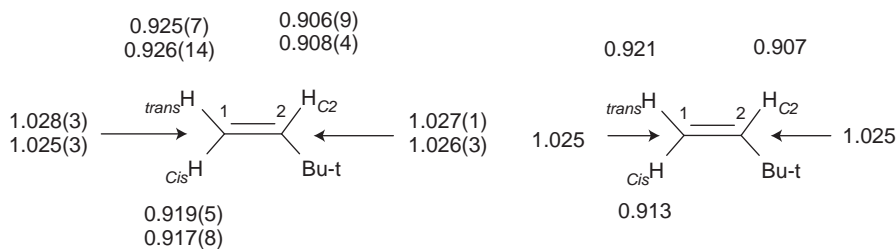
Figure 14 Experimental and calculated KIEs for dihydroxylation of **29** at 3°C.
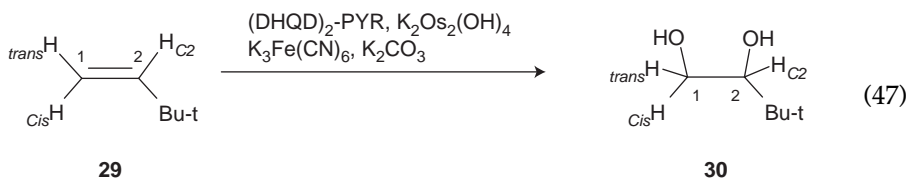
^{2}H and ^{13}C experimental isotope effects are collected in Figure 14.

The best agreement of experimental and predicted isotope effects were found for effects calculated for (3+2) transition structure. For Becke3LYP calculations an effective core potential for osmium with a (341/321/21) basis set for the 'valence' electrons and 6-31G* basis set for other atoms were applied.

Dirhodium *tris*-(diphenyltriftylimidazolidinone)(acetate) [Rh$_2$(OAc)(DPTI)$_3$] was found to be efficient and enantioselective catalyst in cyclopropenations of

alkynes with ethyl diazoacetate. Two-step mechanism involving [2+2] cycloaddition of the alkyne to *tribridged* carbenoid followed by reductive elimination was proposed.[83] Reaction of 1-pentyne or 1-hexyne with ethyl diazoacetate in the presence of $Rh_2(OAc)(DPTI)_3$ or $Rh_2(OAc)_4$ in chlorobenzene at 25°C was studied by means of isotope effects in order to explain the origin of enantioselectivity in formation of cyclopropene **31**.[84]

$$(48)$$

31   R=Me, Et   **32**
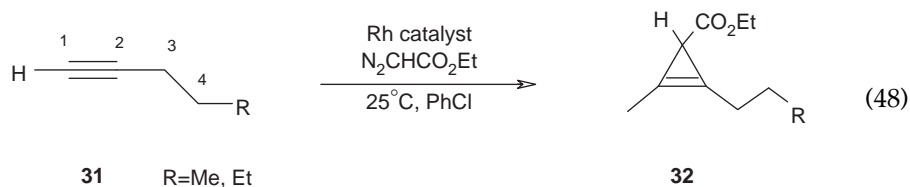
Analysis of ^{13}C distribution in recovered alkynes using C4 atom as an internal standard led to experimental KIEs as collected in Table 4. For both catalysts significant isotope effect was observed for the terminal acetylenic carbon. Experimental KIEs are consistent with cyclopropenation via intact *tetrabridged* rhodium carbenoids and do so to support [2+2] cycloaddition. DFT calculations using B3LYP functional were complicated and did not give conclusive results.

The selenium-dioxide mediated allylic oxidation of alkenes was explored by means of ^2H and ^{13}C KIEs to clarify the mechanism of ene step.[85] Changes of isotopic composition were determined for unreacted 2-methyl-2-butene **33** in reaction with SeO_2 at 25°C in *tert*-butyl alcohol (Equation (49)).

$$(49)$$

33   **34**
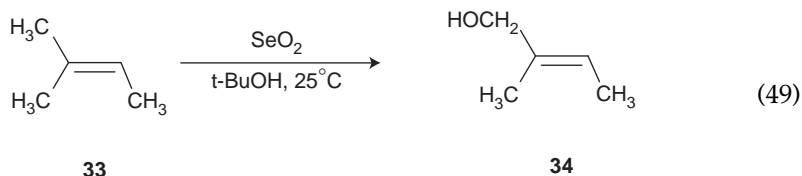
and calculated experimental isotope effects are summarized in Figure 15.

Table 4 Experimental ^{13}C KIEs for cyclopropenations of 1-pentyne or 1-hexyne with ethyl diazoacetate in the presence of rhodium catalyst

	C_1	C_2	C_3
	$Rh_2(OAc)_4$		
Expt. 1 (R = Me)	1.012(3)	1.001(3)	0.999(4)
Expt. 2 (R = Me)	1.012(3)	1.003(3)	1.000(2)
	$Rh_2(OAc)(DPTI)_3$		
Expt. 1 (R = Me)	1.008(3)	1.003(1)	1.000(2)
Expt. 2 (R = Me)	1.007(4)	0.999(2)	0.999(3)
Expt. 3 (R = Et)	1.010(4)	1.003(4)	1.000(4)

^{2}H KIEs

^{13}C KIEs

1.004(1), 1.004(1)
1.004(2), 1.005(2)

1.130(16)
1.127(15)   H$_3$C   H   0.920(10)
                              0.914(7)

1.006(2), 1.006(3) →
1.007(2), 1.007(2)   H$_3$C   H   1.017(3), 1.013(2)
                                                        ← 1.014(3), 1.014(3)

1.100(10) H$_3$C   CH$_3$ 1.00
1.101(10)   (assumed)   H$_3$C   CH$_3$

                 5
              2 3
                 1   4

1.003(1), 1.002(2)   1.00 (assumed)
1.002(1), 1.003(2)
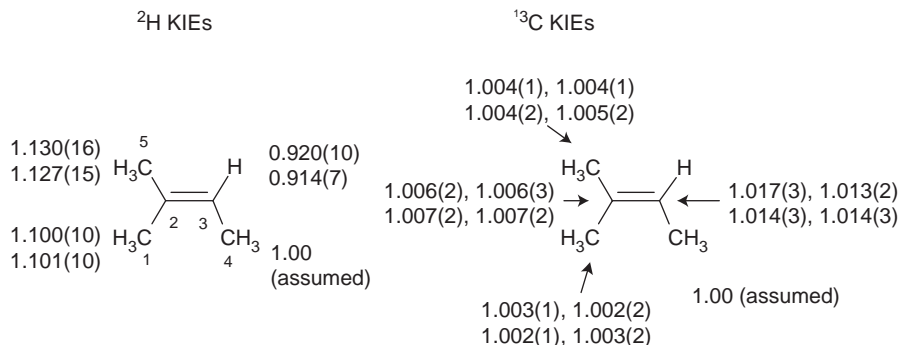
Figure 15 Experimental KIEs for oxidation of 2-methyl-2-butene **33** with selenium dioxide.

Isotope effects at C3 indicate the changes of hybridization (^{2}H KIE) and bonding (^{13}C KIE) at this atom in the rate-determining step. These results are consistent with a rate-limiting concerted ene step proposed by Sharpless.[86] On the other side, KIEs for C1 and C5 (1.002–1.005) seems to be too small for carbons undergoing a hydrogen abstraction and KIE for C2 (1.006–1.007) is too large as can be expected for an ene step. An alternative mechanism including electrophilic attack of SeO$_2$ on alkene and formation of the intermediate zwitterion would be consistent with isotope effects at C2, but not with primary ^{2}H effects at C1 and C5. Transition structures for alternative mechanisms were calculated by Becke3LYP calculations (6-311+G** basis set for selenium and 6-31G* for other atoms). The best agreement of experimental and predicted isotope effects was found for a concerted ene reaction with SeO$_2$ as the active oxidant. The involvement of reversible electrophilic attack by HSeO$_2^+$, followed by rate-limiting proton transfer in the zwitterion was ruled out.

The palladium-catalysed allylic alkylation of dimethylallyl acetate **35** with dimethyl malonate **36** in THF at 25°C was carried out using a combination of Pd$_2$(dba)$_3$ [*tris*(dibenzylideneacetone)dipalladium] and triphenylphosphine with *O,N-bis*(trimethylsilyl)acetamide (BSA) as a base.[87]

MeO$_2$C   CO$_2$Me
                Me
              Me   **37**

O
O   Me
     Me   +   MeO$_2$C   CO$_2$Me

Pd$_2$(dba)$_3$
Ph$_3$P, THF

BSA, 25 °C

+   (50)

CO$_2$Me
              Me
MeO$_2$C
        38   Me

Me

35   **36**
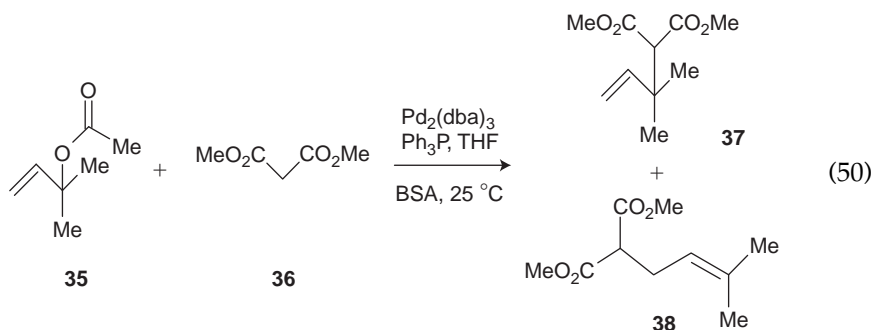
Under these conditions two products **37** and **38** were formed in the ratio 76:24. For ^{13}C NMR analysis the unreacted **35** was recovered from reaction taken above
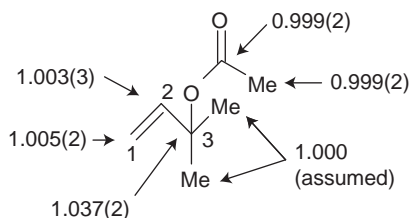
Figure 16 ^{13}C KIEs for the allylic alkylation reaction of **35** with **36** at 25°C.

70% conversion. The average isotope effects from six experiments are shown as in Figure 16.

A very large isotope effect at the tertiary atom C3 indicates the substantial change in bonding at this atom in the rate-determining step. Isotopes affects at C1 and C2 are small and suggest π-complexation to the olefin without significant bonding change. Overall, KIEs are consistent with the rate-limiting C–O bond cleavage. Theoretical calculations for reaction (50) had difficulty of prediction of isotope effects consistent experimental effects, probably due to problems with modelling of the ionization.

4.3 Ene reactions

^{2}H and ^{13}C KIEs were applied to study different types of ene (the Alder-ene) reactions. The reaction of maleic anhydride with allylbenzene was carried out at 175°C in the presence BHT (2,6-di-*tert*-butyl-4-methylphenol).[88]

(51)

39
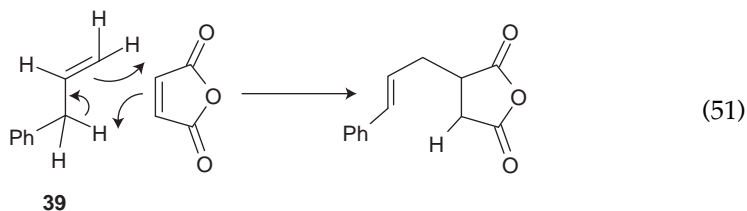
NMR analysis of ^{2}H and ^{13}C composition of recovered allylbenzene **39** was carried out using the *ortho* aromatic deuterium peak and the *para* aromatic carbon peak as internal standards. From integrations the following isotope effects values were calculated as shown in Figure 17.

The combination of small but significant inverse deuterium and normal ^{13}C KIEs at C1 indicate the bond formation to this carbon atom in the early rate-determining transition state. The observed hydrogen and carbon isotope effects in position 3 are consistent with proton transfer in the rate-determining step. Thus, from the qualitative analysis of isotope effect an early concerted pericyclic transition state can be concluded. The more detailed structure of transition state was described on the basis of theoretical calculations (Becke3LYP/6-31G*).
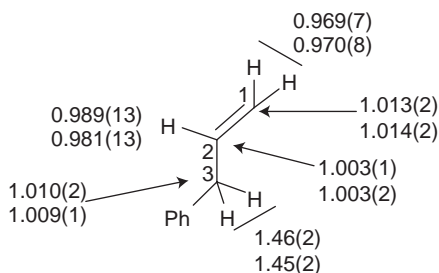
Figure 17 ^{2}H and ^{13}C KIEs for the reaction of maleic anhydride with allylbenzene **39** at 175°C.

The intermolecular and intramolecular ^{13}C isotope effects were used in studies of the mechanism of the ene reaction of singlet ($^1\Delta_g$) oxygen with alkenes.[89] The intermolecular ^{13}C isotope effect was determined for reaction of 3-isopropyl-2,4-dimethylpent-2-ene **40** with $^1O_2$ in methanol/2-propanol (1:1) at 10°C using a sunlamp and Rose Bengal as sensitizer.
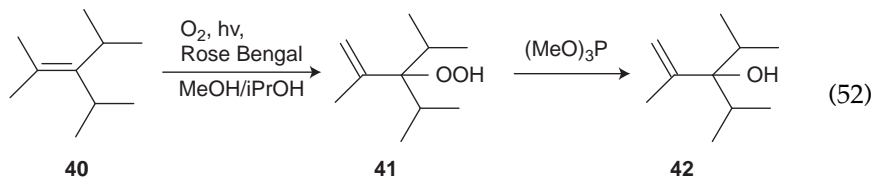
Substrate after 76% of conversion was recovered from reaction mixture treated with trimethyl phosphite to convert product **41** to **42**. Small and similar (1.006) ^{13}C intermolecular isotope effects for the olefinic carbons reflect a synchronous attack of $^1O_2$ in the rate-limiting transition state.

The intramolecular ^{13}C isotope effects on the ene reaction with $^1O_2$ oxygen were determined for 2,3-dimethyl-1-buten-3-ol **43** prepared from 2,3-dimethyl-but-2-ene:[89]
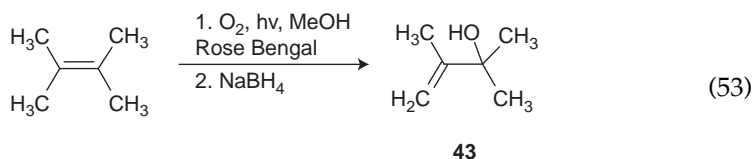
The analysis of ^{13}C integrations in context of different mechanistic models (concerted, biradical or per epoxide) led authors to the conclusion that ^{13}C integration pattern is consistent with the perepoxide model and supports mechanism proposed earlier from ^{2}H KIEs.[90] The following intramolecular ^{13}C isotope effects for formation of **43** were calculated from changes of ^{13}C integrations (Figure 18).

The advanced theoretical calculations were carried out to find the best prediction of experimental isotope effects. In contrast to the other examined theoretical methods the composite CCSD-(T)/6-31G*//B3LYP/6-31G* grid gave
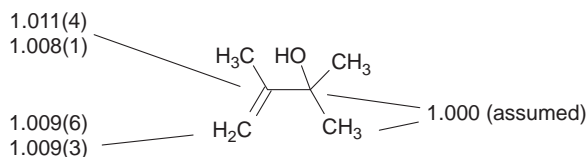
Figure 18 Intramolecular ^{13}C KIEs for synthesis of **43**.
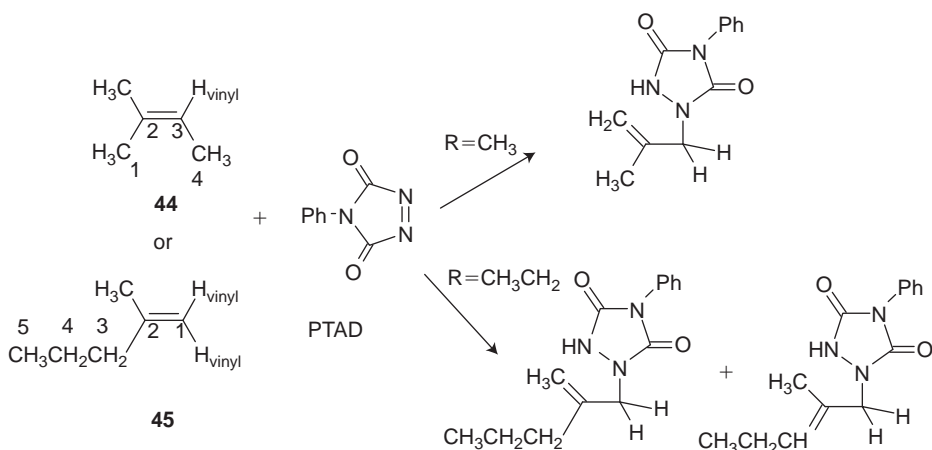
Scheme 7.

the excellent agreement of KIEs. An important conclusion from these studies is experimental evidence for a reaction surface involving two adjacent transition states with no intermediate between them (a two-step no-intermediate mechanism).

^{2}H and ^{13}C KIEs were determined for the ene reaction of 4-phenyl-1,2,4-triazoline-2,5-dione (PTAD) with 2-methyl-2-butene **44** or 2-methyl-1-pentene **45** (Scheme 7).[91] Authors assumed that although in the reaction of 2-methyl-1-pentene two products are formed, reactions should proceed via very similar transition states in the first mechanistic step.

Reaction was carried out in 1,4-dioxane at 25°C and samples of substrates recovered at 65–75% of conversion were isolated for NMR analysis. The changes of ^{2}H and ^{13}C composition were determined using as 'internal standard' C4 methyl group (**44**) or C4 methylene group (**45**). For 2-methyl-2-butene **44** ^{13}C KIEs for C2 [1.014(3), 1.013(2)] and C3[1.026(3), 1.025(3)] were found. In the case of 2-methyl-1-pentene ^{13}C KIE for C1 was 1.036(4). For vinyl protons in **44** and **45** the same highly inverse deuterium KIE equal to 0.87 were found.

Assuming the intermediacy of the aziridinium imide from the qualitative analysis of isotope effect values highly asynchronous C–N bond formation can be

expected. HF and Becke3LYP calculations using 6-31G* basis set for 2-methyl-1-pentene provided transition-state structure leading to biradical intermediate **46**:

46
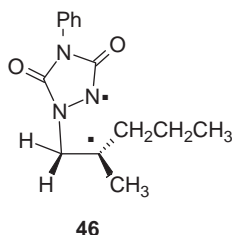
and calculated intermolecular isotope effects are consistent with experimental values except for C2. The predicted value 1.009 is greater than the observed value (1.003). This may suggest less bond formation to C2 in the actual transition state in comparison to the calculated structure.

Comparison of experimental and calculated KIE values for 2-methyl-butene is more complicated due to formation of three stereoisomeric/regioisomeric transition structures:
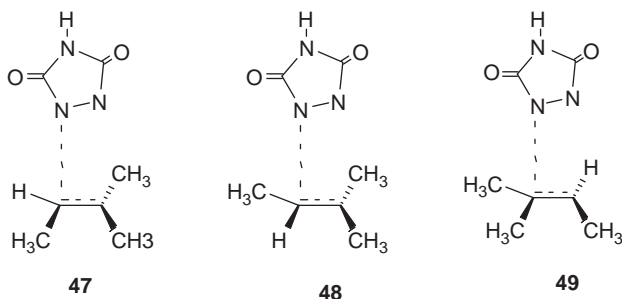
47   **48**   **49**

When in prediction 70:30 mixture of (**47**+**48**)/**49** was taken into consideration, KIEs of 1.014 and 1.026 for C2 and C3 in 2-methyl-2-butene **44** were in perfect agreement with the experimental results.

The mechanism of Lewis acid-catalysed ene reactions was studied for reaction of 2-methyl-butene **44** with formaldehyde in the presence of diethylaluminium chloride in toluene:[92]

(54)
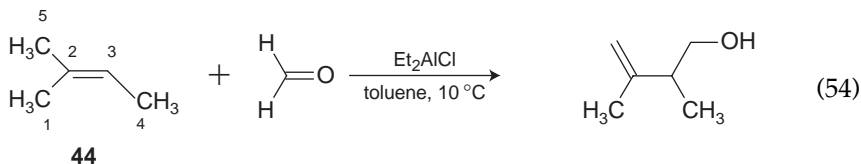
The recovered **44** was analysed by means of ^{2}H and ^{13}C NMR and changes of composition were related to C4 methyl group as internal standard. From these changes the isotope effects were calculated. The overall isotope effect at C5 represents a combination of primary and secondary isotope effects of proton

transfer and change of hybridization, respectively. The observed deuterium effect at C5 1.218–1.228 is consistent with small but significant primary isotope effect of rate-limiting proton transfer and his conclusion is supported by ^{13}C KIE 1.006–1.009 at this atom. The vinylic deuterium KIE 0.89 is consistent with the C3 carbon being fully sp[3]-hybridized in the transition state, however ^{13}C KIE 1.007–1.008 is smaller than carbon isotope effects in similar reactions. On the qualitative basis is impossible to unambiguously distinct between mechanisms involving rate-determining proton transfer and concerted ene transition state with nearly complete bond formation between the attacking electrophile and C3. The Becke3LYP calculations using 6-31G* basis gave consistent with experiment predicted isotope effects for mechanism involving a carbocation intermediate with subsequent proton transfer step being the rate limiting:

(55)
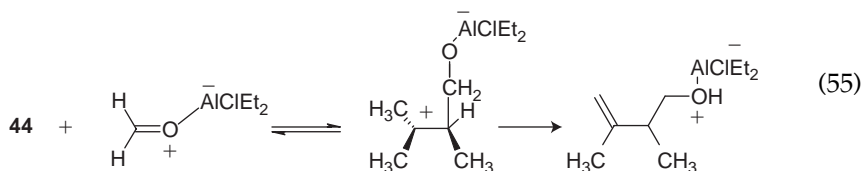
4.4 Coarctate reactions

Fragmentation of 2-phenylimino-Δ^3-1,3,4-oxadiazoline **49** includes break of five σ-bonds in the substrate and formation of five new π-bonds.[93]

(56)
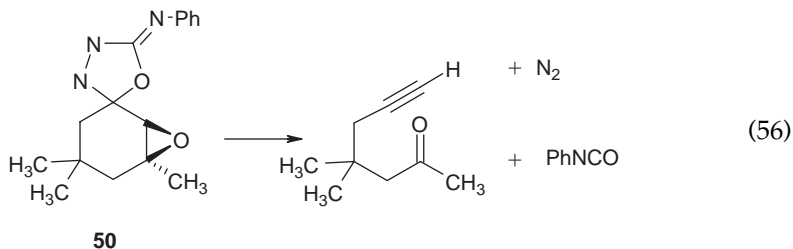
This an example of 'coarctate reaction' in which two bonds are simultaneously formed and broken at an atom not following a cyclic pathway.[94] The ^{13}C KIEs for fragmentation of **50** at 150°C in diphenyl ether were determined for substrate at 65–84% conversion (Figure 19).

The primary ^{13}C KIEs were observed for the C2 and C5 ring carbons and these atoms are undergoing a σ-bonding change in the transition state of the rate-limiting step. The absence of isotope effect at the quaternary epoxide carbon suggests that the epoxide ring remains intact in the rate-limiting step. These qualitative conclusions were confirmed by theoretical calculations (B3LYP/6-31+G(d,p)+zpe) and good agreement of predicted isotope effects with experimental KIEs was achieved.
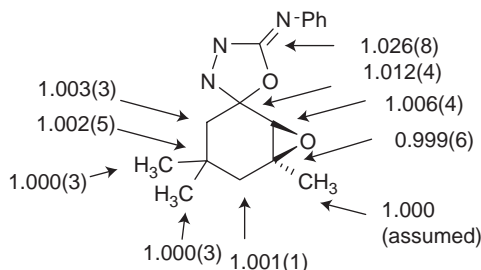
Figure 19 ^{13}C KIEs for fragmentation of **50** at 150°C.

Another example of coarctate reaction studied by means of ^{13}C KIEs is the deoxygenation of styrene oxide **51** with dichlorocarbene.[95]

(57)
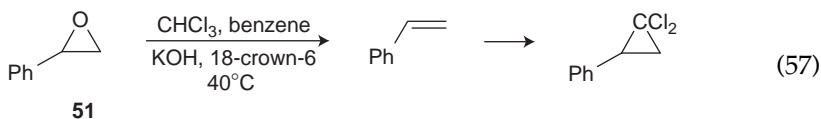
^{13}C KIEs experiments were supposed to help distinguishing the rate-limiting formation of an epoxide–carbene ylide complex **52** versus a rate-limiting deoxygenation process.

52
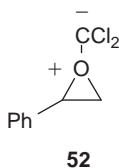
For the rate-limiting ylide complex formation no isotope effects are expected for epoxide carbons. The observed ^{13}C KIEs (Figure 20) rules out that formation of ylide is kinetically important, because effects of C1 and C2 atoms are different than unity. The normal isotope effect of C1 corresponds to the C–O bond breakage in the rate-limiting step. The inverse isotope effect of C2 suggests that the C2–O bond became stranger in transition state than in substrate.

Theoretical calculations (B3LYP/6-311++G(2d,p)) supported this conclusion and gave predicted isotope effects consistent with experimental values.

4.5 Nucleophilic substitution

For thermal decomposition of aryl diazonium cations in water two mechanism are considered: an S_N1 mechanism involving an aryl cation and concerted front-side displacement S_N2Ar. Kinetic, isotopic and theoretical studies delivered arguments for both mechanisms without unambiguous generalization. Application of isotope effects combined with theoretical calculations gave a new view of this problem.[96] *p*-Tolyldiazonium cation **54** was chosen for ^{13}C KIEs studies

1.016(2)

0.995(1)

1.001(3)

1.002(3)

1.000(3)

1.000
(assumed)
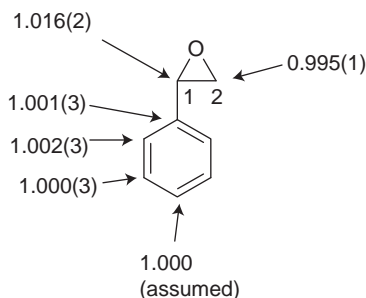
Figure 20 ^{13}C KIEs for the deoxygenation of styrene oxide **51** with dichlorocarbene.

1.017(2)
1.016(2)

1.024(3)
1.024(3)

1.014(2)
1.013(2)

1.000(3)
1.000(3)
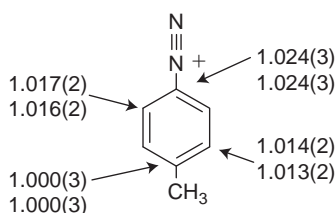
Figure 21 ^{13}C kinetic isotope effects for decomposition of **54** in water at 55°C.

because methyl group could be applied as internal standard.

$$ \text{(58)} $$

53   **54**   **55**
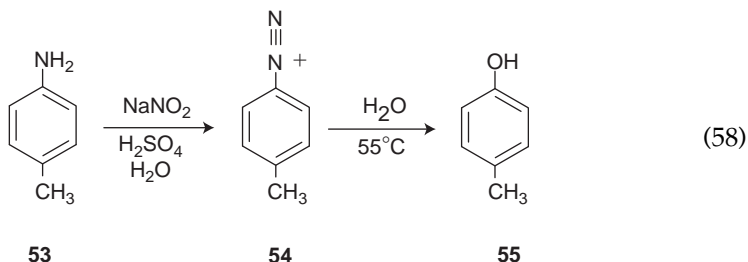
Unreacted substrate was quantitatively converted into *p*-tolyl azide before NMR analysis. ^{13}C KIEs are summarized in Figure 21.

The most surprising observation is ^{13}C KIEs observed not only for undergoing substitution C1 carbon atom, but also for *ortho* and *meta* carbon atoms. The observed isotope effects suggest that the C2–C3 and C5–C6 bonds become weaker in the resembling cation transition state relatively to the substrate. Theoretical calculations (B3LYP/6-31G*, *m*PW1PW91/6-31G*) with fully optimized water as a solvent (a continuum solvent model) were carried out for different structures of transition states, representing a spectrum of S$_N$2Ar mechanisms as well as formation of *p*-tolyl cation. Analysis of predicted isotope effects and dynamics trajectories led to the conclusion that there is no clear dividing line between bimolecular and unimolecular mechanisms.

4.6 Elimination reaction (decarboxylation)

The thermal decarboxylation of 1,3-dimethylorotic acid **56** was studied as a model for uncatalysed decarboxylation of orotidine 5′-monophosphate to form uridine 5′-monophosphate.[97] This reaction catalysed by the enzyme oritidine 5′-monophosphate decarboxylase is the essential step in nucleic acid biosynthesis.[98] Samples of 1,3-dimethylorotic acid were heated at 190°C to conversion over 90% and unreacted substrate was recovered after conversion into the methyl ester.

$$\text{(59)}$$

56
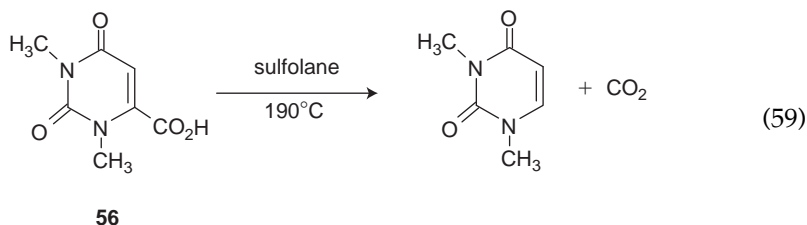
The relative changes in ^{13}C composition were calculated using signal of *N*-3 methyl group as internal standard. The experimental ^{13}KIEs are collected in Figure 22.

The C6 isotope effect of 1.028(2) is consistent with decarboxylation in the rate-determining step. Two mechanistic pathways were explored in Becke3LYP calculations using a 6-31+G* basis set (Scheme 8):

Transition states for decarboxylation of zwitterions **57** and **58** were optimized for different values of distance *r* between C6 carbon atom and carboxylate carbon in the range of 2–4.5 Å. Predicted isotope effects for C6 atom were found to be sensitive to the *r* distance contrary to the KIEs for C2, C4 and C5. As could be expected the predicted isotope effects also varied with the *r* distance. The best correlation of experimental and predicted isotope effects was found for the lower pathway (Scheme 8) including protonation of the O-4 oxygen. In the transition state HO-4 proton is engaged in hydrogen bond with water molecule.

4.7 Polymerization

Mechanism of polymerization of methyl methacrylate (MMA) was studied by means of isotope effects. Deuterium isotope effect of cobalt porphyrin catalysed
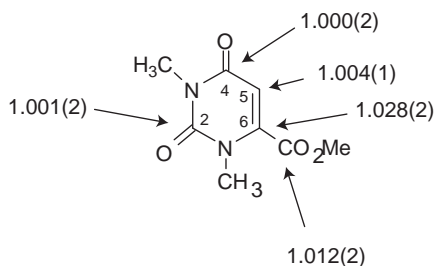
Figure 22 ^{13}C KIEs for decarboxylation of **56** at 190°C.
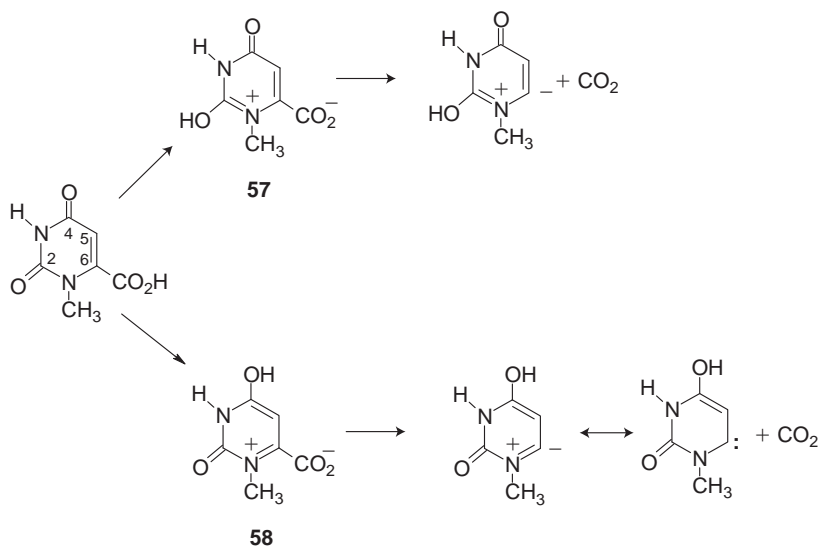
Scheme 8.

chain transfer in MMA free-radical polymerization was determined as the ratio of rate constants for reactions of perdeuterated or not-deuterated monomer.[99] Natural abundance of ^{13}C kinetic isotope was applied to compare mechanisms of free-radical polymerization and atom transfer radical polymerization (ATRP). The reaction was carried out in xylene at 60°C in the presence of CuBr/N-propyl-2-pyridinylmethanimine or AIBN.[100] Experimental isotope effects are summarized in Figure 23.

Substantial ^{13}C isotope effect on C1 is consistent with mechanism of free-radical polymerization, in which radical reacts with double bond at the less substituted carbon. The difference of isotope effects on C2 was assigned to differences in the mechanism of the propagation step in Cu(I) mediated and free-radical polymerization. Part of radicals is present as 'caged' radicals, held within the coordination sphere of the metal. With involvement of the metal catalyst in the addition step of ATRP did not agree Matyjaszewski and Singleton.[101] They applied combination of ^{13}C KIEs and theoretical calculations for MMA polymerization initiated by AIBN or CuBr:2,2′-bypiridine:ethyl 2-bromoisobutyrate in 1,2-dichlorobenzene at 80°C. Four independent reactions for both polymerizations gave eight sets of KIEs, which values were independent on reaction conditions and their statistical combination is presented in Figure 24.

Theoretical calculation (UB3LYP/6-311+G**, UB3LYP/6-31G*, UMPW1K/6-31+G**) for the addition of 2-methoxycarbonyl-2-propyl radical to MMA gave predicted isotope effects on C1(1.0378–1.0388), C2(1.0070–1.0076), C3(1.0008–1.0009) and C4(1.0018–1.0023) in good agreement with experimental values. Thus, observed by Harrison et al.[100] isotope effect of 1.002 on C2 in the free-radical polymerization should be experimentally verified, particularly that association of vinyl monomers and the [Cu^I(PMDETA)]BPh$_4$ was proofed not

Cu(I)-mediated   Free-radical
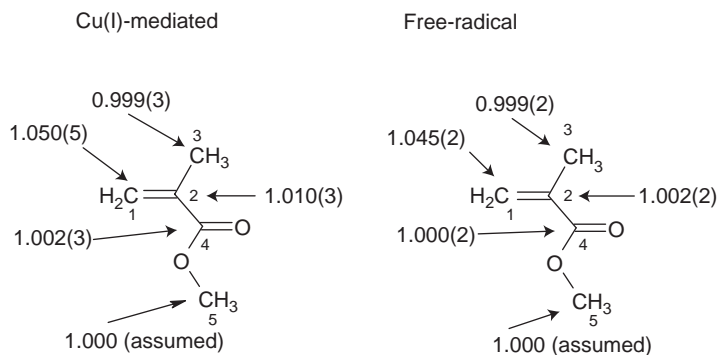
Figure 23 ^{13}C kinetic isotopes for copper(I)-mediated (left) and free-radical polymerization (right) of MMA at 60°C.
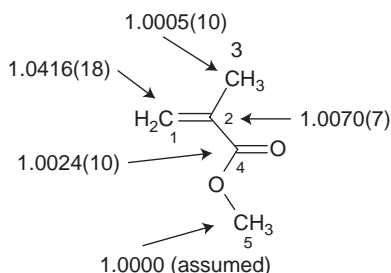
Figure 24 ^{13}C KIEs for polymerization of MMA in 1,2-dichlorobenzene at 80°C.

to affect the reactivity of the monomers in conventional free and ATRP polymerization.[102]

5. CONCLUSIONS

Within last 15 years new application of isotope effects has been developed. Natural abundance precise NMR measurements of deuterium, ^{13}C and sporadically ^{17}O enable determination of isotope effects for all atoms within molecules. This is a new opportunity for organic and physical organic chemists probing the reaction mechanisms. Fast development of sensitivity of modern NMR spectrometers and continuously better access to them should encourage scientists to apply KIEs measured at natural abundance.

ACKNOWLEDGEMENTS

REFERENCES

1. E. M. Purcell, H. C. Torey and R. V. Pound, *Phys. Rev.*, 1946, **69**, 37.
2. F. Bloch, W. W. Hansen and M. Packard, *Phys. Rev.*, 1946, **69**, 127.
3. J. Bigeleisen and M. G. Mayer, *J. Chem. Phys.*, 1947, **15**, 261.
4. H. S. Gutovsky, *J. Chem. Phys.*, 1959, **31**, 1683.
5. P. Muller, *Pure Appl. Chem.*, 1994, **66**, 1077.
6. W. Gombler, *J. Am. Chem. Soc.*, 1982, **104**, 6616.
7. C. J. Jameson and H. J. Osten, *Ann. Rep. NMR Spectrosc.*, 1986, **17**, 1.
8. H. Batiz-Hernandez and R. A. Bernheim, *Progr. NMR Spectrosc.*, 1967, **3**, 63.
9. P. E. Hansen, *Ann. Rep. NMR Spectrosc.*, 1983, **15**, 105.
10. H.-U. Siehl, *Adv. Phys. Org. Chem.*, 1987, **23**, 63–163.
11. H.-H. Limbach, G. S. Denisov and N. S. Golubev, Hydrogen bond isotope effects studied by NMR, in: *Isotope Effects in Chemistry and Biology*, A. Kohen and H.-H. Limbach, eds., CRC Press Taylor and Francis Group, Boca Raton, 2006, p. 193.
12. P. E. Hansen, *Magn. Reson. Chem.*, 2000, **38**, 1–10.
13. S. Bolvig and P. E. Hansen, *Curr. Org. Chem.*, 2000, **4**, 19.
14. T. Dziembowska and Z. Rozwadowski, *Curr. Org. Chem.*, 2001, **5**, 289.
15. T. Dziembowska, P. E. Hansen and Z. Rozwadowski, *Prog. NMR Spectrosc.*, 2004, **45**, 1.
16. P. E. Hansen, NMR studies of isotope effects of compounds with intramolecular hydrogen bonds, in: *Isotope Effects in Chemistry and Biology*, A. Kohen and H.-H. Limbach, eds., CRC Press Taylor and Francis Group, Boca Raton, 2006, p. 253.
17. P. E. Hansen, *J. Labelled Comp. Rad.*, 2007, **50**, 967.
18. J. M. Lopez, F. Maennle, I. Wawer, G. Buntkowsky and H.-H. Limbach, *Phys. Chem. Chem. Phys.*, 2007, **9**, 4498.
19. G. Buntkowsky and H.-H. Limbach, *J. Low Temp. Phys.*, 2006, **143**, 55.
20. J. G. Sośnicki, M. Langaard and P. E. Hansen, *J. Org. Chem.*, 2007, **72**, 4108.
21. M. Pietrzak, M. F. Shibl, M. Broering, O. Kuehn and H.-H. Limbach, *J. Am. Chem. Soc.*, 2007, **129**, 296.
22. T. T. Nguyen, N. Thach, F. Duus, B. K. V. Hansen and P. E. Hansen, *Magn. Reson. Chem.*, 2007, **45**, 245.
23. S. L. Borch and P. E. Hansen, *Z. Phys. Chem.*, 2008, **222**, 1213.
24. P. E. Hansen, Z. Rozwadowski and T. Dziembowska, *Curr. Org. Chem.*, 2009, **13**, 194.
25. C. J. Jameson and H. J. Osten, *J. Am. Chem. Soc.*, 1986, **108**, 2497.
26. C. J. Jameson, Isotope effects on chemical shifts and coupling constants, in: *Encyclopedia NMR*, D. M. Grant and R. K. Harris, eds., Wiley, Chichester, 1996, pp. 2638.–2655.
27. A. K. Jameson and C. J. Jameson, *J. Magn. Reson.*, 1978, **32**, 445.
28. R. E. Wasylishen and N. Burford, *Can. J. Chem.*, 1987, **65**, 2707.
29. Yu. A. Strelenko and N. M. Sergeyev, *J. Mol. Struct.*, 1996, **378**, 61.
30. N. D. Sergeyeva, J. P. Jacobsen and N. M. Sergeyev, *Chem. Commun.*, 1998, 1355.
31. M. Murray, *J. Magn. Reson.*, 1973, **9**, 326.
32. J. E. Del Bene, Anharmonicities, isotopes, and IR and NMR properties of hydrogen-bonded complexes, in: *Isotope Effects in Chemistry and Biology*, A. Kohen and H.-H. Limbach, eds., CRC Press Taylor and Francis Group, Boca Raton, 2006, p. 153.
33. J. Stare, A. Jezierska, G. Ambrozic, I. J. Kosir, J. Kidric, A. Koll, J. Mavri and D. Hadzi, *J. Am. Chem. Soc.*, 2004, **126**, 4437.
34. T. A. Ruden and K. Ruud, Ro-vibrational corrections to NMR parameters, in: *Calculations of NMR and EPR Parameters — Theory and Applications*, M. Kaupp, M. Bühl and V. G. Malkin, eds., Wiley-VCH, Weinheim, 2004 Chapter 10, p. 153.
35. A. A. Auer, *Chem. Phys. Lett.*, 2009, **467**, 230.
36. G. J. Martin and M. L. Martin, *Tetrahedron Lett.*, 1981, **22**, 3525.
37. G. J. Martin and M. L. Martin, *Ann. Rep. NMR Spectrosc.*, 1995, **31**, 81.
38. G. J. Martin, S. Akoka and L. M. Martin, *Mod. Magn. Res.*, 2006, **3**, 1629.
39. M. L. Martin, B. Zhang and G. J. Martin, *Mod. Magn. Res.*, 2006, **3**, 1637.
40. G. J. Martin, M. L. Martin and G. Remaud, *Mod. Magn. Res.*, 2006, **3**, 1647.

41. E. Jamin and G. J. Martin, *Mod. Magn. Res.*, 2006, **3**, 1659.

42. P. Paneth, *Talanta*, 1987, **34**, 877.

43. R. A. Pascal, M. W. Baum, C. K. Wagner and L. R. Rodgers, *J. Am. Chem. Soc.*, 1984, **106**, 5377.

44. R. A. Pascal Jr., M. W. Baum, C. K. Wagner, L. R. Rodgers and D.-E. Huang, *J. Am. Chem. Soc.*, 1986, **108**, 6477.

45. D. A. Singleton and A. A. Thomas, *J. Am. Chem. Soc.*, 1995, **117**, 9357.

46. B.-L. Zhang, M. Trierweiler, C. Jouitteau and G. J. Martin, *Anal. Chem.*, 1999, **77**, 2301.

47. L. Melander and W. H. Saunders Jr., *Reaction Rates of Isotopic Molecules*, John Wiley and Sons, New York, 1980.

48. D. A. Singleton and M. J. Szymanski, *J. Am. Chem. Soc.*, 1999, **121**, 9455.

49. S. Jankowski, J. Marczak, A. Olczak and M. Główka, *Tetrahedron Lett.*, 2006, **47**, 3341.

50. J. Wiktorowicz, *Ph.D. Dissertation*. Faculty of Chemistry, Technical University of Lodz, Lodz, Poland, 2007.

51. R. Criegee, *Justus Liebigs Ann. Chem.*, 1948, **560**, 127. G. R. Krow, *Org. React.*, 1993, **43**, 251.

52. S. R. Merrigan, V. N. Le Gloahec, J. A. Smith, D. H. R. Barton and D. A. Singleton, *Tetrahedron Lett.*, 1999, **40**, 3847.

53. P. Paneth, *J. Am. Chem. Soc.*, 1985, **107**, 7070.

54. J. Pawlak, M. H. O'Leary and P. Paneth, *J. Mol. Struct. (Theochem)*, 1998, **454**, 69.

55. M. Wolfsberg, *Acc. Chem. Res.*, 1972, **5**, 225.

56. B. R. Beno, K. N. Houk and D. A. Singleton, *J. Am. Chem. Soc.*, 1996, **118**, 9984.

57. J. S. Hirschi, T. Takeya, C. Hang and D. A. Singleton, *J. Am. Chem. Soc.*, 2009, **131**, 2397. and references cited therein

58. M. Saunders, K. E. Laidig and M. Wolfsberg, *J. Am. Chem. Soc.*, 1989, **111**, 8989.

59. V. Anisimov and P. Paneth, *J. Math. Chem.*, 1999, **26**, 75.

60. M. P. Meyer, A. J. DelMonte and D. A. Singleton, *J. Am. Chem. Soc.*, 1999, **121**, 10865.

61. J. J. Gajewski, K. B. Peterson, J. R. Kagel and Y. C. J. Huang, *J. Am. Chem. Soc.*, 1989, **111**, 9078.

62. D. A. Singleton, S. R. Merrigan and A. A. Thomas, *Tetrahedron Lett.*, 1999, **40**, 639.

63. D. A. Singleton, S. R. Merrigan, B. R. Beno and K. N. Houk, *Tetrahedron Lett.*, 1999, **40**, 5817.

64. N. J. Saettel, O. Wiest, D. A. Singleton and M. P. Mayer, *J. Am. Chem. Soc.*, 2002, **124**, 11552.

65. R. W. Holder, N. A. Graf, E. Duester and J. C. Moss, *J. Am. Chem. Soc.*, 1983, **105**, 2929.

66. I. Lee, *Chem. Soc. Rev.*, 1995, 223.

67. S. Yamabe and T. Dai, *J. Am. Chem. Soc.*, 1996, **118**, 6518.

68. T. Machiguchi, T. Hasegawa, A. Ishiwata, S. Terashima, S. Yamabe and T. Minata, *J. Am. Chem Soc.*, 1999, **121**, 4771.

69. B. R. Ussing, C. Hang and D. Singleton, *J. Am. Chem Soc.*, 2006, **128**, 7594.

70. D. A. Singleton and B. E. Schulmeier, *J. Am. Chem. Soc.*, 1999, **121**, 9313.

71. D. A. Singleton, Y. Wang, H. W. Yang and D. Romo, *Angew. Chem. Int. Ed.*, 2002, **41**, 1572.

72. S. R. Merrigan and D. A. Singleton, *Org. Lett.*, 1999, **1**, 327.

73. A. E. Keating, S. R. Merrigan, D. A. Singleton and K. N. Houk, *J. Am. Chem. Soc.*, 1999, **121**, 3933.

74. D. A. Singleton and Z. Wang, *J. Am. Chem. Soc.*, 2005, **127**, 6679.

75. E. Weitz and A. Scheffer, *Chem. Ber.*, 1921, **54**, 2327.

76. C. F. Christian, T. Takeya, M. J. Szymanski and D. A. Singleton, *J. Org. Chem.*, 2007, **72**, 6183.

77. U. Nettekoven and J. F. Hartwig, *ibid*, 2002, **124**, 1166.

78. K. Vo Loan and D. Singleton, *Org. Lett.*, 2004, **6**, 2469.

79. D. E. Frantz and D. A. Singleton, *J. Am. Chem. Soc.*, 2000, **122**, 3288.

80. D. E. Frantz, D. A. Singleton and J. P. Snyder, *J. Am. Chem. Soc.*, 1997, **119**, 3383.

81. D. T. Nowlan III, T. M. Gregg, H. M. L. Davies and D. A. Singleton, *J. Am. Chem. Soc.*, 2003, **125**, 15902.

82. A. J. DelMonte, J. Haller, K. N. Houk, K. B. Sharpless, D. A. Singleton, T. Strassner and A. A. Thomas, *J. Am. Chem. Soc.*, 1997, **119**, 9907.

83. Y. Lou, M. Horikawa, R. A. Kloster, N. A. Hawryluk and E. J. Corey, *J. Am. Chem. Soc.*, 2004, **126**, 8916.

84. D. T. Nowlan III and D. A. Singleton, *J. Am. Chem. Soc.*, 2005, **127**, 6190.

85. D. A. Singleton and C. Hang, *J. Org. Chem.*, 2000, **65**, 7554.

86. K. B. Sharpless and R. F. Lauer, *J. Am. Chem. Soc.*, 1972, **94**, 7154.

87. D. A. Singleton and C. F. Christian, *Tetrahedron Lett.*, 2005, **46**, 1631.

88. D. A. Singleton and C. Hang, *Tetrahedron Lett.*, 1999, 8939.

89. D. A. Singleton, C. Hang, M. J. Szymanski, M. P. Meyer, A. G. Leach, K. T. Kuwata, J. S. Chen, A. Greer, C. S. Foote and K. N. Houk, *J. Am. Chem. Soc.*, 2003, **125**, 1319.

90. B. Grdina, M. Orfanopoulos and L. M. Stephenson, *J. Am. Chem. Soc.*, 1979, **101**, 3111.

91. D. A. Singleton and C. Hang, *J. Am. Chem. Soc.*, 1999, **121**, 11885.

92. D. A. Singleton and C. Hang, *J. Org. Chem.*, 2000, **65**, 895.

93. D. A. Singleton and Z. Wang, *Tetrahedron Lett.*, 2005, **46**, 819.

94. R. Herges, *Ang. Chem. Int. Ed. Engl.*, 1994, **33**, 255.

95. D. A. Singleton and Z. Wang, *Tetrahedron Lett.*, 2005, **46**, 2033.

96. B. R. Ussing and D. A. Singleton, *J. Am. Chem. Soc.*, 2005, **127**, 2888.

97. D. A. Singleton, S. R. Merrigan, B. J. King, P. Beak, L. M. Philips and J. K. Lee, *J. Am. Chem. Soc.*, 2000, **122**, 3296.

98. A. Radzicka and R. Wolfenden, *Science*, 1995, **267**, 90.

99. A. A. Gridnev, S. D. Ittel, B. B. Wayland and M. Fryd, *Organometallics*, 1996, **15**, 5116.

100. S. Harrison, J. P. Rourke and D. M. Haddleton, *Chem. Commun.*, 2002, 1470.

101. D. A. Singleton, D. T. Nowlan III, N. Jahed and K. Matyjaszewski, *Macromolecules*, 2003, **36**, 8609.

102. W. A. Braunecker, N. V. Tsarevsky, T. Pintauer, R. R. Gil and K. Matyjaszewski, *Macromolecules*, 2005, **38**, 4081.

CHAPTER 4

Residual Dipolar Couplings for the Configurational and Conformational Analysis of Organic Molecules

G. Kummerlöwe and **B. Luy**

Contents

Department Chemie, Technische Universität München, LS OC II, Lichtenbergstrasse 4, D-85747 Garching, Germany

Abstract   Residual dipolar couplings (RDCs) have already revolutionized biomolecular NMR spectroscopy and are about to do the same in small molecule applications: impressive examples for conformational refinement of small sugars and peptides, the distinction of enantiomers and the determination of relative and absolute configuration have been published in recent years. After a short introduction into the basic theory, this article will give a review of existing alignment media, methods for scaling the alignment, pulse sequences for measuring RDCS and recent applications.

Keywords: NMR spectroscopy; RDCs; residual dipolar couplings; alignment media; structure; chirality; configuration; conformation

1. INTRODUCTION

The structure determination of organic molecules in solution — constitution, configuration and conformation — is probably the most important application of high-resolution NMR spectroscopy. Sophisticated methods based on classical NMR parameters like chemical shifts, *J*-couplings and nuclear Overhauser enhancement (NOE) have been developed for deriving structural models.[1,2] The approach has been successfully applied to a vast number of molecules including thousands of biomacromolecules and uncountable natural and synthetic products.

However, all standard NMR parameters are of short-ranged nature: chemical shifts are typically affected by the first and second sphere of atoms surrounding the nucleus and usually provide only qualitative measures; ^3J-couplings are limited to dihedral angles via three covalent bonds and through space connectivities via NOE can only be found up to 5 Å in favourable cases. As soon as the chain of short-range information is interrupted by NMR-inactive nuclei or a flexible linker, distant parts of a molecule cannot be correlated and the structure determination is bound to fail.

A potential solution to many of these problems can be found by the use of dipolar couplings as they are measured in the solid state[3–5] or in liquid crystalline phases.[6–9] But due to strong signal overlap, the approach is limited to specifically labelled or very small molecules. Only with the advent of residual dipolar couplings (RDCs) about a decade ago, which uses very weak alignment of molecules to largely retain chemical shift resolution, anisotropic NMR parameters are now available for structure determination of larger organic molecules.

Direct RDCs in biomolecules between protons over a distance of up to 8 Å have been measured,[10,11] allowing in principle an extension of atoms to be correlated. But even more important is that the nature of RDCs allows the extraction of angular information relative to the static magnetic field as an *external reference*, making it now generally possible to correlate distant parts of a molecule with NMR spectroscopy.

After the early work on dipolar couplings measured for small organic molecules in liquid crystalline phases, major elements of weak partial alignment have been developed in the field of biomolecular NMR spectroscopy where

RDCs are commonly used for the structure elucidation of proteins and nucleic acids nowadays.[12,13] Only recently the approach was transferred back to also obtain structural information of small- to medium-sized organic molecules. The central application in this case is the determination of relative configurations of distant chiral and prochiral centres, and also conformational studies of biologically active molecules, for example the enantiomeric differentiation of small molecules in chiral alignment media can be achieved.

Recent results have been summarized in a number of articles.[14–20] This review in parts is based on ref. 20 and will focus on the measurement and application of RDCs on small- to medium-sized organic molecules: after a short introduction into dipolar couplings and the alignment tensor, the most important alignment media for small molecule applications and how to scale their alignment properties in order to get ideal measurement conditions are discussed. A selection of pulse sequences adapted specifically to the measurement of RDCs at natural isotope abundance, and a look at the large variety of applications will complete the overview of the method. Finally, a brief summary and outlook to future perspectives of RDCs will be given.

2. THEORY

RDCs belong to the so-called anisotropic NMR parameters which cannot be observed in isotropically averaged samples as, for example, is the case in liquids. Besides RDCs, a number of other anisotropic parameters can be used for structure elucidation, like residual chemical shift anisotropy, residual quadrupolar couplings for spin-1 nuclei, or pseudo-contact shifts in paramagnetic samples. Here, we will focus on RDCs where we give a brief introduction into the dipolar interaction, then into the averaging effects with the description by the alignment tensor and concepts to deal with the flexibility of molecules. For the other anisotropic NMR parameters, we refer the reader to ref 19 for an introduction and to refs. 6–8 for a detailed description.

2.1 Dipolar couplings

Next to scalar couplings via covalent bonds, dipolar couplings through space are probably the most important interactions in NMR spectroscopy. The origin of this interaction can be understood in a simplistic, classical picture if we consider spins as magnets with an inherent rotation at the Larmor frequency. Although spins are not oriented directly along the static magnetic field B_0, the integration over time of the fast rotating magnets yields a secular magnetic moment parallel or antiparallel to B_0 (Figure 1A, B). The magnetic moment of spin I results in the same magnetic field as a classical magnet with the typical r^{-3} dependence of the magnetic field with respect to the distance to the magnet and the $(3\cos^2\theta - 1)$-dependence with respect to the angle θ relative to the axis of the magnetic moment. Since the magnetic moment of the spin is oriented along the static magnetic field B_0, the angle θ is identical to the angle Θ with respect to B_0. The
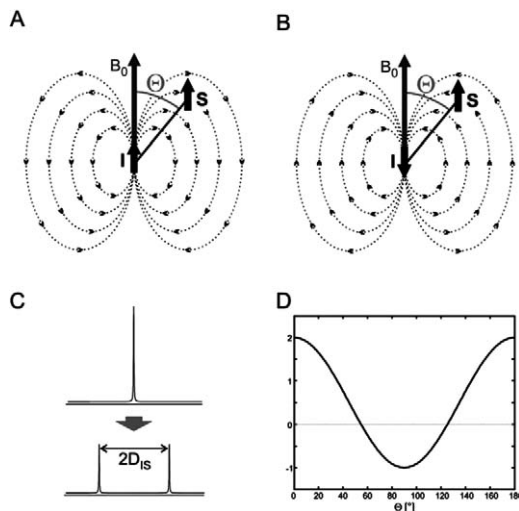
Figure 1 Illustration of the dipolar interaction. (A and B) The magnetic field induced by spin I adds up to the static magnetic field B_0 and leads to a shift of the resonance frequency of the close-by spin S. Since spins parallel and antiparallel to the magnetic field are equally populated, a splitting with the dipolar coupling $2D_{IS}$ is observed (C). If the distance r_{IS} between the two spins is fixed, the dipolar coupling is directly proportional to $3\cos^2\Theta-1$ and can be used as angular information relative to the static magnetic field B_0 (D). (Reprinted from ref. 20. Copyright 2009, with permission from Elsevier.)

magnetic field produced by spin I now adds up to the static magnetic field felt by spin S and causes a shift of its resonance frequency, the so-called dipolar coupling. Depending on the distance between the two spins and their angle Θ of the internuclear vector relative to B_0, the strength and sign of this additional magnetic field varies. The exact formula for the dipolar coupling D_{IS} between two spins in a defined orientation is

$$D_{IS} = -\frac{\hbar\gamma_I\gamma_S\mu_0}{16\pi^2}\left\langle\frac{1}{r_{IS}^3}(3\cos^2\Theta-1)\right\rangle \tag{1}$$

with the gyromagnetic ratios γ_I and γ_S of the two spins, their distance r_{IS}, and the angle Θ of the internuclear vector with B_0, averaged over time as indicated by the brackets. Since the spin I is equally populated parallel and antiparallel to B_0, a dipolar-coupled signal shows a splitting of size $2\,D_{IS}$ (Figure 1C).

Dipolar couplings are typically on the order of several thousand Hertz. In solid-state powder spectra, these couplings lead to broad lines devoid of chemical shift resolution. In liquid-state spectra, however, dipolar couplings are averaged to zero and sharp lines with high resolution are possible. Although dipolar couplings still contribute to relaxation processes like the NOE as a widely used structural parameter in NMR spectroscopy, a large amount of the potential structural information is lost by the averaging, and valuable restraints would be obtained if dipolar couplings could be measured directly.

To be able to measure the desired additional structural information without significant loss in chemical shift resolution, an intermediate state between solid and liquid has to be reached. With the help of so-called alignment media, solute molecules are only oriented for a time average of 0.05% which, for example reduces a 23 kHz dipolar coupling between a carbon and its directly attached proton to a RDC of only 11.5 Hz (or a dipolar splitting of 23 Hz, which in many cases is also called RDC). In this way dipolar interactions can be measured with relatively high accuracy and reasonable RDC-based line broadening. The only drawback of the method is the partial averaging due to the tumbling of the molecule and its inherent flexibility which has to be addressed by an adequate model.

2.2 Motional averaging and the concept of the alignment tensor

The description of the averaging in Equation (1) is by no means trivial, and the development of corresponding models for an effective inclusion of flexibility of molecules on various time scales is still an ongoing field of research. We therefore will start out with the most simple case, the averaging of a completely rigid molecule, before going into effects of conformational averaging.

If we assume a rigid molecule with fixed distances and angles between atoms, the averaging of Equation (1) is only due to molecular tumbling of the molecule. The dipolar coupling in this case is described by

$$D_{IS} = -\frac{\hbar \gamma_I \gamma_S \mu_0}{16\pi^2} \left(\frac{1}{r_{IS}^3} (3\langle \cos^2 \Theta \rangle - 1) \right) \qquad (2)$$

with averaging only over the angle Θ of the internuclear vector relative to the static magnetic field. In an isotropic solution all orientations will be distributed equally, resulting in $\langle \cos^2 \Theta \rangle = 1/3$ and the angular term will lead to a cancellation of all anisotropic interactions. In a partially oriented system, however, reduced dipolar couplings survive.

The description so far is based on the laboratory frame with the static magnetic field fixed along the z-axis and the molecule tumbling in space (Figure 2A). It turns out to be useful for the description of orientational averaging
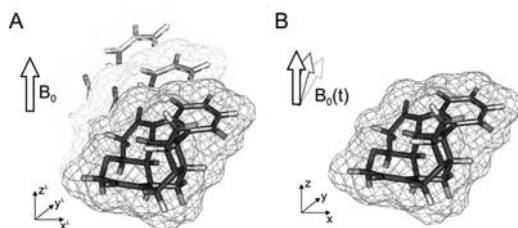
Figure 2   In the laboratory frame (A) the molecule is tumbling with the static magnetic field fixed along the z-axis. The reference frame of a rigid molecule, instead, moves with the compound and leads to an effective variation of the magnetic field vector (B).

to go into an arbitrary frame of reference of the (rigid) molecule itself. In this reference frame, the molecule is fixed in space while the magnetic field vector is changing its position (see Figure 2B). With the cylindrical symmetry of the magnetic field and the assumption of a cylindrically symmetric alignment medium with its director pointing into the same direction as the magnetic field (for the situation that director and magnetic field point in different directions, see Section 4.2), the distribution of the magnetic field can be described by the so-called probability tensor $\mathbf{P}$.[21] This tensor is represented by a (3×3) matrix with the components being time and ensemble averaged probabilities $P_{\alpha\beta} = \langle \cos \vartheta_\alpha \cos \vartheta_\beta \rangle$; $(\alpha, \beta = x, y, z)$ to find the magnetic field at the angles $\vartheta_x, \vartheta_y, \vartheta_z$ relative to the axes of the reference frame of the molecule. Because of its symmetry along the diagonal and the condition for the probability distribution that $P_{xx} + P_{yy} + P_{zz} = 1$, the tensor has a maximum number of five independent components (which might be further reduced by inherent symmetries of the molecule of interest). The tensor represents an ellipsoid and with the coordinate system along the principle axes of the ellipsoid, the matrix becomes diagonal with the three eigenvalues P_{xx}^d, P_{yy}^d, P_{zz}^d which are usually ordered according to their size $P_{xx}^d \leq P_{yy}^d \leq P_{zz}^d$. Although the probability tensor $\mathbf{P}$ is very intuitive and sufficient to describe the resulting anisotropic parameters in a rigid molecule, it is more common to express the partial alignment of the molecule in terms of the so-called alignment tensor $\mathbf{A}$, which is given by

$$\mathbf{A} = \mathbf{P} - \frac{1}{3}\mathbf{1} \tag{3}$$

The alignment tensor has a vanishing trace $A_{xx} + A_{yy} + A_{zz} = 0$, and its eigenvalues are ordered by definition to fulfill $|A_{xx}^d| \leq |A_{yy}^d| \leq |A_{zz}^d|$. With the internuclear vector $\mathbf{r} = (r_x, r_y, r_z)$ in the coordinates of the reference frame, the dipolar coupling between the spins can then be written as

$$D_{IS} = -\frac{\hbar \gamma_I \gamma_S \mu_0}{16\pi^2} \left(\frac{3}{r_{IS}^5} \sum_{\alpha,\beta} A_{\alpha\beta} r_\alpha r_\beta \right) \tag{4}$$

The original nomenclature introduced by Saupe[22] uses the Saupe-matrix $\mathbf{S}$ instead of the alignment tensor $\mathbf{A}$, which are related by

$$\mathbf{S} = \frac{3}{2}\mathbf{A} \tag{5}$$

and sometimes the tensor is characterized by its axial and rhombic components[21]

$$A_a = \frac{3}{2}A_{zz}^d; \qquad A_r = A_{xx}^d - A_{yy}^d \tag{6}$$

Generally, the five independent components of the alignment tensor $\mathbf{A}$ can be derived by mathematical methods like the singular value decomposition (SVD)[23] as long as a minimum set of five RDCs has been measured in which no two internuclear vectors for the RDCs are oriented parallel to each other and no more than three RDC vectors lie in a plane. Any further measured RDC directly

contains valuable structural information as long as the molecule can be considered to be rigid.

Most applications on medium-sized organic molecules reported today are based on an interpretation of RDCs via the concept of the alignment tensor. It is therefore not surprising to find that most studied molecules are relatively rigid. However, it turns out that the concept even allows the approximate description of conformationally averaged structures.

2.3 Conformational flexibility

For a flexible compound, both r_{IS} and Θ from Equation (1) are conformationally dependent and the interconversion of the structures is overlayed with the reorientation of the rigid molecule as described in the previous section. The two processes can be separated, in principle, if their time scales are sufficiently different. Especially if the interconversion rate is fast compared to the reorientation rate, the molecule of interest can be described by an average structure with a single alignment tensor.[24] However, even considering vibrational motions, this condition is only fulfilled for very small molecules. For the case that conformational changes happen on a similar or slower time scale than the corresponding reorientation, each conformer has to be described by its own alignment tensor.[24]

If we concentrate on vibrational motions first, it has been shown early in refs. 25–28 that RDCs for a molecule can be influenced if the motions are coupled to the reorientation processes. The vibrational corrections to RDCs are generally small, estimated to be about 1–2% in the original publications[26] and <5% in later articles.[8] Since the experimental error of many RDCs is larger than this correction, it is usually safely neglected in corresponding configurational and conformational studies of larger molecules. However, it has been shown that vibrational corrections can account for RDCs and other anisotropic parameters measured in molecules with tetrahedral symmetry like methane or tetramethylsilane, which should not show any anisotropic parameters at all in the rigid picture.[29,30]

Models for the treatment of RDCs in flexible molecules can also be based on a mean-field approach. Instead of the alignment tensor, which describes the anisotropic part of the orientational averaging of a rigid molecule, averaging over all orientations and conformations can also be achieved when describing the conformationally dependent probabilities to find a molecule in a certain orientation as a sum of an isotropic and anisotropic potential. The anisotropic potential can then be expanded into a series of functions with their coefficients as fitting parameters. As with the alignment tensor approach, RDCs in addition to the ones used for the fitting process then provide highly useful structural information even for molecules with conformational flexibility. Several models like the additive potential (AP) model,[31] the maximum entropy (ME) approach[32] and their combination into the APME approach[33–37] have been proposed.

Other ways of fitting RDCs to a number of conformations are based on theoretical calculations of potential conformers (e.g. by DFT calculations or by generating an ensemble of structures and sorting out lowest energy conformers

in an QM/MM approach) and directly fitting RDCs to either a set of alignment tensors[38] or to a single alignment tensor as a crude approximation.[39,40] More efficient treatments of flexible molecules in conformational and configurational studies can be expected to be developed in the future.

3. ALIGNMENT MEDIA FOR WEAK ALIGNMENT

In 1963, Saupe and Englert reported the first spectrum of a partially aligned organic molecule: benzene in a nematic liquid crystalline phase, resulting in an approximately 2500 Hz broad multiplet with 32 lines.[41] Only one year later, the full theory of dipolar couplings in partially aligned samples was derived[22] and the potential usefulness of a systematic study of solute molecules in liquid crystalline phases became evident. Since then many different alignment media have been developed for different applications. Some alignment media are designed to achieve maximum dipolar couplings in anisotropic liquids to measure as much structural information as possible and provide a structural model of small compounds in unprecedented detail. Recently developed alignment media, however, are optimized to allow very weak alignment, if possible without lower limit of the alignment strength. As mentioned in the introduction, in this case the measurement of a relatively small number of RDCs is manageable for larger organic compounds up to biomacromolecules like proteins and nucleic acids. In the following, the discussion of alignment media will be focussed on very weakly aligning media.

3.1 Different types of alignment media

Three different ways of partially aligning a molecule are known today: the already mentioned alignment in a liquid crystalline phase, alignment in a stretched gel and the orientation via paramagnetic ions.

While paramagnetic alignment[42] is frequently used in biomolecular NMR, where either paramagnetic ions[43,44] or specifically designed paramagnetic tags[45–48] provide RDCs and so-called pseudo-contact shifts as valuable structural parameters, its use for small molecules is quite limited, since covalently attached paramagnetic centres usually will broaden the lines of neighbouring nuclei beyond detection. The only class of paramagnetic alignment media frequently used for organic molecules are the lanthanide shift reagents[49–52] which form complexes with the solute of interest and thereby introduce pseudo-contact shifts that help to resolve overlap or distinguish enantiomers. RDCs and other anisotropic parameter so far have not been measured with the help of such shift reagents to our knowledge.

The most widely used type of alignment media today are liquid crystalline phases, typically lyotropic mesophases (Figure 3A). A large variety of liquid crystals is known for apolar organic solvents and also aqueous solutions.[9,54] A characteristic feature of liquid crystalline phases is their limitation to certain concentration and temperature ranges. Especially the lower concentration limit
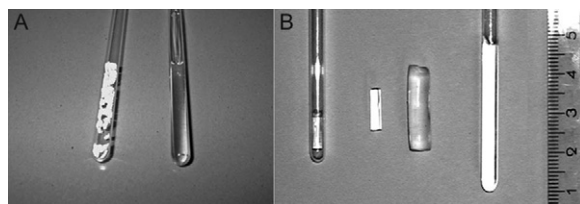
Figure 3   Liquid crystalline (A) and gel-based alignment medium (B) at various stages: (A) dry PBLG and the readily prepared lyotropic mesophase. (B) Cross-linked PS as an unswollen polymer stick in a standard NMR tube (left), polymer stick directly after polymerization, fully swollen polymer stick, polymer stick swollen in an NMR tube with an effective stretching along the tube axis (right). (Reproduced from refs. 17 and 53 with permission from Wiley-VCH Verlag GmbH & Co. KGaA (Copyright).)

for a first-order phase transition leads to a minimum alignment strength. While this minimum alignment is sufficiently low in many aqueous phases, most liquid crystals with apolar solvents align relatively strongly for medium-sized organic molecules.

Stretched polymer gels were introduced by Deloche and Samulski.[55] Their alignment strength is solely determined by the amount of mechanical stretching so that arbitrary scaling of RDCs can be achieved. A common preparation scheme is to put a dry, cross-linked polymer stick into an NMR tube which is then swollen by the addition of a solvent. The swelling gel reaches the glass walls and any further swelling will automatically result in a stretching (Figure 3B). Solute molecules diffused into a stretched gel will be partially oriented by the anisotropic gel matrix. In the meantime, polymer gels for most NMR solvents are known and their flexibility makes them the favoured type of alignment media in our laboratory. Their only disadvantage is the time needed for the solute molecule to diffuse into the polymer gels which typically takes several days.

3.2 Alignment media for aqueous solutions

A large number of alignment media for aqueous solutions have been found in the field of NMR spectroscopy of biomacromolecules which are now partially transferred to applications with organic molecules. Initial aqueous alignment media focussed on liquid crystalline phases. A large variety of so-called bicelles[56–59] has been adjusted to corresponding needs especially in protein NMR. Similarly, the liquid crystals known as Otting phases[60,61] are frequently used because of their relatively low cost and easy preparation. The 'standard' alignment media for nucleic acids are negatively charged filamentous Pf1 phage,[11,62–64] which are also used for negative-to-neutral charged proteins and sugars. There is a large number of less frequently used liquid crystalline phases. Some of them are cellulose crystallites,[65] the so-called Helfrich phases,[66–68] purple membranes[69,70] and mineral liquid crystals.[71,72] Alignment media with interesting features are also liquid crystalline phases that are immobilized in a gel phase.[73–76] Recently reported alignment based on DNA nanotubes[77] and nucleic

acid G-tetrad structures[78] are probably too expensive to be of real use in small molecule NMR.

A second type of alignment media is stretched polymer gels, for which the number of applications in biomolecular NMR spectroscopy is growing fast.[79] The use of gels as alignment media started with poly(acrylamide) (PAA) gels[73,80,81] which are commonly prepared in most biochemical laboratories. The method to use a stretched PAA gel for aligning a solute molecule is called strain-induced alignment in a gel (SAG).[80] It is extended by now to a variety of copolymers of PAA with positively or negatively charged monomeric units[82,83] and a corresponding apparatus is available for an easier sample preparation.[84] Recent developments also include gelatin as an inert, extremely low cost and widely applicable hydrogel[85–89] as well as the closely related collagen.[90,91] A list of alignment media for biomacromolecules with a more detailed characterization of the individual alignment properties can be found in refs. 54 and 92. In Table 1, we have summarized aqueous alignment media and common media for other solvents that have already been applied to RDC measurements of small-to-medium-sized organic molecules.

3.3 Alignment media for apolar organic solvents

For typical apolar organic solvents like chloroform, dichloromethane, benzene, dioxane or tetrahydrofurane, a large variety of liquid crystalline alignment media exists, but typically with quite strong lower alignment limit (see, e.g. refs. 6 and 7). Widely used alignment media for small organic molecules are poly(amino acids) like poly-γ-benzyl-L-glutamate (PBLG),[95,96,107,108] poly-γ-ethyl-L-glutamate (PELG),[98] or poly-ε-carbobenzyloxy-L-lysin (PCBLL).[98] Interestingly, the lower limit of alignment and therefore also the minimum achievable alignment strength of such liquid crystals decreases with an increased persistent length of the polymer,[97] which might lead to more weakly aligning media in the near future. A promising liquid crystalline phase close to a phase transition with good alignment properties also for larger molecules appears to be 4-n-pentyl-4′-cyanobiphenyl (PCBP), especially in its perdeuterated form.[94]

A variety of gel-based alignment media without lower limit with respect to the alignment strength exists for the mentioned solvents. The first published gel-based alignment medium suitable for apolar solvents has been polystyrene (PS),[53] which is compatible with all the above-mentioned solvents, can easily be synthesized chemically and is well characterized.[110] The gel is very robust and has been applied to several systems. In a perdeuterated version, referred to as dPS, the gel matrix is of high interest also for solute molecules at low concentrations.[105] Poly(vinyl acetate) (PVAc) is another robust polymer matrix with the solvent range extended to more polar solvents.[103] Poly(dimethylsiloxane) (PDMS), instead, extends the solvent range to more apolar solvents like hexane and is, maybe, the most widely used apolar gel at the moment.[106] Poly(methyl methacrylate) (PMMA) has properties comparable to PS without aromatic contribution.[104]

Table 1 Selected weakly aligning media

Description	Compatible solvents	Remarks	References
Liquid crystals			
Pf1 phage	D_2O	Charged	62,63
Bicelles, micelles	D_2O		56–58
Purple membranes	D_2O		69
Cellulose crystallites	D_2O		65
V_2O_5	D_2O		71
$H_3Sb_3P_2O_{14}$	D_2O		72
C_mE_n/n-alkyl alcohol (Otting phases)	D_2O		60
Cetylpyridinium halogenides/hexanol (Helfrich phases)	D_2O		66,68
$C_{12}E_5$	$DMSO/D_2O$		93
4-n-pentyl-4′-cyanobiphenyl (PCBP)	n.a.	Orienting solvent	94
Poly-γ-benzyl-L-glutamate (PBLG)	$CDCl_3$, CD_2Cl_2, DMF, THF, Dioxane	Chiral	95,96
Poly-γ-benzyl-L-glutamate (PBLG) (high MW)	$CDCl_3$, CD_2Cl_2, DMF, THF, Dioxane	Chiral, weaker alignment	97
Poly-γ-ethyl-L-glutamate (PELG)	$CDCl_3$, CD_2Cl_2	Chiral	98,99
Poly-ε-carbobenzyloxy-L-lysin (PCBLL)	$CDCl_3$, CD_2Cl_2	Chiral	98
Immobilized media	D_2O	LC in gel	73,74,76
DNA nanotubes	D_2O		77
G-tetrad structures	D_2O		78
Stretched gels			
Gelatin	D_2O	Chiral, cheap	85
Collagen	D_2O	Chiral	90
e^--gelatin	D_2O, DMSO	Chiral	100
Poly (acrylamide) (PAA)	D_2O		73,80
Acrylamide copolymers	D_2O	Charged	82,83
Dimethylacrylamide co-polymers (PH-PDMAA)	D_2O, DMSO, DMF	Charged	101
Poly (acrylonitrile) (PAN)	DMSO, DMF		102
Poly (vinyl acetate) (PVAc)	$CDCl_3$, CD_2Cl_2, CD_3OD, CD_3CN, DMSO, DMF, C_6D_6, acetone, THF, EtOAc, dioxane		103

Table 1 *(Continued)*

Description	Compatible solvents	Remarks	References
Poly (methyl methacrylate) (PMMA)	$CDCl_3$, CD_2Cl_2, CD_3CN, acetone, C_6D_6, EtOAc		104
Polystyrene (PS), deuterated PS (dPS)	$CDCl_3$, CD_2Cl_2, THF, C_6D_6, dioxane		53,105
Poly (dimethylsiloxane) (PDMS)	$CDCl_3$, CD_2Cl_2, THF, C_6D_6, dioxane, *n*-hexane	Single NMR signal	106

An important aspect of very weakly aligning media is undesired signals from the medium itself. Liquid crystals like the poly(amino acids) usually provide relatively strong alignment and the proton signals of the alignment medium are strongly broadened due to the multitude of large homonuclear dipolar couplings. The resulting effect on spectra is just a slight increase of the baseline. The situation is different for weakly aligning polymer gels where broad polymer signals and signals from residual monomers and radical starters might be present. In highly concentrated samples it is usually easy to distinguish such signals from solute peaks, and especially in 2D or 3D spectra, the probability of overlap is quite low. However, at low solute concentrations, large signals from alignment media with their broad feet might impose serious problems for RDC detection. One way to circumvent this problem is to pick an alignment medium with very few NMR signals in regions that do not overlap with the NMR spectrum of the molecule of interest. PMMA, for example does not contain any aromatic signals and might be used instead of PS if signals in this region show overlap. An even better gel in this respect is PDMS, which shows a single signal at 0.1 ppm that can be suppressed by water suppression methods.[106] The best choice, of course, is the use of perdeuterated alignment media. So far, only two deuterated alignment media have been reported to our knowledge: the liquid crystalline phase PCBP[94] and the dPS gel, which combines all the positive features of a robust gel-based alignment medium with a practically artifact-free spectrum[105] (Figure 4). The resulting spectra are of very high quality in both cases. Perdeuteration seems to be a general approach worth considering for the alignment of restricted amounts of valuable samples.

3.4 Alignment media for polar organic solvents

In contrast to aqueous and apolar solvents, weakly aligning media for polar organic solvents, especially DMSO, are sparse. Very few liquid crystalline phases are known, one of them being PBLG with DMF as the polar solvent[95,111,112] or poly(ethylene glycol) based phases with DMSO/water mixtures.[93,113] Most
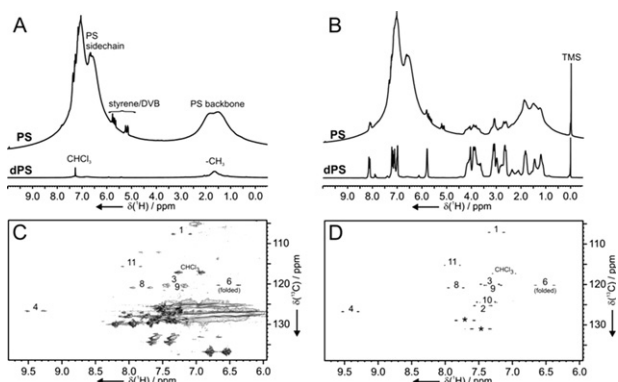
Figure 4 The effect of perdeuteration of the alignment medium on the quality of corresponding spectra. (A) Comparison of 1D spectra of PS and deuterated PS (dPS). (B) Comparison of equivalent samples with ≈ 25 mM strychnine diffused into the gels. (C and D) Aromatic regions of CLIP-HSQC spectra of ≈ 4 mM staurosporine diffused into a PS gel (C) and a dPS gel (D). (Reproduced from ref. 105 with permission from the Royal Chemical Society.)

alignment media for polar organic solvents used today are based on the gel approach: the already mentioned PVAc is a good alignment medium for most polar organic solvents including, for example, methanol, acetone, and acetonitrile, and works reasonably well with DMSO and DMF;[103] the so-called PH-poly (dimethyl acrylamide) (PH-PDMAA) also covers a range of different solvents and can be produced with varying charged groups;[101] finally, poly(acrylonitrile) (PAN) was optimized for the use with DMSO and also works very well with DMF.[102] Especially, PAN with cross-linking via accelerated electrons shows remarkable alignment properties with very few NMR signals from the polymer itself. We are currently working on a perdeuterated PAN gel which then would provide an almost perfect alignment medium for the important solvent DMSO.

3.5 Chiral alignment media

Many of the alignment media presented so far possess stereogenic centres, but only media with a large chiral super structure are referred to as chiral alignment media, since only those are capable of distinguishing enantiomers (see also Section 6.3).

A variety of chiral alignment media for organic solvents is known[98,114–120] with the most widely used and best characterized being the poly(amino acids) PBLG and PCBLL. Both polymers form lyotropic mesophases and possess α-helical structures for which many examples of enantiomeric differentiation have been shown. In addition to chiral poly(amino acids), it was demonstrated that achiral media with chiral cages like cyclodextrines serve as alignment media with the potential of chiral discrimination.[121]

For aqueous solutions, the triple helical gelatin was introduced recently as a chiral hydrogel with excellent performance at an unbeatable low price. Especially, its use with a rubber-based stretching apparatus as described in Section 4.3 promises many interesting applications. Conventional gelatin can be used as a chiral alignment medium in D_2O and $D_2O/DMSO$ mixtures with up to 80% DMSO,[85,87–89] and e^--gelatin (gelatin irradiated and cross-linked with accelerated electrons) allows chiral discrimination with pure DMSO and at temperatures above the melting point of conventional gelatin.[100] A second alignment medium for water-soluble compounds is based on a glucopon/buffered water/n-hexanol lyotropic liquid crystal.[122]

4. SCALING OF ALIGNMENT

To get spectra with the best possible resolution while being able to precisely measure RDCs, it is necessary to carefully adjust the alignment strength. In Figure 5, a resulting spectral region of efrapeptin C, a 15 amino acid peptide, is shown in the very weakly aligning PDMS gel for two different alignment strengths with residual quadrupolar couplings of the solvent $CDCl_3$ of 9 and 35 Hz, respectively. While the spectrum with the lower alignment will certainly allow the straightforward extraction of RDCs, the stronger alignment leads to linewidths of approximately 60 Hz, mainly due to unresolved $^1H,^1H$-RDCs. Clearly in the latter case, extraction of coupling constants becomes much more difficult.

There are various ways of scaling the alignment which will be summarized in the following sections. The direct way, of course, is the variation of the alignment medium itself, which, however, in most cases involves the preparation of a new sample. More sophisticated methods like variable angle sample spinning (VASS) or a specialized stretching device allow the scaling of alignment in a single sample.
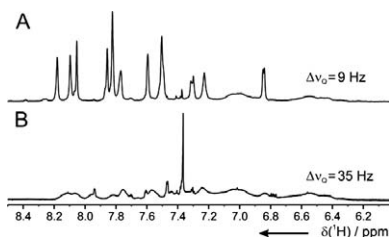
Figure 5 Importance of the right alignment strength. Amide region of the ^1H-1D spectrum of the peptide efrapeptin C in two PDMS/$CDCl_3$ gels with deuterium quadrupolar splittings of the solvent of 9 Hz (A) and 35 Hz (B). The increased alignment strength leads to lines of ≈ 60 Hz of the amide signals which usually prohibits accurate extraction of RDCs.

4.1 Adjusting the alignment medium

In partially aligned samples, the solute molecules typically experience a time-averaged interaction with the alignment medium with only very short contact times at the oriented polymer chains. An increase of the alignment strength in this case can simply be achieved by increasing the number of oriented polymer chains and therefore the number of contacts per time with the solute. Depending on the type of medium, different possibilities exist for achieving this.

Above the first-order phase transition of lyotropic mesophases, their alignment strength can typically be increased by a higher concentration of the solid part of the liquid crystal. A certain percentage of this solid part is automatically oriented by the static magnetic field and the time-averaged alignment is approximately linear with the concentration of the polymer chain or other oriented structures. In Figure 6A, the concentration dependence of the alignment strength is shown for filamentous Pf1 phage with a very small lower limit of alignment. In this way, by just adding phage or by diluting the liquid crystalline phase one can easily adjust the alignment strength.

In liquid crystals for apolar organic solvents, the same rules apply; however, due to the relatively large lower limit of alignment, the variation in alignment strength can only be achieved down to the first-order phase transition of the mesophase. Unfortunately, the lower limit of alignment is quite large already for medium-sized organic molecules, although recent work to some degree allows the reduction of the alignment strength by an increase of the persistence length.[97] For strychnine in PBLG as one of the weakest aligning liquid crystalline phases
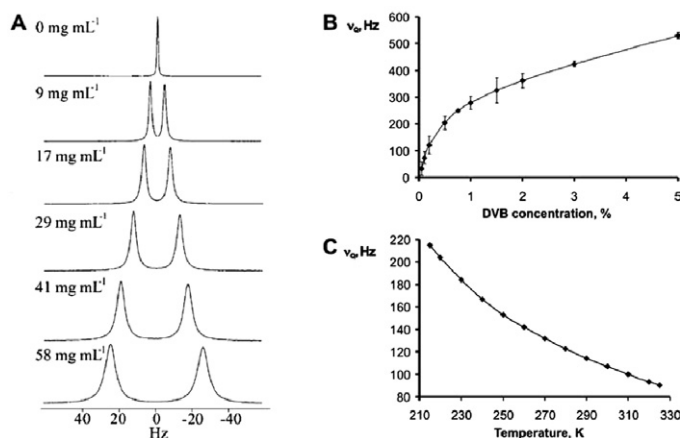
Figure 6 Scaling of alignment. In a lyotropic liquid crystal the alignment is roughly proportional to the concentration of the solid part (A). Stretched gels can be varied by the cross-linker concentration (B) (PS/CDCl$_3$ gel with divinylbenzene (DVB) as cross-linker) or by temperature variation (C). (Reprinted by permission from Macmillan Publisher Ltd. ref. 63, copyright (1998). And reprinted with permission from ref. 110. Copyright 2005 American Chemical Society.)

with CDCl$_3$, for example the ^{1}H-coupled ^{13}C-spectrum shows second-order artifacts for some of the signal,[123] making it almost impossible to accurately extract RDCs for these carbons. In such a case, more sophisticated ways of scaling the alignment must be applied as introduced in the next section.

In an unstretched gel, polymer chains are randomly distributed in all three dimensions and solute molecules, although interacting constantly with the gel matrix, on time-average are not aligned. As soon as the gel is stretched, however, more polymer chains are oriented in the stretching direction than perpendicular to it and a net alignment results.

It is clear that the alignment strength increases with the strain put on the gel. The strain can be increased in many ways. When using the stretching-by-restricted-swelling approach shown in Figure 3B, simply the diameter of the dry stick relative to the inner diameter of the NMR tube can be varied.[110] For a given stick, the usage of 4 mm or even 3 mm tubes instead of the standard 5 mm tubes can be of interest and smaller variations might be achieved by the use of thin wall tubes. When synthesizing the polymer sticks, however, the diameter of the stick can be varied to basically any size and fine-tuning of the alignment is possible. Since the swelling strength of a polymer stick in different solvents can vary dramatically, the stretching, of course, also depends on the solvent used.[110]

Another possibility of scaling the alignment lies in the variation of polymerization parameters of the polymer gel. In a chemical synthesis, the amount of radical starter defines the average length of polymer chains and the amount of cross-linker added to the reaction influences the stiffness of the polymer network.[53,110,103,104] The longer the average chain length of the polymer and the more cross-linked the gel is, the stronger the alignment gets (see Figure 6B for a dependence of the alignment strength on the amount of cross-linker used). The same rule applies for polymer gels cross-linked via accelerated electrons, where in turn the irradiation dose defines the amount of cross-linking in the gel.[106] Finally, within the limits of the melting and boiling point of the solvent used, the alignment can also be varied by a change of temperature. For a PS/CDCl$_3$ gel, for example a factor of 2.4 in alignment strength can be achieved over the accessible temperature range[106,110] (Figure 6C).

The main disadvantage of changing the polymer gel for a given sample in order to adjust the alignment strength is the necessity to prepare a new sample with the relevant swelling and diffusion times. Methods to vary the alignment in a single sample as discussed in the next two sections are therefore highly desirable.

4.2 Variable angle sample spinning

Dipolar couplings were introduced in Equation (1) of Section 2.1 with the averaging over all orientations. Later on the averaging was included in the alignment tensor assuming that the average director of the alignment medium is parallel to the magnetic field. A more detailed description introducing a possible

deviation of the average director relative to the magnetic field by the angle Θ_{dB} leads to the expression

$$D_{IS} = -\frac{\hbar\gamma_I\gamma_S\mu_0}{16\pi^2}\left(\frac{3}{2}\cos^2\boldsymbol{\Theta}_{dB} - \frac{1}{2}\right)\left\langle\frac{1}{r_{IS}^3}(3\cos^2\boldsymbol{\Theta}_{md} - 1)\right\rangle \tag{7}$$

with Θ_{md} now defined as the angle between the internuclear vector within a molecule and the average director of the alignment medium. The equation implies that RDCs can generally be scaled if the director can be varied independently of the static magnetic field, which has already been derived by Saupe in his original theory of NMR in liquid crystalline phases.[22]

In contrast to solid-state NMR where a sample is simply rotated to change the orientation of a crystal relative to the magnetic field, the average director of a nematic liquid crystalline phase will always orient parallel or perpendicular to the magnetic field, depending on the sign of the anisotropy of the magnetic susceptibility $\Delta\chi = \chi_{||}-\chi_\perp$ of the particular liquid crystal.[8] However, the orientation along the magnetic field takes place with a certain time constant which depends on the rotational viscosity coefficient γ_1 as defined in refs. 124–126 and the square of the magnetic field B_0^2. As originally suggested theoretically by Hornreich[127] and later on verified in EPR[128] and NMR,[129–131] sample spinning above a certain threshold frequency $\omega_{th} = \Delta\chi B_0^2/\sqrt{3}\gamma_1$ can then be used to align the average director of a nematic phase with positive magnetic susceptibility anisotropy along the rotational axis as long as the angle Θ_{dB} of the rotational axis relative to the static magnetic field fulfills the condition $\Theta_{dB} < 54.7°$ (Figure 7A). For angles larger than the magic angle, the average director aligns perpendicular to the magnetic field which leads to strongly modulated spectra, and at the magic angle itself, the orientation of the director is not defined.[130] For nematic phases with negative magnetic susceptibility anisotropy, a stable rotation axis is only obtained for $\Theta_{dB} > 54.7°$.[130]

Since most liquid crystalline phases used today are lyotropic mesophases with a relatively small magnetic susceptibility anisotropy, it should be noted that the orientation of the director is also influenced by the inertial torque when
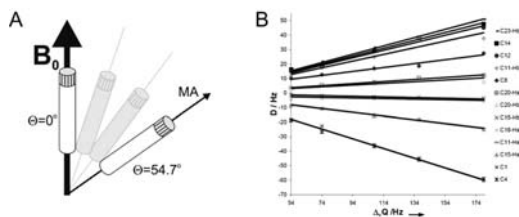
Figure 7 With variable angle sample spinning (VASS) it is possible to scale the alignment by $3\cos^2\Theta_{dB}-1$ for angles up to 54° for liquid crystals with positive $\Delta\chi$ (A). A linear scaling of RDCs with the measured quadrupolar splitting of the solvent is observed (here: VASS-NMR on strychnine in PBLG/CDCl$_3$ at various angles). (Experimental data reproduced from ref. 132 with permission from Wiley-VCH Verlag GmbH & Co. KGaA (Copyright).)

spinning fast.[133,134] The effect leads to an upper limit for the sample spinning frequency under which stable conditions for director alignment are obtained. It is generally the case that the window of rotational frequencies is the smaller the lower the magnetic susceptibility anisotropy $\Delta\chi$ is.

With the according probe head, VASS[134] allows the scaling of alignment and therefore the scaling of all anisotropic interaction close to 0, as is demonstrated for RDCs measured on strychnine in PBLG/CDCl$_3$ in Figure 7B. Many applications have been reported using the approach (see, e.g. refs. 130, 135–142) and many more can be expected in the future. However, the method is, of course, limited by the necessary hardware, as not everybody has access to a VASS probe head. The kind of probe head is usually designed for solid-state applications so that a lock channel might be missing and the shimming at an angle to the magnetic field is never trivial. Better suited are HR-MAS-type probe heads with lock and rotors with a spherical volume for an optimal shim.

Yet unpublished data[143] show that the change of the average director of the alignment medium can also be applied to gel-based alignment media. In this case, the director is given by the mechanical stretching and sample spinning is not necessary. Also, variable angle (VA) NMR with stretched gels can be used for the whole range of Θ_{dB} angles from $0°$ to $90°$, including the magic angle for complete removal of anisotropic interactions.

4.3 Gel stretching apparatus

Several devices have been developed to stretch gels. One of the first stretching devices for biomolecular NMR is the one introduced by Chou et al.[84] which squeezes a PAA gel into an open-cut NMR tube via a funnel. However, the device just helps to prepare the sample but is not able to adjust the alignment strength. The method introduced by Ishii and Tycko[80,81] uses a Shigemi plunger to compress the gel in an NMR tube and, depending on the pressure put on the plunger, different alignment strengths can be obtained. Apparently, the approach has been applied to apolar gels in the meantime with good results (R. Gil, personal communication). A drawback of the method can be the decreased T_2 relaxation times observed for proteins. A similar approach based on the strong swelling capacity of charged hydrogels uses the Shigemi plunger simply as a restriction for gel swelling.[83] The alignment strength in this case can be increased by slightly loosening the plunger and letting the hydrogel swell stronger with an increased effective stretching. However, this approach is a one-way street, since a swollen gel can hardly be pushed back to a smaller size without destruction.

A totally different stretching apparatus was introduced by Kuchel et al.[86] by using a rubber tube to stretch a gel inside it. A slightly modified version of the apparatus[89] is shown in Figure 8. A silicone rubber tube containing the gel is fixed inside an open-cut NMR tube by a teflon plug at the bottom. After stretching the gel to the desired strength by pulling the rubber tube, the position of the latter one is fixed by a corresponding screwing device at the top of the NMR tube. Since the gel is stretched homogeneously inside the rubber tube, no equilibration time is needed and the shimming results are generally good with
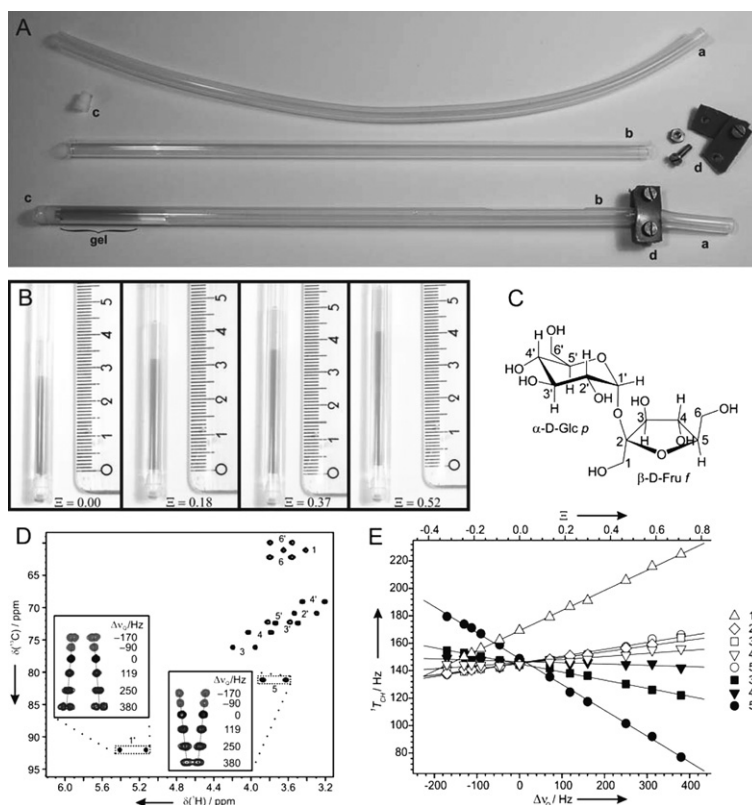
Figure 8 Stretching apparatus for the variable scaling of alignment in a single gel. (A) The components of the apparatus: (a) flexible rubber tube, (b) open-cut NMR tube, (c) teflon plug for the bottom, (d) fixation device for the top of the apparatus. In the readily prepared gel sample, the gel is inside the rubber tube. (B) The gel at different extension factors Ξ for different alignment strengths. (D) CLIP-HSQC of sucrose (C) in gelatin/D_2O (black contours) with inlets showing two cross-peaks at various states of stretching (dark grey) and compression (light grey) with corresponding quadrupolar splittings of the deuterated solvent. (E) $^1T_{CH}$ couplings of sucrose at different extension factors result in an linear relation to the quadrupolar splitting of D_2O with the slope proportional to RDCs. (Reproduced from ref. 89.) (See Plate 1 in Color Plate Section)

potential linewidths below 1 Hz in our hands. Also no special NMR equipment is needed for the apparatus. The alignment of the gel increases approximately linear with the so-called extension factor (Ξ = (stretched gel length/relaxed gel length)−1) as can be nicely seen in Figure 8B–E for sucrose in gelatin at various stretchings.

With gelatin as the alignment medium, the preparation is very simple and in addition the gel in this case can also be compressed by first stretching the gel, relaxing the gel via heating above the melting temperature and releasing the cooled rubber tube again (Figure 8D and E;[87–89]). For covalently cross-linked gels, the apparatus is limited to gel stretching.

The stretching apparatus using a silicone rubber tube is limited to polar solvents. We tested several gels including poly(acrylonitrile) for DMSO with good results.[89] However, silicone allows humidity to diffuse into the gel which is usually unwanted and might alter the swelling properties of the alignment medium. A stretching apparatus based on perfluorinated elastomers is currently developed in our lab in collaboration with DuPont Perfomance Elastomers which is impermeable for humidity and can also be used for apolar solvents.

5. PULSE SEQUENCES

In weakly aligned samples, RDCs simply contribute to the splitting of scalar couplings. Therefore, the difference between coupling constants measured in an isotropic sample and the corresponding partially aligned sample directly results in the desired RDCs (see Figure 9). In principle, most experiments for measuring scalar couplings can be used this way to extract dipolar couplings. In practice, however, the required precision for measuring RDCs is usually higher than for scalar couplings and the sign information of the measured couplings is needed. As a result, existing methods have been strongly revised and extended during the last decade and further techniques can be expected in the future. Since we focus on organic molecules which are usually only available at natural isotope abundance, we neglect the multitude of experiments specifically designed for labelled macromolecules and limit ourselves to the basic methods applicable in this case. The set of pulse sequences shown in Figure 10 corresponds to the
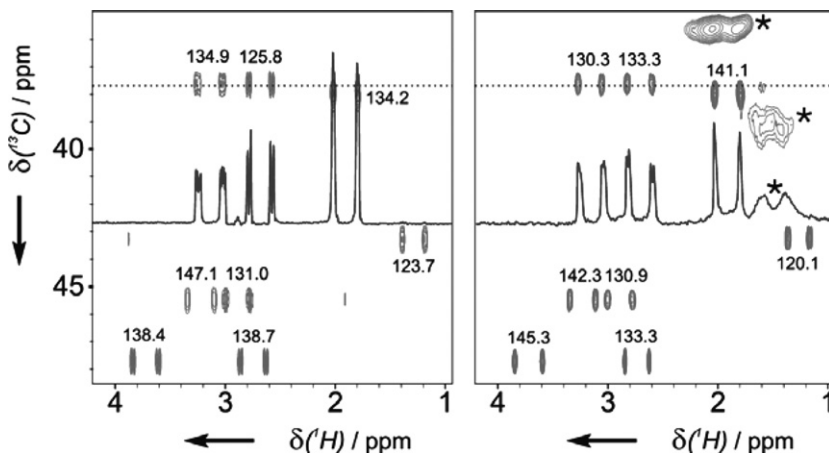
Figure 9 Example for measuring RDCs. t_2-coupled HSQC spectra of strychnine result in cross-peaks that are split by the $^1J_{CH}$ coupling in the conventional CDCl$_3$ sample (left) and by $^1J_{CH}+2D_{CH}$ in the sample aligned by a PS/CDCl$_3$ gel (right). A slice at 37.8 ppm is shown to give an impression of spectral quality; cross-peaks originating from the alignment medium are marked with an asterisk. (Reproduced from ref. 53 with permission from Wiley-VCH Verlag GmbH & Co. KGaA (Copyright).)
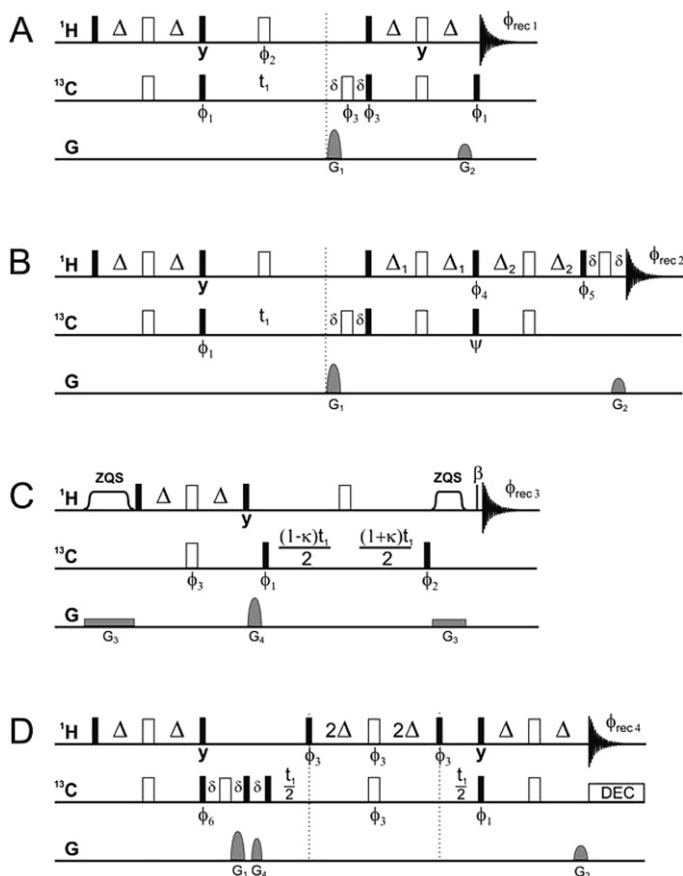
Figure 10 Pulse sequences used frequently in our laboratory. (A) The CLIP-HSQC for the measurement of $^1T_{CH}$ couplings with pure absorptive multiplets (see also Fig. 11).[144] (B) HSQC-IP/AP for measurement of $^1T_{CH}$ couplings with samples at low concentrations. By acquiring spectra with the phase $\Psi = x$ and $\Psi = -x$, the corresponding added/subtracted spectra can also be used to extract $^2T_{HH}$ couplings of CH_2 groups (see ref. 145 for details). (C) The P.E.-HSQC is routinely used in our laboratory to extract $^2T_{HH}$ and $^1T_{CH}$ couplings in a single experiment. It results in an E.COSY-type pattern with the two couplings in the direct dimension and $\kappa \cdot {}^1T_{CH}$ in the indirect dimension.[146] (D) The J-BIRD^{d,x}-HSQC with heteronuclear J-evolution in the indirect dimension is designed for maximum resolution and is especially useful for the distinction of enantiomers (see also Fig. 15B).[85] Filled and open bars indicate 90° and 180° pulses unless indicated otherwise. The delays δ are determined by the duration of applied gradients, $\Delta = 1/(2^1T_{CH})$, and the corresponding delay Δ_1 and Δ_2 have to be adjusted to the expected spin systems according to ref. 145. The β-pulse refers to a short pulse with a flip angle of typically 30°–40°. Phases are $\phi_1 = \phi_{rec2} = x, -x$; $\phi_2 = 4(x), 4(-x)$; $\phi_3 = 2(x), 2(-x)$; $\phi_6 = 4(y), 4(-y)$; $\phi_{rec1} = -x, x, x, -x$; $\phi_{rec2} = \phi_{rec4} = x, -x, x, -x, -x, x, -x, x$; HSQC-IP and HSQC-AP experiments are obtained for $(\phi_6 = y, \phi_7 = x)$ and $(\phi_6 = x, \phi_7 = y)$, respectively. Gradients must fulfill the ratios $G_1:G_2 = 40.1:10$ for carbon as the heteronucleus and G_4 as purge gradient should not be a multiple of G_1 or G_2. Gradient G_3 together with adiabatic inversion pulses indicated by ZQS have to be adjusted for the Keeler z-filter scheme as described in ref. 147.

standard experiments used in our lab to record spectra for the extraction of heteronuclear one-bond couplings and homonuclear couplings between geminal protons.

5.1 One-bond RDCs

The most easily measured RDCs are along one-bond heteronuclear couplings like $^1D_{CH}$ or $^1D_{NH}$ as the difference from $^1T_{CH} = {}^1J_{CH} + 2\,{}^1D_{CH}$ (and $^1T_{NH} = {}^1J_{NH} + 2\,{}^1D_{NH}$, respectively) measured in the partially aligned sample and the corresponding scalar couplings $^1J_{CH}$ ($^1J_{NH}$) of the isotropic sample. If the alignment strength is adjusted correctly, RDCs are significantly smaller than corresponding scalar couplings of known sign, and sign-sensitive measurement of RDCs is most easily achieved. Since the distance between directly bound nuclei is usually well known and fixed, RDCs can also directly be translated into relative angular information. Regarding the actual pulse sequences used for coupling measurements, conventional heteronuclear multiple-quantum correlation (HMQC) or heteronuclear single-quantum correlation (HSQC) experiments can be recorded without heteronuclear decoupling during acquisition. However, if transfer delays are not well matched with the $^1T_{CH}$ ($^1T_{NH}$) couplings, dispersive antiphase contributions to the signals are obtained, for which the individual multiplet components have to be phased separately to obtain correct coupling constants.[148] An elegant way to circumvent individual phasing of the multiplet components is achieved by the CLIP-HSQC which removes dispersive antiphase components prior to detection (Figure 11). If sensitivity is not the primary problem (i.e. NMR sample concentrations of approximately 5 mM or higher), we therefore recommend the experiment for spectra with outstanding overall quality[144] (Figure 10A), which is even improved when using recently optimized BEBOP[149–151] excitation and BIBOP[151] inversion pulses and corresponding universal rotation pulses using the construction scheme described in ref. 152. For overlap of α and β components of multiplets, the CLAP-HSQC in a kind of IPAP approach provides additional resolution.[144] A second set of experiments for samples at low concentrations, where the most sensitive approach for coupling measurement at good resolution is needed, is
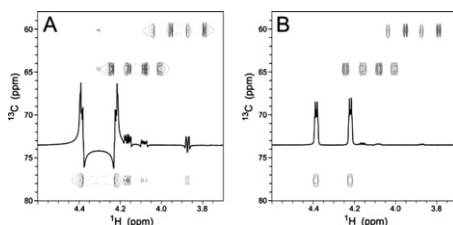
Figure 11 Spectral region of a conventional t_2-coupled HSQC (A) and a CLIP-HSQC spectrum (B) of strychnine in CDCl$_3$ for a mismatched delay for heteronuclear coherence transfer. The conventional HSQC has strong dispersive antiphase components and contributions from long-range connectivities which are practically absent in the CLIP-HSQC.[144]

given by the HSQC-IP/AP sequences reported in ref. 145 (Figure 10B). Phases have to be corrected individually in this case and obtained couplings might not be as accurate as for the CLIP-HSQC, but for low signal-to-noise ratios the pulse sequences represent a very good compromise.

Generally, scalar and dipolar couplings can also be measured with the coupling evolution in the indirect dimension. This method is usually preferred for measuring RDCs in biomacromolecules,[59] since the linewidth of the heteronuclei in the indirect dimension is much smaller than the proton linewidth in the directly detected dimension. However, for small molecules with the much wider chemical shift range, the acquisition of a ridiculous number of t_1 increments or multiple folding of spectra would be required in order to obtain the desired spectral resolution. Spectra for recording $^1T_{CH}$ couplings in the indirect dimension are described in ref. 17 and an experiment optimized for CH_2 groups using an HMQC-type experiment with coupling evolution in the indirect dimension is given in ref. 153. Interestingly, a comparison of RDCs obtained in the indirect and direct dimension for a sugar led to deviations of up to 5 Hz.[154] The origin of the deviating measurements is yet unclear (cross-correlated relaxation in the carbon dimension or potential strong coupling artefacts for the directly detected dimension might play a crucial role), and hopefully future analyses will show if t_1 or t_2 evolved couplings will be more accurate.

In all the experiments mentioned so far, signal widths are generally broadened by either heteronuclear long-range couplings or passive homonuclear couplings. The situation can significantly be improved by selective decoupling using BIRD filter elements.[155,156] The approach has been applied in several versions for measuring RDCs using $(J+D)$-evolution periods with a central BIRD^{d,X}-filter.[85,157–159] In Figure 10D, an experiment with $(J+D)$ evolution in the indirect dimension with the acquisition scheme taken from refs. 160 and 161 optimized for resolution in the coupling dimension is shown.[85]

5.2 RDCs between geminal protons

A second class of easily measured RDCs with fixed geometry is along homonuclear $^2J_{HH}$ scalar couplings found in methylene and methyl groups. A number of sophisticated experiments have been developed for the sign-sensitive measurement of these couplings: the most easily applied experiment is probably the P.E.HSQC[146] (Figure 10C) which we recommend in cases where overlap is not a problem; other techniques resulting in further reduced multiplet structures require a couple or more spectra to be acquired and combined, but potentially lead to spectra with better resolved signals.[145,162,163] In Figure 10B, the extension of the HSQC-IP/AP approach to the closely related HSQC-IP(x)/IP($-x$) and HSQC-AP(x)/AP($-x$) allows the sign-sensitive measurement of $^2T_{HH}$ couplings in separated subspectra.[145] A general problem with the extraction of homonuclear two-bond couplings is frequently observed as second-order artefacts which often prohibit a simple extraction of coupling constants in all of the available experiments.

5.3 Others

Especially in small molecules with few protons available, the additional measurement of other RDCs is important for obtaining sufficient structural information. If the amount of material is nearly unlimited and solubility is no problem, INADEQUATE spectra have been shown to provide RDCs along $^1J_{CC}$[164] and even $^2J_{CC}$ couplings.[165] Such carbon–carbon RDCs are one order of magnitude smaller than the corresponding proton–carbon or proton–proton RDCs, which should be taken into account. The same is the case for long-range proton–carbon RDCs, which are very difficult to measure with the necessary accuracy. Publications that review state-of-the-art methods for their measurement can be found, for example, in refs. 166 and 167.

The extraction of homonuclear proton–proton RDCs is difficult because of the multitude of long-range RDCs contributing to the proton multiplet. Sign-sensitive measurement of RDCs can be achieved using E.COSY-type experiments when multiplets are not too strongly broadened.[168–170] Also the measurement of 2D multi-quantum-filtered spectra has been proposed lately in a series of publications.[171–176] Other methods that give only the magnitude but not the sign of the coupling constants are based on integration of cross-peaks originating from constant time COSY experiments[177,178] or the conventional COSY[179] with the typical error in integration. An approach with accurate coupling measurement is the SIAM-TOCSY[180,181] which involves the measurement of inphase and antiphase multiplets and subsequent extraction of couplings using the Keeler–Titman fitting procedure.[182] Methods using heteronuclear correlation for the measurement of $^1H,^1H$ couplings are, for example based on spin-state-selective excitation[183] or XLOC type experiments.[184] The methods allow extraction of coupling constants with a much higher resolution due to the heteronucleus, but the implementation with many planar mixing periods is difficult to achieve equally for all spin systems because of the inherent variation of heteronuclear one-bond couplings in partially oriented samples. Finally, it must be noted that $^1H,^1H$-RDCs other than those between geminal protons are potentially difficult to interpret, since the interproton distance is strongly modulated by the inherent flexibility of molecules.

RDCs to other NMR-active nuclei like ^{19}F or ^{31}P in principle can be measured with similar techniques as the corresponding heteronuclear $^1H,^{13}C$-RDCs. Sequences using the special properties of ^{19}F of geminal HF groups for the measurement of $^1H,^{19}F$ long-range RDCs can be found in refs. 185 and 186. Experiments designed for the measurement of long-range $^1H,^{31}P$-RDCs are reported in refs. 187–189.

The inclusion of average Hamiltonian theory derived pulse sequence building blocks specifically designed for the measurement of RDCs is highly desirable. The homonuclear dipolar decoupling sequences used in ref. 190 lead to the less complex multiplet structures observed in isotropic samples with the chemical shift resolution reduced by a factor of $\approx 2–3$, depending on the multiple pulse

sequence used. However, additional hardware might be necessary for the implementation of such building blocks and the rf-power applied to the sample in this case is quiet high.

Other sequences based on average Hamiltonian theory involve the efficient or suppressed coherence transfer due to RDCs in TOCSY-type experiments. As has been shown for a number of conventional TOCSY multiple pulse sequences, resulting coherence transfer can vary significantly depending on the sequence used[181,191–194] and even coherence transfer via spins without effective multiplet splitting can be observed.[192] The underlying change in transfer is due to different effective mixing conditions, varying from isotropic[195–197] to cylindrical[198,199] and fully dipolar[200] coupling conditions. Especially, the MOCCA-XY16 sequence with most effective transfer via RDCs[201] and inherently optimal relaxation properties[202] provides interesting possibilities for the efficient distribution of magnetization.[105,185,186,203] The *J*-ONLY-TOCSY based on the Jester-XY16 multiple pulse sequence,[203] on the other hand, provides TOCSY transfer only via *J*-couplings even in the presence of RDCs. It is a very valuable tool in cases where the assignment cannot be deduced directly from other experiments.[105,203]

6. APPLICATIONS

6.1 Conformational studies

Many applications have been reported in the field of biomolecular NMR spectroscopy which use RDCs for the refinement of three-dimensional structures. The approach is quite powerful and can also be applied to smaller molecules whenever the conformation of a molecule is important, as for example in the case of rational drug design. Traditionally, NMR in liquid crystals is applied on a multitude of small organic compounds to obtain their fully characterized structure. Most examples are measured on all kinds of aromatic systems as reported in refs. 204–212; other recent examples deal with substituted alkanes,[213–215] aldehydes[216,217] or bridged systems like norbornadiene.[218] In general, these very detailed studies can be applied to molecules with up to ≈12 protons.

Concerning applications to biologically interesting molecules with usually more than 12 protons, by now a good number of applications are reported for sugars in aqueous solution[219–229] (see also a listing of most applications of RDCs measured in weakly aligned samples in Table 2). Especially, the dynamics of the relatively flexible molecules are of interest.[33–37,231,252] As a second class of molecules, various peptides have been structurally investigated or refined by RDCs: a small number of short peptides,[232,236] the highly defined average conformation of relatively large cyclic peptides[230,234] and the conformation of peptides with unnatural amino acids[235,253] were examined using RDCs measured in organic solvents. Finally, the conformations of some synthetic[113] and natural products[105,153,242] have been examined in detail with RDCs. The resulting data are quite impressive, since for the first time RDCs allow for correlations of distant

Table 2 Selected RDC applications using weak alignment media

Compound	Alignment medium	Year	Refs.
Conformation			
Oligosaccharides	Bicelles (D_2O)	2000	219
Pentasaccharide	Bicelles (D_2O)	2000	220
Heptasaccharide	Bicelles (D_2O)	2001	221
Sucrose and raffinose	Bicelles (D_2O)	2001	222
Tri- and tetrasaccharides	Bicelles (D_2O)	2002	223
Sucrose	Bicelles (D_2O)	2002	225
Trisaccharides	Bicelles (D_2O)	2002	224
Lactose	Helfrich phase (D_2O)	2003	227
Hexa-and tetrasaccharides	Bicelles (D_2O)	2003	226
Methyl α-D-xylopyranoside	Otting phase (D_2O)	2004	228
Macrocyclic arenes	PBLG ($CDCl_3$)	2004	113
Cyclosporin A	PDMS ($CDCl_3$)	2005	230
Lactose	Otting phase (D_2O); Helfrich phase (D_2O)	2005	231
Tripeptide	Helfrich phase (D_2O)	2005	232
Tetrasaccharide	Otting phase (D_2O)	2005	233
Hormaomycin	PH-PDMAA (DMSO)	2006	234
Disaccharide	Bicelles (D_2O)	2006	36
Tetrasaccharide	Pf1 phage (D_2O)	2008	229
Cylindramide	PAN (DMSO)	2008	153
α-, β- and γ- cyclodextrins	V_2O_5 (D_2O)	2008	37
Tripeptides	PDMS ($CDCl_3$)	2009	235
Di- and tetrapeptides	Otting phase (D_2O)	2009	236
Piperidine base	PBLG (high MW) ($CDCl_3$)	2009	237
Phenylmenthol	PELG ($CDCl_3$)	2009	238
Prochiral assignment			
Strychnine	PBLG ($CDCl_3$)	2003	123
	PELG ($CDCl_3$)	2004	99
	PS ($CDCl_3$)	2004	53
Sphaeropsidin A	PVAc (DMSO)	2005	103
Relative configuration			
4,6-O-ethylidene-D-glucopyranose	Pf1 phage (D_2O)	2003	148
Dihydropyridone	PBLG ($CDCl_3$)	2003	239
Sodium cholate	PAA (D_2O)	2003	240
Spiroindene	PDMS ($CDCl_3$)	2004	106
Five-membered ring	Pf1 phage, bicelles (D_2O)	2004	241
Methylene-butyrolactone	Otting phase (D_2O)	2006	38
Sagittamide A	PH-PDMAA, PAN (DMSO)	2007	39
Sucro-neolambertellin	PH-PDMAA, PAN (DMSO)	2008	40
Ludartin	PMMA ($CDCl_3$)	2008	104

Table 2 *(Continued)*

Compound	Alignment medium	Year	Refs.
Archazolide A	PH-PDMAA (DMSO)	2008	242
Staurosporine	Deuterated PS (CDCl$_3$)	2008	105
Dextramorphan	PS (CDCl$_3$)	2009	243
Enantiomeric discrimination			
Dibromopropane, trichlorobutyric-β-lactone	PBLG (CDCl$_3$)	2002	244
Phosphine oxides/boranes	PBLG, PCBLL (CDCl$_3$)	2003	245
Chloropropanoic acid	PBLG (CDCl$_3$)	2004	246
Arene chromium carbonyl complexes	PBLG (CDCl$_3$, DMF)	2005	247
Alanine	Gelatin (D$_2$O)	2005	85
	Collagen (D$_2$O)	2006	90
Propargylic fluorides	PBLG (CD$_2$Cl$_2$)	2006	248
Propylene carbonate/oxide	PBLG (CDCl$_3$)	2006	142
Acyclic phosphonium salts	PBLG (DMF)	2006	249
Ibuprofen	PBLG (CDCl$_3$)	2007	250
Sign of *J*-couplings			
Five-membered ring	Pf1 phage, bicelles (D$_2$O)	2004	251
Dipolar resolution			
J-BIRD^{d,X}-HSQC	Pf1 phage (D$_2$O)	2007	159
Exchange transferred RDCs			
Transducin	Purple membranes	2000	70

structural features which make the corresponding overall average structures more reliable. A very instructive example for the influence of RDCs on the overall structure is shown in Figure 12 for cyclosporin A measured in CDCl$_3$ and a stretched PDMS/CDCl$_3$ gel:[230] the RDC-refined average structure has a bend which complies with all NOE restrains. The crystal structure and the conventionally NOE-derived structure are much flatter in comparison and do not fulfill the experimental RDCs.

6.2 Prochiral assignment and relative configuration

The assignment of prochiral protons and the determination of the relative configuration within a small organic compound are everyday tasks in a chemical laboratory. In most cases, either a crystal structure or classical NMR parameters like *J*-couplings and NOEs lead to an unambiguous identification, but many problems still cannot be solved by these means. Especially, far apart stereogenic centres and five-membered rings are notoriously difficult in this respect. RDCs already helped in a number of cases to solve such problems, usually in combination with *J*-couplings and NOEs.
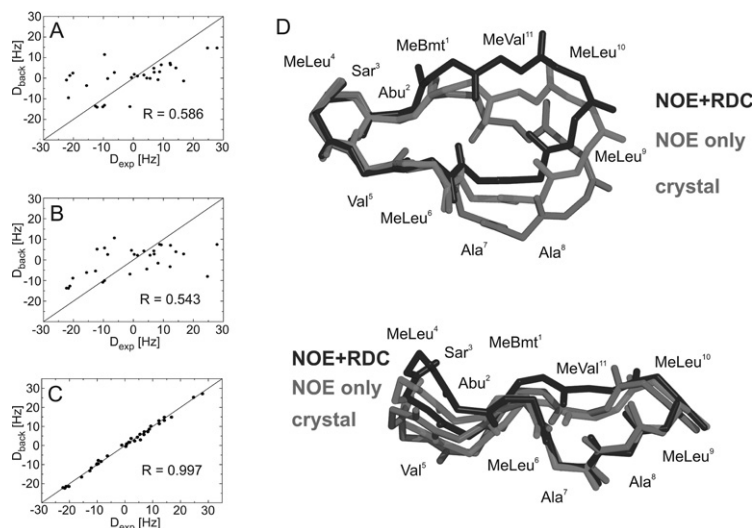
Figure 12 Comparison of experimentally determined RDCs and RDCs back-calculated from the crystal structure (A), an NOE-derived structural model (B) and the (NOE+RDC)-refined structure (C) of cyclosporin A. (D) Evaluation of the resulting models for the average structures show a flat geometry in the crystal, an already bent backbone for the structure based only on NOE data, and a further twist in the RDC-refined backbone, which does not violate any NOE data. (Reproduced from ref. 230 with permission from Wiley-VCH Verlag GmbH & Co. KGaA (Copyright).) (See Plate 2 in Color Plate Section)
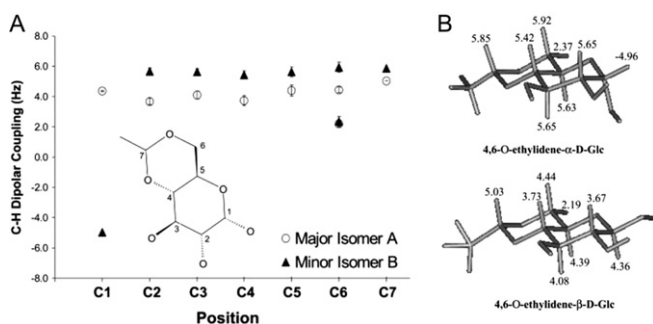
Figure 13 Distinction of the anomeric centre of 4,6-O-ethylidene-D-glucose using RDCs. (A) α and β isomers are easily distinguished from RDCs at position C1. (B) The two anomeric forms with corresponding RDCs. (Adapted with permission from ref. 148. Copyright 2003 American Chemical Society.)

The basic principle can be understood easily by looking at the distinction of axial versus equatorial protons in a six-membered ring: since all axial ^{1}H,^{13}C-vectors are parallel or antiparallel, they also have the same average angle to the static magnetic field and very similar resulting RDCs. All protons with ^{1}H,^{13}C-RDCs significantly different from the RDCs of an axial proton therefore must be equatorial[148] (Figure 13).

A more general way for assigning prochiral protons or determining the relative configuration of a molecule from RDCs involves the concept of the alignment tensor as described in Section 2.2. If more than five independent RDCs per rigid molecular structure are known, its alignment tensor can be derived and additional RDCs can directly be translated into angular and/or distance information. Example molecules for which the assignment of diastereotopic protons has been specifically reported are six-membered rings,[148,238] strychnine,[123] dextramorphan[243] and the five-membered ring within sphaeropsidin A,[103] which could not be obtained otherwise because of the inherent uncertainty in such a system.

Closely related to the prochiral assignment is the determination of relative configuration in organic compounds. Using SVD for fitting experimental data to a back-calculated alignment tensor can be done in two effective ways:[99] one is to simply fit all RDCs to the potential compounds with all permutations of prochiral and chiral centres; the other one is to only use RDCs of unambiguous internuclear vectors for the fit and predict the RDCs of prochiral and chiral centres by the fitted alignment tensor. Relative configurations using one of these approaches have been obtained for many natural products like a dihydropyridone derivative,[239] a spiroindene (Figure 14A),[106] sodium cholate as a steroid,[240] ludartin,[104] staurosporine[105] and archazolide A;[242] other applications include the very difficult to get relative configuration of five-membered rings.[241] The relative configurations of flexible compounds have been reported for the five-membered ring of a lactone (Figure 14B),[38] the glycoside sucro-neolambertillin[40] and the extended chain of sagittamide A.[39] While the five-membered ring was solved by fitting RDCs, NOEs and J-couplings to minimum energy structures obtained from *ab initio* calculations, the latter two flexible molecules were fitted using an
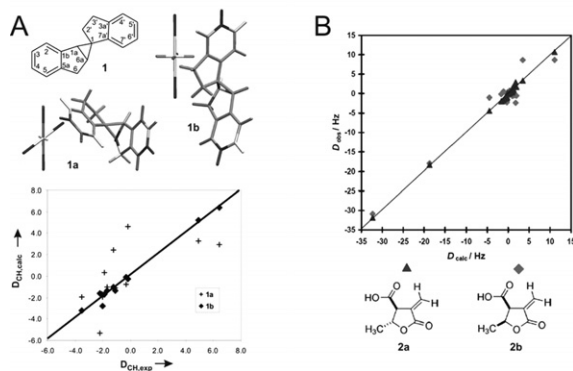
Figure 14 Examples for the determination of relative configuration. (A) The spiroindene **1** in principle can adopt two configurations **1a** and **1b**. The two configurations are shown with the principle axes of the fitted alignment tensors (see ref. 106 for colour coding). By plotting experimental versus back-calculated RDCs, clearly **1b** is identified as the correct configuration. (B) Similar procedure for the potential lactones **2a** and **2b**, respectively, with the additional difficulty of the flexibility in the five-membered ring. (Reprinted with permission from ref. 106. Copyright 2004 American Chemical Society. And reproduced from ref. 17 with permission from Wiley-VCH Verlag GMBH & Co. KGaA (Copyright).) (See Plate 3 in Color Plate Section)

ensemble of structures compatible with NOE and *J*-coupling data against a single alignment tensor, making the assumption that the alignment tensor would not change significantly for the conformations within the ensemble. Although the assumption is crude and might not be applicable in many cases, the apparent success of the method justifies it in retrospective for the reported molecules. A method based on molecular dynamics simulations using the implementation of RDCs in GROMACS has so far only been applied for the rigid molecule staurosporine,[105] but it certainly has the potential for applications on more flexible compounds.

6.3 Distinction of enantiomers and absolute configuration

The average orientation of two enantiomers differs if they are dissolved in a chiral alignment medium. As has been shown very nicely by the group of scientists around Jacques Courtieu in a long series of publications (see, e.g. refs. 96, 108, 109, 119, 254–256), this effect can be used to measure enantiomeric excess even in cases where chiral HPLC could not separate the compounds. Molecules with axial chirality,[257] planar chirality,[247] threefold symmetries,[258] rotational isomerism,[259] invertomers,[260] unlike/like stereoisomers,[261] enantiotopic differentiation in molecules with C_s and C_{2v} symmetry,[262] secondary alcohols,[263] fluorinated alkanes[215] and even chiral alkanes[264] have been successfully studied. Although mostly the quadrupolar splitting of deuterium has been used for enantiomeric distinction in the liquid crystalline phase PBLG,[108,265] residual chemical shift anisotropies and RDCs[85,109,245,266–268] can also be used. Figure 15 shows two examples for the distinction of enantiomers: a mixture of two enantiomeric lactones in PBLG/CDCl$_3$ using ^{1}H,^{1}H-RDCs and L-alanine/D-alanine in gelatin/D$_2$O using ^{1}H,^{13}C-RDCs measured with the sequence shown in Figure 10D.
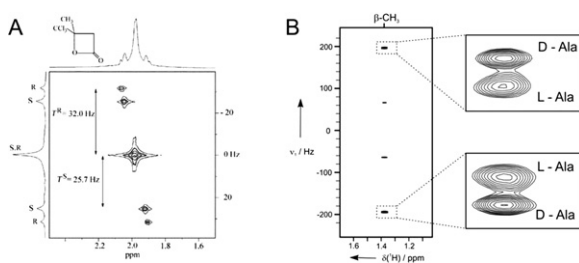
Figure 15 Distinction of enantiomers. (A) The distinction of enantiomers in a sample of 3-methyl-4,4,4-trichlorobutyric-β-lactone 21.5% enriched with the *S* enantiomer and dissolved in PBLG/CDCl$_3$ by ^{1}H-^{1}H-RDCs between the methyl protons using a SERF 2D experiment. (B) Separation of enantiomers using a two-dimensional *J*-^{1}H,^{13}C-BIRD^{d,x}-HSQC (see Figure 10D) recorded for a mixture of L-Ala/D-Ala (1.2:1) in gelatin. Determination of enantiomeric excess is possible by integration. (Reprinted from ref. 244 Copyright 2002, with permission from Elsevier and reproduced from ref. 85 with permission from Wiley-VCH Verlag GMBH & Co. KGaA (Copyright).)

If enantiomers can be distinguished by RDCs, the determination of absolute chirality should also be possible in principle. A general approach for this task has not yet been derived, but two examples using the conformational difference of enantiomers bound to the chiral alignment medium[250] and the comparison of experimental multiplet patterns with similar compounds of known chirality[269] were successful in determining the correct absolute chirality.

6.4 Other applications

RDCs can be used not only for structure determination, but also for the determination of isotropic NMR quantities. A very interesting example is demonstrated in ref. 251, where the authors used RDCs to determine the sign of underlying scalar couplings. Starting from back-calculated RDCs from the known structure and the measurement of corresponding couplings in the isotropic and partially aligned phase, the sign of six different types of *J*-couplings could be obtained simultaneously in a fluorinated compound.

Usually, RDCs result in more complex multiplet patterns and therefore on average broader lines with lower overall resolution of spectra. However, as was demonstrated on a small protein,[159] spectra on partially aligned samples with small signal widths due to the application of BIRD^{d,X}-filters can lead to increased resolution due to RDCs. This type of resolution might be of special interest for resolving otherwise unresolved signals: since the strength of RDCs and also the alignment tensor can be varied by using methods described in Section 4 or by a different alignment medium, two signals can be resolved as long as their internuclear vectors do not point into the same direction.

Of special interest for pharmaceutical studies is also the possibility to measure exchange-transferred RDCs of a small ligand with intermediate binding affinity to a receptor. The small molecule in this case remembers the RDCs when bound to the strongly aligned receptor and the resulting RDCs measured on the free, practically unaligned ligand mirror its conformation in the bound state.[19] In the only example reported so far by Koenig et al.,[70] the conformation of a peptide binding to a rhodopsin-containing bicellar phase is studied.

7. CONCLUSION AND OUTLOOK

Although the measurement of RDCs in partially aligned molecules has been introduced about 45 years ago, only recent advances in the development of alignment media made it possible to easily extract a limited number of RDCs for structural investigations of medium-sized organic molecules. The angular information content relative to the static magnetic field makes one- and two-bond RDCs the first high-resolution NMR parameters to connect distant parts of a molecule, and also long-range RDCs can in principle be used as combined distance and angular restraints in structure calculations.

Current disadvantages of the approach are certainly the sample preparation and structural interpretation: the sample preparation with gel-based alignment

media is relatively straightforward but typically takes several days for diffusion and equilibration, while liquid crystalline phases are more difficult to handle but allow a sample preparation within hours; the structural interpretation of RDCs is complicated by the overall tumbling of the molecules and usually has to be done by specialized software. Most software available today, like the freely available program PALES used in our laboratory, is designed for biomacromolecules and self-written conversion scripts are sometimes needed. Future developments, like the recently started implementation of an RDC toolbox in MestreNova,[238] will most certainly lead to significant improvements here.

Typical applications of the method are cases where conventional high-resolution NMR parameters do not provide sufficient configurational information or when the precise conformation of a molecule in solution is desired. Impressive examples for the power of RDCs have been reported for the determination of relative configurations in natural products and for conformational studies of sugars and peptides. While initial studies have been limited to rigid compounds, now also more and more flexible molecules are investigated.

In addition to applications in achiral environments, chiral alignment media have been shown to allow the effective distinction of enantiomers and the measurement of enantiomeric excess (ee). This fast and non-destructive way of measuring ee can be of special interest for quality control of many small molecule syntheses.

With the elegant methods available for scaling the alignment and corresponding pulse sequence developments, the authors are confident that the reliable measurement of long-range RDCs will be possible in the near future. This increase of accessible RDCs will further widen the applicability of the approach to solve most questions concerning the relative configuration of molecules. In a more distant future, even the more general determination of the absolute chirality of molecules by RDCs measured in chiral alignment media seems to be in reach.

ACKNOWLEDGEMENTS

REFERENCES

1. K. Wüthrich, *NMR of Proteins and Nucleic Acids*, Wiley & Sons, New York, 1986.
2. S. Berger and D. Sicker, *Classics in NMR Spectroscopy: Isolation and Structure Elucidation of Natural Products*, Wiley-VCH, Weinheim, 2009.
3. R. R. Ernst, G. Bodenhausen and A. Wokaun, *Principles of Nuclear Magnetic Resonance in One and Two Dimensions*, Clarendon Press, Oxford, 1987.
4. K. Schmidt-Rohr and H. W. Spiess, *Multidimensional Solid-State NMR and Polymers*, Academic Press, London, 1994.
5. M. H. Levitt, *Spin Dynamics: Basics of Nuclear Magnetic Resonance*, Wiley, Chichester, 2007.

6. J. W. Emsley and J. C. Lindon, *Nuclear Magnetic Resonance Spectroscopy Using Liquid Crystal Solvents*, Pergamon Press, Oxford, 1975.

7. R. Y. Dong, *Nuclear Magnetic Resonance of Liquid Crystals. Partially Ordered Systems*, Springer, Berlin, 1994.

8. J. W. Emsley, Liquid-crystalline materials, in: *Solid-State NMR Spectroscopy*, M. J. Duer, ed., Blackwell Science, Oxford, 2002, p. 512.

9. R. Y. Dong, *Nuclear Magnetic Resonance Spectroscopy of Liquid Crystals*, Imperial College Press, London, 2009.

10. M. R. Hansen, M. Rance and A. Pardi, *J. Am. Chem. Soc.*, 1998, **120**, 11210.

11. M. R. Hansen, P. Hanson and A. Pardi, *Methods Enzymol.*, 2000, **317**, 220.

12. B. Simon and M. Sattler, *Angew. Chem. Int. Ed.*, 2002, **41**, 437.

13. A. Bax, *Protein Sci.*, 2003, **12**, 1.

14. J. L. Yan and E. R. Zartler, *Magn. Reson. Chem.*, 2005, **43**, 53.

15. R. M. Gschwind, *Angew. Chem. Int. Ed.*, 2005, **44**, 4666.

16. C. M. Thiele, *Conc. Magn. Reson. A*, 2007, **30**, 65.

17. C. M. Thiele, *Eur. J. Org. Chem.*, 2008, 5673.

18. B. Luy and H. Kessler, Partial alignment for structure determination of organic molecules, in: *Modern Magnetic Resonance*, G. A. Webb, ed., Springer, Dordrecht, 2006, p. 1261.

19. B. Luy, A. O. Frank and H. Kessler, Conformational analysis of drugs by nuclear magnetic resonance spectroscopy, in: *Methods and Principles in Medicinal Chemistry*, R. Mannhold, H. Kubinyi and G. Folkers, eds., Vol. 37, Wiley-VCH, Weinheim, 2008, p. 207.

20. G. Kummerlöwe and B. Luy, *Trends Anal. Chem.*, 2009, **28**, 483.

21. F. Kramer, M. V. Deshmukh, H. Kessler and S. J. Glaser, *Conc. Magn. Reson. A*, 2004, **21**, 10.

22. A. Saupe, *Z. Naturforsch. A*, 1964, **19**, 161.

23. J. A. Losonczi, M. Andrec, M. W. F. Fischer and J. H. Prestegard, *J. Magn. Reson.*, 1999, **138**, 334.

24. E. E. Burnell and C. A. De Lange, *J. Magn. Reson.*, 1980, **39**, 461.

25. J. Bulthuis and C. Maclean, *J. Magn. Reson.*, 1971, **4**, 148.

26. N. J. D. Lucas, *Mol. Phys.*, 1971, **22**, 147.

27. N. J. D. Lucas, *Mol. Phys.*, 1971, **22**, 233.

28. N. J. D. Lucas, *Mol. Phys.*, 1972, **23**, 825.

29. J. G. Snijders, C. A. De Lange and E. E. Burnell, *J. Chem. Phys.*, 1982, **77**, 5386.

30. J. G. Snijders, C. A. De Lange and E. E. Burnell, *J. Chem. Phys.*, 1983, **79**, 2964.

31. J. W. Emsley, G. R. Luckhurst and C. P. Stockley, *Proc. R. Soc. Lond. A*, 1982, **381**, 117.

32. D. Catalano, L. Dibari, C. A. Veracini, G. N. Shilstone and C. Zannoni, *J. Chem. Phys.*, 1991, **94**, 3928.

33. B. Stevensson, C. Landersjö, G. Widmalm and A. Maliniak, *J. Am. Chem. Soc.*, 2002, **124**, 5946.

34. B. Stevensson, D. Sandström and A. Maliniak, *J. Chem. Phys.*, 2003, **119**, 2738.

35. J. Thaning, B. Stevensson and A. Maliniak, *J. Chem. Phys.*, 2005, 123.

36. C. Landersjö, B. Stevensson, R. Eklund, J. Östervall, P. Söderman, G. Widmalm and A. Maliniak, *J. Biomol. NMR*, 2006, **35**, 89.

37. J. Thaning, B. Stevensson, J. Östervall, K. J. Naidoo, G. Widmalm and A. Maliniak, *J. Phys. Chem. B*, 2008, **112**, 8434.

38. C. M. Thiele, A. Marx, R. Berger, J. Fischer, M. Biel and A. Giannis, *Angew. Chem. Int. Ed.*, 2006, **45**, 4455.

39. A. Schuetz, J. Junker, A. Leonov, O. F. Lange, T. F. Molinski and C. Griesinger, *J. Am. Chem. Soc.*, 2007, **129**, 15114.

40. A. Schuetz, T. Murakami, N. Takada, J. Junker, M. Hashimoto and C. Griesinger, *Angew. Chem. Int. Ed.*, 2008, **47**, 2032.

41. A. Saupe and G. Englert, *Phys. Rev. Lett.*, 1963, **11**, 462.

42. A. A. Bothnerby, P. J. Domaille and C. Gayathri, *J. Am. Chem. Soc.*, 1981, **103**, 5602.

43. M. John, G. Pintacuda, A. Y. Park, N. E. Dixon and G. Otting, *J. Am. Chem. Soc.*, 2006, **128**, 12910.

44. G. Pintacuda, M. John, X. C. Su and G. Otting, *Acc. Chem. Res.*, 2007, **40**, 206.

45. J. Wöhnert, K. J. Franz, M. Nitz, B. Imperiali and H. Schwalbe, *J. Am. Chem. Soc.*, 2003, **125**, 13338.

46. G. Pintacuda, A. Moshref, A. Leonchiks, A. Sharipo and G. Otting, *J. Biomol. NMR*, 2004, **29**, 351.

47. P. Haberz, F. Rodriguez-Castañeda, J. Junker, S. Becker, A. Leonov and C. Griesinger, *Org. Lett.*, 2006, **8**, 1275.
48. X. C. Su, T. Huber, N. E. Dixon and G. Otting, *ChemBioChem*, 2006, **7**, 1599.
49. C. C. Hinckley, *J. Am. Chem. Soc.*, 1969, **91**, 5160.
50. D. Parker, *Chem. Rev.*, 1991, **91**, 1441.
51. H. Friebolin, *Basic 1 and 2 Dimensional NMR Spectroscopy*, Wiley-VCH, Weinheim, 1993.
52. T. J. Wenzel and J. D. Wilcox, *Chirality*, 2003, **15**, 256.
53. B. Luy, K. Kobzar and H. Kessler, *Angew. Chem. Int. Ed.*, 2004, **43**, 1092.
54. J. H. Prestegard, C. M. Bougault and A. I. Kishore, *Chem. Rev.*, 2004, **104**, 3519.
55. B. Deloche and E. T. Samulski, *Macromolecules*, 1981, **14**, 575.
56. N. Tjandra and A. Bax, *Science*, 1997, **278**, 1111.
57. M. Ottiger and A. Bax, *J. Biomol. NMR*, 1998, **12**, 361.
58. J. A. Losonczi and J. H. Prestegard, *J. Biomol. NMR*, 1998, **12**, 447.
59. M. Ottiger, F. Delaglio and A. Bax, *J. Magn. Reson.*, 1998, **131**, 373.
60. M. Rückert and G. Otting, *J. Am. Chem. Soc.*, 2000, **122**, 7793.
61. J. H. Prestegard, K. L. Mayer, H. Valafar and G. C. Benison, *Nucl. Magn. Reson. Biol. Macromol. C*, 2005, **394**, 175.
62. G. M. Clore, M. R. Starich and A. M. Gronenborn, *J. Am. Chem. Soc.*, 1998, **120**, 10571.
63. M. R. Hansen, L. Mueller and A. Pardi, *Nat. Struct. Biol.*, 1998, **5**, 1065.
64. M. Zweckstetter and A. Bax, *J. Biomol. NMR*, 2001, **20**, 365.
65. K. Fleming, D. Gray, S. Prasannan and S. Matthews, *J. Am. Chem. Soc.*, 2000, **122**, 5224.
66. L. G. Barrientos, C. Dolan and A. M. Gronenborn, *J. Biomol. NMR*, 2000, **16**, 329.
67. L. G. Barrientos, K. Gawrisch, N. Cheng, A. C. Steven and A. M. Gronenborn, *Langmuir*, 2002, **18**, 3773.
68. R. S. Prosser, J. A. Losonczi and I. V. Shiyanovskaya, *J. Am. Chem. Soc.*, 1998, **120**, 11010.
69. J. Sass, F. Cordier, A. Hoffmann, A. Cousin, J. G. Omichinski, H. Löwen and S. Grzesiek, *J. Am. Chem. Soc.*, 1999, **121**, 2047.
70. B. W. Koenig, D. C. Mitchell, S. König, S. Grzesiek, B. J. Litman and A. Bax, *J. Biomol. NMR*, 2000, **16**, 121.
71. H. Desvaux, J.-C. P. Gabriel, P. Berthault and F. Camerel, *Angew. Chem. Int. Ed.*, 2001, **40**, 373.
72. J.-C. P. Gabriel, F. Camerel, B. J. Lemaire, H. Desvaux, P. Davidson and P. Batail, *Nature*, 2001, **413**, 504.
73. H. J. Sass, G. Musco, S. J. Stahl, P. T. Wingfield and S. Grzesiek, *J. Biomol. NMR*, 2000, **18**, 303.
74. S. A. Riley, J. R. Giuliani and M. P. Augustine, *J. Magn. Reson.*, 2002, **159**, 82.
75. J. F. Trempe, F. G. Morin, Z. C. Xia, R. H. Marchessault and K. Gehring, *J. Biomol. NMR*, 2002, **22**, 83.
76. K. Ruan and J. R. Tolman, *J. Am. Chem. Soc.*, 2005, **127**, 15032.
77. S. M. Douglas, J. J. Chou and W. M. Shih, *Proc. Natl. Acad. Sci. U.S.A.*, 2007, **104**, 6644.
78. J. Lorieau, L. S. Yao and A. Bax, *J. Am. Chem. Soc.*, 2008, **130**, 7536.
79. A. A. Shahkhatuni, A. G. Shahkhatuni, H. A. Panosyan, A. B. Sahakyan, I. J. L. Byeon and A. M. Gronenborn, *Magn. Reson. Chem.*, 2007, **45**, 557.
80. R. Tycko, F. J. Blanco and Y. Ishii, *J. Am. Chem. Soc.*, 2000, **122**, 9340.
81. Y. Ishii, M. A. Markus and R. Tycko, *J. Biomol. NMR*, 2001, **21**, 141.
82. S. Meier, D. Haussinger and S. Grzesiek, *J. Biomol. NMR*, 2002, **24**, 351.
83. T. Cierpicki and J. H. Bushweller, *J. Am. Chem. Soc.*, 2004, **126**, 16259.
84. J. J. Chou, S. Gaemers, B. Howder, J. M. Louis and A. Bax, *J. Biomol. NMR*, 2001, **21**, 377.
85. K. Kobzar, H. Kessler and B. Luy, *Angew. Chem. Int. Ed.*, 2005, **44**, 3145.
86. P. W. Kuchel, B. E. Chapman, N. Müller, W. A. Bubb, D. J. Philp and A. M. Torres, *J. Magn. Reson.*, 2006, **180**, 256.
87. C. Naumann, W. A. Bubb, B. E. Chapman and P. W. Kuchel, *J. Am. Chem. Soc.*, 2007, **129**, 5340.
88. C. Naumann and P. W. Kuchel, *J. Phys. Chem. A*, 2008, **112**, 8659.
89. G. Kummerlöwe, F. Halbach, B. Laufer and B. Luy, *The Open Spectrosc. J.*, 2008, **2**, 29.
90. U. Eliav and G. Navon, *J. Am. Chem. Soc.*, 2006, **128**, 15956.
91. J. H. Ma, G. I. Goldberg and N. Tjandra, *J. Am. Chem. Soc.*, 2008, **130**, 16148.

92. E. de Alba and N. Tjandra, Orientational restraints, in: *Methods and Principles in Medicinal Chemistry*, R. Mannhold, H. Kubinyi and G. Folkers, eds., Vol. 16, Wiley-VCH, Weinheim, 2003, p. 179.
93. V. V. Klochkov, A. V. Klochkov, C. M. Thiele and S. Berger, *J. Magn. Reson.*, 2006, **179**, 58.
94. B. Bendiak, *J. Am. Chem. Soc.*, 2002, **124**, 14862.
95. P. Doty, A. M. Holtzer, J. H. Bradbury and E. R. Blout, *J. Am. Chem. Soc.*, 1954, **76**, 4493.
96. A. Meddour, I. Canet, A. Loewenstein, J. M. Péchiné and J. Courtieu, *J. Am. Chem. Soc.*, 1994, **116**, 9652.
97. A. Marx and C. Thiele, *Chem. Eur. J.*, 2009, **15**, 254.
98. C. Aroulanda, M. Sarfati, J. Courtieu and P. Lesot, *Enantiomer*, 2001, **6**, 281.
99. C. M. Thiele, *J. Org. Chem.*, 2004, **69**, 7403.
100. G. Kummerlöwe, M. Udaya Kiran and B. Luy, *Chem. Eur. J.*, accepted.
101. P. Haberz, J. Farjon and C. Griesinger, *Angew. Chem. Int. Ed.*, 2005, **44**, 427.
102. G. Kummerlöwe, J. Auernheimer, A. Lendlein and B. Luy, *J. Am. Chem. Soc.*, 2007, **129**, 6080.
103. J. C. Freudenberger, S. Knör, K. Kobzar, D. Heckmann, T. Paululat, H. Kessler and B. Luy, *Angew. Chem. Int. Ed.*, 2005, **44**, 423.
104. R. R. Gil, C. Gayathri, N. V. Tsarevsky and K. Matyjaszewski, *J. Org. Chem.*, 2008, **73**, 840.
105. G. Kummerlöwe, S. Knör, A. O. Frank, T. Paululat, H. Kessler and B. Luy, *Chem. Commun.*, 2008, 5722.
106. J. C. Freudenberger, P. Spiteller, R. Bauer, H. Kessler and B. Luy, *J. Am. Chem. Soc.*, 2004, **126**, 14690.
107. M. Panar and W. D. Phillips, *J. Am. Chem. Soc.*, 1968, **90**, 3880.
108. J. P. Bayle, J. Courtieu, E. Gabetty, A. Loewenstein and J. M. Péchiné, *New J. Chem.*, 1992, **16**, 837.
109. M. Sarfati, P. Lesot, D. Merlet and J. Courtieu, *Chem. Commun.*, 2000, 2069.
110. B. Luy, K. Kobzar, S. Knör, J. Furrer, D. Heckmann and H. Kessler, *J. Am. Chem. Soc.*, 2005, **127**, 6459.
111. P. Doty, J. H. Bradbury and A. M. Holtzer, *J. Am. Chem. Soc.*, 1956, **78**, 947.
112. J. C. Mitchell, A. E. Woodward and P. Doty, *J. Am. Chem. Soc.*, 1957, **79**, 3955.
113. V. V. Klochkov, B. I. Khairutdinov, A. V. Klochkov, M. S. Tagirov, C. M. Thiele, S. Berger, I. S. Vershinina, I. I. Stoikova, I. S. Antipin and A. I. Konovalov, *Russ. Chem. Bull.*, 2004, **53**, 1466.
114. A. S. Tracey and P. Diehl, *FEBS Lett.*, 1975, **59**, 131.
115. A. S. Tracey, *Mol. Phys.*, 1977, **33**, 339.
116. K. Baczko, C. Larpent and P. Lesot, *Tetrahedron: Asymmetry*, 2004, **15**, 971.
117. E. Lafontaine, J. P. Bayle and J. Courtieu, *J. Am. Chem. Soc.*, 1989, **111**, 8294.
118. E. Lafontaine, J. M. Péchiné, J. Courtieu and C. L. Mayne, *Liq. Cryst.*, 1990, **7**, 293.
119. I. Canet, J. Courtieu, A. Loewenstein, A. Meddour and J. M. Péchiné, *J. Am. Chem. Soc.*, 1995, **117**, 6520.
120. B. E. Weiss-Lopéz, M. Azocar, R. Montecinos, B. K. Cassels and R. Araya-Maturana, *Langmuir*, 2001, **17**, 6910.
121. J. M. Péchiné, A. Meddour and J. Courtieu, *Chem. Commun.*, 2002, 1734.
122. A. Solgadi, A. Meddour and J. Courtieu, *Tetrahedron: Asymmetry*, 2004, **15**, 1315.
123. C. M. Thiele and S. Berger, *Org. Lett.*, 2003, **5**, 705.
124. F. M. Leslie, *Q. J. Mech. Appl. Math.*, 1966, **19**, 357.
125. F. M. Leslie, *Arch. Ration. Mech. Anal.*, 1968, **28**, 265.
126. F. M. Leslie, G. R. Luckhurst and H. J. Smith, *Chem. Phys. Lett.*, 1972, **13**, 368.
127. R. M. Hornreich, *Phys. Rev. A*, 1977, **15**, 1767.
128. C. H. Yo, R. Poupko and R. M. Hornreich, *Chem. Phys. Lett.*, 1978, **54**, 142.
129. J. Courtieu, D. W. Alderman and D. M. Grant, *J. Am. Chem. Soc.*, 1981, **103**, 6783.
130. J. Courtieu, D. W. Alderman, D. M. Grant and J. P. Bayles, *J. Chem. Phys.*, 1982, **77**, 723.
131. R. Teeäär, M. Alla and E. Lippmaa, *Org. Magn. Reson.*, 1982, **19**, 134.
132. C. M. Thiele, *Angew. Chem. Int. Ed.*, 2005, **44**, 2787.
133. J. P. Bayle, F. Perez and J. Courtieu, *Liq. Cryst.*, 1988, **3**, 753.
134. J. Courtieu, J. P. Bayle and B. M. Fung, *Prog. Nucl. Magn. Reson. Spectrosc.*, 1994, **26**, 141.
135. T. Väänänen, J. Jokisaari and M. Seläntaus, *Chem. Phys. Lett.*, 1986, **129**, 399.

136. T. Väänänen, J. Jokisaari and M. Seläntaus, *J. Magn. Reson.*, 1987, **72**, 414.
137. W. A. Heeschen, D. W. Alderman and D. M. Grant, *J. Phys. Chem.*, 1988, **92**, 6504.
138. N. T. Lai, J. P. Bayle, J. M. Ouvrard and J. Courtieu, *Liq. Cryst.*, 1988, **3**, 745.
139. F. Tian, J. A. Losonczi, M. W. F. Fischer and J. H. Prestegard, *J. Biomol. NMR*, 1999, **15**, 145.
140. R. H. Havlin, G. H. J. Park, T. Mazur and A. Pines, *J. Am. Chem. Soc.*, 2003, **125**, 7998.
141. N. Lancelot, K. Elbayed, A. Bianco and M. Piotto, *J. Biomol. NMR*, 2004, **29**, 259.
142. L. Beguin, J. Courtieu, L. Ziani and D. Merlet, *Magn. Reson. Chem.*, 2006, **44**, 1096.
143. G. Kummerlöwe, S. Grage, C. M. Thiele and B. Luy, *47th ENC Conference*, 2006, 62.
144. A. Enthart, J. C. Freudenberger, J. Furrer, H. Kessler and B. Luy, *J. Magn. Reson.*, 2008, **192**, 314.
145. P. Nolis, J. F. Espinosa and T. Parella, *J. Magn. Reson.*, 2006, **180**, 39.
146. P. Tzvetkova, S. Simova and B. Luy, *J. Magn. Reson.*, 2007, **186**, 193.
147. M. J. Thrippleton and J. Keeler, *Angew. Chem. Int. Ed.*, 2003, **42**, 3938.
148. J. L. Yan, A. D. Kline, H. P. Mo, M. J. Shapiro and E. R. Zartler, *J. Org. Chem.*, 2003, **68**, 1786.
149. T. E. Skinner, T. O. Reiss, B. Luy, N. Khaneja and S. J. Glaser, *J. Magn. Reson.*, 2003, **163**, 8.
150. T. E. Skinner, T. O. Reiss, B. Luy, N. Khaneja and S. J. Glaser, *J. Magn. Reson.*, 2004, **167**, 68.
151. K. Kobzar, T. E. Skinner, N. Khaneja, S. J. Glaser and B. Luy, *J. Magn. Reson.*, 2004, **170**, 236.
152. B. Luy, K. Kobzar, T. E. Skinner, N. Khaneja and S. J. Glaser, *J. Magn. Reson.*, 2005, **176**, 179.
153. N. Cramer, S. Helbig, A. Baro, S. Laschat, R. Diestel, F. Sasse, D. Mathieu, C. Richter, G. Kummerlöwe, B. Luy and H. Schwalbe, *ChemBioChem*, 2008, **9**, 2474.
154. B. Yu, V. Subramanian and D. I. Freedberg, *50th ENC conference*, 2009, 51.
155. J. R. Garbow, D. P. Weitekamp and A. Pines, *Chem. Phys. Lett.*, 1982, **93**, 504.
156. D. Uhrín, T. Liptaj and K. E. Kover, *J. Magn. Reson. A*, 1993, **101**, 41.
157. K. Feher, S. Berger and K. E. Kover, *J. Magn. Reson.*, 2003, **163**, 340.
158. L. Ziani, J. Courtieu and D. Merlet, *J. Magn. Reson.*, 2006, **183**, 60.
159. J. Furrer, M. John, H. Kessler and B. Luy, *J. Biomol. NMR*, 2007, **37**, 231.
160. B. Luy and J. P. Marino, *J. Magn. Reson.*, 2003, **163**, 92.
161. B. Luy, G. Hauser, A. Kirschning and S. J. Glaser, *Angew. Chem. Int. Ed.*, 2003, **42**, 1300.
162. T. Carlomagno, W. Peti and C. Griesinger, *J. Biomol. NMR*, 2000, **17**, 99.
163. E. Miclet, D. C. Williams, G. M. Clore, D. L. Bryce, J. Boisbouvier and A. Bax, *J. Am. Chem. Soc.*, 2004, **126**, 10560.
164. L. Verdier, P. Sakhaii, M. Zweckstetter and C. Griesinger, *J. Magn. Reson.*, 2003, **163**, 353.
165. L. Jin and D. Uhrín, *Magn. Reson. Chem.*, 2007, **45**, 628.
166. B. L. Marquez, W. H. Gerwick and R. T. Williamson, *Magn. Reson. Chem.*, 2001, **39**, 499.
167. K. Kobzar and B. Luy, *J. Magn. Reson.*, 2007, **186**, 131.
168. C. Griesinger, O. W. Sørensen and R. R. Ernst, *J. Am. Chem. Soc.*, 1985, **107**, 6394.
169. C. Griesinger, O. W. Sørensen and R. R. Ernst, *J. Chem. Phys.*, 1986, **85**, 6837.
170. C. Griesinger, O. W. Sørensen and R. R. Ernst, *J. Magn. Reson.*, 1987, **75**, 474.
171. B. Baishya and N. Suryaprakash, *J. Chem. Phys.*, 2007, **127**, 214510.
172. B. Baishya and N. Suryaprakash, *J. Phys. Chem. A*, 2007, **111**, 5211.
173. B. Baishya, G. N. M. Reddy, U. R. Prabhu, T. N. G. Row and N. Suryaprakash, *J. Phys. Chem. A*, 2008, **112**, 10526.
174. B. Baishya, U. R. Prabhu and N. Suryaprakash, *J. Magn. Reson.*, 2008, **192**, 92.
175. S. Hebbar and N. Suryaprakash, *J. Magn. Reson.*, 2008, **194**, 192.
176. G. N. M. Reddy, T. N. G. Row and N. Suryaprakash, *J. Magn. Reson.*, 2009, **196**, 119.
177. F. Tian, P. J. Bolon and J. H. Prestegard, *J. Am. Chem. Soc.*, 1999, **121**, 7712.
178. Z. R. Wu and A. Bax, *J. Magn. Reson.*, 2001, **151**, 242.
179. F. Delaglio, Z. R. Wu and A. Bax, *J. Magn. Reson.*, 2001, **149**, 276.
180. T. Prasch, P. Gröschke and S. J. Glaser, *Angew. Chem. Int. Ed.*, 1998, **37**, 802.
181. A. Möglich, M. Wenzler, F. Kramer, S. J. Glaser and E. Brunner, *J. Biomol. NMR*, 2002, **23**, 211.
182. J. J. Titman and J. Keeler, *J. Magn. Reson.*, 1990, **89**, 640.
183. A. Meissner, J. O. Duus and O. W. Sørensen, *J. Magn. Reson.*, 1997, **128**, 92.
184. A. Meissner and O. W. Sørensen, *Magn. Reson. Chem.*, 2001, **39**, 49.
185. B. Luy and J. P. Marino, *J. Biomol. NMR*, 2001, **20**, 39.
186. B. Luy, J. J. Barchi and J. P. Marino, *J. Magn. Reson.*, 2001, **152**, 179.

187. C. H. Gotfredsen, A. Meissner, J. O. Duus and O. W. Sørensen, *Magn. Reson. Chem.*, 2000, **38**, 692.
188. Z. R. Wu, N. Tjandra and A. Bax, *J. Biomol. NMR*, 2001, **19**, 367.
189. T. Carlomagno, M. Hennig and J. R. Williamson, *J. Biomol. NMR*, 2002, **22**, 65.
190. J. Farjon, W. Bermel and C. Griesinger, *J. Magn. Reson.*, 2006, **180**, 72.
191. F. Kramer, B. Luy and S. J. Glaser, *Appl. Magn. Reson.*, 1999, **17**, 173.
192. F. Kramer and S. J. Glaser, *J. Magn. Reson.*, 2002, **155**, 83.
193. F. Kramer and S. J. Glaser, *J. Magn. Reson.*, 2004, **168**, 238.
194. F. Kramer, A. Jung, E. Brunner and S. J. Glaser, *J. Magn. Reson.*, 2004, **169**, 49.
195. L. Braunschweiler and R. R. Ernst, *J. Magn. Reson.*, 1983, **53**, 521.
196. O. Schedletzky and S. J. Glaser, *J. Magn. Reson. A*, 1996, **123**, 174.
197. B. Luy, O. Schedletzky and S. J. Glaser, *J. Magn. Reson.*, 1999, **138**, 19.
198. D. M. Taylor and A. Ramamoorthy, *J. Magn. Reson.*, 1999, **141**, 18.
199. B. Luy and S. J. Glaser, *J. Magn. Reson.*, 2001, **148**, 169.
200. B. Luy and S. J. Glaser, *J. Magn. Reson.*, 2000, **142**, 280.
201. F. Kramer, W. Peti, C. Griesinger and S. J. Glaser, *J. Magn. Reson.*, 2001, **149**, 58.
202. J. Furrer, F. Kramer, J. P. Marino, S. J. Glaser and B. Luy, *J. Magn. Reson.*, 2004, **166**, 39.
203. J. Klages, H. Kessler, S. J. Glaser and B. Luy, *J. Magn. Reson.*, 2007, **189**, 217.
204. G. Celebre, G. De Luca, M. Longeri, D. Catalano, C. A. Veracini and J. W. Emsley, *J. Chem. Soc. Faraday Trans.*, 1991, **87**, 2623.
205. G. Celebre, G. De Luca, M. Longeri and J. W. Emsley, *J. Phys. Chem.*, 1992, **96**, 2466.
206. G. Celebre, G. De Luca, J. W. Emsley, E. K. Foord, M. Longeri, F. Lucchesini and G. Pileio, *J. Chem. Phys.*, 2003, **118**, 6417.
207. G. Celebre, G. De Luca, M. Longeri, G. Pileio and J. W. Emsley, *J. Chem. Phys.*, 2004, **120**, 7075.
208. G. Celebre, G. De Luca, M. Longeri and G. Pileio, *Mol. Cryst. Liq. Cryst.*, 2007, **465**, 289.
209. G. Celebre, G. Cinacchi, G. De Luca, B. M. Giuliano, F. Iemma and S. Melandri, *J. Phys. Chem. B*, 2008, **112**, 2095.
210. J. W. Emsley, G. Celebre, G. De Luca, M. Longeri, D. Catalano and C. A. Veracini, *Gazz. Chim. Ital.*, 1996, **126**, 429.
211. A. B. Sahakyan, A. G. Shahkhatuni, A. A. Shahkhatuni and H. A. Panosyan, *Magn. Reson. Chem.*, 2008, **46**, 144.
212. A. Yethiraj, A. C. J. Weber, R. Y. Dong and E. E. Burnell, *J. Phys. Chem. B*, 2007, **111**, 1632.
213. E. E. Burnell, C. A. de Lange, J. B. S. Barnhoorn, I. Aben and P. F. Levelt, *J. Phys. Chem. A*, 2005, **109**, 11027.
214. G. Celebre, M. Concistre, G. De Luca, M. Longeri and G. Pileio, *Chem. Phys. Chem.*, 2006, **7**, 1930.
215. J. W. Emsley, M. Longeri, D. Merlet, G. Pileio and N. Suryaprakash, *J. Magn. Reson.*, 2006, **180**, 245.
216. G. Celebre, M. Concistre, G. De Luca, M. Longeri, G. Pileio and J. W. Emsley, *Chem. Eur. J.*, 2005, **11**, 3599.
217. M. Concistre, G. De Luca, M. Longeri, G. Pileio and J. W. Emsley, *Chem. Phys. Chem.*, 2005, **6**, 1483.
218. C. Aroulanda, G. Celebre, G. De Luca and M. Longeri, *J. Phys. Chem. B*, 2006, **110**, 10485.
219. M. Martín-Pastor and C. A. Bush, *Biochemistry*, 2000, **39**, 4674.
220. M. Martín-Pastor and C. A. Bush, *Carbohydr. Res.*, 2000, **323**, 147.
221. M. Martín-Pastor and C. A. Bush, *J. Biomol. NMR*, 2001, **19**, 125.
222. H. Neubauer, J. Meiler, W. Peti and C. Griesinger, *Helv. Chim. Acta*, 2001, **84**, 243.
223. H. F. Azurmendi and C. A. Bush, *Carbohydr. Res.*, 2002, **337**, 905.
224. H. F. Azurmendi, M. Martín-Pastor and C. A. Bush, *Biopolymers*, 2002, **63**, 89.
225. D. I. Freedberg, *J. Am. Chem. Soc.*, 2002, **124**, 2358.
226. J. Adeyeye, H. F. Azurmendi, C. J. M. Stroop, S. Sozhamannan, A. L. Williams, A. M. Adetumbi, J. A. Johnson and C. A. Bush, *Biochemistry*, 2003, **42**, 3979.
227. M. Martín-Pastor, A. Canales-Mayordomo and J. Jimenez-Barbero, *J. Biomol. NMR*, 2003, **26**, 345.
228. T. N. Pham, S. L. Hinchley, D. W. H. Rankin, T. Liptaj and D. Uhrín, *J. Am. Chem. Soc.*, 2004, **126**, 13100.
229. A. Silipo, Z. Zhang, F. J. Cañada, A. Molinaro, R. J. Linhardt and J. Jiménez-Barbero, *ChemBioChem*, 2008, **9**, 240.
230. J. Klages, C. Neubauer, M. Coles, H. Kessler and B. Luy, *ChemBioChem*, 2005, **6**, 1672.

231. M. Martín-Pastor, A. Canales, F. Corzana, J. L. Asensio and J. Jiménez-Barbero, *J. Am. Chem. Soc.*, 2005, **127**, 3589.

232. A. V. Klochkov, B. I. Khairutdinov, M. S. Tagirov and V. V. Klochkov, *Magn. Reson. Chem.*, 2005, **43**, 948.

233. C. Landersjö, J. L. M. Jansson, A. Maliniak and G. Widmalm, *J. Phys. Chem. B*, 2005, **109**, 17320.

234. U. M. Reinscheid, J. Farjon, M. Radzom, P. Haberz, A. Zeeck, M. Blackledge and C. Griesinger, *ChemBioChem*, 2006, **7**, 287.

235. M. B. Schmid, M. Fleischmann, V. D'Elia, O. Reiser, W. Gronwald and R. M. Gschwind, *ChemBioChem*, 2009, **10**, 440.

236. V. V. Klochkov, R. F. Baikeev, V. D. Skirda, A. V. Klochkov, F. R. Muhamadiev, I. Baskyr and S. Berger, *Magn. Reson. Chem.*, 2009, **47**, 57.

237. R. S. Stoll, M. V. Peters, A. Kuhn, S. Heiles, R. Goddard, M. Buhl, C. M. Thiele and S. Hecht, *J. Am. Chem. Soc.*, 2009, **131**, 357.

238. V. M. Sánchez-Pedregal, R. Santamaría-Fernández and A. Navarro-Vázquez, *Org. Lett.*, 2009, **11**, 1471.

239. C. Aroulanda, V. Boucard, F. Guibe, J. Courtieu and D. Merlet, *Chem. Eur. J.*, 2003, **9**, 4536.

240. A. Mangoni, V. Esposito and A. Randazzo, *Chem. Commun.*, 2003, 154.

241. J. L. Yan, F. Delaglio, A. Kaerner, A. D. Kline, H. P. Mo, M. J. Shapiro, T. A. Smitka, G. A. Stephenson and E. R. Zartler, *J. Am. Chem. Soc.*, 2004, **126**, 5008.

242. C. Farès, J. Hassfeld, D. Menche and T. Carlomagno, *Angew. Chem. Int. Ed.*, 2008, **47**, 3722.

243. J. D. Swarbrick and T. D. Ashton, *Chirality,* 2009, DOI: 10.1002/chir.20703, available online.

244. J. Farjon, D. Merlet, P. Lesot and J. Courtieu, *J. Magn. Reson.*, 2002, **158**, 169.

245. M. Rivard, F. Guillen, J.-C. Fiaud, C. Aroulanda and P. Lesot, *Tetrahedron: Asymmetry*, 2003, **14**, 1141.

246. J. Farjon, J.-P. Baltaze, P. Lesot, D. Merlet and J. Courtieu, *Magn. Reson. Chem.*, 2004, **42**, 594.

247. O. Lafon, P. Lesot, M. Rivard, M. Chavarot, F. Rose-Munch and E. Rose, *Organometallics*, 2005, **24**, 4021.

248. V. L. Manthati, A. Sai Krishna Murthy, F. Caijo, D. Drouin, P. Lesot, D. Grée and R. Grée, *Tetrahedron: Asymmetry*, 2006, **17**, 2306.

249. A. Meddour, J. Uziel, J. Courtieu and S. Jugé, *Tetrahedron: Asymmetry*, 2006, **17**, 1424.

250. V. M. Marathias, G. J. Tawa, I. Goljer and A. C. Bach II, *Chirality*, 2007, **19**, 741.

251. J. L. Yan, A. D. Kline, H. P. Mo, M. J. Shapiro and E. R. Zartler, *Magn. Reson. Chem.*, 2004, **42**, 962.

252. R. M. Venable, F. Delaglio, S. E. Norris and D. I. Freedberg, *Carbohydr. Res.*, 2005, **340**, 863.

253. M. Udaya Kiran, A. Sudhakar, J. Klages, G. Kummerlöwe, B. Luy and B. Jagadeesh, submitted.

254. C. Aroulanda, P. Lesot, D. Merlet and J. Courtieu, *J. Phys. Chem. A*, 2003, **107**, 10911.

255. O. Lafon, P. Lesot, H. Zimmermann, R. Poupko and Z. Luz, *J. Phys. Chem. B*, 2007, **111**, 9453.

256. P. Lesot, V. Baillif and I. Billault, *Anal. Chem.*, 2008, **80**, 2963.

257. W. Smadja, S. Auffret, P. Berdague, D. Merlet, C. Canlet, J. Courtieu, J. Y. Legros, A. Boutros and J. C. Fiaud, *Chem. Commun.*, 1997, 2031.

258. P. Lesot, D. Merlet, M. Sarfati, J. Courtieu, H. Zimmermann and Z. Luz, *J. Am. Chem. Soc.*, 2002, **124**, 10071.

259. P. Lesot, O. Lafon, H. B. Kagan and C. A. Fan, *Chem. Commun.*, 2006, 389.

260. M. Sarfati, C. Aroulanda, J. Courtieu and P. Lesot, *Tetrahedron: Asymmetry*, 2001, **12**, 737.

261. K. Ben Ali, O. Lafon, H. Zimmermann, E. Guittet and P. Lesot, *J. Magn. Reson.*, 2007, **187**, 205.

262. C. Aroulanda, D. Merlet, J. Courtieu and P. Lesot, *J. Am. Chem. Soc.*, 2001, **123**, 12059.

263. A. Meddour, D. Atkinson, A. Loewenstein and J. Courtieu, *Chem. Eur. J.*, 1998, **4**, 1142.

264. M. Sarfati, J. Courtieu and P. Lesot, *Chem. Commun.*, 2000, 1113.

265. D. Merlet, B. Ancian, J. Courtieu and P. Lesot, *J. Am. Chem. Soc.*, 1999, **121**, 5249.

266. P. Lesot, D. Merlet, A. Meddour, J. Courtieu and A. Loewenstein, *J. Chem. Soc. Faraday Trans.*, 1995, **91**, 1371.

267. M. Jakubcova, A. Meddour, J. M. Péchiné, A. Baklouti and J. Courtieu, *J. Fluorine Chem.*, 1997, **86**, 149.

268. A. Meddour, P. Berdague, A. Hedli, J. Courtieu and P. Lesot, *J. Am. Chem. Soc.*, 1997, **119**, 4502.

269. L. Ziani, P. Lesot, A. Meddour and J. Courtieu, *Chem. Commun.*, 2007, 4737.
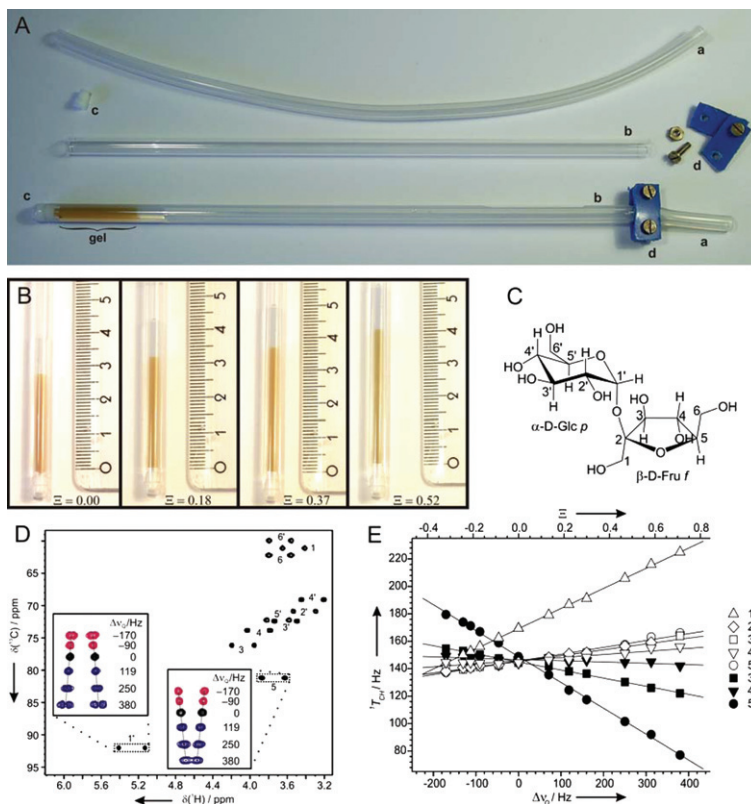
Plate 1 Stretching apparatus for the variable scaling of alignment in a single gel. (A) The components of the apparatus: (a) flexible rubber tube, (b) open-cut NMR tube, (c) teflon plug for the bottom, (d) fixation device for the top of the apparatus. In the readily prepared gel sample, the gel is inside the rubber tube. (B) The gel at different extension factors Ξ for different alignment strengths. (D) CLIP-HSQC of sucrose (C) in gelatin/D_2O (black contours) with inlets showing two cross-peaks at various states of stretching (dark grey) and compression (light grey) with corresponding quadrupolar splittings of the deuterated solvent. (E) $^1T_{CH}$ couplings of sucrose at different extension factors result in an linear relation to the quadrupolar splitting of D_2O with the slope proportional to RDCs. (Reproduced from ref. 89.) (For B/W version, refer page 211, Figure 8)
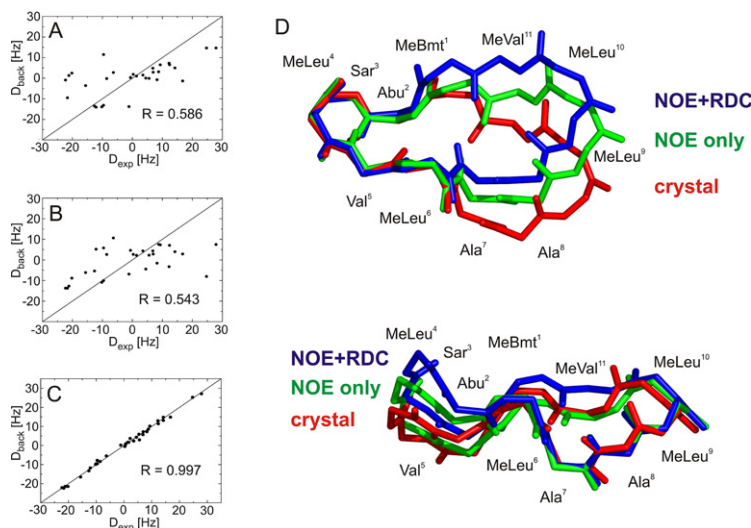
Plate 2 Comparison of experimentally determined RDCs and RDCs back-calculated from the crystal structure (A), an NOE-derived structural model (B) and the (NOE+RDC)-refined structure (C) of cyclosporin A. (D) Evaluation of the resulting models for the average structures show a flat geometry in the crystal, an already bent backbone for the structure based only on NOE data, and a further twist in the RDC-refined backbone, which does not violate any NOE data. (Reproduced from ref. 230 with permission from Wiley-VCH Verlag GmbH & Co. KGaA (Copyright).) (For B/W version, refer page 220, Figure 12)
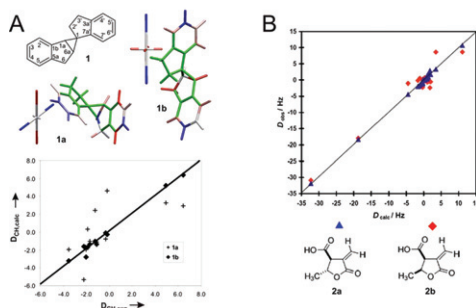
Plate 3 Examples for the determination of relative configuration. (A) The spiroindene **1** in principle can adopt two configurations **1a** and **1b**. The two configurations are shown with the principle axes of the fitted alignment tensors (see ref. 106 for colour coding). By plotting experimental versus back-calculated RDCs, clearly **1b** is identified as the correct configuration. (B) Similar procedure for the potential lactones **2a** and **2b**, respectively, with the additional difficulty of the flexibility in the five-membered ring. (Reprinted with permission from ref. 106. Copyright 2004 American Chemical Society. And reproduced from ref. 17 with permission from Wiley-VCH Verlag GMbH & Co. KGaA (Copyright).) (For B/W version, refer page 221, Figure 14)

SUBJECT INDEX